Accelerator Division

Collider-Accelerator Department

Configuration Manual

Last revision Nov. 2006

Table of Contents

CRYOGENIC SYSTEM (WBS 1.3)

VACUUM SYSTEM

BEAM TRANSFER AND INJECTION SYSTEM (WBS 1.5)

BEAM DUMP SYSTEM (WBS 1.6)

CONVENTIONAL FACILITIES (WBS 1.10)

COLLIDER INSTALLATION (WBS 1.0)

SAFETY SYSTEMS (WBS 1 .12)

INTRODUCTION

The Relativistic Heavy Ion Collider facility at the Brookhaven National Laboratory enables studies of nuclear phenomena in collisions of light and heavy ions, and polarized protons. The collider was constructed in an existing 3.834 km long ring tunnel, and is in operation since 2000. The major performance design requirements for the collider was a beam energy ranging up to 100 GeV/n for the heaviest ions, e.g. for Au-Au, and an average luminosity at top energy of 2×10^{26} $cm^{-2}s^{-1}$ at each of the possible six crossing points. This luminosity goal has been exceeded, and the new performance goals are called the Enhanced Design parameters. These call for a four-fold increase in the average heavy ion luminosity. In addition, a polarized proton program was developed. The Enhanced Performance parameters for polarized protons are a maximum energy of 250 GeV, an average store luminosity of 150×10^{30} $cm^{-2}s^{-1}$, an average store polarization of 70%, and the availability of longitudinally polarized beams at 2 interaction points.

This Configuration Manual shows the current and future expected collider performance and, at the same time, the accelerator physics and engineering parameters of the machine. It also gives the locations of all major ring components, notably the location of magnets, rf cavities, beam position monitors, and injection and beam dump equipment. The Configuration Manual, together with drawings and specifications, establishes the configuration of the RHIC facility.

In order to prevent confusion caused by outdated information, each page of the Configuration Manual will be coded as to its Accelerator System, the page number within an Accelerator System, and the revision date. The Table of Contents indicates the valid revision of the Configuration Manual.

FACILITY SCOPE

The Relativistic Heavy Ion Collider at Brookhaven National Laboratory has been in operation since 2000. The research objectives of RHIC involve the study of collisions of heavy ion beams (e.g., beams of the nuclei of gold atoms) at energies up to 100 GeV/n, and polarized protons at energies up to 100 GeV. Since 2000, RHIC has delivered luminosity to 5 experiments, STAR, PHENIX, PHOBOS, BRAHMS, and PP2PP. In heavy ion operation a greater operational flexibility than at other hadron colliders is required. Species and collision energy are changed frequently. The heavy ion program has produced a number of striking results, including the discovery of a fascinating new form of matter. Unexpectedly, this extremely hot and dense matter, often referred to as the strongly interacting quark gluon plasma or sQGP, behaves more like a perfect liquid than an ideal gas. In polarized proton operation, both luminosity and polarization are important. The figure of merit for the experiments is either LP^2 or LP^4 where L is the luminosity and P the beam polarization. RHIC can deliver vertically polarized beam to all experiments, and longitudinally polarized beam to STAR and PHENIX. Currently the main goal of the polarized proton program is to reveal the source of the proton spin.

The Configuration Manual covers technical areas, which are related to the beam transfer lines and the collider. The following sections address performance objectives of the collider, the overview on the collider rings, and the collider operational scenario.

Performance Objectives

The performance objectives for a heavy-ion collider were originally formulated in 1983 by a *Task Force for Relativistic Heavy Ion Physics*. The project scope for RHIC was finalized with input from scientific and technical review committees and has been endorsed by the DOE/NSF Nuclear Science Advisory Committee in its December 1989 Long Range Plan for Nuclear Science. The agreed upon design parameters for heavy ions were exceeded after a few years of operation. New goals were formulated and are called "Enhanced Design" parameters. The major RHIC performance parameters (Design, Achieved, and Enhanced Design) are summarized in Table 1.

Energy. The top kinetic energy will be 100 × 100 GeV/n for gold ions. At a $B\rho = 839.5$ T·m of the magnet system set for 100 GeV/n Au beams, the operational momentum increases with

the charge-to-mass ratio, resulting in kinetic energies of 125 GeV/n for lighter ions and 250 GeV for protons. The collider will be able to operate over a wide range from injection to top energies. In order to limit magnet aperture, and thus cost, full luminosity and lifetime requirements were specified at energies above 30 × 30 GeV/n.

Luminosity. The collider was designed for an average Au-Au luminosity of about 2×10^{26} $cm^{-2}s^{-1}$ at top energy, while maintaining the potential for future upgrades by an order of magnitude. Operation with the heaviest ions imposes the most demanding requirements on the collider design, and gold-on-gold is taken as the prototypical example. The luminosity is energy dependent and decreases in first approximation quadratically to the operating energy (the beam size increases linearly with $1/\gamma$, and the β^* is also increased with $1/\gamma$). The luminosity for lighter ions is higher, since approximately the same charge per bunch can be stored. The Enhanced Design goal for Au-Au luminosity is 4 times larger than the design goal, 8×10^{26} $cm^{-2}s^{-1}$. The Enhanced Design goal for the average p-p luminosity at 250 GeV is 150×10^{30} $cm^{-2}s^{-1}$.

Polarization. RHIC is the only existing collider of spin-polarized protons. The Enhanced Design goal for polarization is 70% on average during stores of energies up to 250 GeV.

Range of ion masses. The expectations for interesting physics phenomena require a broad range of nuclei from the heaviest to the lightest, including protons. Asymmetric operation with heavy ions colliding on deuterons or protons is crucial for the experimental program. The collider will allow collisions of beams of equal ion species from Au-Au all the way down to p-p. It will also allow operation of unequal species such as deuteron or protons on gold ions. Uranium is a viable species and can be considered as a future upgrade with the Electron Beam Ion Source EBIS.

Intersection Regions. The existing tunnel and the magnet lattice configuration provides for six experimental areas where the circulating beams cross. Four of the experimental areas presently have completed experimental halls with a support building for utilities (IR2, IR6, IR8, IR10). IR4 houses the rf systems, IR12 the polarized hydrogen jet.

A warm space of about ±9 m at each crossing point is provided for the experimental detectors, with a free space of ±7.12 m space available for the experimental beam pipes. The crossing point configuration foresees head-on collisions, but allows crossing angles up to 1.7 mrad.

Table 1. RHIC Design, Achieved, and Enhanced Performance Objectives.

Mode	No of bunches	Ions/bunch [10^9]	β* [m]	Emittance [μm]	$\mathcal{L}_{peak}$ [$cm^{-2}s^{-1}$]	$\mathcal{L}_{store\ ave}$ [$cm^{-2}s^{-1}$]	L_{week}
			Design values (1999)				
$Au^{79+} + Au^{79+}$	56	1.0	2	15-40	9×10^{26}	2×10^{26}	50 μb^{-1}
$p^+ + p^+$	56	100	2	20	5×10^{30}	4×10^{30}	1.2 pb^{-1}
			Achieved values (2006)				
$Au^{79+} + Au^{79+}$	45	1.1	1	15-40	15×10^{26}	4×10^{26}	160 μb^{-1}
$p^+\uparrow + p^+\uparrow$ *	111	135	1	18-25	35×10^{30}	20×10^{30}	7.0 pb^{-1}
$d^+ + Au^{79+}$	55	110d / 0.7Au	2	15	7×10^{28}	2×10^{28}	4.5 nb^{-1}
$Cu^{29+} + Cu^{29+}$	37	4.5	0.9	15-30	2×10^{28}	0.8×10^{28}	2.4 nb^{-1}
			Enhanced design values (~2008)				
$Au^{79+} + Au^{79+}$	112	1.1	1	15-40	36×10^{26}	8×10^{26}	330 μb^{-1}
$p^+\uparrow + p^+\uparrow$ **	112	200	1	20	225×10^{30}	150×10^{30}	55 pb^{-1}

* Blue and Yellow ring polarization of 65% in RHIC stores at 100GeV.
** Blue and Yellow ring polarization of 70% in RHIC stores at 250GeV.

The beta function at each crossing point is continuously adjustable from β* = 10 m down to 1 m (and possibly to 0.5 m) at top energy by changing the currents in the insertion quadrupoles. In operation at lower energies, β* is adjusted such as to maintain the same beam size in the triplet magnets as at top energy.

The Collider Rings

The RHIC facility is a complex set of accelerators interconnected by beam transfer lines. The injector system can be operated independently of the collider. The main 3.834 km long tunnel is connected to the AGS through the injection tunnels. The collider has support buildings, four completed experimental areas (two additional undeveloped experimental areas also exist), and a cryogenic refrigerator system with the capacity to meet RHIC requirements. The RHIC tunnel is located towards the northwest corner of the Brookhaven site. The site plan in Fig. 1 shows all major components of the RHIC complex.

Bending and focusing of the ion beams is achieved by the ring magnets. In view of the fixed tunnel circumference, a cost optimization lead the choice of relatively low-field superconducting magnets. At a magnetic field of 3.458 T, the beam energy is 100 GeV/n for fully stripped gold ions, and 250 GeV for protons. The required field is generated with single-layer cosine-theta magnets, which, for maximum operational flexibility, are contained in vacuum vessels separate for each ring, except those near the collision points. The collider consists of two rings of superconducting magnets. The main components of the magnet system are 288 arc-size dipoles and 108 insertion dipoles, and 276 arc and 216 insertion quadrupoles. In addition to dipoles and quadrupoles, there is an inventory of smaller magnets consisting of 72 trim quadrupoles, 288 sextupoles and 492 corrector magnets at each quadrupole. For polarized proton spin manipulations there are 24 superconducting helical magnets in each ring, grouped into 2 snakes and 4 spin rotators. The arc dipoles have a physical length of 9.728 m (9.45 m effective), are bent with a 4.85 cm sagitta and have a coil aperture of 8 cm in order to accommodate the requirements due to intrabeam scattering. The cold bore beam tube aperture is 69 mm in diameter. The beams in the arcs are 90 cm apart.

The magnets are cooled to a temperature of <4.6 K by circulating supercritical helium, which is supplied by a 24.8 kW refrigerator. The various ring magnets are excited by an appropriate power supply system and protected by a quench protection system. The beam tube in the superconducting magnets is at the temperature of liquid helium. An extremely good vacuum with an equivalent warm pressure $<10^{-11}$ Torr is obtained, in the absence of leaks into the cold bore. In order to avoid the formation of electron clouds, beam loss and radiation background, a vacuum of about 7×10^{-11} Torr is required in the warm beam tube sections of the insertion regions. The cryostats for the superconducting magnets require a separate insulating vacuum of less than 10^{-5} Torr in order to avoid a heat load due to convection.

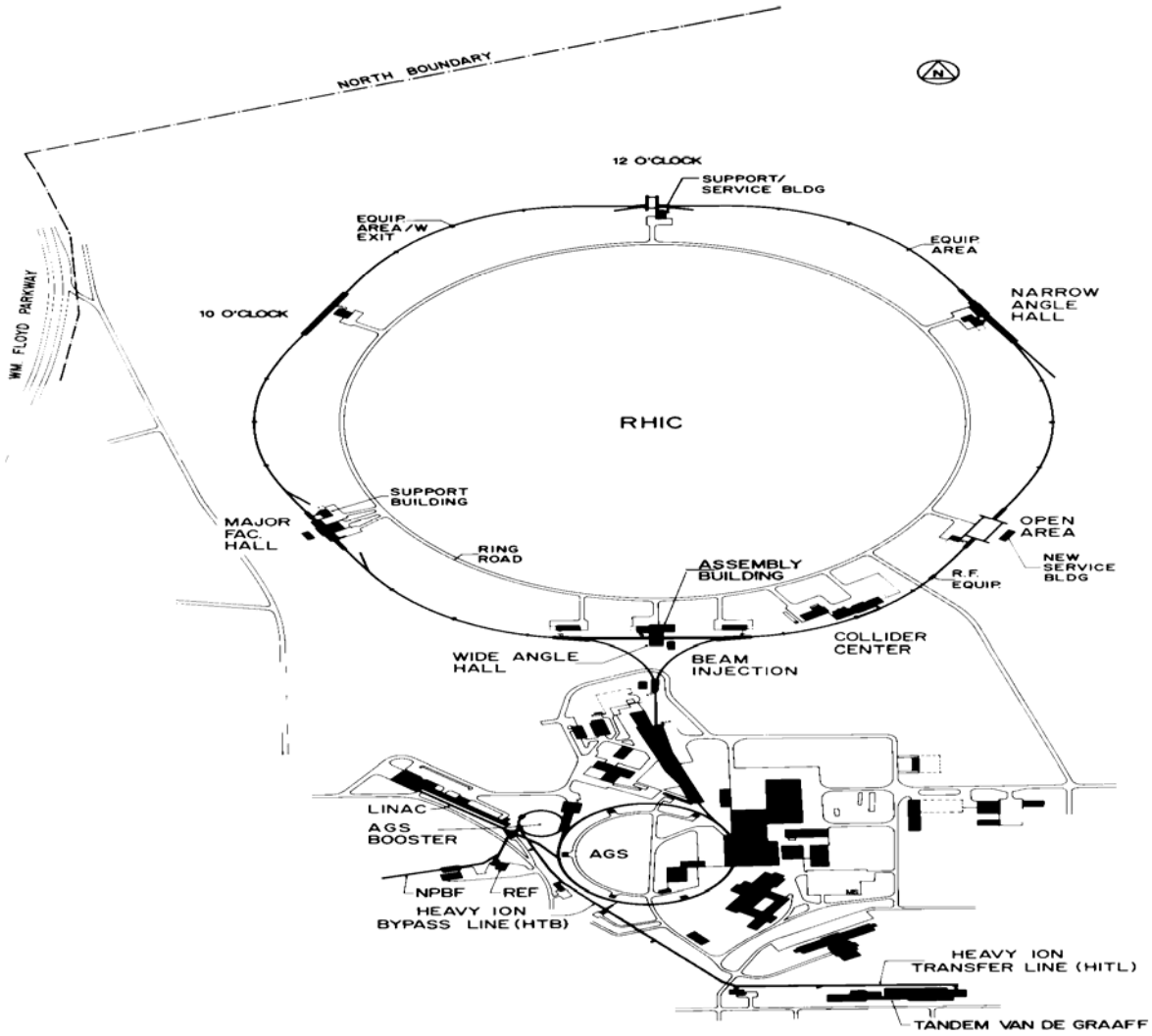

Fig. 1. Layout of RHIC facility – injectors and collider.

The Collider Scenario

An important choice in the RHIC design was the utilization of short bunches colliding head-on to enhance the luminosity while keeping the average current and stored beam energy low. Formation of thebunches occurs prior to injection. The injector chain for ions consists of the Tandem Van de Graaff accelerators, the Booster synchrotron, and the Alternating Gradient Synchrotron (AGS). The sequence of steps in the chain of accelerators is shown in Fig. 2 for the prototypical example of gold ions. The injector chain for polarized protons consists of the optically pumped polarized proton source, the 200 MeV proton linac, the Booster, and the AGS.

Two Tandem Van de Graaff accelerators are available. They can be used for two different ion species, or one as a backup for the other. A two-stage operation is employed with the negative ion source at ground potential. The negative ions, with charge -1, are accelerated from ground to +15 MV potential. They pass through a stripping foil in the high voltage terminal yielding partially stripped ions, with a positive charge, Q_T, which is a function of the element being accelerated. The partially stripped ions are accelerated back to ground potential, increasing their energy by $15 \times Q_T$ MeV. For the prototypical example of gold beams, the ions exit the Tandem at the kinetic energy of 1 MeV/n and with $Q = +12$ charge state.

Exiting from the Van de Graaff, the ions are further stripped to charge state +32. They then traverse a long (~ 550 m) heavy ion transfer line to the AGS (HITL), continue in a new, shorter section by-passing the AGS (HTB) and proceed to be injected into the Booster synchrotron. The beam from the Tandem will be stacked in both horizontal and vertical betatron space by adding linear coupling to the Booster lattice. The 700 μsec Tandem pulse yields 45 Booster turns for gold. The stacking/capture efficiency is about 50%, so for gold, the 4.5×10^9 ions from Tandem yield 2.2×10^9 ions accelerating in the Booster.

The Booster can accelerate this beam to 0.65 T in less than 100 ms. A single rf system (two cavities) operating on the 6th harmonic of the revolution frequency provides the accelerating voltage over this range. The kinetic energy of the six bunches at extraction is 100 MeV/n. In the Booster-to-AGS (BtA) transfer line, the ions are stripped once again by a foil to charge state +77 (only K-shell electrons remaining) and then enter the AGS.

Four such Tandem/Booster cycles, occurring at a 5 Hz repetition rate, fill the circumference of the AGS using 600 ms of the AGS repetition period. The bunches are injected into matching AGS rf buckets (h = 12). After the fourth transfer, the beam is debunched and rebunched into 4 bunches.

With 75% acceleration efficiency (Booster and AGS together), this bunch would contain 1×10^9 ions [(75% acc eff)×(60% BtA foil stripping)×(2.2×10^9)].

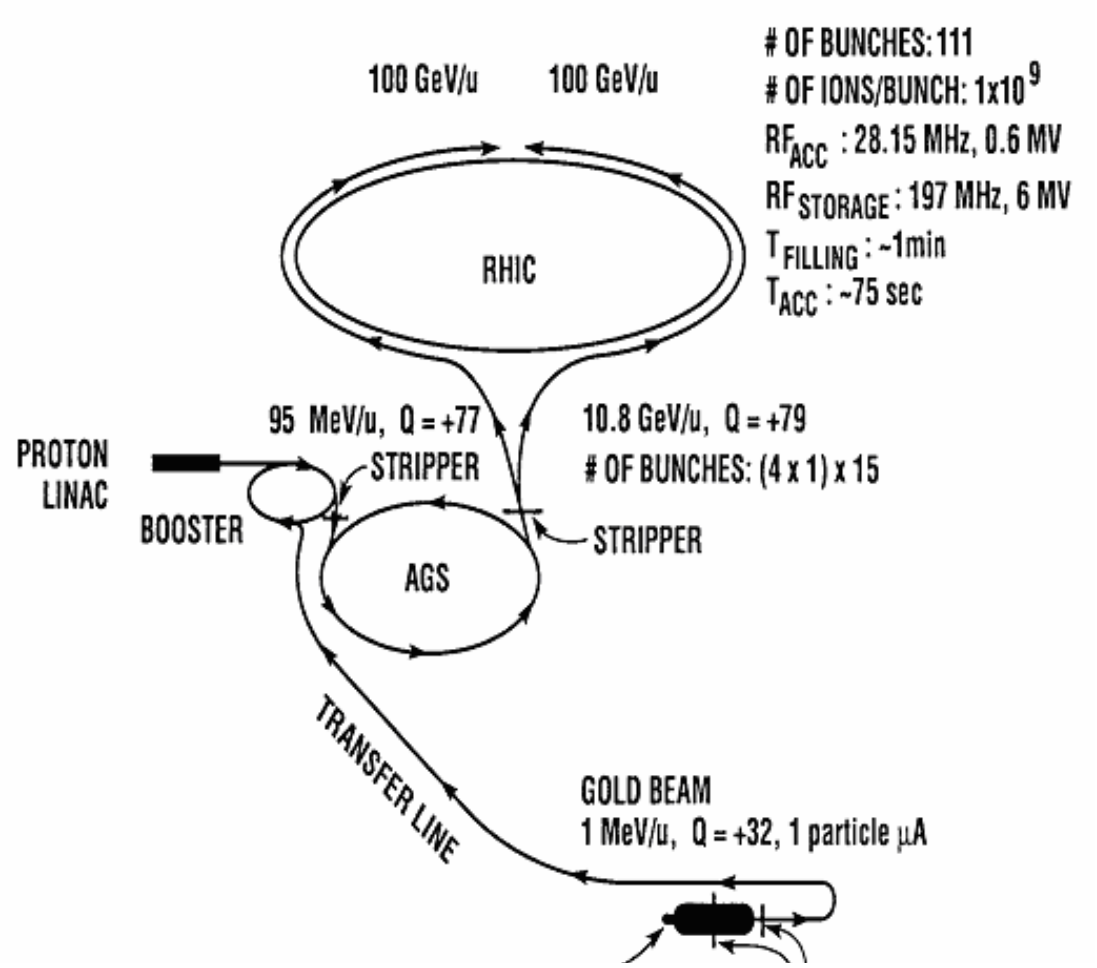

Fig. 2. RHIC Acceleration Scenario for gold.

Finally, the beam is fast extracted into the existing AGS to RHIC (AtR) transfer line tunnel. A final stripping from +77 to +79 takes place at the start of this line. For protons the acceleration strategy is simplified, the merges are unnecessary, since intensity is not a problem. For heavy ion and proton cycles, the final kinetic energies (8.9 GeV/n and 22.9 GeV respectively) correspond to a peak AGS $B\rho$ of 80 Tm.

The AGS to RHIC (AtR) transfer line uses conventional room temperature magnets, some of which exist from procurements for the former CBA project, and employs a magnetic septum magnet and fast kicker system to deposit the beam vertically onto the injection closed orbit.

A total of up to 111 bunches are injected into each collider ring in bunch-to-bucket fashion. The AGS extraction system will allow single-bunch transfer of the four AGS bunches into one of the two collider rings. Filling both rings with ions requires about 1 minute, currently only 1 polarized proton bunch is accelerated per AGS cycle and filling both rings with polarized protons takes about 10 min. Minimizing the filling time is important in order to prevent bunch area dilution due to intrabeam scattering. For the lightest ions, protons and deuterium, approximately 2×10^{11} ions/bunch can be stored in the collider. The nominal number of ions per bunch transferred to the collider is given in Table 2. The intensity is estimated from Tandem currents after allowing for some losses in the Booster and the AGS.

Beam parameters, i.e. bunch area S and normalized transverse emittance ε_N, at RHIC injection are given in Table 2. The beam parameters for ions from the Tandem are taken to be the same for all species, i.e. 0.5 eV·s/n and 10 mm ·mrad. Those for protons are different, with a larger emittance, i.e. 20 mm.mrad, since they come from a different source. The bunch area containing 95% of the beam population, S, is defined by $S = 6\pi\,\sigma_\tau\,\sigma_E$ where σ_τ is the rms bunch length in units of time and σ_E the rms energy spread. Correspondingly, the normalized emittance, is defined by $\varepsilon_N = (\beta\,\gamma)\,\varepsilon = (\beta\,\gamma)\,6\,\sigma_{H,V}^2\,/\,\beta_{H,V}$ where $\sigma_{H,V}$ is the rms beam width or height and $\beta_{H,V}$ the horizontal or vertical amplitude lattice function. By local convention, the energy spread is quoted as $\pm\sqrt{6}\,\sigma$ and the (total) bunch length as $2\sqrt{6}\,\sigma$.

The beam parameters are quoted for a typical set of ion species in order to illustrate the variation of the collider performance over the entire mass range. The Tandem Van de Graaff source is capable of delivering many other elements, most of them in adequate intensity. In fact, the choice of ^{16}O and ^{28}Si may entail operational difficulties due to the mass-to-charge ratio being $A/Z = 2$,

potentially leading to beam contamination with lighter fragments of equal rigidity. Since this problem could be circumvented by the use of isotopes or different elements such as ^{11}B and ^{35}Cl, the discussion is limited here to the few illustrative examples of Table 2.

The bunch separation in the collider ring is 108 ns, and this corresponds to a rise time of 95 nsec. The injection kicker allows the transfer of single bunches from the AGS. The adoption of beam transfer from the AGS to RHIC in the single-bunch mode allows considerable freedom in the choice of the harmonic number and bunch pattern. The bunches are captured in stationary buckets of the so-called acceleration rf system operating at 28.15 MHz, corresponding to a harmonic h = 360. The acceleration rf system has 2 cavities per ring capable of providing a total of 300 kV peak voltage. In order to avoid bunch area dilution, it is essential to match the shape of the bunches from the AGS to the shape of the buckets of the collider rf. The harmonic chosen together with the rf voltage available provide adequate bucket area in the collider but require for protons bunch rotation in the AGS prior to the bunch transfer. The beams are injected into RHIC at 300 kV for gold and heavy ions, but 150 kV for protons. The nominal bunch parameters at injection into the collider are quoted in Table 2.

After injection of the beam, the rf voltage can be adjusted adiabatically to optimum values for acceleration and the crossing of the transition energy (nominally 300 kV for the prototypical gold beam). In order to avoid bunch area dilution at transition, a γ-transition jump is executed, limiting the bunch area growth. Proton beams are injected above but close to transition.

After having reached the operating kinetic energy corresponding to a $B\rho$ = 839.5 T·m, ion bunches are transferred from the acceleration (28.15 MHz) to the storage rf system at 197 MHz. The harmonic number of the storage rf is $h = 360\times7 = 2520$, resulting in a bucket length of 1.52 m. This frequency was chosen in order to limit the growth of the bunch due to intrabeam scattering to an rms bunch length of <25 cm. The resulting rms diamond length is less than ~18 cm.

With a bunch area after transition of 0.7 eV·s/n, the length of a gold bunch is before rebucketing longer than the storage bucket length. Shortening of the bunch is necessary for all ion species and is accomplished by a non-adiabatic bunch rotation in the acceleration system. Each of the RHIC rings has 3 storage system cavities and shares additional 4 common cavities with the other ring for a total voltage of 6 MV. The 3 cavities provide the marginal voltage required to accept the shortened bunches. After transfer, the storage rf voltage is adiabatically raised to its maximum value available and kept constant during the storage cycle.

The stored ion beam energy is 350 kJ per ring for ions, and 900 kJ for polarized protons, small enough to be aborted onto an internal beam dump at the end of the storage period or in case of equipment malfunction. The beam will be dumped in a single turn (13 μsec) by activating the abort kicker, which deflects the beam horizontally onto a dump block. In order to facilitate the beam abort design, a gap of ~ 1 μsec is provided.

Operation of the collider and achievement of full performance requires continuous monitoring of many beam characteristics, and appropriate beam instrumentation is provided. A central control system allows the control of, and communication among, the various collider systems.

The major parameters of the collider are listed in Table 3. The accelerator systems are described in greater detail in the subsequent sections of this Configuration Manual.

Table 2. General Beam Parameters for the Collider

Element	Proton	Deuterium	Oxygen	Silicon	Copper	Iodine	Gold
Atomic Number Z	1	1	8	14	29	53	79
Mass Number A	1	2	16	28	63	127	197
Rest Energy (GeV/u)	0.93827	0.93781	0.93093	0.93046	0.92022	0.93058	0.93113
Injection:†							
Kinetic Energy (GeV/u)	28.3	13.7	13.7	13.7	12.6	11.3	10.8
Energy, γ	31.2	15.6	15.7	15.7	14.5	13.1	12.6
Norm. Emittance (mm·mrad)	20	10	10	10	10	10	10
Bunch Area (eV·s/n)	0.5	0.5	0.5	0.5	0.5	0.5	0.5
Bunch Length (m)	2.58	4.1	4.1	4.1	4.6	5.32	5.62
Energy Spread ($\times 10^{-3}$)	±1.26	±1.63	±1.63	±1.63	±1.59	±1.52	±1.49
No. ions/Bunch ($\times 10^{9}$)	100	100	8.3	5.6	2.7	1.5	1.0
*Top Energy, @ transfer:**							
Kinetic Energy (GeV/u)	250.7	124.9	124.9	124.9	114.9	104.1	100.0
Energy, γ	268.2	134.2	135.2	135.3	124.5	112.9	108.4
rms Bunch Length (m)	0.10	0.17	0.17	0.17	0.18	0.19	0.19
Energy Spread ($\times 10^{-3}$)	±0.83	±1.35	±1.35	±1.35	±1.41	±1.46	±1.49

†Acceleration rf System $h = 360$, $V_{rf} = 300$ kV, except 170 kV @ p; *Storage rf System $h = 2520$, $V_{rf} = 6$ MV

Table 3. Major Parameters for the Collider

Kinetic Energy, Injection-Top (each beam), Au	8.9-100	GeV/u
p↑	22.9-250	GeV
Luminosity, Au-Au @ 100 GeV/n, store average, Enhanced Design	8×10^{26}	$cm^{-2}\ s^{-1}$
p↑-p↑ @ 250 GeV, store average, Enhanced Design	150×10^{30}	$cm^{-2}\ s^{-1}$
Proton polarization, store average, Enhanced Design	70	%
No. of bunches/ring, max	111	
No. of ions/bunch, Au	1×10^{9}	
p↑	2×10^{11}	
Luminosity lifetime Au @ $\gamma > 30$	2.5	h
p↑	>10	h
Diamond length	18	cm rms
Circumference, 4-3/4 C_{AGS}	3833.845	m
Beam separation in arcs	90	cm
Number of crossing points	6	
Free space at crossing point	±9	m
Beta @ crossing, horizontal/vertical	10	m
low-beta insertion	1	m
Crossing angle, nominal (maximum)	0 (< 1.7)	mrad
Betatron tune, horizontal/vertical, Au	28.22/29.23	
p↑	28.685/29.695	
Transition Energy, γ_T	22.89	
Magnetic Rigidity, $B\rho$: @ injection / @ top energy	81.1 / 839.5	T·m
Bending radius, arc dipole	242.781	m
No. of dipoles (192/ring + 12 common)	396	
No. of quadrupoles (276 arc + 216 insertion)	492	
Dipole field @ 100 GeV/u, Au	3.458	T
Arc dipole length, effective	9.45	m
Arc Dipole length, physical	9.728	m
Dipole current	5.093	kA
Arc quadrupole gradient	~71	T/m
Arc quadrupole length, effective	1.11	m
Coil i.d. arc magnets	8	cm
Beam tube i.d.	6.9	cm
Operating temperature, Helium refrigerant	< 4.6	K
Refrigeration capacity at 4 K	24.8	kW
Cooldown time, entire system, 80K to 4K	10	d
Vacuum, warm beam tube sections	$\sim10^{-11}$	Torr
Filling mode	Bunch-to-bucket	
Injection kicker strength (95 nsec)	~0.18	T·m
Beam stored energy Au / p↑	350/900	kJ
rf voltage, h=360	600	kV
rf voltage, h=2520	6	MV

LATTICE AND BEAM DYNAMICS (WBS 1.11)

The collider is composed of two identical non-circular concentric rings in a common horizontal plane, oriented to intersect with one another at six crossing points. Each ring consists of three inner arcs and three outer arcs and six insertions joining the inner and outer arcs. Each arc is composed of 11 FODO cells. The insertion has nine quadrupoles and six dipoles (four for dispersion matching and two for the beam crossing) on each side of the crossing point. A general layout of the collider ring is shown on Fig. 11-1.

In the current lattice version RHIC 92 Rev. 0.5, the insertion is tunable from $\beta^* = 1$ m to β^* 10 m and beyond. The curves for the gradients versus β^* are smooth and continuous. Furthermore, the crossing point β^* is variable at different betatron tunes ranging from $\nu_{H,V} = 27.823$ to 29.195. The selected operating point will be at $\nu_H = 28.19$ and $\nu_V = 29.18$.

The ring structure conforms closely to the geometry of the existing tunnel. In the standard configuration, there is reflection symmetry with respect to each arc bisector. The polarity sequence of all quadrupoles is anti-symmetric with respect to the crossing points. This gives rise to three superperiods, with one sextant consisting of an inner arc plus insertion and its neighboring sextant consisting of an outer arc plus insertion as the fundamental period. The superperiodicity will be reduced if the insertions are not all identically tuned, e.g., in order to provide different crossing point conditions (crossing angles, beta values, detector magnets). On the other hand, machine functions, such as beam injection and beam abort, can be accommodated by the standard insertion. It is expected that the collider will initially be operated in its simplest configuration, i.e., one with the highest possible superperiodicity and $\beta^* = 10$ m, and that departure from this configuration will be introduced as operational experience grows.

It proved to be too expensive to place the transition energy outside the operating range from 10 - 100 GeV/u, so that the heavy ion beams will have to be accelerated through transition. Stored beam operation near the transition energy is not possible; this leaves a small gap in the operating range for beam energies very close to the nominal $\gamma_T = 22.89$.

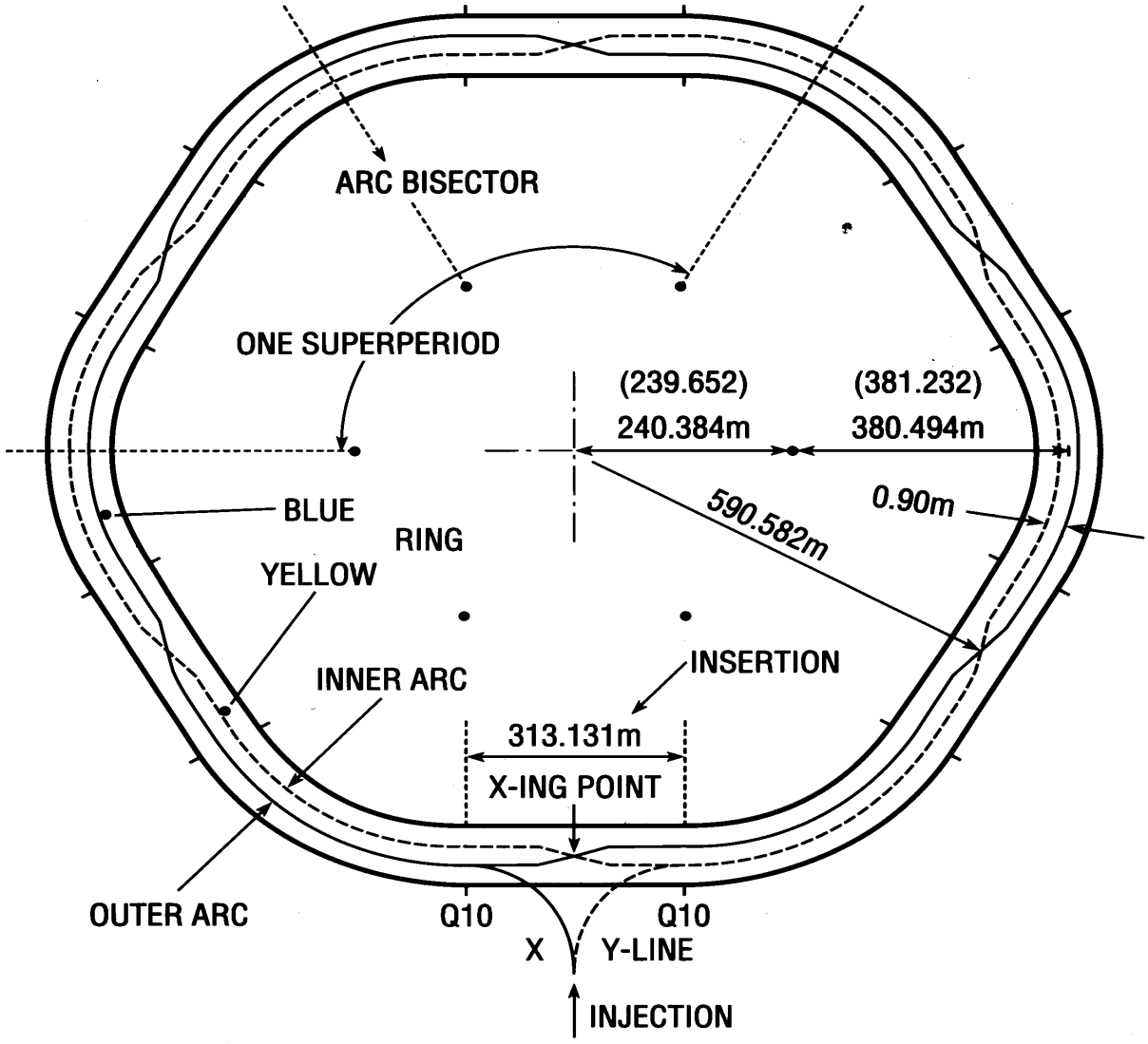

Fig. 11-1. Layout of the collider and in parenthesis of the tunnel. The ring circumference is 3833.845 m.

i. Arcs

The choice of the arc structure has a profound impact on the performance and the cost of the collider. Intrabeam scattering in the case of heavy ions results in larger longitudinal and transverse emittances and thus larger aperture requirements relative to a proton accelerator. The desire to keep the aperture requirements small points to a lattice solution with stronger focusing and higher transition energy. On the other hand, the requirements of the chromaticity sextupole system, the rf requirements at low energies, the desire to avoid passage through transition with protons, and quadrupole cost considerations favor weaker focusing and limit the transition energy to below the AGS energy. These arguments lead to the adoption of a solution with 11 FODO arc cells per sextant, with a transition energy of $\gamma_T = 22.89$ and a tune $\nu_H = 28.19$ and $\nu_V = 29.18$. The half cell geometry is shown in Fig. 11-2. Each cell is ~ 29.622 m long; it deflects the beam by ~ 77.85 mrad and has a betatron phase advance which varies from $\mu_H = 80.55^o$ and $\mu_V = 85.40^o$ to $\mu_H = 82.42^o$ and $\mu_V = 87.25^o$ with $\beta^* = 10$ to 1 m respectively. The cell betatron and dispersion functions are shown in Fig. 11-3, and the principal characteristics are tabulated in Table 11-1.

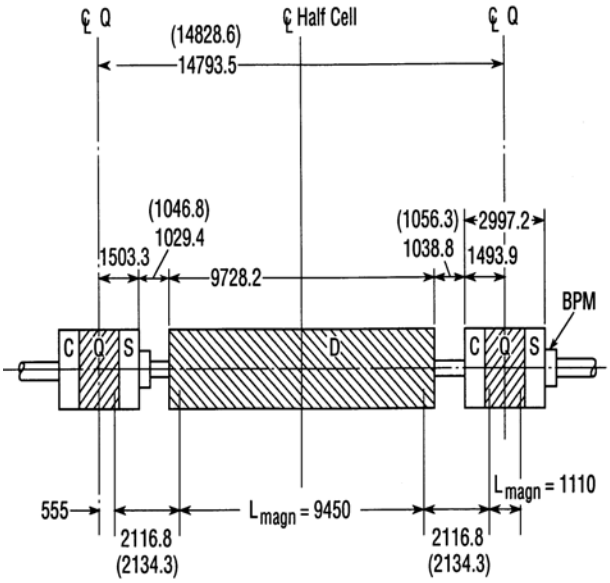

Fig. 11-2. Layout of inner (outer) arc half cell. (Dimensions in mm.)

Table 11-1. Principal Characteristics of Arc Cell

	Inner Arc		Outer Arc
Length (m)	29.5871		29.6571
Deflection Angle (mrad)		77.8481	
Average Radius of Curvature (m)*	380.0443		380.9443
Dipole Bending Radius (m)		242.7806	
Distance between Centerlines (m)		0.9000	
Dipole Strength $\int B\mathrm{d}l/B\rho$		0.038924	
Quadrupole Strength (all insertions at $\beta^* = 10$ m)			
$\int B'\,\mathrm{d}l/B\rho$, ($m^{-1}$) F&D	0.09020 & 0.09320		
Betatron Phase Advance (all insertions at $\beta^* = 10$ m)			
$\Delta\mu_H/2\pi$, $\Delta\mu_V/2\pi$	0.2234 & 0.2369		0.2241 & 0.2376
$\hat{\beta}_H$ & $\breve{\beta}_H$ in quadrupole midplanes (m)	49.71 & 10.56		49.84 & 10.53
$\hat{\beta}_V$ & $\breve{\beta}_V$	48.55 & 9.82		48.70 & 9.79
$\hat{X}_p$ & $\breve{X}_p$ in quadrupole midplanes (m)	1.841 & 0.939		1.837 & 0.936
$\chi_{H,V} = \Delta\nu/(\Delta p/p)$	-0.273 & -0.284		-0.275 & -0.286

*Defined by quad centers

The inner and outer arcs are constructed with the same magnet types and are identical, except for the small difference in average radii, obtained from adjustments in the drift space lengths. The inner and outer arcs of a magnet sextant are concentric. The quadrupole center-to-center distance between two rings is chosen to be 90 cm so that each ring line can be housed in a separate vacuum vessel. There are eleven identical cells in each arc, each with two quadrupoles and two dipoles, resulting in a count of 132 arc dipoles and 138 arc quadrupoles per ring (since Q10 must be double counted). Note, however, that D8 is identical to the arc dipole, resulting in a count of 144 arc-size dipoles.

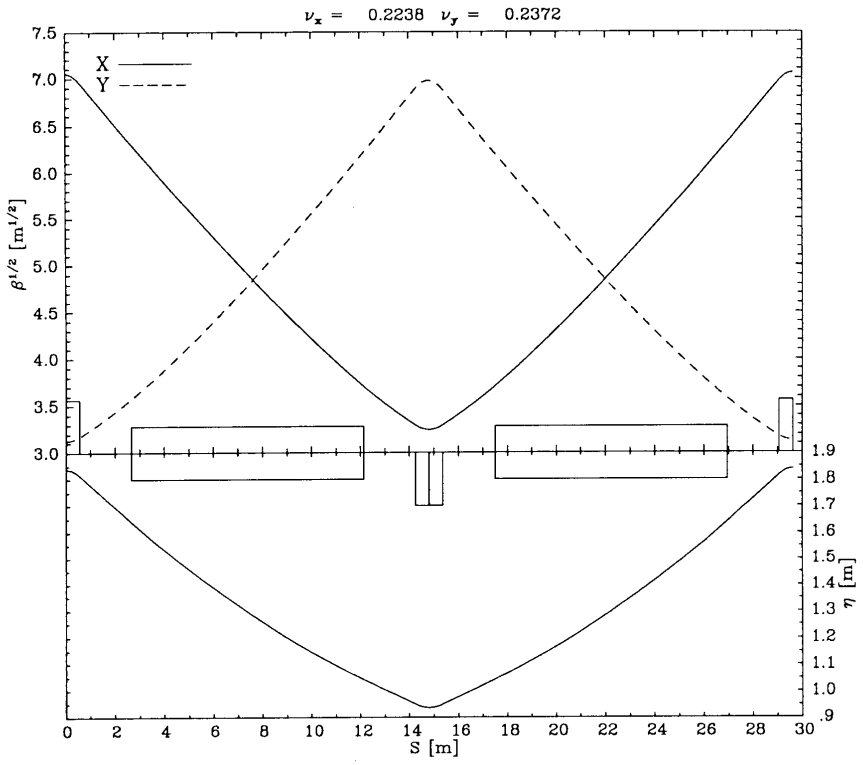

Fig. 11-3. β and X_p functions of RHIC regular arc cell for β.

ii. Insertions

The insertions serve two functions: they transport the beams from arc to arc, and they control the lattice parameters at the crossing points. For injection, we require a β* at the crossing point where all the β's throughout the insertion are small, β* = 10 m was found to be a good choice. During experiments, the smallest practical β* would lead to the largest luminosities. This leads to the β function range at the crossing point of $\beta^* = \beta_H^* = \beta_V^*$ _ *1-10* m. Furthermore, the crossing angle is adjustable from α _ 0-7.7 mrad. Note, the actual range is limited by the aperture of the DX dipole.

As the insertion is tuned, the phase advance across the insertion changes as well. This can create a mismatch when each insertion is tuned to a different β*. The worst case situation is when one insertion is at β* = 1 m and 5 insertions are at β* = 10 m, then $\Delta\beta/\beta$, $\Delta X_p/X_p$ <5%. Since a_1 and b_1 errors could cause a larger ripple, this may be of little consequence. However, the ripple can be reduced by tuning the lattice differently, such as imposing fixed phase advance across the insertion, etc.

Figure 11-4 shows the half-insertion at 6 o'clock and Fig. 11-5 an expanded layout of an insertion on one side of the interaction point. Each half-insertion is composed of (1) a dispersion matching section (D9, Q9, D8, Q8, Q7, D6, Q6 and D5); (2) a straight betatron function matching section ("telescope") with the quadrupole doublet Q5, Q4 and the triplet Q3, Q2 and Q1; and (3) the beam crossing dipoles D0 and DX. D5 of the inner and outer half-insertions serve also to bring the beam-beam separation from 90 cm to 41.5 cm at the edge of D0. The magnets D6 and D9 are identical with a magnet length of 2.95 m. The insertion dipoles D8 are identical to the arc dipoles, and D0 has a magnetic length of 3.6 m. The magnets Q3, Q2, Q1, and D0 of inner and outer insertions sit in common vacuum vessels. The large aperture dipole DX is common to both rings, but electrically and cryo connected to the blue ring. The dipole DX, as well as D0 in the insertions, are separately adjustable to allow for unequal species or finite crossing angle operation.

The dipoles D0, D6 and D9 are assumed to be curved. However, if any of these dipoles are manufactured as straight, additional correction is required. An adequate correction scheme was found by adding shunt correction supplies to Q1, Q7 and on the trims of Q5 and Q6 where $\Delta G/G$ ~0.1%.

Note, Q9I is identical to Q8O and they are sometimes denoted as QFA in lattice calculations. Similarly, Q8I and Q9O are also referred to as QDA.

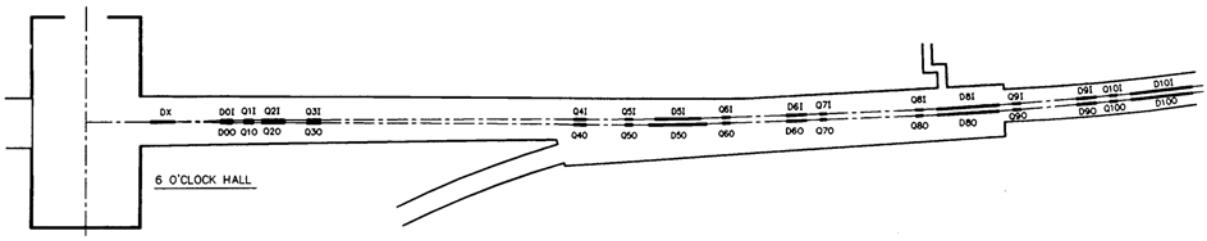

Fig. 11-4. RHIC half-insertion at 6 o'clock.

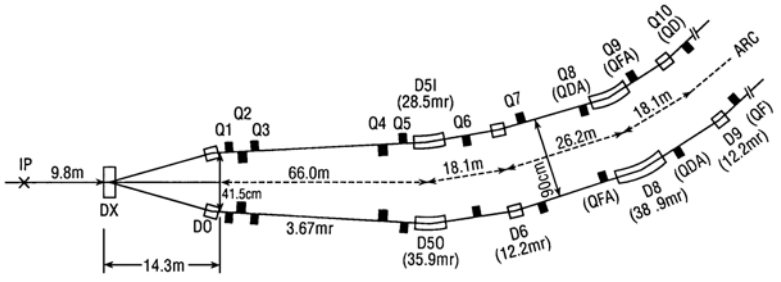

Fig. 11-5. Expanded layout of half-insertion.

Table 11-2. Principal Characteristics of Insertions

Number of insertions 6			
Crossing angle (mrad)0 - 7.7			
Nominal free space @ crossing† (m)		±9.8	
Half-insertion length, @ Q10O-center (m)		156.608	
@ Q10I-center (m)		156.523	
β^* (m)	1¶	2¶	10
$\hat{\beta}_{H,V}$ (m)	1318	667	146
$\alpha^*_{H,V}$	0	1×10^{-3}	2×10^{-3}
X_p^* (m)	8×10^{-3}	2×10^{-3}	0
$X_{p'}^*$	22×10^{-3}	9×10^{-3}	4×10^{-3}
$\chi_{H,V} = \Delta v/(\Delta p/p)$	-17.97	-9.83	-3.79
$\chi_{H,V}$, Ring Total	-68.7, -71.0	-52.9, -54.4	-40.8, -41.6
$\int B'' \, dl/B\rho$ @ QF in arc‡ (m^{-2})	0.20	0.14	0.11
@ QD in arc‡ (m^{-2})	-0.37	-0.27	-0.21

†The actual free space available for detector equipment is ±9 m.
‡For zero chromaticity with two sextupole families.
¶Two low-beta insertions plus four 10 m insertions.

Each insertion may be subdivided into an inner and an outer half insertion which are joined at the crossing point. There is near perfect reflection anti-symmetry relative to the crossing point in component location and component strength. A small deviation from symmetry is caused by the differences ($\sim 2\times10^{-3}$) in drift space lengths imposed by geometrical constraints and the differences between QF and QD ($\sim 2\times10^{-3}$). The symmetry breaking will result in arc beta and dispersion function flutter of $<5\times10^{-3}$ if the insertion quadrupoles were excited with exact anti-symmetry. A fully matched lattice, i.e. without lattice function flutter in the arcs, could be obtained by allowing differences in the inner/outer quadrupole excitations of $\sim 10^{-2}$. The principal characteristics of the

insertion are given in Table 11-2, and the behaviors of the betatron and dispersion functions are shown in Fig. 11-6.

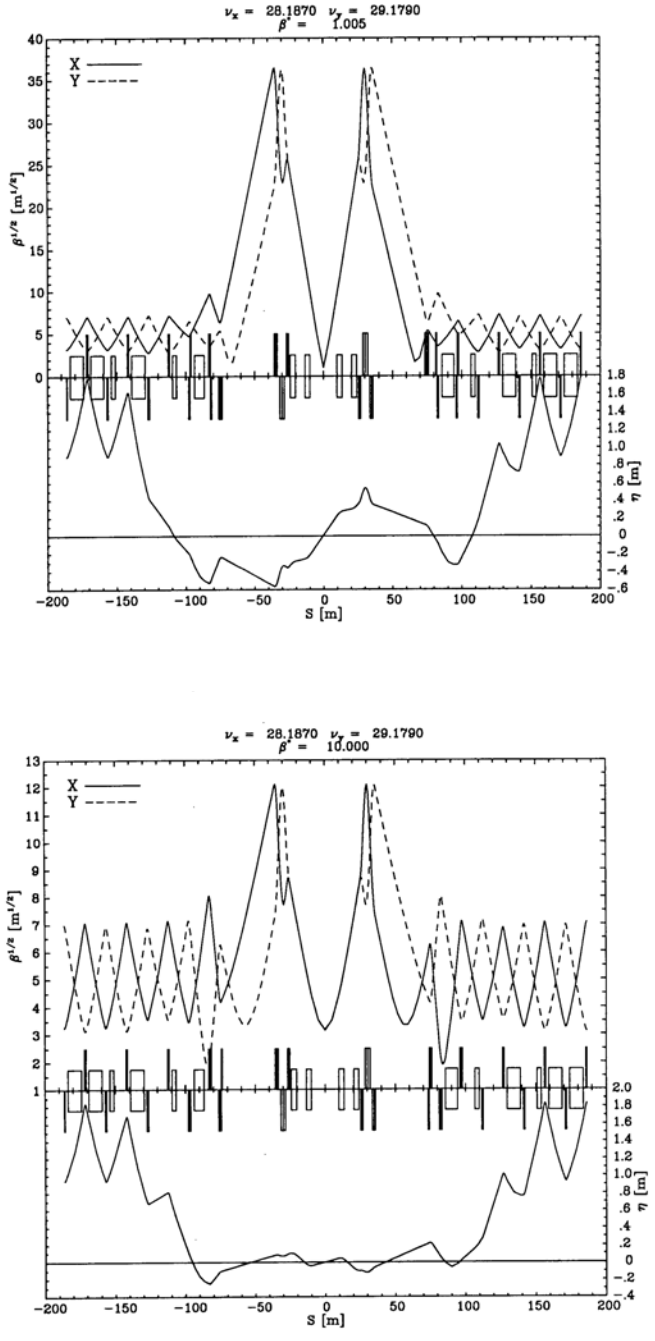

Fig. 11-6. Betatron and dispersion functions in the insertion region.

The beam crossing geometry is shown in Fig. 11-7. DX is common to both beams, D0 of inner and outer insertions are separately excited to accommodate variations in beam crossing angles as well as collisions between unequal species. For unequal species, such as p on Au, the line of head-on collision is rotated by about 3.85 mrad with respect to the longitudinal center axis. For nonzero-angle collisions the insertion quadrupoles have to be readjusted in strength by less than 1% in order to preserve the dispersion characteristics.

The dynamic aperture in the low β* configuration is dominated by the coil radius of the high-beta quadrupoles Q1, Q2, Q3 and D0 dipole. Since the large-aperture quadrupoles are frozen at 13 cm coil i.d. by available tooling, the "matched" aperture of D0 would be $(\beta @ D0/\beta @ Q3)^{1/2} \times 13$ cm ≈ 8.7 cm. Tracking studies suggest that the dynamic aperture can be increased with a D0 aperture of 10 cm. In order to accommodate yoke dimensions, D0 cannot be placed any closer than the 7 m to DX as shown in Fig. 11-7. A summary of major lattice dipole and quadrupole parameters is given in Table 11-3.

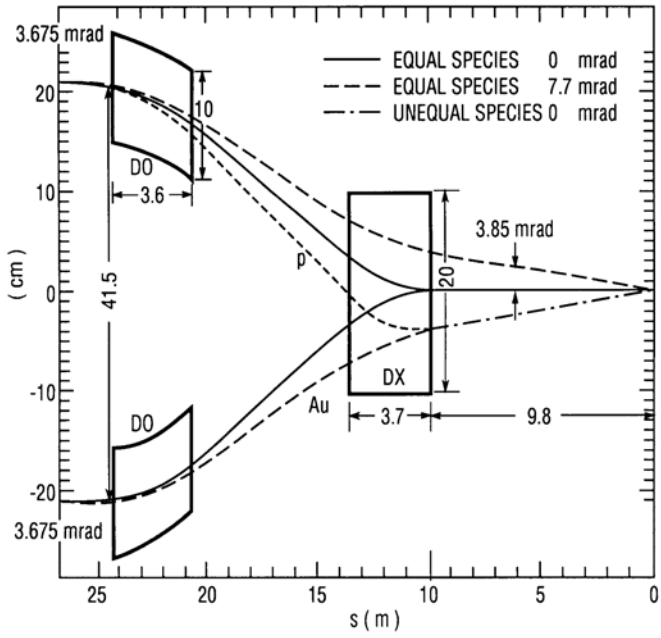

Fig. 11-7. Beam crossing geometry (magnetic lengths are shown).

Table 11-3. Summary of Dipole and Quadrupole Parameters

	Coil i.d. (mm)	Eff. Length (m)	Field @ 100 GeV/u† (T;T/m)		Location	Number
DIPOLES	80	9.45**	3.45		ARC, D8	288
	80	2.95	3.45		D6, D9	48
	80	8.71	3.45		D5O	12
	80	6.92	3.45		D5I	12
Subtotal, 80 mm						360
	100	3.60	3.52		D0	24
	200	3.70	4.27		DX	12
QUADRUPOLES			β*=10 m	β*=1 m		
	80	1.11	68.2	69.5	QF	138
	80	1.11	70.5	71.8	QD	138
	80	1.11	65.4	73.5	QFA (Q9I, Q8O)	24
	80	1.11	66.4	74.6	QDA (Q9O, Q8I)	24
	80	1.11	75.5	75.5	Q5, Q6¶	48
	80	0.93	76.3	72.0	Q7	24
	80	1.81	75.5	75.5	Q4¶	24
Subtotal, 80 mm						420
	130	1.44	46.7	48.5	Q1	24
	130	3.40	46.3	47.1	Q2	24
	130	2.10	46.0	47.3	Q3	24
Subtotal, 130 mm						72
TOTAL, dipole and quadrupole magnets						888

**physical length 9.728 m (383.0 in.)

† Quench field in

80 mm Dipole 4.6 T
100 mm Dipole 4.42 T
200 mm Dipole 5.14 T
80 mm Quad 107 T/m
130 mm Quad 75.3 T/m

¶ Trim quadrupoles at Q4, Q5, Q6 provide gradient changes from β* = 10 to 1 m.

Injection into the collider, acceleration and low-energy operation will be done with the β* = 10 m configuration. The low-beta configuration with β* = 1 m can be obtained at high energies, nominally above 30 GeV/u, by changing the insertion quadrupole excitations. Depending on the operational experience gained, this change may require activation of all available corrector magnets and thus stronger and/or additional power supplies, but no physical changes of the magnet system will be needed.

The luminosity and the crossing point conditions (β* values and crossing angle) are interrelated and limited by the magnet apertures, the beam energy, the range of quadrupole power supplies of the insertion, and the available chromaticity sextupoles. Figure 11-8 shows the maximum amplitude function $\hat{\beta}^{1/2}$ and the chromaticity contribution of one insertion as a function of β*. Figure 11-9 shows the corresponding quadrupole gradients as a function of β* at the design tune.

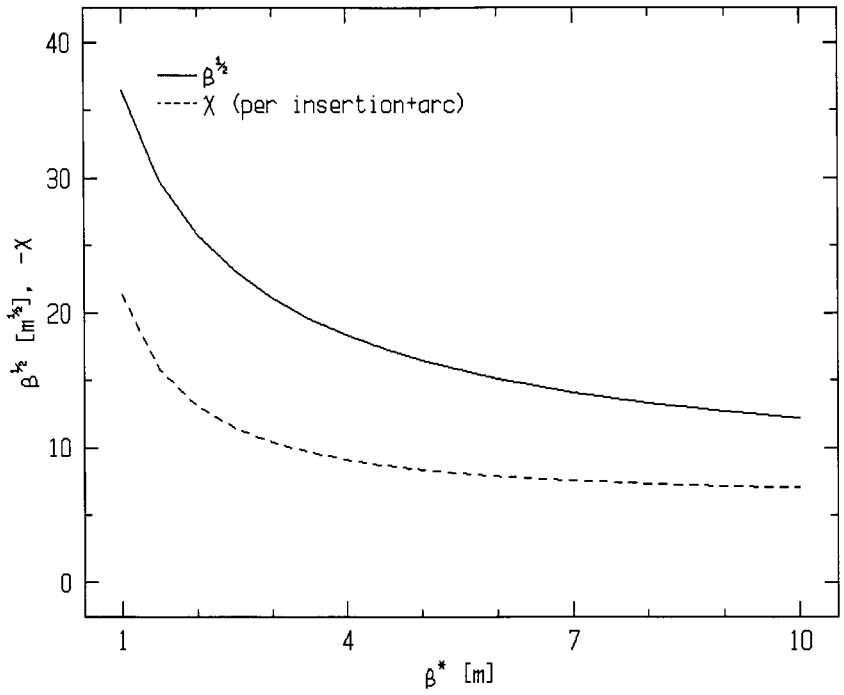

Fig. 11-8. The maximum amplitude function and the total natural chromaticity is shown as a function of β*.

Possible alternative operating tunes range from $\nu_{H,V}$ = 27.82 to 29.20. The tune of the machine can be changed by varying the phase advance in the arc cells as well as the focusing strength of the insertion quadrupoles while maintaining matched conditions. It has been demonstrated that the insertion is tunable over the full β* range at the following 7 different machine tunes:

ν_H =	28.83	ν_V =	28.82	Equal tune
	28.56		28.55	Half integer tune
	28.83		27.82	Split tune
	29.20		28.20	Split tune
	28.20		28.20	Alternate tune
	28.96		28.95	Integer tune
	28.19		29.18	Nominal tune

The power supplies installed assure that these β* tune combinations are reachable.

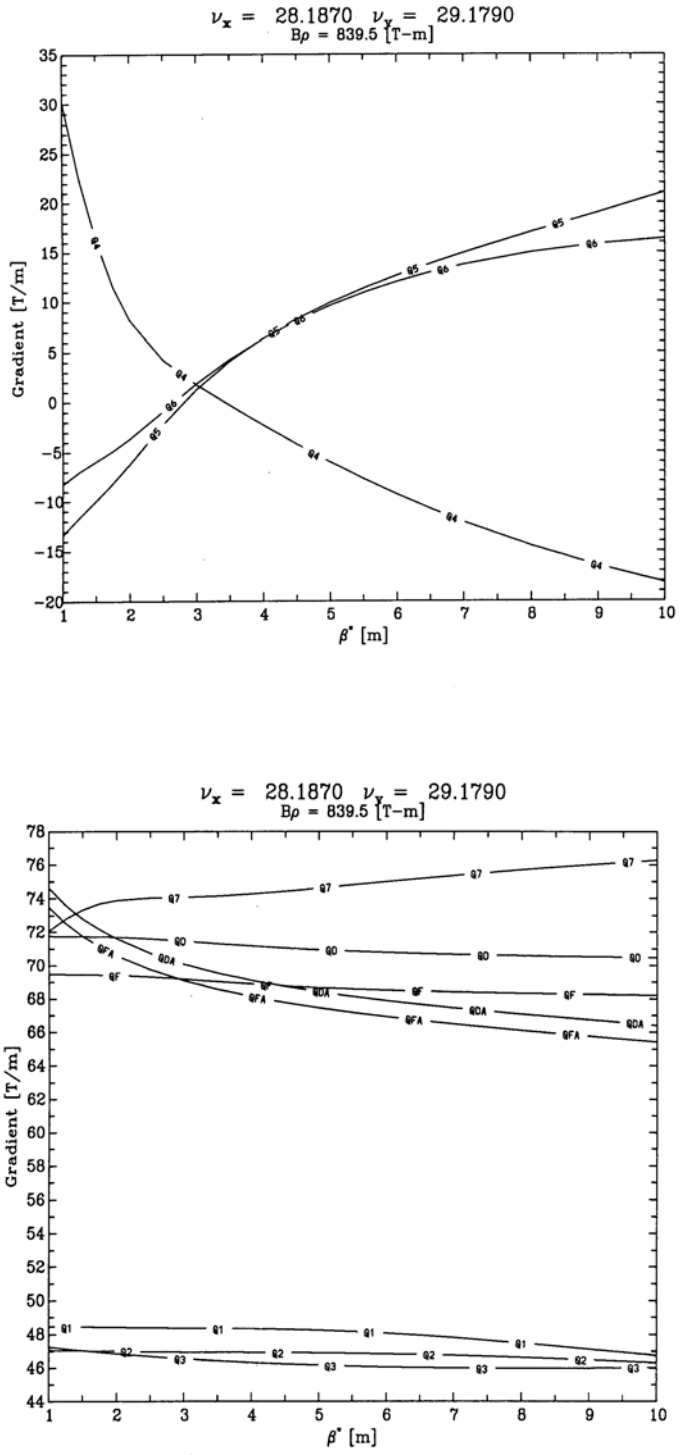

Fig. 11-9. Strength of Insertion Quadrupoles versus β* at the nominal operating H/V tune of 28.19/29.18.

iii. Chromatic Effects

If the insertions are all identical and set up for β* = 10 m the natural chromaticities ($\chi = p\ dv/dp$) are $\chi_H \approx \chi_V \approx -42$ to which the six arcs contribute -23 units. These large negative values of the chromaticities must be reduced to zero or a small positive value. This can be done by having sextupoles next to each quadrupole in which there is significant dispersion. A configuration with 24 sextupoles per arc was adopted (the sextupole at the quadrupole Q9 in the 3-4, 7-8, 11-12 o'clock insertion is functionally part of the arc). The placement of the sextupoles of one ring relative to their associated quadrupoles is antisymmetric with respect to the crossing point; the sextupole placement in the two rings has mirror symmetry with respect to a radius through the crossing point. A plan view of the sextupole configuration is shown in Fig. 11-10.

All the leads to the sextupoles are available so that any sextupole configuration can be implemented. The simplest sextupole scheme is a two family scheme involving the families S_F and S_D as shown in Fig. 11-10. Figure 11-11 shows the variation of lattice functions for off-momentum particles in an idealized lattice with no magnetic errors. The increases of the β- and X_p-functions affect the linear aperture, and indirectly affect the dynamic aperture. One way to decrease these distortions is to increase the number of sextupole families, especially in the arcs adjacent to experimental (low-beta) interaction points. The day-one nominal configuration invokes two

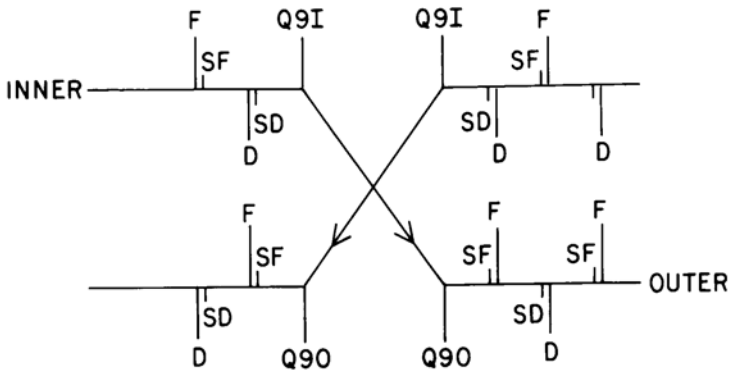

Fig. 11-10. Sextupole arrangement in the inner and outer arcs (shown at 6 o'clock insertion).

sextupole families and two octupole families. This will certainly be adequate for β* = 10 m operation. Figure 11-12 shows the tune variation with momentum, in the absence of magnetic errors. The linear and quadratic parts of the chromaticities will be corrected by the sextupole and octupole families, respectively.

Chromatic optics distortions and nonlinear chromaticities are much stronger in error free optics when the value of β* is relatively small, since the main sources are the insertion region quadrupoles. Systematic magnetic errors are also important, for example in the arc dipoles, but the chromatic effects caused by magnetic errors tend to be independent of the optical configuration. Commissioning will decide whether the β* = 1 m low-beta optics require activation of more sextupole families per arc, or of the two decapole families that are also available, but which are not nominally activated. The use of additional families of correctors would require additional power supplies but no modification of the electrical bus configuration of the magnets.

The sextupoles required in the lattice to correct the chromaticity introduce intrinsic nonlinear effects by which the betatron tunes will be shifted proportionally to the particle emittances. For the

$$\Delta\nu_H = \bullet(0.38\ \varepsilon_H + 1.20\ \varepsilon_V)\ x10^{-3}/\pi\ \text{mm}\bullet\text{mrad}$$

worst case where β* = 1 m in two insertions and with the arrangement described above one finds

$$\Delta\nu_V = +(0.13\ \varepsilon_V \bullet 1.20\ \varepsilon_H)\ x10^{-3}/\pi\ \text{mm}\bullet\text{mrad}$$

where ε_H and ε_V are actual emittance values. The coefficients drop an order of magnitude for β* = 10 m. Thus this effect does not seem to be very important.

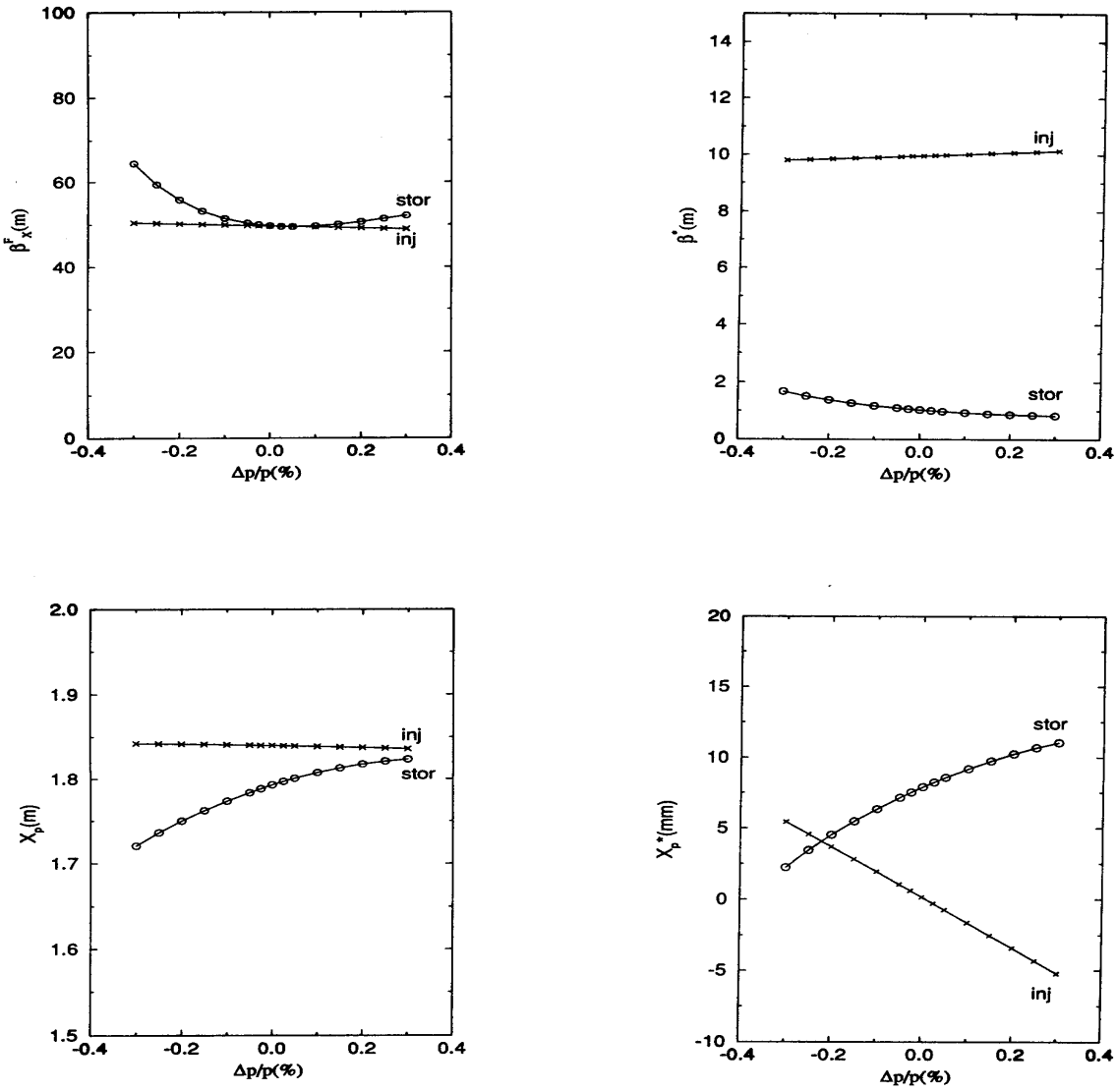

Fig. 11-11. Variation of betatron and dispersion functions versus momentum at the center of inner arcs (left) and at the crossing point (right) at injection ($6 \times \beta^*=10$ m) and storage ($2 \times \beta^*=1$ m & $4 \times \beta^*=10$ m). The chromaticity is corrected with 2 families of sextupoles.

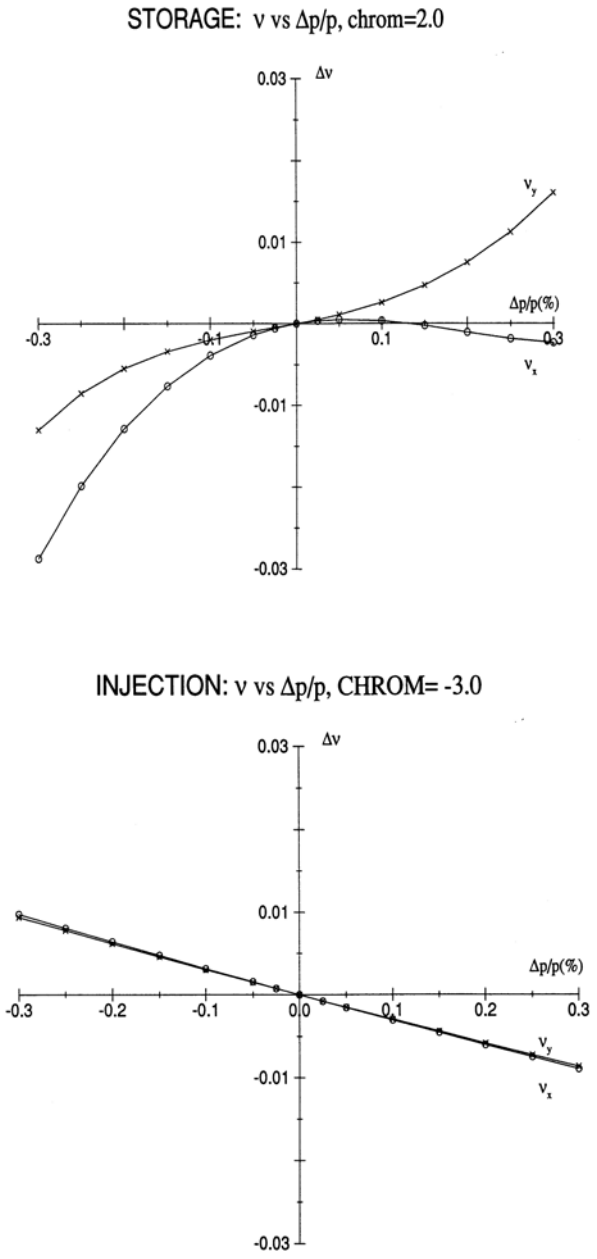

Fig. 11-12. Variation of betatron tunes with momentum at injection ($6 \times \beta^*=10$ m) and storage ($2 \times \beta^*=1$ m & $4 \times \beta^*=10$ m). The chromaticity is corrected with 2 families of sextupoles.

iv. γ_T-jump

With the exception of protons, all ions are injected below the transition energy and, consequently, have to be accelerated through transition to reach the top energy for storage. The acceleration is provided by the 28.15 MHz rf system with a maximum peak voltage of 600 kV. In order to successfully transfer the ion beams from the acceleration rf system (28.15 MHz) to the storage rf system (197 MHz), it is of primary importance to avoid particle loss and to preserve the initial bunch area of 0.3 eV·s/u during the transition crossing.

Problems related to transition crossing can mainly be divided into two categories: single- and multi-particle. The former category mainly includes the effect of chromatic non-linearities, while the latter includes bunch-shape mismatch and microwave instability induced by low- and high-frequency self fields, respectively. In addition, the remnant voltage of the 197 MHz rf cavities induced by the circulating beam causes further complication.

Both analytical and numerical studies have been performed to investigate the various problems. It has been shown that the transition crossing can be achieved with no particle loss and negligible bunch-area growth, when a γ_T-jump of 0.8 unit is employed in a time period of 60 ms. The γ_T-jump scheme will be used with the RHIC lattice when all the insertions are tuned to $\beta^* = 10$ m where $\gamma_T = 22.89$. A γ_T-jump of 0.8 units could be achieved with one family of b_1-correctors located at the horizontally focussing quadrupoles in the arcs. However, since γ_T can only be increased by this second-order scheme, a symmetric γ_T-jump *cannot* be achieved. A first-order matched γ_T-jump can be obtained with two quadrupole families and will be used in the RHIC lattice.

One family of quadrupoles will change the dispersion function through the dipoles which provides essentially linear dependence of γ_T on quad excitation. A second family of quadrupoles is added in low-dispersion regions of the lattice to correct for any tune change. These families are arranged in pairs of quadrupoles (denoted as doublets) with phase differences of $\pi/2$ to cancel any betatron waves.

The first family of doublets determines the value of the γ_T change. The γ_T change achievable is given by

$$\Delta\,(1/\gamma_T^2) = -\frac{1}{C}\,\Sigma\;\; K_i\;\; X_p^*\,X_p$$

where C is the ring circumference, K_i the quadrupole strength and X_p^* and X_p are the dispersion functions at the places where the additional quadrupoles are when the jump is "on" and under regular conditions, respectively. The maximum contribution to $\Delta\ (1/\gamma_T^2)$ is obtained where $(X_p)^2$ has a maximum. This condition shows that the best positions for the γ_T jump quadrupole doublets are where the horizontal dispersion has maximum values. The design follows this condition by placing this family of four b_1 correctors per sextant at the arc quadrupoles.

The second family of quadrupole doublets is located within the insertion where the dispersion is very close to zero. This family does not affect the value of the γ_T change; they are used to keep the tunes unchanged. The condition for the tunes to remain unchanged ($\Delta\nu_x = 0$) is:

$$\Delta\nu_x = \frac{1}{4\pi} \Sigma\, \beta_i K_i = 0$$

There are two doublets per interaction region where the dispersion has maximum values and an additional two doublets at locations where the dispersion is close to zero. Because the RHIC basic FODO cell has a phase difference close to $\pi/2$, the conditions for the γ_T design are very favorable. The total number of the additional γ_T quadrupoles per ring in RHIC is 48.

A total $\Delta\gamma_T = 0.8$ can be achieved symmetrically with $\Delta\gamma_T = +0.4$ and $\Delta\gamma_T = -0.4$ units by positive and negative quadrupole excitations as shown in Fig. 11-13. The properties of the correction γ_T quadrupole are listed in the Magnet System section of this manual. The nominal value of the strength of the correction γ_T jump quadrupoles at the current of $I = 50$ A is $K\gamma_T = 0.0084\ \text{m}^{-1}$. The required change of the γ_T is thus obtained with one half of the "nominal" $I = 50$ A condition.

The betatron and dispersion function dependence on the γ_T quadrupole excitation were examined and are shown in Fig. 11-14. As mentioned above, the horizontal and vertical betatron tunes were always kept unchanged. The maximum value of the dispersion function in the present RHIC lattice, with the horizontal and vertical tunes split by one integer, is $X_{pmax} = 1.841$ m.

The RHIC γ_T-jump will maintain a physically small beam size during the jump and will not exceed the beam size at injection.

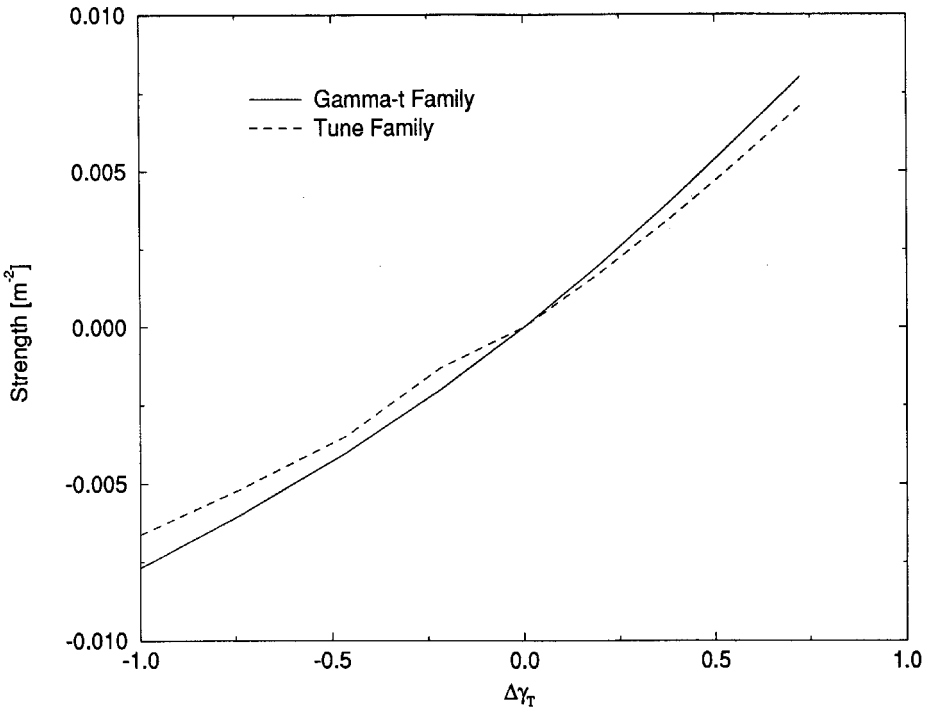

Fig. 11-13. b_1-corrector strength versus the change in γ_T .

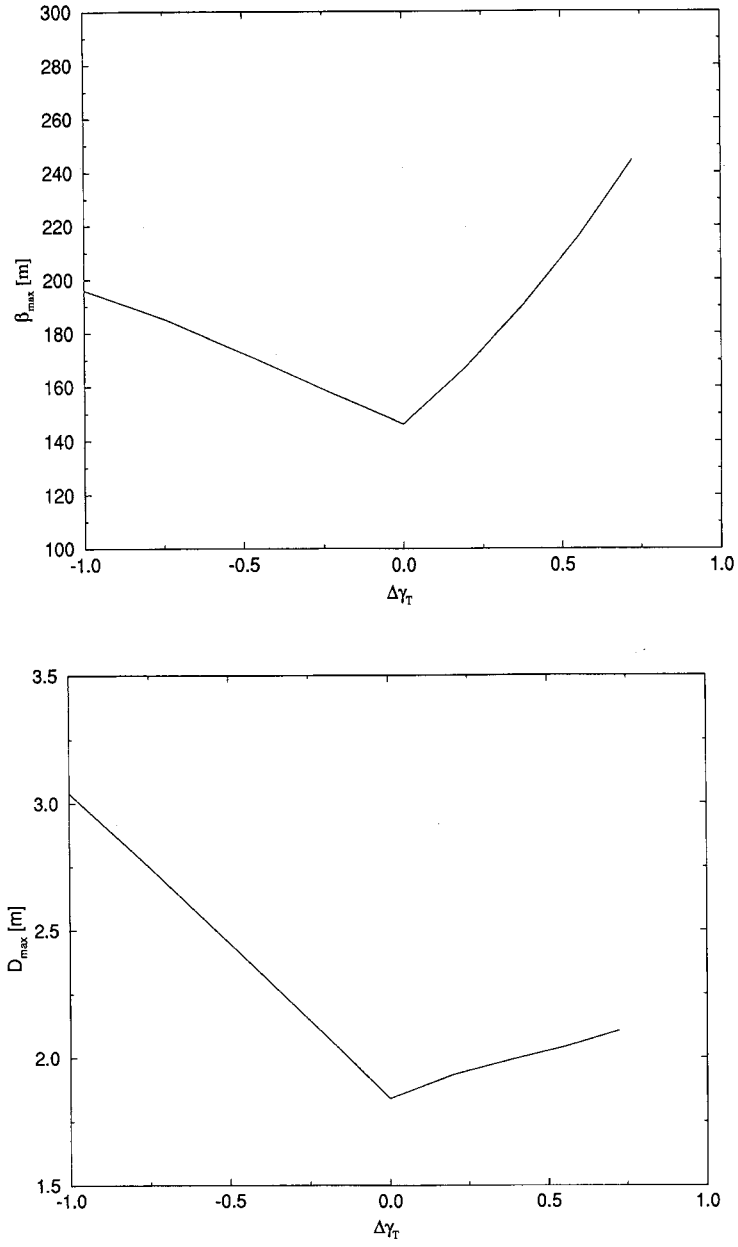

Fig. 11-14. The maximum beta function and the maximum dispersion during the γ_T-jump.

v. Lattice Correction Systems

The lattice configuration described above would be completely adequate to assure stable motion of single particles assuming ideal properties of all magnet elements. Real magnets depart unavoidably from the ideal situation and will exhibit 1) systematic errors due to design or intrinsic material properties such as iron saturation or superconductor magnetization and 2) random errors due to fabrication and installation tolerances. Furthermore, the goal of high luminosity implies intense beams imposing additional operational requirements. Proper operation of the collider as built therefore requires additional systematic trim and random error correction magnets.

The primary objectives for the correction of beam optics distortions are to assure 1) that the orbit is centered in the good field aperture of the magnets and 2) that the operating tune remains in a range which is free from 10th order and lower resonances. The tune diagram for RHIC is shown in Fig. 11-15 with the selected working point at $\nu_x = 28.19$ and $\nu_y = 29.18$ as well as the neighboring sum resonances $n\,\nu_x + m\,\nu_y = p$ where n, m, and p are positive integers and n + m denotes the order of the resonance. The nominal tune is located between the 5th order systematic resonance at 28.20 and the 6th order resonance at 28.166 yielding a useable tune range of 33×10^{-3}. The trim/correction magnet systems for RHIC with a brief description of the beam optical purpose are listed in Table 11-4, and their ring location is shown in Fig. 11-16.

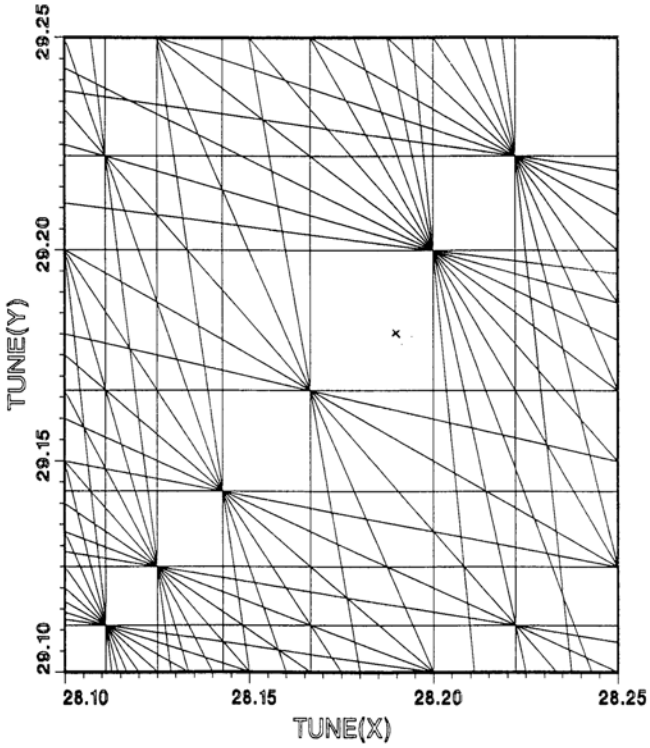

Fig. 11-15. Tune diagram showing the selected working point of RHIC at $v_x = 28.19$, $v_y = 29.18$ with neighboring sum and difference resonances.

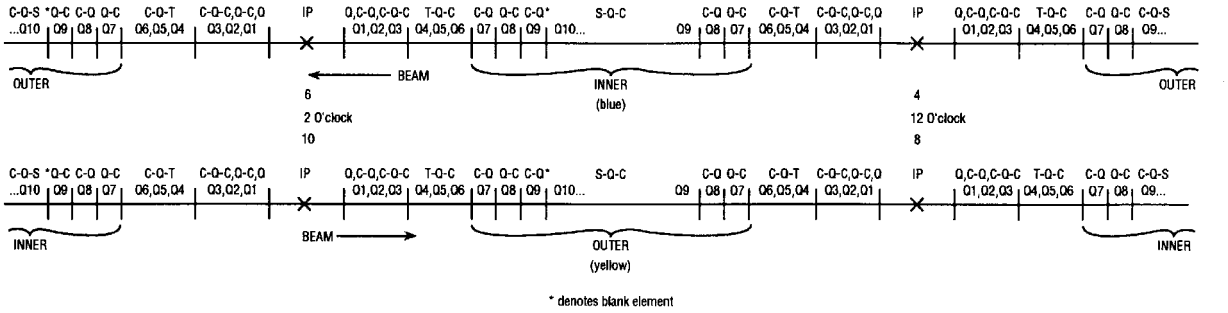

Fig. 11-16. Ring location of trim-quadrupole T, sextupole S and corrector C magnets. Note that Q9O at 6 o'clock is a CQ (not CQ*) assembly.

Table 11-4. Trim/Correction Magnet Systems Per Ring with Power Supplies on Day-One

Magnet System	Beam Optical Purpose	Units/Ring, Location, Strength
Dipole	Correct closed orbit, beam separation @ crossing point during acceleration and storage	222 b_o/a_o units, 0.3 T·m each @ each QF/QD, Q4-Q9, and focussing Q2, Q3 individually powered
		12 a_o units/insertion, 0.3 T·m each @ defocussing Q2, Q3 individually powered
Quadrupole	γ_T-jump	8 b_1 units/sextant, 1.5 T each @ QF in insertion and arc 2 families*/sextant
	Correct β_x, β_y, X_p @ crossing points and arcs	Trim power supplies @ Q1 - Q3, Q7, QFA, QDA Trim magnets, 21 T each @ Q4, Q5, Q6
Skew Quadrupole	Correct linear coupling and tune splitting	8 a_1 units/insertion, 1.5 T each 2 families/insertion
		2 a_1 units/insertion, 0.8 T each @ Q2, individually powered
	Correct vertical dispersion @ crossing points	Future option
Sextupole	Correct skew chromaticity	2 b_2 and 2 a_2 units/insertion individually powered
Octupole	Correct quadratic chromaticity	15 b_3 units/sextant, 3.6 kT/m^2 each 2 F + 2 D families/sextant
	Triplet correction	4 b_3 units/insertion, 240 T/m^2 @ Q2, Q3 in low beta insertions individually powered
Decapole	Correct tune spread due to $\langle b_4 \rangle \neq 0$ in dipoles iron saturation	Future option
	Triplet correction	2 b_4 units/insertion, 565 kT/m^3 each @ Q2, Q3 in low beta insertions individually powered
Dodecapole	Correct tune spread due to $\langle b_5 \rangle \neq 0$ in high-beta quads iron saturation	4 b_5 units/insertion, 4.9 MT/m^4 each @ Q2, Q3 in low beta insertions individually powered

*A family of corrector magnets is powered by one supply.

MAGNET SYSTEM (WBS 1.1)

i. Overview

The magnet system of the collider consists primarily of the superconducting dipole and quadrupole magnets for guiding and focusing the counter-circulating ion beams into well-defined orbits in the regular arcs of the machine lattice, as well as a large complement of special magnets ("insertion magnets") required for steering the beams into collisions at the six interaction points where the highly charged ion beams interact.

The magnet system is designed to allow operation in the energy range corresponding to a $B\rho$ from 97 to 840 T·m. Operation with either equal or unequal ion species in the colliding beams is required, imposing a ratio of up to 2.5:1 in the magnetic fields of the two rings. The superconducting magnets are optimized for heavy ion (in particular ^{197}Au) operation, with beam energies between 30 and 100 GeV/u. Operation above 100 GeV/u corresponding to 3.458 T in the arc dipoles might be possible.Besides reaching fields with substantial margins above the required field range, all of the RHIC magnets must meet stringent requirements on field quality, reproducibility, and long-term reliability. Existing technology was being used for the magnet design and construction, measuring and analysis procedures, cooling method, quench protection, instrumentation, and quality control standards. Improvements that were developed and tested during the R&D phase were incorporated into designs and fabrication methods.

The RHIC magnet lattice is designed to fit into the existing tunnel of ~3.8 km circumference. The lattice is divided into 6 arcs and 6 insertions for each of the two rings. In the arcs, the rings are separated radially by 90 cm. In the two rings of the collider, there are 408 dipoles, 492 quadrupoles, 72 trim quadrupoles, 288 sextupoles, and 492 magnets for correction of field perturbations. Table 1-1 gives the RHIC magnet inventory.

The field quality of accelerator magnets is characterized by normal and skew field harmonics, b_n and a_n, which are quoted in "primed units" and can be defined in terms of the field at the reference radius R which is taken as ~2/3 of the inner coil radius (i.e. R is 25 mm for the 80 mm aperture dipoles and quadrupoles, 40 mm for the 130 mm aperture quadrupoles, 31 mm for the 100 mm aperture dipoles and 67 mm for the 200 mm aperture dipole. The horizontal and vertical field

components, B_x and B_y, throughout the magnet aperture are then given in polar coordinates (r, θ) by

$$B_y + i\ B_x = 10^{-4}\, B(R) \sum_{n=0}^{\infty} \left(b_{n'} + i\ a_{n'}\right)\left(\cos\ n\theta + i\ \sin\ n\theta\right) \left(\frac{r}{R}\right)^n$$

where i is the imaginary unit and $B(R)$ is the magnitude of the field due to the *fundamental* at the

$$B_x(x) = 10^{-4}\ B(R) \sum_n a_{n'} (x/R)^n$$

reference radius. The field components on the median plane (i.e. θ = *0*) follow as

$$B_y(x) = 10^{-4}\, B(R) \sum_n b_{n'} (x/R)^n$$

In a normal dipole, $b_{0'} = 10^4$ and $B(R) = B_0$. In a normal quadrupole, $b_{1'} = 10^4$ and $B(R) = GR$ where G is the gradient $\partial B_y / \partial x$ at the magnet center. In general, for a 2 (m+1)-pole magnet $b_{m'} = 10^4$ and

$$B(R) = \frac{R^m}{m!} \left(\frac{\partial^m B_y}{\partial x^m}\right)_{x=0}$$

Magnet Nomenclature

A naming convention has been established for the various types of magnets to facilitate record keeping and physical tracking:

- Each cold mass will be named as indicated in the "Magnet/Cold Mass" Table 1-2. When a single cold mass is installed in a cryostat, the resulting magnet will be identified with the name of the cold mass inside.
- When several cold masses are combined as a cold mass assembly in a cryostat (the assembly magnets: CQS, CQT, etc) the resulting magnet will be identified as shown in the "Assembly" Table 1-3.

Table 1-1. RHIC Magnet Inventory

REGULAR ARC COMPONENTS	
Dipoles	264
Quadrupoles	276
Sextupoles	276
Correctors	276
INSERTION COMPONENTS	
Standard Aperture (8 cm) Magnets	
Dipoles (D5I, D5O, D6, D8, D9)	96
Quadrupoles (Q4-Q9)	144
Trim quadrupoles (@ Q4, Q5, Q6)	72
Sextupoles at Q9	12
Correctors	144
Intermediate Aperture (10 cm) Magnets	
Dipoles (D0)	24
Helical Dipoles	12
Intermediate Aperture (13 cm) Magnets	
Quadrupoles (Q1-Q3)	72
Correctors	72
Large Aperture (18 cm) Magnets	
Dipoles (DX)12	
TOTALS	
Dipoles	408
Quadrupoles	492
Trim quadrupoles	72
Sextupoles	288
Correctors	492
Total magnets	1752

Table 1-2 Magnet Nomenclature - Magnet/Cold Mass

Magnet/Cold Mass	Quan.†	∅(cm)	L(m)	Location	Fabr.	Magnet ID	Coil ID
Dipole	264 (-)	8	9.45	Arc	GAC	DRG###	DCG####
	13 (1)	8	6.92	D5I	GAC	D5I###	DCJ####
	13 (1)	8	8.71	D5O	GAC	D5O###	DCK####
	25 (1)	8	2.95	D6	GAC	D96###	DCH####
	34 (10*)	8	9.45	D8	GAC	DR8###	DCG####
	24 (-)	8	2.95	D9	GAC	D96###	DCH####
	26 (2)	10	3.6	D0	BNL	DRZ###	DCZ####
	12 (2)	10	10.4	IR's	BNL	HRD###	HSD###
	13 (1)	18	3.7	DX	BNL	DRX###	DCX####
Quadrupole	282 (6)	8	1.13	Arc	GAC	QRG###	QCG####
	26 (2)	8	1.83	Q4	GAC	QR4###	QCH####
	25 (1)	8	1.13	Q5	GAC	QRG###	QCG####
	24 (-)	8	1.13	Q6	GAC	QRG###	QCG####
	26 (2)	8	0.95	Q7	GAC	QR7###	QCF####
	25 (1)	8	1.13	Q8	GAC	QRG###	QCG####
	24 (-)	8	1.13	Q9	GAC	QRG###	QCG####
	26 (2)	13	1.44	Q1	BNL	QRI###	QCI####
	26 (2)	13	3.40	Q2	BNL	QRK###	QCK####
	26 (2)	13	2.10	Q3	BNL	QRJ###	QCJ####
Trim quads	78 (6)	8	0.75	Q4,5,6	EEC	QRT###	QCT####
Corrector	100 (4)	8	0.5	Arc + Ins - Style B	BNL	CRB###	
	136 (4)	8	0.5	Arc + Ins - Style C	BNL	CRC###	
	78 (-)	8	0.5	Arc + Ins - Style D	BNL	CRD###	
	78 (-)	8	0.5	Arc + Ins - Style E	BNL	CRE###	
	40 (4)	8	0.5	Arc + Ins - Style F	BNL	CRF###	
	13 (1)	13	0.5	Q2 Outer - Style I	BNL	CRI###	
	13 (1)	13	0.5	Q3 Inner - Style J	BNL	CRJ###	
	26 (2)	13	0.5	Q3 - Style K	BNL	CRK###	
	13 (1)	13	0.5	Q3 Inner - Style L	BNL	CRL###	
	13 (1)	13	0.5	Q3 Outer - Style M	BNL	CRM###	
Sextupole	300 (12)	8	0.75	Arc,Q9	EEC	SRE###	SCE####

† Quantities listed include spares which are listed in parentheses, ( )
* The total of 10 spares are constructed as DR8 type and are interchangeable with DRG type, but not vice versa.

Table 1-3. Magnet Nomenclature - Assembly

Assembly	Quan.†	∅(cm)	L(m)	Location	Fabr.	Magnet ID
CQS	282 (6)	8	3.4	Arc	BNL	CQS###
	12 (-)	8	3.4	Q9	BNL	CQS###
CQT	26 (2)	8	4.1	Q4	BNL	CQ4###
	25 (1)	8	3.4	Q5	BNL	CQ5###
	24 (-)	8	3.4	Q6	BNL	CQ6###
CQ	26 (2)	8	2.5	Q7	BNL	CQ7###
CQ	25 (1)	8	2.6	Q8	BNL	CQ8###
CQBlank	12 (-)	8	3.4	Q9	BNL	CQ9### ††
Dipole	13 (1)	10	4.4	D0	BNL	DIZ###
Q	13 (1)	13	1.9	Q1	BNL	CQ1###
CQ	13 (1)	13	4.4	Q2	BNL	CQ2###
CQC	13 (1)	13	4.0	Q3	BNL	CQ3###
Dummy Assembly	24 (-)	8	2.6	Q4/Q5	BNL	DU4###
	24 (-)	8	6.0	Q6/D6	BNL	DU6###
	24 (-)	8	11.9	Q7/Q8	BNL	DU7###
	24 (-)	8	6.0	Q9/D9	BNL	DU9###

† Quantities listed include spares which are listed in parentheses, ( )
†† 2 assemblies do not contain blank iron

ii. Superconductor

30-Strand Superconducting Cable

The 30-strand (or wire) superconductor cable is used in the fabrication of all of the dipole and quadrupole magnets with 8 and 10 cm aperture. A similar cable has been fabricated and used for many years in the RHIC and in the SSC 40 mm R&D programs. Consequently, the wire and cable fabrication methods are well developed. During magnet fabrication the cable was insulated just prior to use for winding coils.

The dimensional, mechanical and electrical properties of the superconducting strand used to fabricate the cable are summarized in Table 2-1. Each strand consists of 3510 Nb-Ti alloy superconducting filaments with nominal diameter of 6μm and spacing >1μm. The exact number of filaments has been chosen by the superconductor vendor based on the details of the billet design, and will be maintained within ±20 for every billet assembled. Copper is used as the matrix between filaments, it occupies a >10% cross section central core, and provides an outer covering for the wire. Copper represents about 69% of the wire cross section and is important for the cable and magnet operational stability. The wire diameter of 0.648 mm is tightly controlled during final stages of manufacturing and is checked with a laser micrometer.

The wire minimum critical current is defined at a temperature of 4.22 K, an applied magnetic field of 5.0 T perpendicular to the wire axis and a resistivity of 1×10^{-14} Ω·m based on the total wire cross section. This current requirement corresponds to a minimum current density in the Nb-Ti superconductor of 2600 A/mm^2 at 5.0 T. This modest requirement was chosen for the RHIC magnets because higher values were unnecessary to meet the accelerator design objectives, and because the emphasis for superconductor manufacturing was placed on uniformity of wire and cable properties. In manufacturing, about 2800 A/mm^2 was achieved. An upper limit was placed on wire critical current at 3.0 T in order to control the effects of superconductor magnetization at injection. The relatively high proportion of copper in the strand was chosen to add stability against quenching and to lower peak temperatures during a quench.

Thirty wires are fabricated into a Rutherford-type cable by first twisting them around a "mandrel" and then immediately rolling them into a flat, keystoned shape with dimensions given in Table 2_2 and Fig. 2-1 . The variations of the cable dimensions, especially the cable mid-thickness, are tightly controlled because the magnetic field quality of the magnets and the coil prestress are strongly dependent on them. The cable lay (or twist) pitch is chosen to be opposite to the wire twist

and requires a cabler operating in a planetary mode for fabrication. The cable minimum critical current (see Table 2-2) is defined in a similar way to that for the wire, but with the magnetic field perpendicular to the wide surface of the cable and with compensation for self-field. The cable minimum critical current can be obtained from the "wire minimum critical current at 5.0 T" times 30 (number of wires in cable) and multiplying by 0.95 (allowance for 5% degradation in cabling). All cable lengths were produced without cold welds.

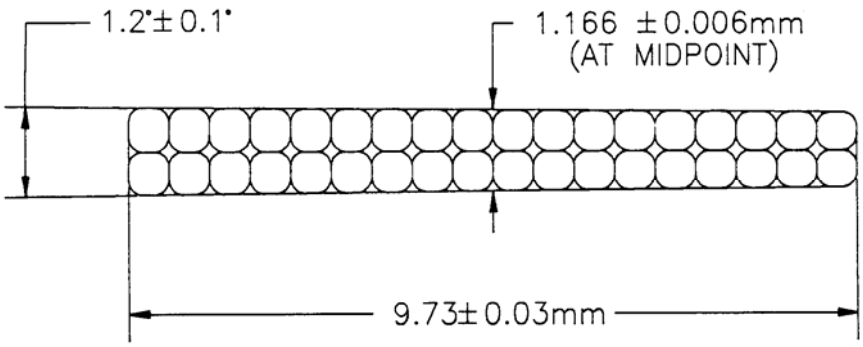

Fig. 2-1. Cross section of the cable used to fabricate coils for RHIC dipole and quadrupole magnets with 8 cm aperture and the 10 cm D0 dipole.

Table 2-1 . Wire Requirements for 30-Strand Cable

Requirement	Value	
DIMENSIONAL AND MECHANICAL		
Nominal Filament Diameter	6	μm
Nominal Filament Spacing	>1	μm
Nominal Copper to Non-Copper Ratio	(2.25±0.1):1	
Number of Filaments	3510±20	
Wire Diameter	(0.0255±0.0001 in.) 0.648±0.003	mm
Wire Twist Direction	Right	
Wire Twist Pitch	(1.9±0.2 twists/in.) 0.75±0.08	twists/cm
ELECTRICAL		
Wire Minimum Critical Current at 5.0 T, 4.2 K	264	A
Wire Maximum Critical Current at 3.0 T	1.6 × measured I_{crit} @ 5.0	T
Wire Maximum R(295 K)	0.0765	Ω/m
Wire Minimum RRR	38	

Table 2-2 . 30-Strand Cable Requirements

Requirement	Value	
DIMENSIONAL AND MECHANICAL		
Number of Wires in Cable	30	
Cable Mid-Thickness	(0.04590±0.00025 in.) 1.166±0.006	mm
Cable Width	(0.383±0.001 in.) 9.73±0.03	mm
Cable Keystone Angle	1.2±0.1	deg
Cable Lay Direction	Left	
Cable Lay Pitch	(2.9±0.2 in.) 74±5	mm
Wire Twist Pitch in Cable	(1.9±0.2 twists/in.) 0.75±0.08	twists/cm
ELECTRICAL		
Cable Minimum Critical Current at 5.0 T, 4.2 K	7524	A
Cable Maximum R (295 K)	0.00268	Ω/m
Cable Minimum RRR	38	

36-Strand Superconducting Cable

The insertion quadrupole and dipole magnets with 13 and 20 cm apertures respectively have a single-layer coil. While considering the design alternatives, it was decided to take advantage of superconductor wire and cable which were well-developed for another, similar magnet program. The conductor chosen was that used for outer-layer coils of the SSC Collider Dipole Magnet with 50 mm aperture.

The dimensional, mechanical and electrical properties of the strand (or wire) used to fabricate the cable are given in Table 2-3. The copper-to-non-copper ratio of 1.8:1 requires that the number of Nb-Ti superconductor filaments be approximately 4100. Copper represents 64% of the wire cross section. The filament diameter of 6 μm and spacing of >1 μm are standard parameters for wires of this type to control low field magnetization and coupling. As for most twisted wires, a central copper core is required with >10% cross section.

The critical current characteristics of the wire are given in Table 2-3 ; for the 36-strand cable they are given in Table 2-4. The minimum critical currents are defined at a temperature of 4.22 K, a magnetic field of 5.6 T and a resistivity of 1×10^{-14} Ω·m. The critical current requirement of the wire corresponds to a minimum current density in the superconductor of 2750 A/mm^2 at 5.0 T or 2420 A/mm^2 at 5.6 T, both without self-field effects. The cable critical current allows for 2% degradation during cabling and includes self-field effects.

The cable dimensional requirements given in Table 2-4 and Fig. 2-2 for the most part correspond exactly to what was being fabricated for SSC. Cable with keystone angle of 1.0^o was used for RHIC 13 cm aperture quadrupoles; this is the angle chosen for SSC magnets. A smaller keystone angle of 0.6^o was used for the RHIC 18 cm dipole. The cable was fabricated in a "planetary" mode, where the original twist of the wire is preserved during the cabling operation. All cable lengths were produced without cold welds.

Table 2-3. Wire Requirements for 36-Strand Cable

Requirement	Value	
DIMENSIONAL AND MECHANICAL		
Nominal Filament Diameter	6	μm
Nominal Filament Spacing	>1	μm
Nominal Copper to Non-Copper Ratio	(1.80±0.1):1	
Number of Filaments	(4100 - 4200)±20	
Wire Diameter	(0.0255±0.0001 in.) 0.648±0.003	mm
Wire Twist Direction	Right	
Wire Twist Pitch	(1.9±0.2 twists/in.) 0.75±0.08	twists/cm
ELECTRICAL		
Wire Minimum Critical Current at 5.6 T, 4.2 K	286	A
Wire Maximum R(295 K)	0.0827	Ω/m
Wire Minimum RRR	36	

Table 2-4 . 36-Strand Cable Requirements

Requirement	Value	
DIMENSIONAL AND MECHANICAL		
Number of Wires in Cable	36	
Cable Mid-Thickness	(0.04550±0.00025 in.) 1.156±0.006	mm
Cable Width	(0.460+0.002/-0.000 in.) 11.68+0.05/-0	mm
Cable Keystone Angle - 13 cm quadrupoles	1.0±0.1	deg
- 20 cm dipoles	0.6±0.1	deg
Cable Lay Direction	Left	
Cable Lay Pitch	(3.7±0.2 in.) 94±5	mm
Wire Twist Pitch in Cable	(1.9±0.2 twists/in.) 0.75±0.08	twists/m
ELECTRICAL		
Cable Minimum Critical Current at 5.6 T, 4.2 K	10100	A
Cable Maximum R (295 K)	0.00240	Ω/m
Cable Minimum RRR	36	

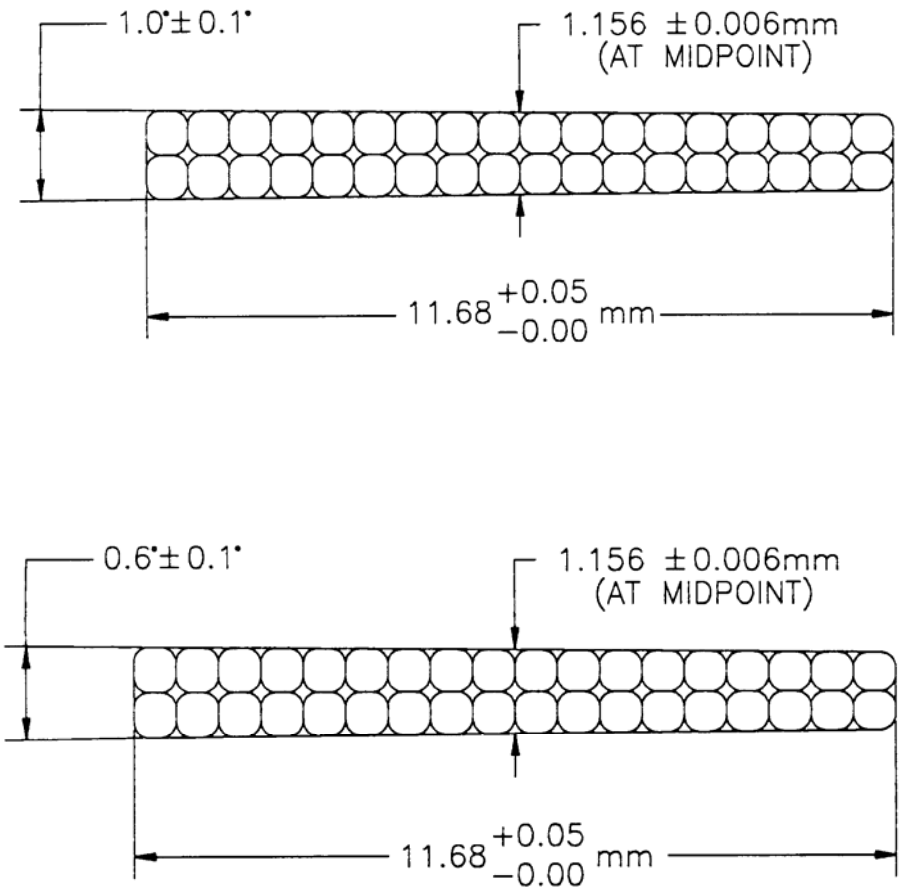

Fig. 2-2. Cross sections of the cable used to fabricate coils for RHIC insertion quadrupoles with 13 cm aperture (1^o keystone angle) and insertion dipoles with 20 cm aperture (0.6^o keystone angle).

Sextupole, Trim Quadrupole and Corrector Wire

The same wire was used to fabricate coils for the sextupole and trim quads and a similar wire for the corrector magnets. It should be noted that the coils are wound from insulated wire, not from cable, and, therefore, the integrity and uniformity of the wire along the length is extremely important for the operation of the magnets. The magnets and superconductor are designed with considerable margin between the expected operating current, in order to raise confidence in the operating reliability.

The dimensional, mechanical and electrical properties of the superconducting wires for the sextupole and corrector magnets are summarized in Table 2-5. The nominal filament diameter of 10 μm is somewhat larger than that for RHIC cable magnets, but this reflects a reduced concern about magnetization effects in these magnets. The nominal copper-to-non-copper ratios of 3.0:1 and 2.5:1 are based on experience from RHIC R&D magnets. The wire diameters of 0.508 and 0.330 mm were chosen in order to accommodate the necessary insulation in the design coil space (to be applied later) and because wires of these diameters match the desired operating currents. The 0.33 mm (plus insulation) wire for the corrector is the maximum size usuable in the Multiwire machine.

The wire minimum critical current is defined at the standard values of 2.0 T magnetic field, 4.22 K temperature and at a resistivity of 1×10^{-14} Ω·m over the total cross section of the wire. The wire was delivered with the copper in the annealed state to enhance wire ductility and to facilitate coil winding. Careful eddy current testing was done over the full length of all delivered wire to eliminate any wire sections with inclusions which may locally damage the superconductor filaments and reduce the critical current.

Table 2-5. Sextupole, Trim Quad and Corrector Wire Requirements

Requirement	Value	
	Sextupole and Trim Quad	Corrector
DIMENSIONAL AND MECHANICAL		
Nominal Filament Diameter	10 μm	10 μm
Nominal Filament Spacing	>1 μm	>1 μm
Nominal Cu to Non-Cu Ratio	(3.0±0.1):1	(2.5±0.1):1
Number of Filaments	645±10	310±5
Diameter, bare	0.508±0.003 mm (0.0200±0.0001 in.)	0.330±0.003 mm (0.0130±0.0001 in.)
Twist Direction	Right	Right
Twist Pitch	0.79±0.08 twists/cm (2.0±0.2 twists/in.)	0.79±0.08 twists/cm (2.0±0.2 twists/in.)
ELECTRICAL		
Minimum I_{crit} @ 2.0 T, 4.2 K	230 A	120 A
Maximum Ratio $I_{crit}(2T)/I_{crit}(5T)$	1.90	1.90
Wire Maximum R (295 K)	0.112 Ω/m	0.280 Ω/m
Wire Minimum RRR	90	90

iii. Standard Aperture Dipoles

The arc dipole magnets have a coil i.d. of 80 mm, are 9.7 m long and, with 264 of these magnets required, represent by far the largest single cost item for the collider. In addition, there are 24 insertion dipoles "D8" which are identical to the arc dipoles, and 72 insertion dipoles "D9, D6, D5I and D5O" which are shorter in length.

Dipole Cold Mass

Figure 3-1 shows a cross-section of the dipole cold mass. The dipole design is based on a single-layer "cosine theta" coil, wound from a partially keystoned, 30-strand NbTi superconducting cable and mechanically supported by a laminated "cold steel" yoke encased in a stainless steel helium containing cylinder. The helium vessel is also a load bearing part of the yoke assembly. This cold mass assembly is mounted within a cryostat consisting of a cylindrical vacuum vessel, an aluminum heat shield, blankets of multilayer thermal insulation, cryogenic headers, and the magnet support system. The nominal dipole operating field is 3.458 T at a current of 5.050 kA and an operating temperature between 4.3 and 4.6 K.

The RHIC dipole cold mass design incorporates a relatively large bore (80 mm), a modest operating field (3.45 T), a single-layer coil, a steel yoke assembled as collars, and no internal trim coils. The general design parameters are listed in Table 3-1.

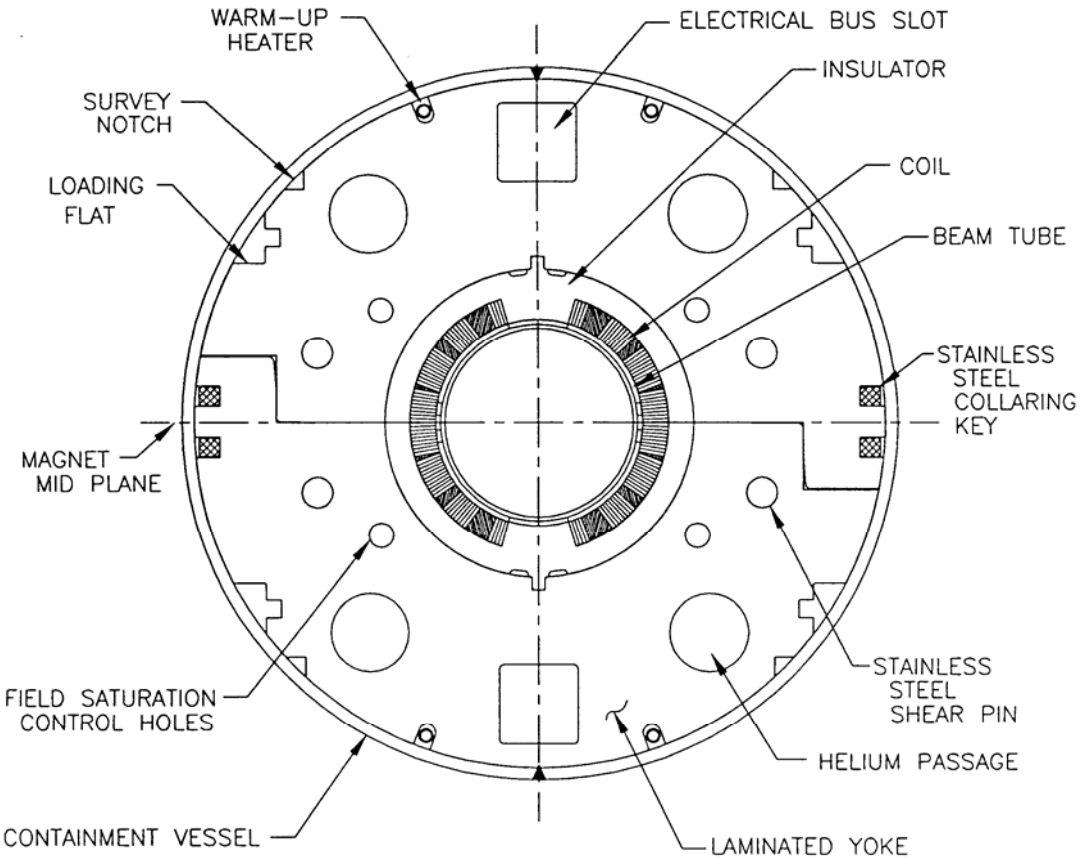

Fig. 3-1. Standard-aperture dipole cold mass cross-section (coil i.d. = 80 mm).

Table 3-1. Standard Aperture Dipole Parameters

Coil i.d.	(3.15 in.) 80	mm
"ARC" DIPOLES		
No. arc dipoles, two rings	264	
No. insertion dipoles, D8	24	
Magnetic length, arc and D8	9.45	m
Magnet rigidity - Injection	97.5	T·m
- Top energy	839.5	T·m
Integrated field strength, top energy	32.677	T·m
Dipole field - Injection	0.401	T
- Top energy	3.458	T
Quench field	~ 4.6	T
Operating temperature, max.	4.6	K
Ramp rate, nominal	0.042	T/s
Current - Injection	568	A
- Top Energy	5.093	kA
Lamination length	(379.4 in.) 9.64	m
Cold mass length	(383 in.) 9.73	m
Dipole bending radius, cold	243	m
Mechanical sagitta for 383 in. cold mass length	(1.91 in.) 48.5	mm
Cold mass, including interconnect cans and flange	(7952 lb) 3607	kg
Inductance	28	mH
Stored energy	351	kJ
INSERTION DIPOLES		
No. insertion dipoles, 6.92 m - D5I	12	
8.71 m - D5O	12	
2.95 m - D6 & D9	48	

Table 3-2. Dipole Beam Tube

Outside diameter	(2.875 in.) 73.0 mm
Outside diameter inc. Kapton wrap	(2.883 in.) 73.2 mm
Wall thickness(77 mil)	1.96 mm
Inner diameter, nominal	69 mm
Weight, nominal	(79 lb) 36 kg
Beam tube-coil radial gap	(133 mil) 3.4 mm

Dipole Beam Tube

The dipole utilizes a cold beam tube with dimensions given in Table 3-2. It is centered horizontally inside the coils with 2.7 mm thick by 76 mm long, G-10, longitudinal bumpers with 0.3 m axial spacing and vertically by the RX630 pole pieces, thus defining a helium buffer space. The tube is wrapped with 25 μm Kapton with 60% overlay, providing 76 μm of insulation which is hi-pot tested at 5 kV. The tube is made of seamless, type 316 LN stainless steel, manufactured by Mannesmann Edelstahlrohr, Germany in accordance with the chemical composition requirements of the ASTM A213/A231M specification, but with a nickel content toward the upper part of the allowable range to mitigate potential welding problems at the ends of the tubes. No copper coating on the tube inner surface was required in the RHIC machine. The beam tubes were welded to the end volumes at each end of the magnet, with no intervening bellows.

Dipole Coil

The superconducting coil is assembled from two half-coils that are wound on automated machinery and then formed into a specified size in a precision molding operation. It consists of a single layer of 32 turns per half-coil arranged in four blocks with intervening copper wedges; the size and positions of the wedges and the coil pole spacer have been designed to result in field harmonics meeting the rigid field quality specifications required for RHIC. The four current block design, which has 3 symmetric wedges, is identified as 9B84A in the DRE dipoles. The coil design parameters are given in Table 3-3.

The cable length per half-coil is 1220 m. This cable was insulated with 2 double layers of newly-developed Kapton CI film [AN93a]. The first double layer has polyimide adhesive on the

outer side of the tape; the second has it on both sides. This marked the first use of all-polyimide electrical insulation in the coils of superconducting accelerator magnets, an advance that has greatly improved their electrical integrity. It has also reduced size variations in molded coils, leading directly to improved magnet field quality. The coil ends were designed for relatively simple construction and low harmonic content [KA93a, MO93a]. There are 8 (9) separate spacers in the lead (return) end of each coil, molded of Ultem 6200 plastic. The coils were keyed to the yoke laminations through the precision-molded, glass-filled phenolic (RX630) insulator-spacers. The phenolic insulators separate the coil from the steel yoke and provide both electrical isolation of the coil from ground as well as reduced magnetic saturation effects at high field. The coil design used sufficiently thick midplane caps to allow adjustment of sextupole and decapole harmonics during production [GU94].

Table 3-3. Arc Dipole Coil Design

Inner diameter	(3.146 in.) 79.9 mm
Outer diameter	(3.938 in.) 100.0 mm
Length, overall	(379.75 in.) 9.646 m
Length, coil straight section	(364.80 in.) 9.266 m
Cable length per magnet	(4002 ft) 1220 m
Cable mass per magnet, bare	(220 lb) 100 kg
Effective cable mid-thickness with insulation under compression	(0.05322 in.) 1.352 mm
Minimum creep path, conductor to ground	(0.2 in.) 5.1 mm
Dielectric strength:current to ground @ 5 kV	< 200 μA
Yoke-coil insulating spacer thickness	10 mm
Midplane Kapton thickness	(0.004 in.) 0.10 mm
Cable wrap material thickness, Kapton	(0.001 in.) 25 μm
Pole angle (coil center radius)	73.178 deg
Number of turns	32
Number of turns, 1st block (closest to pole)	4
Number of turns, 2nd block	8
Number of turns, 3rd block	11
Number of turns, 4th block	9

WEDGE PARAMETERS

Wedge #	Angle	Inner Edge Thickness	Height
1	16.684°	(0.2802 in.) 7.12 mm	(0.382 in.) 9.70 mm
2	9.833°	(0.1217 in.) 3.09 mm	(0.382 in.) 9.70 mm
3	8.105°	(0.0155 in.) 0.39 mm	(0.380 in.) 9.65 mm

Dipole Yoke

The steel yoke performs several functions: it serves as a magnetic return path and thereby enhances the central field, it acts as a "collar" that applies mechanical prestress to the coils through the phenolic insulator-spacer that references the coils to the yoke, and finally, it acts as a shield to reduce stray field in the adjacent ring of magnets. The yoke laminations contain holes for the necessary busses and for the flow of helium. The sizes and positions of these holes, and of the locating notch for the RX630 spacers, were carefully determined to minimize saturation effects [GU94]. Special strain gauge instrumentation and test methods were developed to ensure that the stresses in the magnet met the design goals [GO88a]. Using the yoke laminations as collars dictated the lamination thickness. The magnetic uniformity of the steel was a concern because randomizing of the steel properties through shuffling of laminations was not practicable in a job this large.

The yoke laminations were punched (fine blanked) from 6.35 mm thick ultra-low-carbon steel plate furnished by the Kawasaki Steel Corporation, Japan. Both the mechanical and magnetic characteristics of the steel are important in this application [MO92a]. The yield strength of the steel was specified to be no less than 221 MPa, a level achieved through cold-rolling thickness reduction. This allowed the laminations to be pressed onto the coils without significant yielding on the midplane where the forces during collaring are high. To achieve control of the important high-field saturation magnetization (M_s), the chemical composition (impurities) was strictly specified. This control of the chemistry also ensured that important low field parameters like the coercivity H_c remained under control. Measurements on ring samples [TH92a, MO94a] and chemical analysis of extracted pieces of the production steel were used to monitor the quality of the steel, but the tight quality control exercised by the company in producing the steel ensured that all the material delivered was of the required accelerator quality.

The laminations have an inner diameter of 119.4 mm and an outer diameter of 266.7 mm. They were pinned together in pairs to allow the yoke elements to act as collars. To meet the rms tolerances for the magnetic field integrated over the length of the dipoles, it was required that the weight of steel in the yoke be controlled to within 0.07%. To achieve this tolerance, the lamination pairs that make up the yoke were weighed and their number adjusted to meet the weight specification. The selection of yoke pairs for the top and bottom halves was done in such a way that the total weight of the top half was slightly lower than that for the bottom half [JA95a]. This helped to reduce the skew quadrupole at high fields resulting from a vertically off-centered cold mass in the

cryostat (see Fig. 3-2). During magnet assembly, a press compressed the yoke around the coils. The yoke was subsequently held together with stainless steel keys pushed into notches on the outer circumference. The design preload of 70 MPa acting on the coils was routinely achieved. The yoke laminations extend the full length of the magnet and are not terminated prior to the coil ends as is done in many designs to reduce the field in the mechanically difficult end region of the coils.

Shell

After completion, the coil-in-yoke assembly was surrounded with two, 4.9 mm thick, type 304L stainless steel half-shells, which were then welded along the vertical midplane. The root pass of this weld joined the shell directly to the yoke laminations; no backing strip was used. Extensive testing at Brookhaven confirmed that the joining of these two dissimilar materials gave acceptable results. Nevertheless, a high-nickel-content filler material, type 385LN, was used in this and in the subsequent fill passes to increase the fracture toughness of the joint. In production, these welds were made by automated TIG machines.

Before the welding began, the magnet was placed in a fixture that introduced the required 48.5 mm sagitta; this sagitta was locked in place when the stainless steel half-shells were then welded together. The welding operation also formed the outer, high-pressure (2.1 MPa) helium containment vessel. The shrinkage of the weld compressed the steel collar block, ensuring closure of the mid-plane yoke gap. Further compression was realized at operating temperature from the differential contraction of the stainless steel shell relative to the steel yoke. Compression of the coil increased only until the yoke mid-plane gap closed.

The yoke design parameters are listed in Table 3-4.

Table 3-4. Arc Dipole Yoke and Yoke Containment Design Parameters

YOKE	
Inner diameter	(4.700 in.) 119.4 mm
Outer diameter	(10.5 in.) 266.7 mm
Lamination length	(379.4 in.) 9.64 m
Length, including end plates	(383.0 in.) 9.73 m
Lamination thickness	(0.250 in.) 6.35 mm
Length, lamination packs	(0.500 in.) 12.70 mm
Weight of steel	(6079 lb) 2757 kg
Mechanical sagitta for 383 in. cold mass length	(1.91 in.) 48.5 mm
Bus cavity - width	(1.25 in.) 31.75 mm
- height	(1.25 in.) 31.75 mm
Number of cooling channels	4
Diameter of cooling channels	(1.187 in.) 30.15 mm
YOKE CONTAINMENT SHELL	
Inner diameter, prior to assembly	(10.516 in.) 267.1 mm
Wall thickness	(0.192 in.) 4.9 mm
Weight of shell	(674 lb) 306 kg
ASSEMBLY PRESTRESS	
Room temperature	> (10 kpsi) 68.9 MPa
Cold	> (4.8 kpsi) 33.1 MPa

Table 3-5. Dipole, Electrical Design Requirements

Dipole bus stabilization copper	58	mm^2
Quadrupole bus stabilization copper	58	mm^2
Bus expansion joint motion	46	mm
Warmup heater, resistance/heater @ 300 K	2.24	Ω
Warmup heater, power/heater	938	W
Quench protection diode, max. energy	140	kJ
Quench protection diode, max. reverse leakage current @ 1 kV	10	mA
Quench protection diode, 4.2 K forward voltage threshold @ 10 mA	3.0	V

Electrical Connections and Quench Protection

The design of the machine uses separate main electrical bus systems for the dipoles and the quadrupoles. The bus conductor for these and the various corrector magnets is placed inside an insulating "pultrusion" that is then installed as a completed package into the bus slots at the top and bottom of the yoke. The electrical connections between bus conductors and magnet leads are at the ends of the magnets, within the volume contained by the stainless steel helium containment vessel and end bellows. The end volume also contains the thermal expansion joints for the bus conductors and quench protection diodes. A heater consisting of a stainless steel pipe will accelerate the occasional warm-up of the cold mass.

The quench protection diodes were constructed using a 76.2 mm diameter doped silicon element manufactured by Powerex Corporation, Youngwood, PA. The elements were from an existing compression style hockey puck product line, with the diffusion process modified to achieve the cryogenic requirements. For the RHIC application, a non-hermetic assembly was required. The assembly includes two large copper masses as heat sinks and as compression contacts to the element, and a stainless shell with a threaded top cap. The surface contact with the element is a 76.2 mm circle, loaded to 53.4 kN contact force. The pressure loading is through two 19 mm diameter ceramic balls axially configured to assure an even, concentric loading of the diode element. The top cap is finally welded to the assembly body to prevent thread disengagement during the application of 7000 A test pulses, done at cryogenic temperature. Since the diodes are not hermetic, the polyimide passivation of the junction edge is of paramount importance, and required both visual and electrical

screening to verify passivation integrity. The dipoles were measured to be self-protecting. Quenches of production magnets, mostly near or at the limit of the conductor, had $\int I^2 dt < 12.5$ MIITS, where a MIIT is 10^6 A^2 s. Worst-case situations were simulated by using spot heaters to initiate quenches at the midplane of the coil at 5 kA on the last two full-length R&D magnets. (These magnets were nearly identical to the production dipoles.) These spot-heater quenches produced 13.2 and 13.5 MIITS. For these magnets, 11 MIITS corresponded to 300 K, with the temperature determined from voltage taps located near the spot heaters. This measurement was extrapolated to 500 K for 13 MIITS. The threshold temperature for damage was 835 K.

The electrical design parameters for the dipole magnet are listed in Table 3-5.

Dipole Cryostat

The cryostat is the structure which must make the transition from the 4 K environment of the magnet cold mass to ambient temperature as shown in Fig. 1-4. The cryostat must accurately position the magnet cold mass to a given point in the accelerator lattice, while at the same time, minimizing the refrigeration load, by a method that can be implemented reliably in an industrial production setting.

The major components are the carbon steel (ASTM A53) vacuum vessel (outer diameter 610 mm, wall thickness 6.4 mm), the aluminum heat shield (1100-H14) maintained at a nominal temperature of 55 K, blankets of multilayer aluminized Mylar thermal insulation, various cryogenic headers including bellows at their ends, and post-type supports [SO91a] that carry the cold mass weight to the wall of the vacuum tank. Each support post is comprised of two identical molded plastic "hats" attached end to end. They were precision molded as tubes with flanges from Ultem 2100 glass-filled plastic. A standard arc dipole has three such supports. They make sliding contact (where necessary) to the cold mass to support the cold mass inside the cryostat. A spring was incorporated into this contact assembly to maintain the horizontal alignment of the cold mass. In the tunnel, only two stands carry the load to the ground. The weight distribution is 40 % on the center post and 30 % on each of the outer posts. The post inner diameter is 212.8 mm with a wall thickness of 4.8 mm. The heat shield is captured between the top and bottom hats. The heat leak per leg is 0.1 W to 4.5 K and 1.0 W to 55 K. The superinsulation blankets use alternating layers of reflectors (6 μm non-crinkled Mylar, aluminized on two sides) and spacers (0.15 mm REEMAY 2006). In order to minimize the heat load, the thickness of the aluminum on the Mylar used at 4.5 K is thicker (600 Å) than that on the Mylar at 55 K (380 Å) because of the difference in wavelength of the shielded radiation. The legs of the vacuum chamber are carbon steel castings welded to the vacuum vessel. Sockets machined into these legs are used to provide the exterior survey fiducial references; survey fixtures translate the positional information provided by the cold mass to these references.

The cryostat design parameters are given in Table 3-6.

Table 3-6. Dipole Cryostat

Vacuum vessel, o.d.	(24 in.) 610	mm
Vacuum tank, wall thickness	(0.25 in.) 6.4	mm
Heat shield, o.d.	(21.0 in.) 533	mm
Heat shield, wall thickness, upper section	(0.09 in.) 2.3	mm
Heat shield, wall thickness, lower section	(0.125 in) 3.2	mm
Recooler supply header, i.d.	(2.71 in.) 68.8	mm
Helium return header, i.d.	(2.71 in.) 68.8	mm
Utility header, i.d.	(2.71 in.) 68.8	mm
Shield cooling pipe, i.d.	(2.157 in.) 54.8	mm
Number supports	3	
Support spacing	(141.5 in.) 3.59	m
Weight distribution		
Center post	40%	
	(3395 lb) 1540	kg
Outer post ea.	30%	
	(2532 lb) 1148	kg
Post, i.d.	(8.38 in.) 212.8	mm
Post, wall thickness	(0.189 in.) 4.8	mm
Heat leak per leg at 4.5 K	0.1	W
Heat leak per leg at 55 K	1.0	W
Superinsulation layers, cold mass only	17 Reflector, 32 Spacer	
Superinsulation layers, cold mass plus piping	38 Reflector, 53 Spacer	
Superinsulation layers, shield	62 Reflector, 62 Spacer	

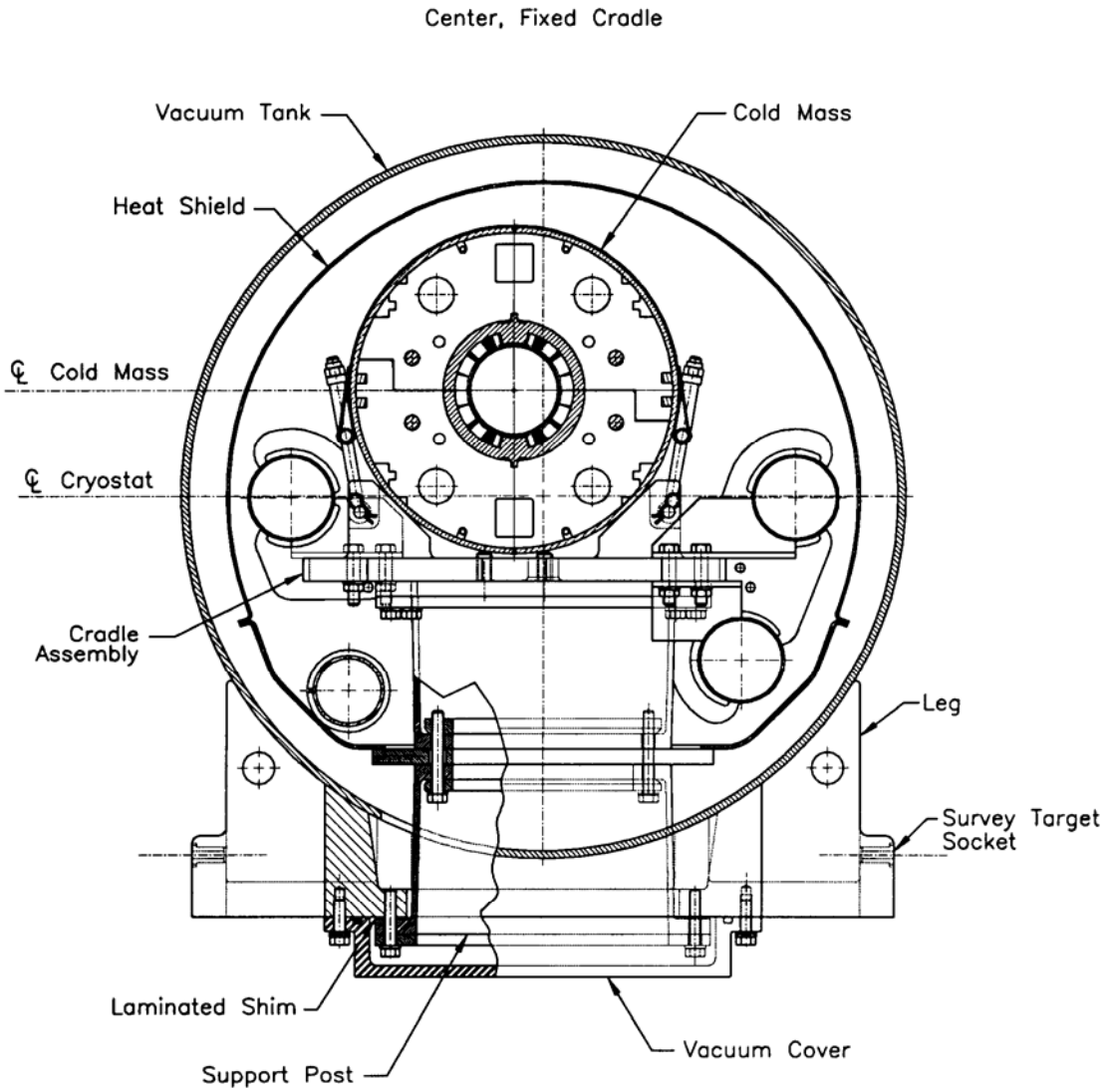

Fig. 3-2. Arc dipole cross-section (610 mm vacuum vessel o.d.).

Magnet Manufacture, Delivery and Acceptance

A total of 373 dipole magnets was manufactured at Grumman according to prints and specifications developed by Brookhaven [WA95b, AN95a, FI99a]. They were delivered as complete units ready for installation into the RHIC lattice. Superconducting cable, beam tubes and quench protection diodes were supplied by Brookhaven; all other components were procured by Grumman. During their construction, the magnets were subjected to rigorous quality and performance checks designed to prevent the manufacture of any faulty magnets. This goal was achieved; all magnets delivered to Brookhaven were acceptable for machine use. The initial 30 magnets were cold tested at Brookhaven. Upon confirmation that their performance validated their design and manufacture, only about 10% of the remaining magnets were cold tested. This reduced level of testing, and the resultant significant cost savings, has been proven sound by the subsequent stellar magnet performance in the machine. Warm magnetic measurements were made on all magnets, both at Grumman [GU95a] and at Brookhaven, and the good warm-cold correlation has been used in tracking calculations at Brookhaven to predict machine performance.

Performance

Quench test results for the 51 arc dipoles tested at 4.5 K are shown in Fig. 3-3. The magnets were quenched until a "plateau," where there was little variation in quench current, was reached, typically within a few quenches. The quench performance of the magnets was excellent. The initial quench current and the plateau quench current of each magnet exceeded the 5 kA operating current. The plateau quench currents were consistent with the currents expected for magnets operating at the current-carrying limit of the superconductor. In RHIC operations, the rings have reached 5 kA without quenching the arc dipoles, confirming the good construction of these magnets.

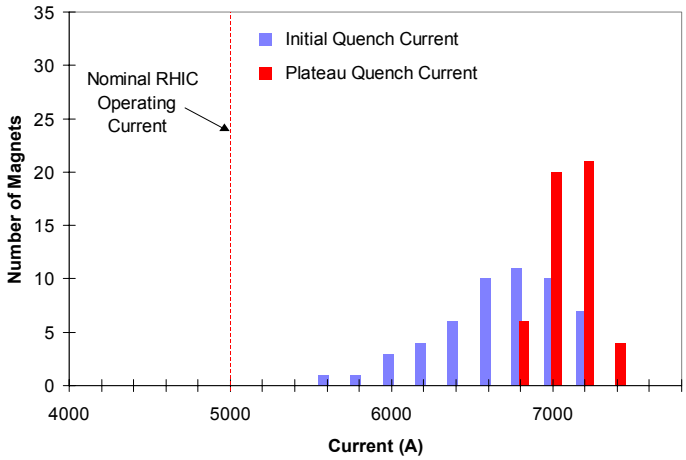

Fig. 3-3. Quench performance of 51 arc dipoles, tested at 4.5 K. The average plateau quench current of these 51 magnets was 7101 A; the field at this average quench current is 4.52 T.

Magnetic measurements were made with two probes: a 1 m-long rotating coil with attached gravity sensor and a 10 m-long stationary coil. The 1 m coil was used to measure the harmonics and the field angle. Integral values of the harmonics and field angles at 4.5 K were obtained by moving the coil in ten 1 m steps at three currents: near the planned injection current (660 A), at transition in RHIC (1450 A), and at full energy (5 kA). Measurements were also made at closely spaced current steps with the coil at a fixed axial position near the center of each magnet. The 10 m stationary coil was used to measure the integral dipole field. The 1 m and the 10 m coils were also used for "warm" measurements with the magnets at room temperature.

During production, several changes were made to the magnet cross section and, thus, to the geometric harmonics [WA98]. Planned changes were introduced in order to reduce the harmonics. Some unplanned changes in transfer function occurred due to variations in the materials used in the magnets. These changes were corrected before too many magnets were affected. The impact of affected magnets on RHIC was reduced by carefully assigning magnets with lower than normal transfer function to lattice locations next to magnets with higher than normal transfer function [WE95].

The field quality of the magnets at room temperature ("warm") was well correlated with the field quality at 5 kA ("cold"). Integral measurements of the low-order harmonics (normal and skew quadrupole, normal sextupole, and normal decapole) are shown in Figs. 3-4 through 3-7. (The data do not lie on the straight line in the plots because of effects such as saturation.) Measurements of

these same four harmonics as a function of current, in the straight section of the magnets, are shown in Figs. 3-8 through 3-11, along with the calculated values. Warm and cold measurements of the harmonics through the 22-pole term are given in Table 3-7. (Note that the quadrupole term is denoted by n = 1. Harmonics are expressed in "units", where a unit is 10^{-4} of the main field.)

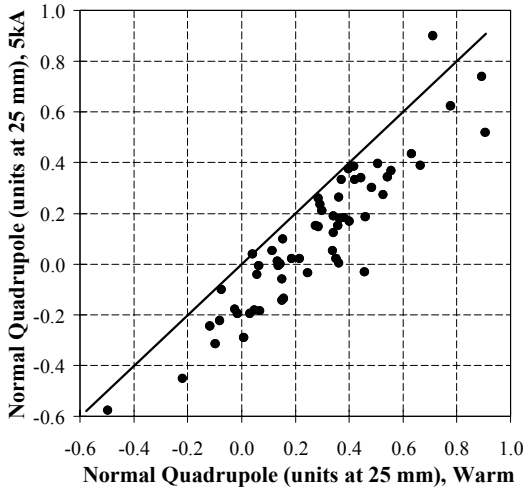

Fig. 3-4. Measured warm-cold normal quadrupole correlation.

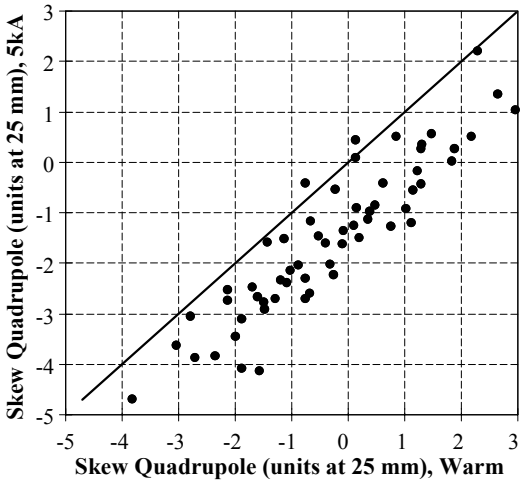

Fig. 3-5. Measured warm-cold skew quadrupole correlation.

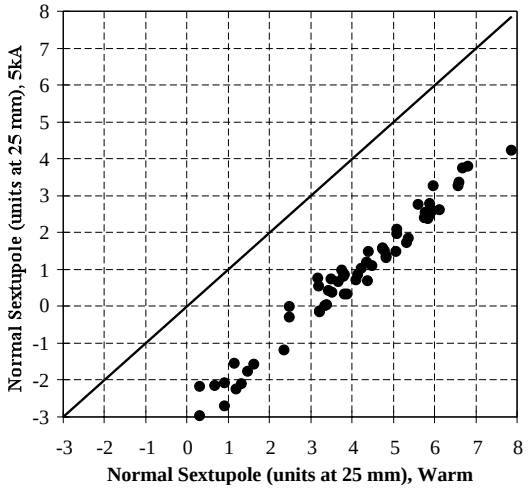

Fig. 3-6. Measured warm-cold sextupole correlation.

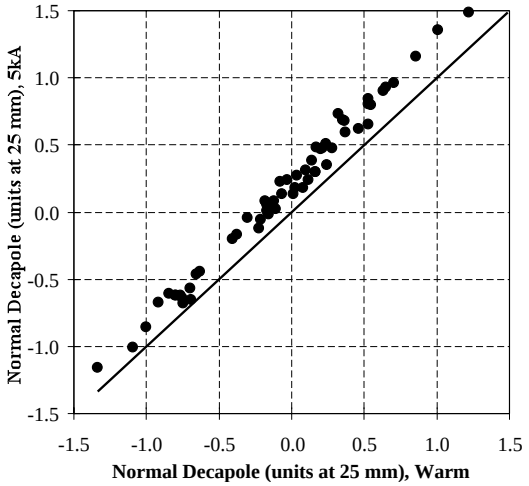

Fig. 3-7. Measured warm-cold decapole correlation.

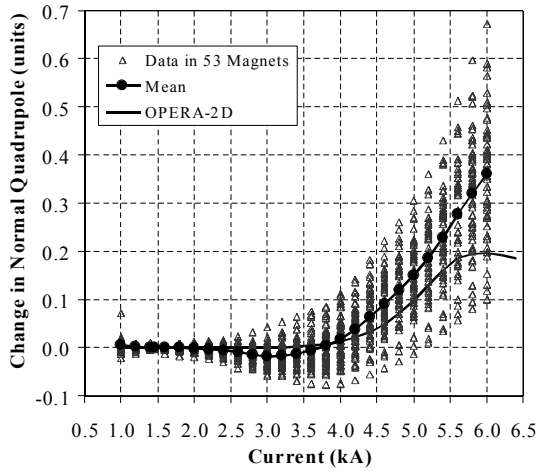

Fig. 3-8. Current dependence of the normal quadrupole component in the 80 mm dipole.

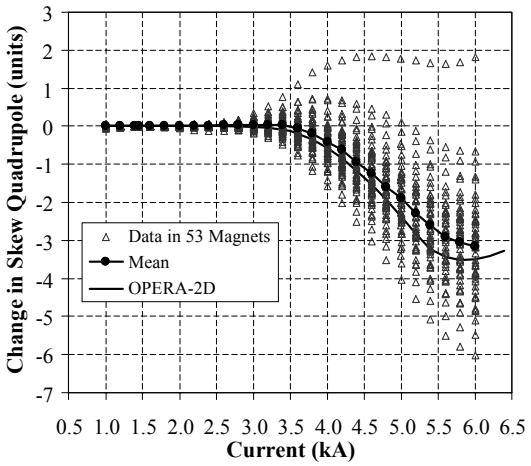

Fig. 3-9. Current dependence of the skew quadrupole component.

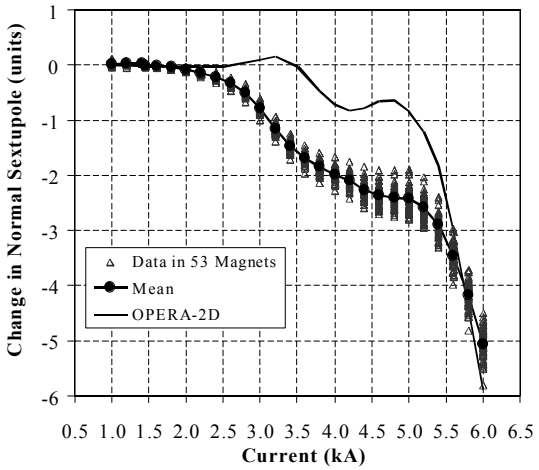

Fig. 3-10. Current dependence of the normal sextupole component.

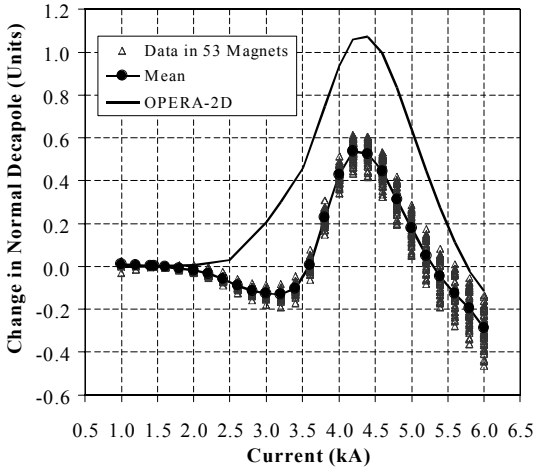

Fig. 3-11 Current dependence of the normal decapole component.

Table 3-7. Summary of the measured integral field harmonics in the 80 mm aperture, 9.7 m long dipoles. The 30 A measurements were done while the magnet was at room temperature. Harmonic b_1 is the normal quadrupole term.

Harmonic	Mean			Standard Deviation		
	30 A (296 magnets)	660 A (58 magnets)	5000 A (59 magnets)	30 A (296 magnets)	660 A (58 magnets)	5000 A (59 magnets)
b_1	0.25	0.08	0.10	0.37	0.28	0.28
b_2	3.54	-0.17	0.83	1.74	2.22	1.76
b_3	-0.03	0.00	0.01	0.10	0.08	0.08
b_4	0.22	-0.33	0.15	0.44	0.57	0.59
b_5	0.01	0.00	-0.03	0.03	0.03	0.04
b_6	0.12	-0.13	1.19	0.11	0.13	0.14
b_7	0.00	-0.01	-0.01	0.01	0.01	0.01
b_8	0.09	0.14	0.12	0.11	0.12	0.12
b_9	0.00	0.02	0.02	0.01	0.02	0.02
b_{10}	-0.53	-0.58	-0.58	0.02	0.02	0.02
a_1	-0.20	0.28	-1.51	1.62	1.53	1.51
a_2	-1.11	-1.03	-1.07	0.20	0.17	0.18
a_3	-0.01	-0.03	-0.36	0.49	0.42	0.41
a_4	0.18	0.21	0.20	0.07	0.06	0.06
a_5	-0.01	0.02	-0.06	0.17	0.15	0.16
a_6	-0.11	-0.10	-0.10	0.03	0.02	0.02
a_7	0.00	-0.01	-0.01	0.05	0.05	0.05
a_8	0.02	0.02	0.02	0.01	0.01	0.01
a_9	0.00	0.04	0.04	0.01	0.02	0.02
a_{10}	-0.01	-0.01	-0.01	0.00	0.01	0.01

The rms variation of the integral transfer function B/I measured warm in all the 9.7 m dipoles was 3.2 $x10^{-4}$. The distribution of the ratio between the integral transfer functions measured warm and at 1.45 kA had an rms of 1.8 x 10^{-4}. A measurement of the transfer function in the straight section of the magnet whose transfer function is closest to the mean is shown in Fig. 3-12. The mean systematic twist of the dipoles was 0.6 mrad, with a rms of 2.2 mrad.

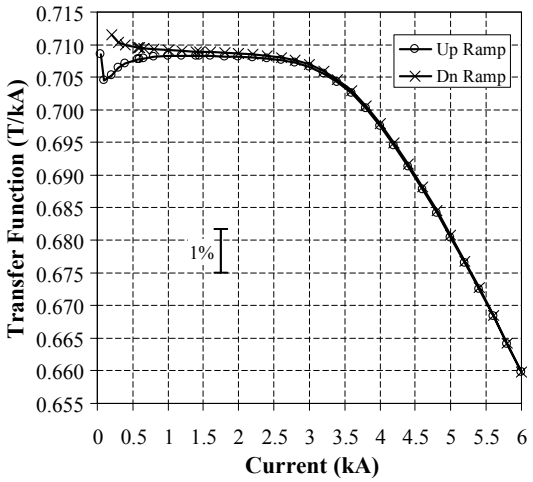

Fig. 3-12. Transfer function for a typical 80 mm dipole in the straight section.

The time dependence of the 80 mm dipoles was determined from measurements in one of the 2.95 m-long magnets built for the D6 and D9 positions (see Table 1-1). The measurements were focussed on the time dependence during injection and at the start of the ramp up [JA00]. The 1 m tangential measuring coil was located in the straight section of the magnet. Measurements were made with a time resolution of ~ 0.66 sec. A smooth current ramp with a quadratic dependence of current on time was used. Prior to the measurement, the magnet was cycled from 25 A to 5.1 kA and back to 25 A at 60 A/sec. The magnet was then ramped to 470 A at 40 A/sec, held at that current, and then ramped up at 40 A/sec. The time variation of the transfer function and the current for injection and the initial part of the ramp up are shown in Fig. 3-13. The change of the transfer function at injection current and the "snapback" at the start of the ramp can be seen in the data. The drift and snapback of the sextupole were ~ 1.5 units. The snapback to the initial value occurs when the current has increased from 470 A to ~ 498 A. The snapback is faster at higher ramp rates (~ 5-6 sec at 20 A/sec, ~ 2 sec at 70 A/sec.). Because the superconductor was purchased as a single lot, it was expected that magnets of the same type would behave in a similar way. This was confirmed by measurements made on the RHIC beam [FI00].

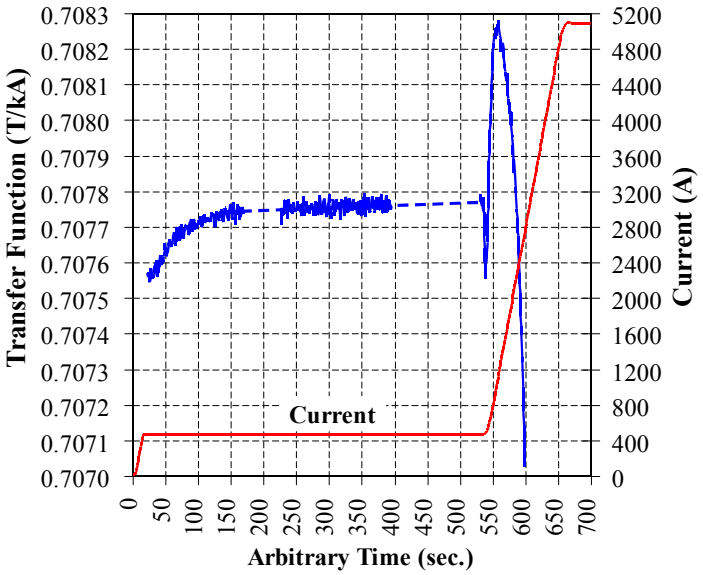

Fig. 3-13. Time decay and snapback in D96525.

iv. Standard Aperture Quadrupoles

The two rings require 276 arc quadrupoles and 144 insertion quadrupoles of standard 8 cm aperture. The magnetic length of the arc quadrupoles is 1.11 m and of the insertion quadrupoles Q4 1.81 m; Q5, Q6, Q8, Q9 1.11 m; Q7 0.93 m.

There are strong economic and technical reasons for maximizing commonality of the designs for all the magnet types; thus the quadrupole is based as much as possible upon the dipole design discussed above. Parameters which have been chosen to be identical are: 1) superconducting cable; 2) operating current; 3) cryogenic design; 4) beam tube; 5) one-layer coil; 6) coil radii; and 7) yoke assembly.

The arc quadrupoles, sextupoles, correctors, and beam position monitors need to be accurately located with respect to the beam and relative to each other. For this reason, they are designed to form one rigid mechanical assembly, as shown in Fig. 4-1 . All insertion quadrupoles have a corrector package, and half of the Q9 insertion quads also have a sextupole magnet.

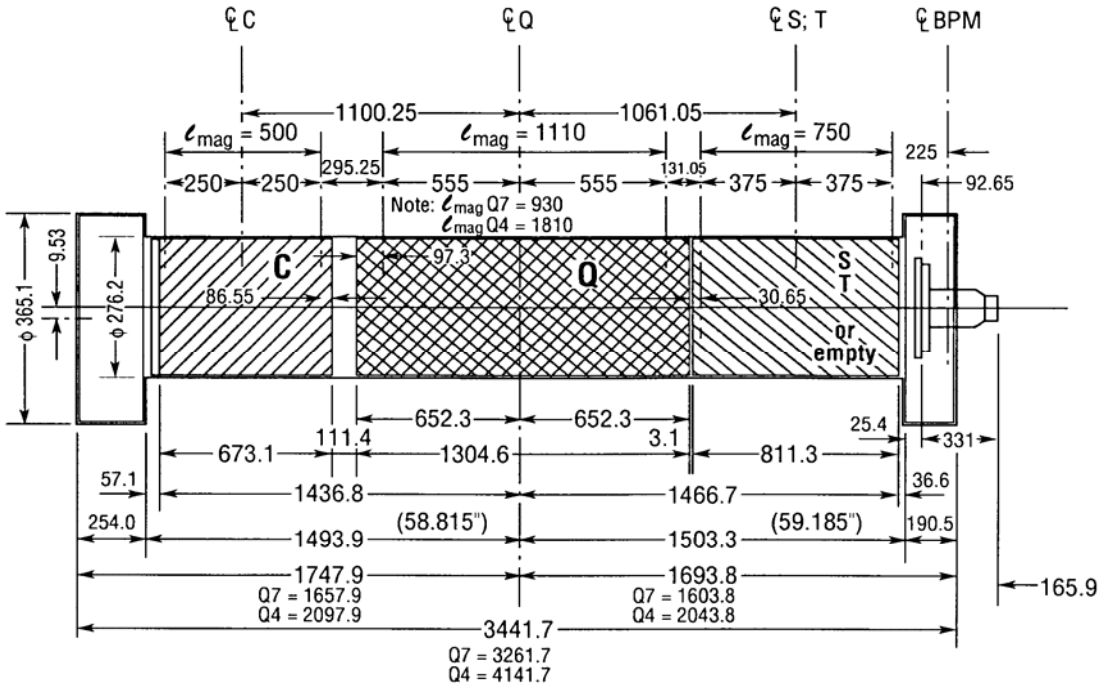

Fig. 4-1. Corrector, quadrupole, sextupole (CQS) assembly. Lamination length is shown (dimensions in mm).

The quadrupole coil design is based on a single-layer "cosine two-theta" coil, wound from a partially keystoned, 30-strand NbTi superconducting cable and mechanically supported by a laminated "cold steel" yoke encased in a cylindrical stainless steel helium containment vessel which is common to the corrector and sextupole. The helium vessel is also a load-bearing part of the yoke assembly. This cold mass assembly is mounted within a cryostat consisting of a cylindrical vacuum vessel, an aluminum heat shield, blankets of multilayer thermal insulation, cryogenic headers, and the magnet support system. Figure 4-2 shows a cross-section of the quadrupole magnet proper or "cold mass." The principal arc quadrupole parameters are given in Table 4-1. The nominal arc gradient requirement is ~71 T/m at top energy, which is obtained with a current of 4.72 kA. The insertion quadrupoles require up to ~6% higher gradients. Larger tuning capabilities are provided by trim quadrupoles at Q4, Q5, Q6.

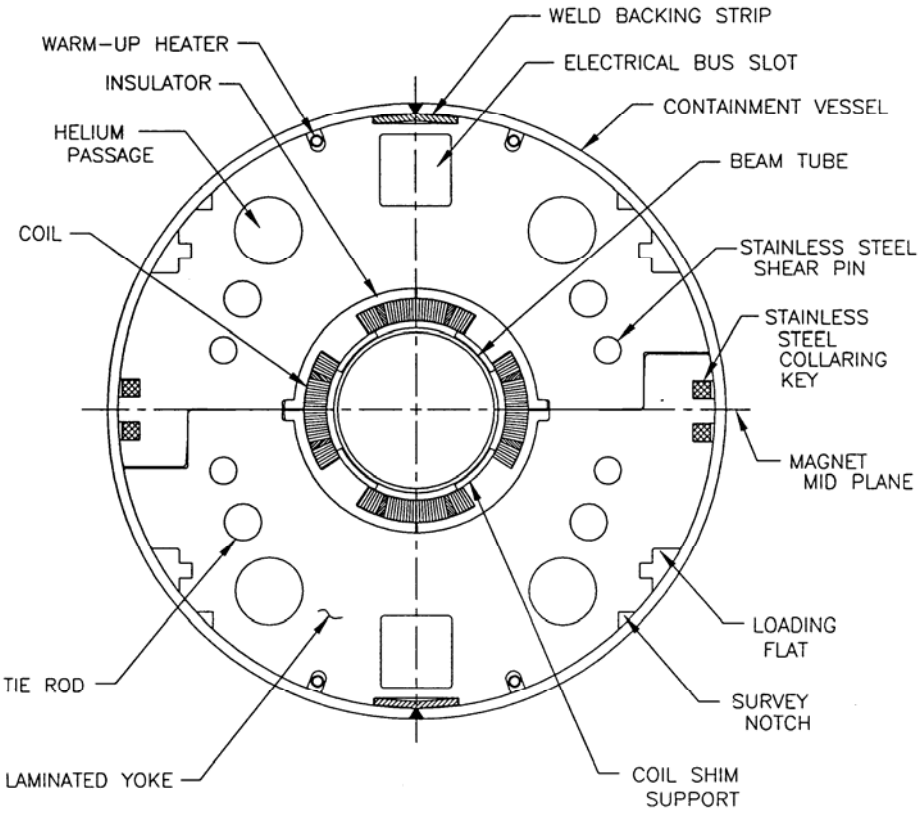

Fig. 4-2. RHIC Arc Quadrupole cross-section (coil i.d. = 79.9 mm).

Table 4-1. Standard Aperture Quadrupole Design Parameters

Coil i.d.	(3.146 in.) 79.9	mm
Coil o.d.	(3.938 in.) 100.0	mm
Number of turns per pole	16	
Number of turns, 1st block (closest to pole)	6	
Number of turns, 2nd block	10	
Wedge angle, bare	13.6	deg
Wedge height, bare	(0.396 in.) 10.06	mm
Effective cable mid-thickness with insulation under compression	(0.05292 in.) 1.344	mm
ARC QUADRUPOLES		
No. quadrupoles, arc	276	
Gradient, @ top energy	~71	T/m
Current, @ top energy	4.72	kA
Gradient, quench	107	T/m
Current, quench	7.65	kA
Magnetic length, arc	1.11	m
Lamination length	(48.4 in.) 1.23	m
Coil length, overall	(48.75 in.) 1.24	m
Coil length, straight section	(39.78 in.) 1.010	m
Cable length per magnet	(504 ft) 154	m
Cable mass per magnet	(27.8 lb) 12.6	kg
Cold mass, CQS package	(2091 lb) 948	kg
Inductance	~2	mH
Stored energy at top energy	20	kJ
INSERTION QUADRUPOLES		
No. quadrupoles, 1.81 m - Q4	24	
0.93 m - Q7	24	
1.11 m - Q5, Q6, Q8, Q9	96	
Gradient @ top energy, Q4, Q5, Q6	75.5	T/m

The quadrupole utilizes a cold stainless steel beam tube of ~69 mm inner diameter. The beam tube design for the CQS package follows the dipoles, except that bumpers are not used because the CQS assembly is straight. The superconducting coil is assembled from quarter-coils that are wound on automated machinery and then formed into a specified size in a precision molding operation - much like the dipole coils. It consists of a single layer of 16 turns per quarter-coil arranged in two blocks with an intervening copper wedge; the size and positions of the wedge and the coil pole spacer have been designed to result in a single-layer coil with field harmonics meeting the rigid field quality specifications required for RHIC. The conductor is the same as that used in the arc dipoles. The cable is insulated with two 50% overlap layers of Kapton film coated with a polyimide adhesive.

The quadrupole yoke design follows directly the dipole design. The yoke laminations are punched from 6.35 mm thick low-carbon steel plate. The lamination surface is phosphate treated. During magnet assembly, a press is utilized to load the coil-in-yoke assembly; it is subsequently held together with stainless steel keys on the outer steel surface to the design preload at room temperature of nominally 69 MPa acting on the coils. After completion, the quadrupole cold mass assembly, together with the sextupole and corrector cold mass assemblies, is inserted snugly into the two halves of a 4.9 mm thick, split stainless steel shell which is then welded along the vertical midplane. The welding operation forms the outer, high-pressure (2.1 MPa) helium containment vessel. This vessel also gives the structure its rigidity and maintains the relative alignment of the component cold masses, which is established by fixturing during the welding operations. This overall assembly is referred to as the CQS cold mass assembly. The CQS assembly is mechanically similar to the dipole assembly, performed with much the same tooling; the principal difference is that the CQS assembly is straight, with no sagitta. The shrinkage of the welds on solidification causes compression of the steel collar blocks, relieving the stress on the keys. Additional compression of the blocks is caused by differential contraction of the stainless steel shell relative to the steel yoke. Since the yoke is completely closed during keying, the coils do not experience any of this increased compressive force.

The design requirements for quadrupole beam tube, yoke, and yoke containment shell are given in Table 4-2.

Table 4-2. Quadrupole Beam Tube, Yoke, and Yoke Containment Shell Parameters

CQS BEAM TUBE	
Outer diameter, bare	(2.875 in.) 73.0 mm
Wall thickness	(0.077 in.) 1.96 mm
Weight, nominal	(29 lb) 13.4 kg
Beam tube-coil radial gap	(0.133 in.) 3.4 mm
Magnetic permeability, 300 K	< 1.005
ARC QUADRUPOLE YOKE	
Inner diameter	(4.300 in.) 109.2 mm
Outer diameter	(10.500 in.) 266.7 mm
Lamination length	(48.4 in.) 1.23 m
Length, including end plates	(51.36 in.) 1.305 m
Lamination thickness	(0.250 in.) 6.35 mm
Length, lamination packs	(0.500 in.) 12.7 mm
Weight of steel	(773 lb) 351 kg
Bus cavity width, height	(1.25 in.) 31.75 mm
Number of cooling channels	4
Diameter of cooling channels	(1.187 in.) 30.15 mm
YOKE CONTAINMENT SHELL	
Inner diameter (prior to assembly)	(10.516 in.) 267.1 mm
Wall thickness	(0.192 in.) 4.9 mm
Weight of common shell for CQS	(215 lb) 97.5 kg
Assembly prestress - Room temperature	(10 kpsi) 69 MPa
- Cold	> (4.8 kpsi) 33 MPa

All quadrupoles quenched well above their operating current and most reached the conductor limit in a few quenches (Fig. 4-3). Measurements of the integral quadrupole field and the first allowed term are shown for a typical quadrupole in Figs. 4-4 and 4-5 . Measurements of the transfer function during injection and the initial part of the ramp up are shown in Fig. 4-6 for a Q7

quadrupole. Measurement conditions were essentially identical to those for the dipole measurements discussed previously, except that the measuring coil was 0.23 m long. The drift and snapback of the dodecapole were ~ 1.5 units. Field quality data for the quadrupoles are summarized in Table 4-3.

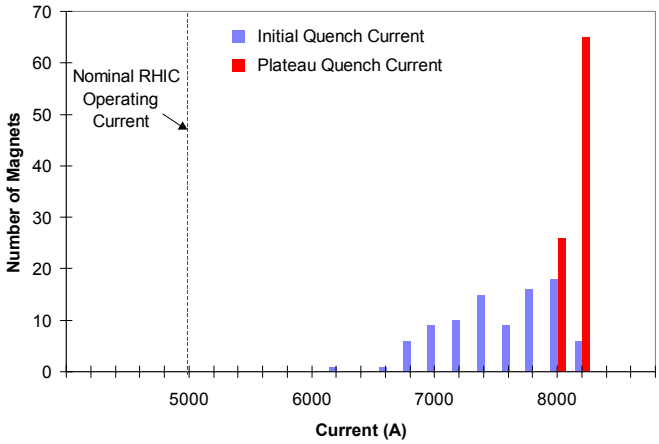

Fig. 4-3. Quench performance of 91 arc quadrupoles, tested at 4.5 K. The average plateau quench current of these 91 magnets was 8152 A.

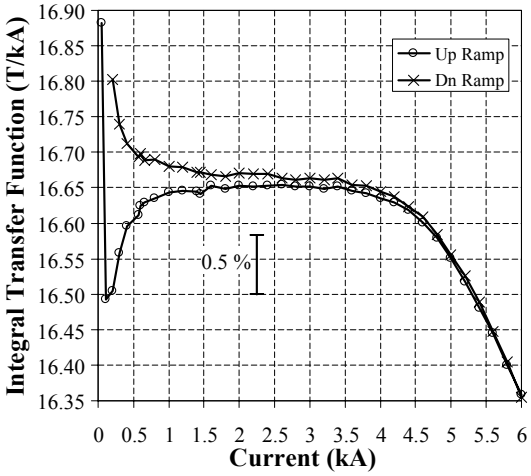

Fig. 4-4. Integral transfer function in QRG316.

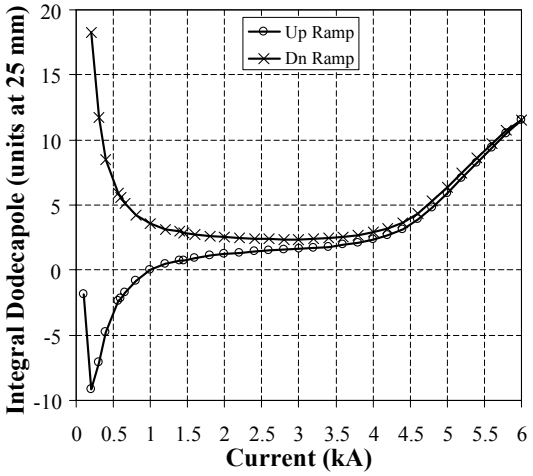

Fig. 4-5. Integral dodecapole in QRG316.

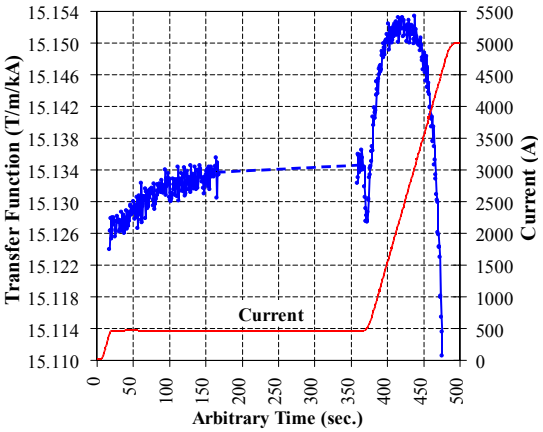

Fig. 4-6. Time decay and snapback in QR7109.

Table 4-3. Summary of Integral Field Quality in RHIC Arc Quadrupoles.

Harmonic at 25 mm	Mean		Standard Deviation	
	10 A (380 magnets)	5000 A (91 magnets)	10 A (380 magnets)	5000 A (91 magnets)
b_2	-0.61	-0.21	1.61	1.77
b_3	-1.51	-0.61	0.95	1.39
b_4	0.14	0.57	0.49	1.57
b_5	1.42	5.70	0.42	0.62
b_6	0.01	0.05	0.13	0.13
b_7	-0.52	-0.52	0.09	0.11
b_8	0.01	0.06	0.05	0.14
b_9	-1.29	-1.44	0.06	0.08
b_{10}	0.00	0.00	0.02	0.02
a_2	-1.93	-1.83	1.66	1.68
a_3	0.48	0.23	0.95	0.90
a_4	0.06	-0.26	0.48	1.40
a_5	-3.76	-3.84	0.29	0.31
a_6	0.04	0.06	0.13	0.14
a_7	0.01	0.04	0.11	0.09
a_8	0.00	0.03	0.05	0.10
a_9	0.35	0.39	0.02	0.04
a_{10}	0.00	0.00	0.02	0.02

v. Sextupoles

Sextupole magnets are required in order to compensate for the natural chromaticity of the machine and to correct for the sextupole field generated in the dipoles, by saturation and superconductor magnetization. The sextupoles have an effective length of 0.75 m and are located at each arc quadrupole and at the Q9 quadrupoles in the 3-4, 7-8 and 11-12 o'clock insertions, resulting in a total number of 144 per ring.

The parameters of the sextupole magnets are given in Table 5-1. The sextupoles must be rather strong, capable of $\int B''dl = 1150$ T/m. This strength makes it desirable to build separate correctors rather than correction coils internal to the dipoles. Because there may be more than the initial two families of these magnets, it is best to design them for a relatively modest current; this reduces the size of the bus work, power supplies and heat leak due to cryogenic feed-throughs. Figure 5-1 shows a cross-section of the sextupole magnet (the cold mass), and Fig. 5-2 shows the pole tip-coil winding configuration in greater detail. The sextupole design uses accurately stamped steel laminations for the yoke and pole tips. The field shape is dominated by the iron, easing the construction tolerances for the coils. The coils are wound from NbTi multifilamentary wire, and the laminated "cold" steel yoke is mounted within a cryostat common to the corrector-quadrupole-sextupole package.

Referring to Fig. 5-1, the sextupole magnet surrounds a cold stainless steel beam tube of standard aperture common to the CQS assembly. The beam tube is welded at one end to a beam position monitor assembly which, in turn, is fastened to the stainless steel end plate of the sextupole yoke; thus, everywhere within the sextupole bore the beam tube fits loosely within the confines of the pole tips. The coils consist of 200 turns of 0.5 mm diameter multifilamentary wire wrapped with 25 μm Kapton insulation with 48% overlay and embedded in a fiberglass/epoxy matrix; they are wound on a machined G-10 form and secured to the pole tips by a scheme employing beryllium copper retainer springs and aluminum locking wedges with intervening G10 insulator strips (Fig. 5-2). The characteristics of the wire are given in Table 2-5.

Table 5-1 . Sextupole Magnet Parameters

No. sextupoles - in arcs	276	
- @ Q9	12	
Magnetic length	0.75	m
∫B″ dl @ 100 A	1150	T/m
∫B (25 mm) dl @ 100 A	0.360	T·m
Maximum operating current	100	A
Quench Current	200	A
Burnout current	250	A
Coil, number of turns	200	
Wire diam., bare	(0.020 in.) 0.5	mm
Coil length, overall	(32.0 in.) 0.81	m
Inductance @ 100A	530	mH
Stored energy @ 100A	2.64	kJ
Yoke, iron length	(31.94 in.) 0.81	m
Yoke, length inc. end plates	(32.25 in.) 0.82	m
Yoke, o.d.	(10.5 in.) 266.7	mm
Yoke, inscribed diam.	(3.070 in.) 78	mm
Lamination thickness	(0.0598 in.) 1.519	mm
Weight of steel	(550 lb) 249	kg
Number of cooling channels	4	
Diameter of cooling channels	(1.187 in.) 30.15	mm
Bus cavity width, height	(1.25 in.) 31.75	mm

The yoke laminations are stamped from 1.5 mm thick low-carbon steel sheet. They have the same external configuration as the quadrupole laminations. Assembly and alignment is as described for the arc quadrupole, with which the sextupole and corrector share a common support structure and helium containment vessel.

The cryostat is the structure which must make the transition from the 4 K environment of the magnet cold mass to ambient temperature; the sextupole, quadrupole, and corrector are mounted in one common cryostat.

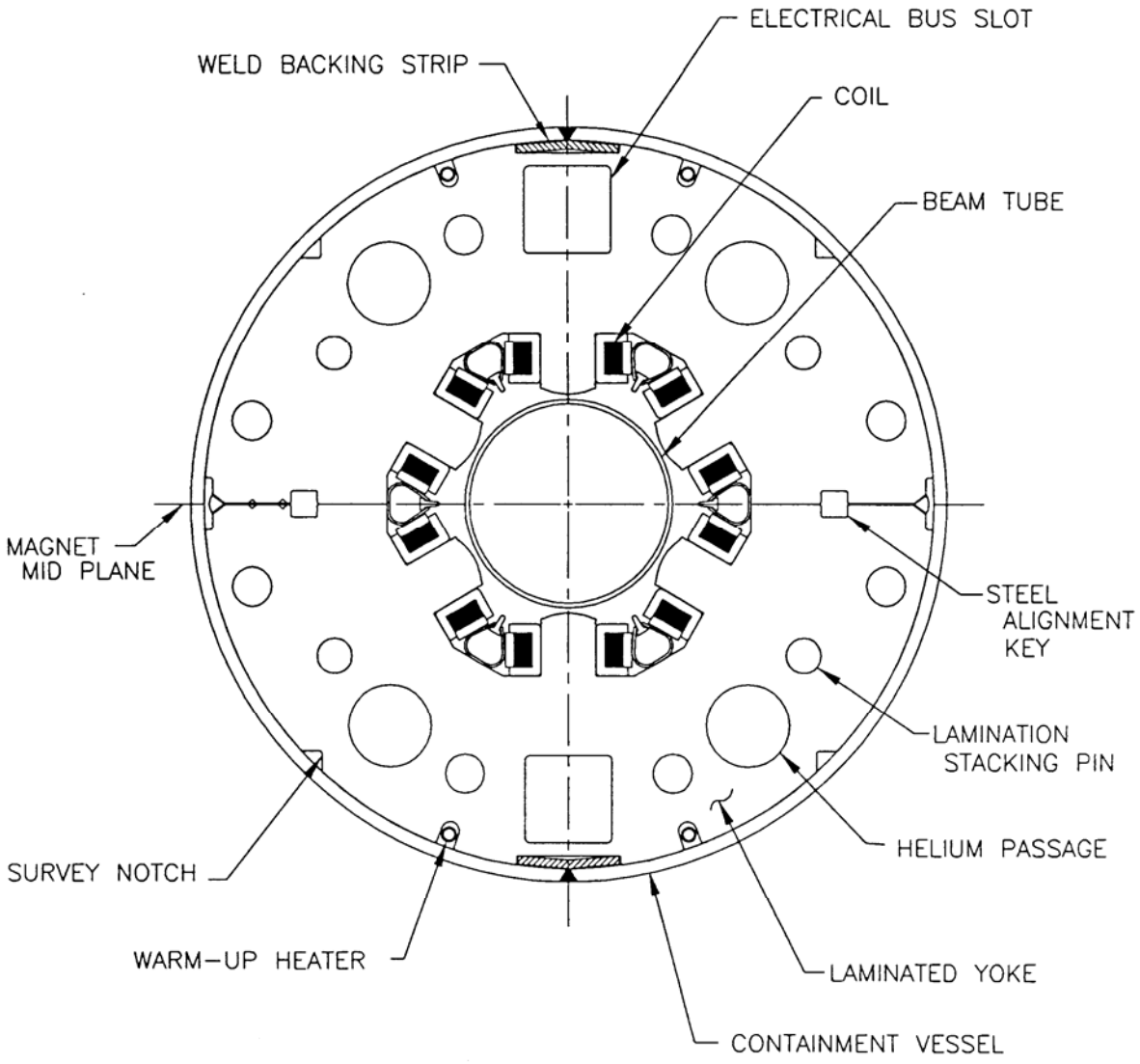

Fig. 5-1. Arc sextupole cross-section (yoke i.d. = 78 mm).

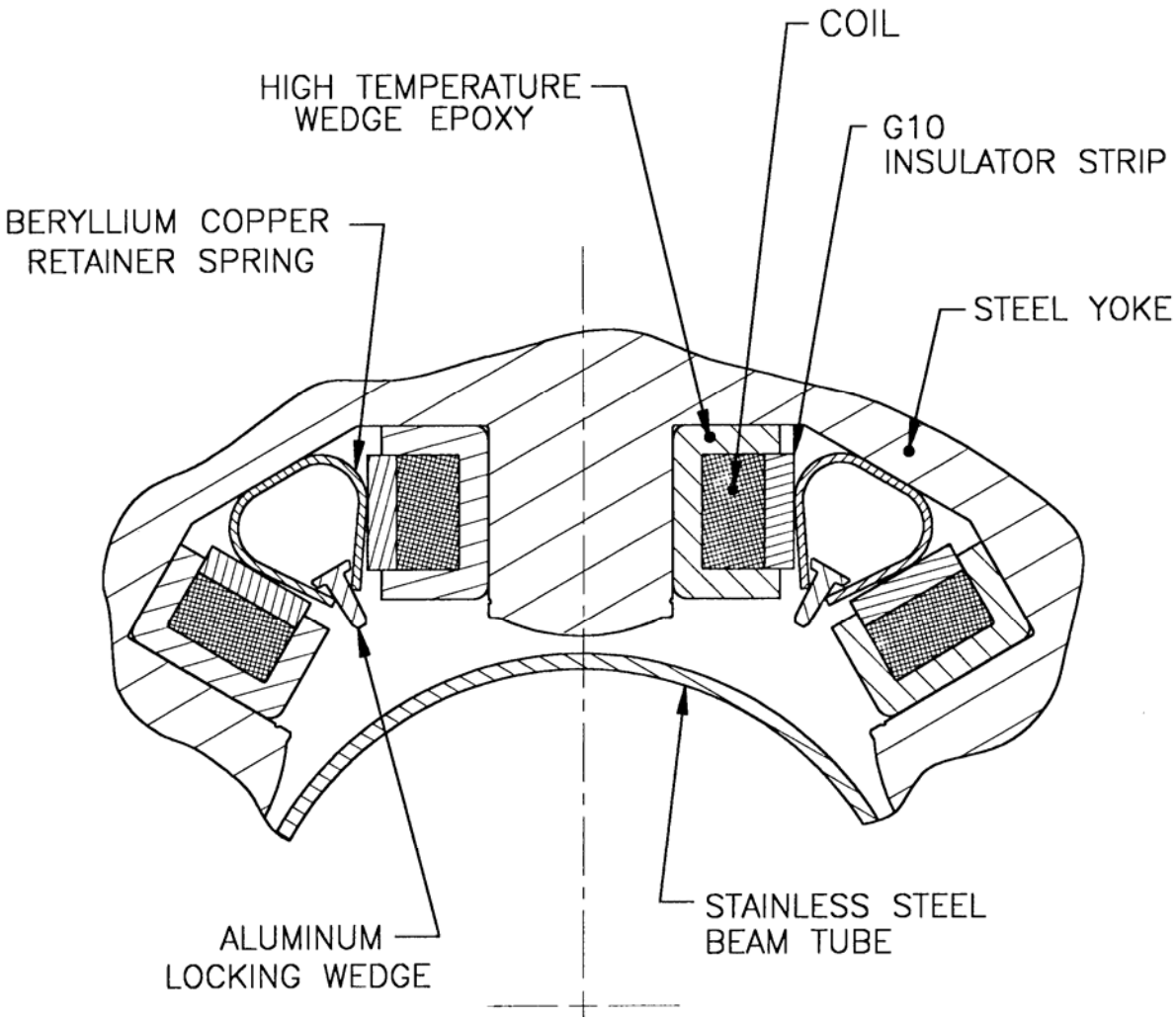

Fig. 5-2. Sextupole details.

The quench performance of sextupoles built as prescribed was excellent, with the magnets usually reaching the limit of the conductor in a few quenches, in both polarities. However, the quench performance of about 30 magnets was poorer, although adequate for operation at currents below 50 A. The cause of the problem was traced to an unauthorized change in production procedures. Fortunately, places were found in the lattice where the operating current was not expected to exceed 50 A. Thus far, no sextupole has quenched in RHIC.

The integral transfer function for a typical sextupole is shown in Fig. 5-3. The saturation of the pole tip is responsible for the decrease of the transfer function at high current and is in agreement with calculation. The large value (~1%) of the first allowed harmonic (Fig. 5-4) is a consequence of the simplicity of the coil construction and is acceptable for these magnets.

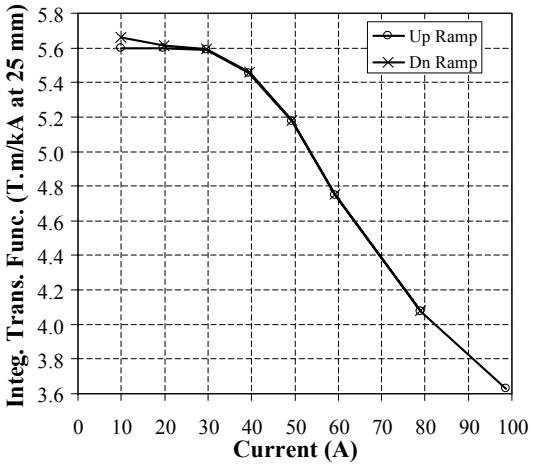

Fig. 5-3. Integral transfer function in SRE211.

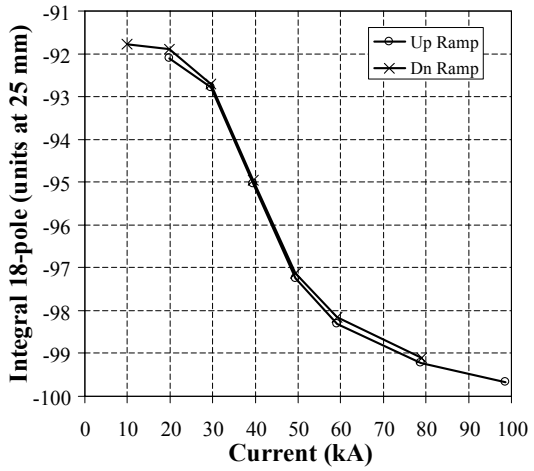

Fig. 5-4. Integral of the first allowed harmonic (b_8) in SRE211.

vi. Trim Quadrupoles

There are no sextupole magnets in the 8 cm aperture CQS assemblies 4 through 8 in the insertion region. The space normally occupied by sextupoles in CQS assemblies 4, 5 and 6 is used for individually powered trim quadrupoles. The construction of the trim quadrupole cold mass is substantially the same as that of the sextupole cold mass. The wire to be used is identical; its parameters are given in Table 2-5. The number of turns is the same and the winding profile of the coils is similar. There are four coils required for each trim quadrupole cold mass. These fit around the four poles of the trim quadrupole yoke. At a radius beyond that of the coil/yoke poles, the yoke cross section is identical to that of the sextupole cold mass. The low carbon steel laminations making up the yoke must be accurately stamped, because the field shape in these magnets is dominated by the iron, relieving the construction tolerances for the coils. The coil and yoke lengths are the same for the trim quadrupole cold mass as for the sextupole cold mass. The coils are held in place in the slots in the steel stampings by thin, beryllium-copper springs between the coil and the pole on each side, expanding the coil in the direction of the Lorentz force against the slot wall.

Figure 6-1 shows a cross section of the trim quadrupole cold mass. The parameters of the trim quadrupole cold mass are given in Table 6-2.

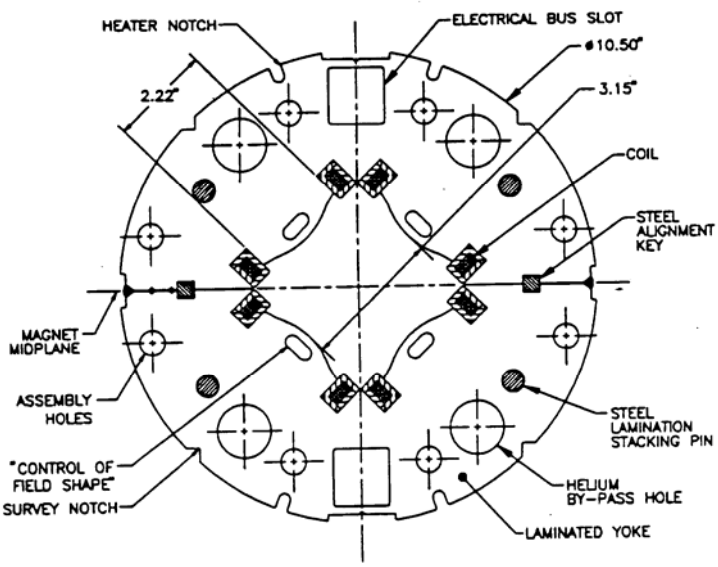

Fig. 6-1. Cross section of the trim quadrupole cold mass. All lamination dimensions outside the pole area are identical to those in the sextupole lamination.

Table 6-1. Design Parameters for the 80 mm Aperture RHIC Trim Quadrupole

GENERAL		
Total number required	72	
Gradient @ 100 A	29.4	T/m
Transfer function @ 100 A	28.3	$G \cdot cm^{-1}/A$
Nominal operating current	100	A
Quench current	182	A
Inductance @ 100 A	590	mH
Effective length	0.75	m
Stored energy @ 100 A (kJ)	3	
COIL		
Number of turns	200	
Coil length, overall	(31.9 in.) 0.81	m
Final molded coil width	(3.03 in.) 77.0	mm
Length of wire per coil, estimated	(14400 in.) 366	m
Wire diameter, bare	(0.020 in.) 0.5	mm
YOKE		
Pole width	(2.22 in.) 56.39	mm
Length of stacked laminations	(31.9 in.) 0.81	m
Weight of steel	(550 lb) 249	kg
Outer diameter	(10.5 in.) 266.70	mm
Lamination thickness (16 gauge)	(0.060 in.) 1.5	mm
(18 gauge)	(0.048 in.) 1.2	mm
Number of helium by-pass holes	4	
Diameter of helium by-pass holes	(1.187 in.) 30.15	mm
Bus cavity width & height	(1.25 in.) 31.75	mm

The quench performance of the trim quadrupoles was excellent, with the magnets reaching the conductor limit in a few quenches. The transfer function (Fig. 6-2) and first allowed harmonic (Fig. 6-3), plotted for a typical magnet, show a saturation behavior similar to but smaller than that of the sextupole.

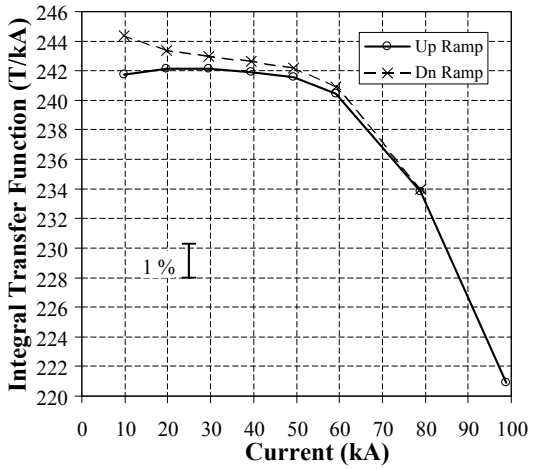

Fig. 6-2. Integral transfer function in trim quadrupole QRT148.

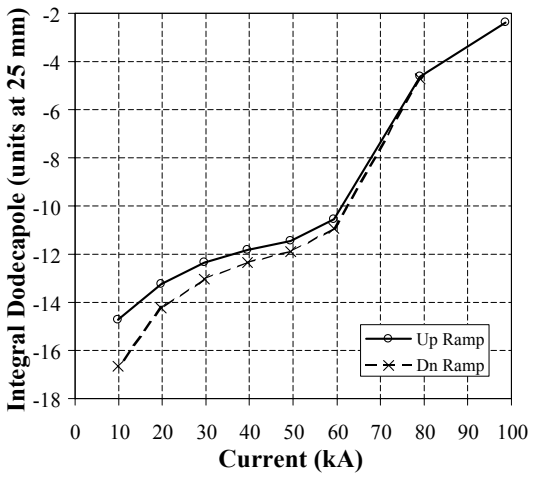

Fig. 6-3. Integral of the first allowed harmonic (b_5) in trim quadrupole QRT148.

vii. Standard Aperture Corrector Magnets

Corrector/trim magnets will be provided at each quadrupole in the arcs, as well as in the insertions (except at Q1 whose corrector is attached to Q2) to compensate for systematic and random errors of the magnets and to control various beam dynamic properties as discussed in the Lattice and Beam Dynamics section.

The correctors have the same aperture as their quadrupoles implying the count of 420 standard-aperture (i.e. 8 cm) correctors and 72 large aperture (i.e. 13 cm) correctors.

Standard Aperture Correctors

The 8 cm correctors are nominally 0.5 m in effective length and are an integral part of the CQS package. They contain either four multipole elements (132 per ring) or a lone dipole element (78 per ring). The following 8 cm quadrupole-corrector combinations are required for the two rings

- b_0, b_1, b_3, b_4 @ 96 QF
- b_0, a_1, b_3, b_4 @ 36 QF
- a_0, a_1, b_3, b_4 @ 132 QD
- b_0 @ 78 QF
- a_0 @ 78 QD

The dipole correctors correct the closed orbit error resulting primarily from random dipole rotational errors and quadrupole misalignments around the ring, necessitating individual current control in each corrector. For this reason, a design using relatively low current has been adopted; this reduces the size of the electrical bus work, power supplies and heat leaks in cryogenic current leads. The normal quadrupoles are used for the gamma-transition jump. The skew quadrupole correctors correct: 1) the effect of random skew quadrupole errors in the dipole, an effect which can be reduced and perhaps eliminated by a shuffling/sorting procedure, and 2) random installation errors in the quadrupoles. The decapole correctors compensate for dipole iron saturation effects. The octupole correctors are used for the correction of second order chromaticity effects; b_4 will remain initially without power supplies.

Figure 7-1 shows a cross-section of the four-element arc corrector magnet (the "cold mass"), and Fig. 7-2 shows the cross-section in greater detail. The magnet utilizes a cold stainless steel beam tube of ~69 mm inner diameter common to the CQS assembly. In radially increasing order, the coil structures are decapole, octupole, quadrupole, and dipole coils, respectively. Each of the

inner three structures consists of a double layer of racetrack coils wound with superconducting wire, with one coil per pole. The outermost winding, the dipole, has three double layers of superconducting wire arranged to minimize field harmonics. Each double layer is wound on a flat, flexible substrate using the specially developed technology which incorporates the MULTIWIRE process. Subsequently,

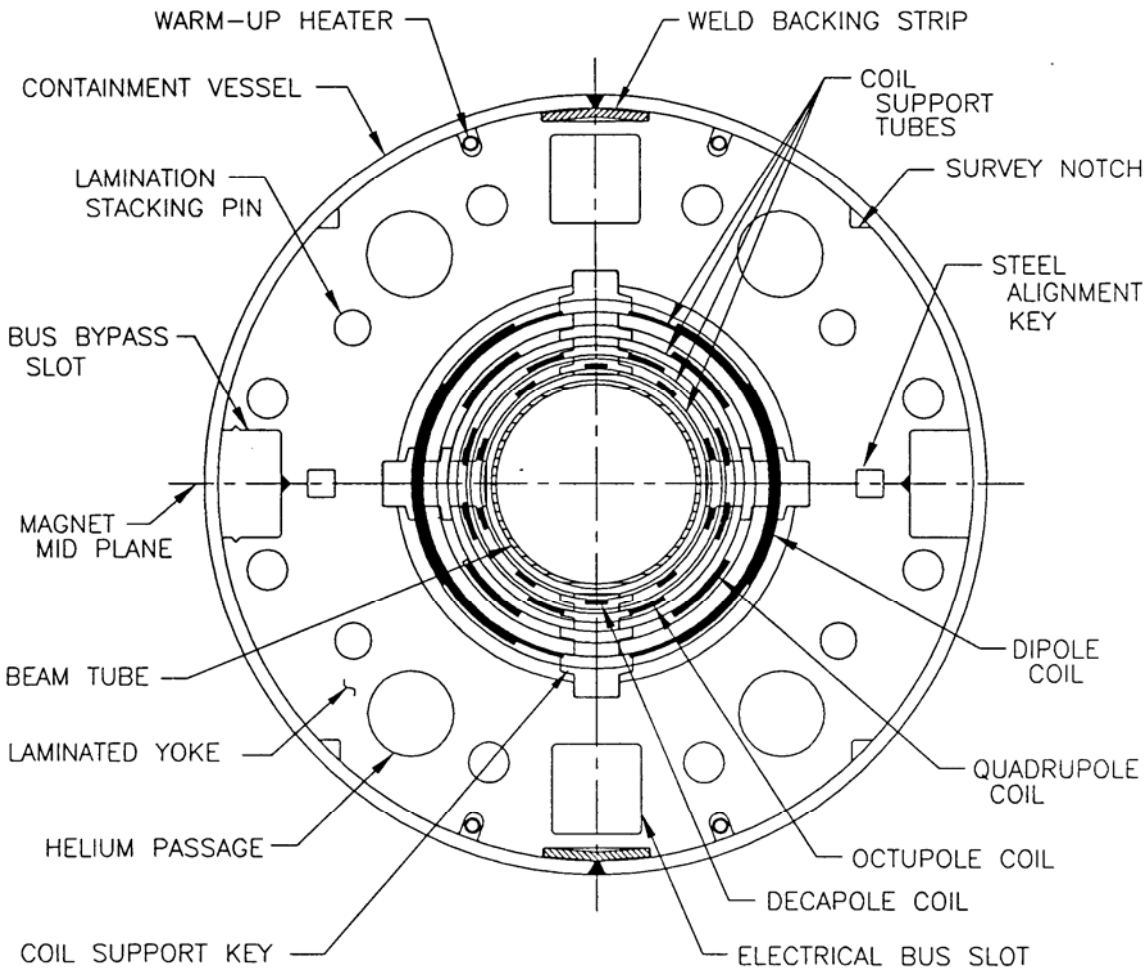

Fig. 7-1. Arc corrector cross-section (beam tube i.d. = 69 mm).

the substrate is epoxy-bonded to a stainless steel support tube which is previously wrapped with Kapton and fitted with aluminum locating pins. The wire is a multifilamentary NbTi composite wire, the parameters of which are given in Table 2-5.

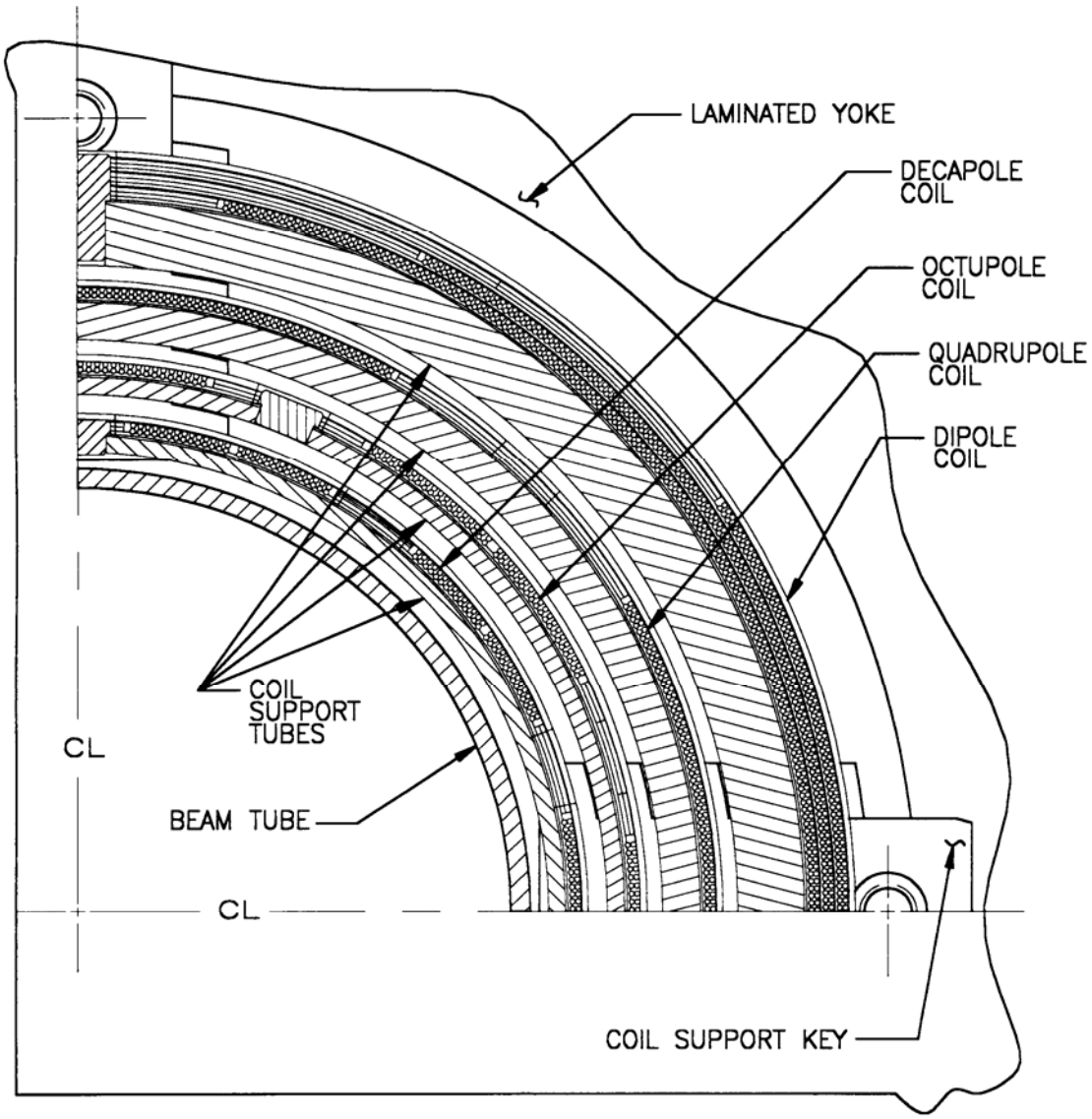

Fig. 7-2. Arc corrector coil cross-section (beam tube i.d. = 69 mm).

Table 7-1. Standard-Aperture Corrector Magnets

Number of correctors, arc and Q9	300	
Number of insertion correctors	120	
Effective length, nominal*	~0.5	m
Coil length, nominal*	(~23 in.) ~580	mm
Wire diameter	(0.013 in.) 0.33	mm
Length, lamination	(26.50 in.) 0.673	m
Outer diameter	(10.50 in.) 266.7	m
Weight of steel	(430 lb) 195	kg
Lamination thickness	(0.0598 in.) 1.519	mm
Number of cooling channels	4	
Diameter of cooling channels	(1.187 in.) 30.15	mm
Bus cavity width, height	(1.25 in.) 31.75	mm

*For exact values see Tables 7-2 and 7-3.

The beam tube fits loosely within the bore of the decapole coil support tube. It is actually the end portion of a continuous beam tube for the corrector-sextupole-quadrupole (CQS) package. It is fixed at one end to a beam position monitor located near the far end of the sextupole magnet; the other end of the beam tube is secured outside the end of the corrector magnet.

The major standard-aperture corrector design parameters are given in Table 7-1. The physical length of the various coils is nominally 0.58 m, a length short enough that the stainless steel support tubes can be supported solely at their ends. The tube diameters were selected from commercially available standard size to minimize machining. The dipole and quadrupole support tube thicknesses were chosen to give acceptable distortions due to the predicted magnetic forces, and the octupole and decapole support tube thicknesses were determined by machining requirements. The end support is provided by separators, four at each end, which serve to position the tubes radially, azimuthally, and axially, and which tie into the overall corrector/quadrupole/sextupole support and alignment structures.

Table 7-2. Mechanical Parameters of Arc Correctors coils. All coils are double layers.

Multipole	Support tube o.d. ((in.)/mm)	Turns/Pole	Overall length ((in.)/m)	Wire length (m)
Decapole	(3.231) 82.1	28	(22.980) 0.584	306
Octupole	(3.624) 92.0	38	(22.962) 0.583	359
Quadrupole	(4.126) 104.8	90	(23.016) 0.585	426
Dipole/1	(4.824) 122.5	278	(22.850) 0.580	660
Dipole/2		226		544
Dipole/3		122		307

The yoke laminations are stamped from 1.5 mm thick low-carbon steel sheet. They have the same external configuration as the quadrupole laminations. Assembly and alignment is as described for the arc quadrupole, with which the sextupole and corrector share a common support structure and helium containment vessel.

A summary of the arc corrector coil parameters required for each multipole is given in Table 7-2, and Table 7-3 gives the operating parameters of the corrector magnets. In general, all the correctors are designed to operate conservatively at ~25-33% of their quench limit.

All correctors were quench tested because the conductor consists of a single strand, increasing the consequences of damage to a strand at any stage of production. In particular, careful study indicated that it would be difficult to detect damage during the automated coil winding process. Therefore, all corrector layers except for the dipole were tested to ± 100 A, twice the maximum operating current. Dipoles were tested to ± 70 A, since quenches at higher current could damage the magnet. Correctors other than the dipole were tested in self field and in the background field of the dipole at 70 A. In all, 1229 layers were tested [MU97]. About 2/3 of the layers reached the maximum current without quenching. Seven layers failed during quench test and were replaced.

Table 7-3. Operating Parameters of Arc Correctors

Multipole	Inductance (mH)	I_{op} (A)	B @ 2.5 cm (T)	L_{eff} (m)	I_Q (A)
Decapole	5.0	59.0	0.016	0.575	202
Octupole	8.0	50.6	0.017	0.571	198
Quadrupole	29.0	49.8	0.067	0.555	190
Dipole	840	52.2	0.596	0.508	160

Table 7-4. Integral field quality measured in the 80 mm corrector coils.

Layer Type	Transfer Function, T.m/kA @25 mm (warm)	Std. Dev. in T.F.	Change in T.F. on Cooldown	Harmonics as Fraction of the Fundamental Field
b_0/a_0	5.5549	0.16%	+1.0%	<0.3%
b_1	0.7627	0.18%	+0.7%	<0.6%
a_1	0.7570	0.09%	+0.7%	<0.6%
b_3	0.1920	0.53%	+0.9%	<2%
b_4	0.1494	0.48%	+1.2%	<2%

The correlation between warm and cold field quality measurements was good enough that the only ~20% were measured cold. The data for all the 80 mm correctors are summarized in Table 7-4. The reproducibility of the integral transfer function is typically 0.2%, and the harmonics are at the level expected for a corrector, ~ 1% of the fundamental. The standard deviation of the warm-cold difference in the integral transfer functions is less than 0.1% of the transfer function for the dipole and quadrupole coils and ~ 0.3% for the octupole and decapole coils.

viii. Standard Aperture CQS Assemblies

The CQS assemblies consist of various combinations (over 80 types) of quadrupole, sextupole and corrector elements assembled together into a common cold mass containment and vacuum vessel [MU95a]. The weight of a CQS assembly is typically 948 kg. The quadrupole and sextupole elements were manufactured industrially, the corrector elements were manufactured in-house at Brookhaven. These elements, along with numerous other components, make up the single complete unit for the RHIC ring. Components included are recoolers for the main helium distribution circuit, beam position monitors, power leads for the included corrector magnets [SH93a], and instrumentation and heater leads with the leads exiting the cryostat locally. Special tooling to control the positions and rotations of the elements during assembly, and instrumentation to measure these parameters afterwards [GO93a, TR95a, JA97a], was developed. A special shell-welding technique was developed to remove any excessive residual twist in these assemblies as well as in the larger 130 mm assemblies [CO97a]. Because of their ubiquitous location around the machine, a rigorous analysis of bellows' strength and operational range was performed [SH90a, SH91a]. This analysis describes the bellows required for interconnecting these devices to their neighbors in the rings. Figure 8-1 shows the magnets of a CQS unit on the assembly bench.

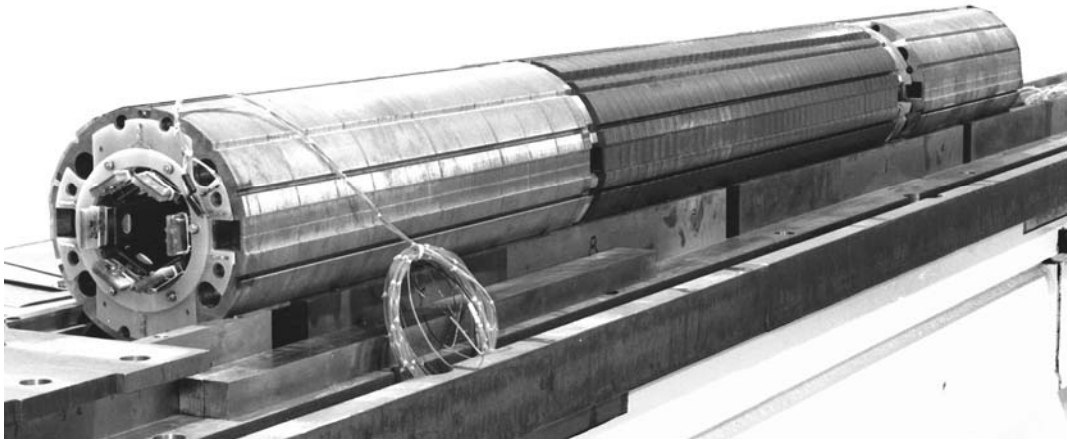

Fig. 8-1. The magnets of a CQS unit on the assembly bench. In the foreground is a sextupole cold mass, followed by quadrupole and corrector cold masses.

The magnetic centers of the CQS elements were measured by two unusual methods: colloidal cell and harmonic antenna. A number of quadrupoles were measured by shining polarized light through a cylindrical glass cell containing a colloidal suspension of iron filings [TR95a]. In a sufficiently strong field, the iron filings lined up along field lines enough to rotate the plane of polarization of the light. The light was viewed through a second filter, which was rotated 90° with respect to the first. The transmitted light produced field patterns that were accurate to ± 50 μm. Because of limitations in this technique, a more versatile device, the harmonic antenna, was developed. With this device, the field center was measured on all three elements of the CQS. The harmonic antenna is a stationary coil, 23 cm long, that senses the fields produced by AC currents in the range 10 – 20 Hz. The coil also has crossed wires mounted precisely across its ends, allowing its position to be surveyed relative to external fiducials to within 0.025 mm. The field center relative to the coil is also determined within 0.025 mm, even in measurements at room temperature [JA97a].

The installation procedure for the CQS called for the centers of the quadrupole and sextupole to be installed on the central beam orbit, so the measurements were analyzed to report the "corrector offset," the distance between the center of the corrector and the beam orbit. After a learning curve, rms corrector offsets of 0.5 mm were achieved [WE96].

To establish the warm-cold correlations, the first 30 CQS units plus 18 of the remaining units were cold tested. For CQS units, the main focus of the correlation is the field angles. For both the quadrupole and the sextupole, the mean warm-cold difference in field angles was –0.2 mrad, with an rms of 0.4 mrad (Fig. 8-2). For dipole correctors, the mean field angle difference was –0.3 mrad with an rms of 0.5 mrad. The centers of the magnetic field were measured warm and cold in one CQS (Fig. 8-3). The field center was measured at three axial positions in the quadrupole and two in the sextupole. The change in vertical position, about 1.75 mm, agrees with the change expected due to thermal contraction. The change in horizontal position is about 0.25 mm.

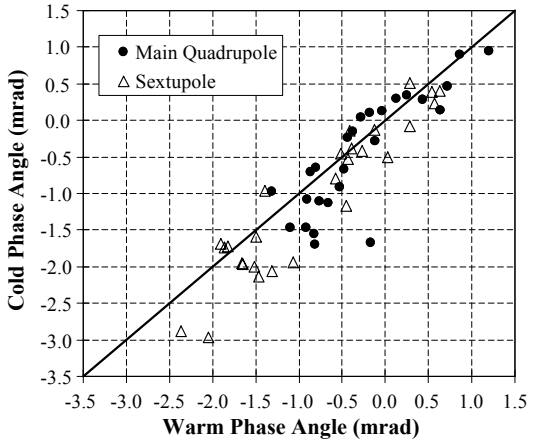

Fig. 8-2. Warm-cold correlations of CQS field angles.

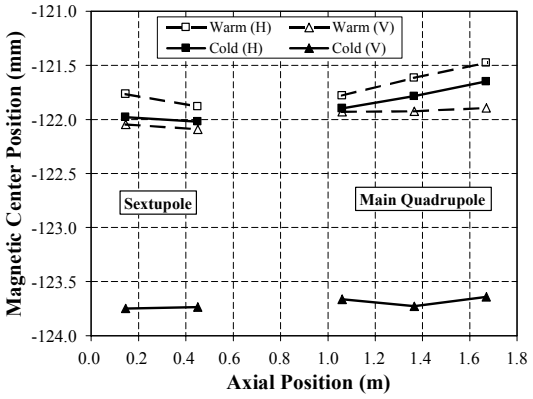

Fig. 8-3. Correlation between warm and cold centers in a CQS assembly.

CQS Cryostat

The cryostat is the structure which must make the transition from the 4 K environment of the magnet cold mass to ambient temperature; the corrector, quadrupole and sextupole (CQS) units are mounted in one common cryostat. In addition, five 50 W "recoolers" per sextant are located under the CQS assembly in the space between the support posts in the 4 K environment. The CQS cryostat design parameters are summarized in Table 8-1. The major components comprising the cryostat are the 6.4 mm thick carbon steel (ASTM A53) vacuum vessel of 610 mm outer diameter, the aluminum heat shield (1100-H14) maintained at nominal 55 K, blankets of multilayer aluminized Mylar thermal insulation, the various cryogenic headers, and the post-type supports which carry the loads generated by the magnet cold masses to the ground. The superinsulation blankets use alternating layers of reflectors (0.25 mil non-crinkled Mylar, aluminized on two sides) and spacers (6 mil REEMAY 2006).

The support posts are the same as used in the arc dipoles. The standard arc CQS assembly is supported by two posts, one located at the sextupole and the other at the corrector. They were precision molded as tubes with flanges from a glass-filled plastic material under the name Ultem 2100. The tubes are in two parts, bolted together at the heat shield. The cold mass is attached to cradles which rest atop each post; the cradles are machined from stainless steel castings. Both cradles are free to move during cooldown; stops on the posts are spaced such that each post is deflected 0.5 mm after cooldown.

The cryostat must accurately position the magnet cold masses to a given point in the accelerator lattice, while at the same time minimizing the refrigeration load. The legs of the vacuum chamber are carbon steel castings. The surfaces of these legs are used to provide the exterior survey fiducial references; survey fixtures will translate the positional information provided by the reference features to a location outside the vacuum tank.

Table 8-1. CQS Cryostat Parameters

Vacuum vessel, outer diameter	(24 in.) 610	mm
Vacuum tank, wall thickness	(0.25 in.) 6.4	mm
Heat shield, outer diameter	(21 in.) 533	mm
Heat shield, wall thickness, upper section	(0.090 in.) 2.29	mm
Heat shield, wall thickness, lower section	(0.125 in) 3.18	mm
Recooler supply header, inner diameter	(2.709 in.) 68.8	mm
Helium return header, inner diameter	(2.709 in.) 68.8	mm
Utility header, inner diameter	(2.709 in.) 68.8	mm
Shield cooling pipe, inner diameter	(2.157 in.) 54.8	mm
Number of supports	2	
Support spacing	(74 in.) 1.88	m
Post, inner diameter	(8.38 in.) 212.8	mm
Post, wall thickness	(0.189 in.) 4.8	mm
Heat leak per leg at 4.5 K	0.1	W
Heat leak per leg at 55 K	1.0	W
Superinsulation layers, cold mass only	17 Reflector, 32 Spacer	
Superinsulation layers, cold mass plus piping	38 Reflector, 53 Spacer	
Superinsulation layers, shield	62 Reflector, 62 Spacer	

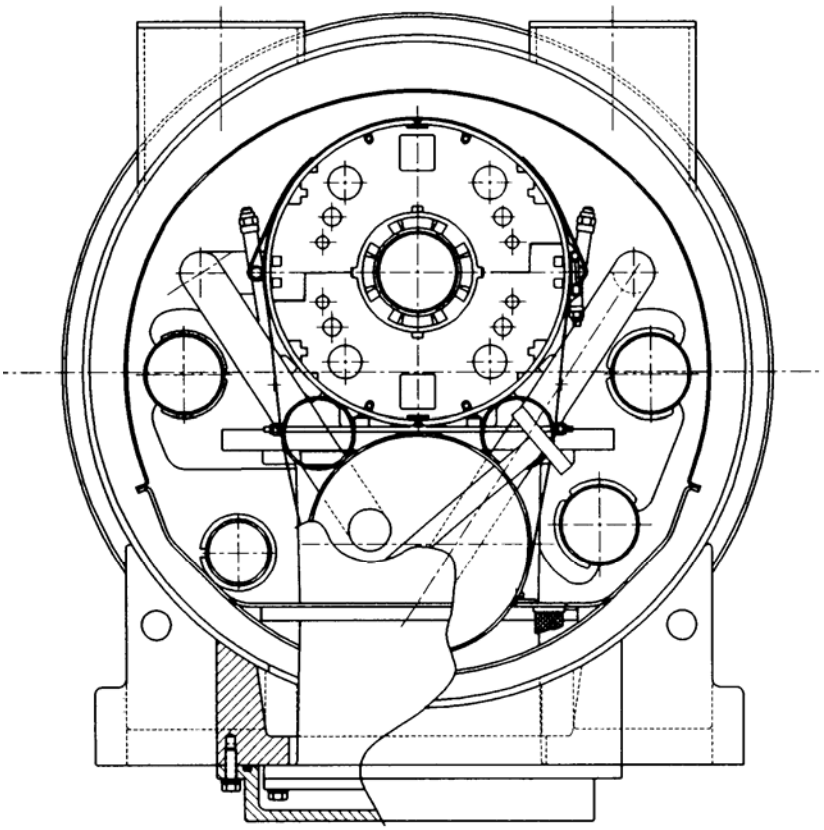

Fig. 8-3. Quadrupole cryostat cross-section, showing recooler.

ix. Large Aperture Correctors

Triplets of large bore, i.e. 13 cm, quadrupoles will be antisymmetrically placed on either side of all six intersection points of RHIC. In RHIC collision optics, the triplets at the two experimental detectors are intended to enable the collision beta function to be reduced to the design goal of $\beta^* = 1$ m in both planes, in order to minimize the spot size and maximize the luminosity. This requires running with $\beta_{MAX} \approx 1400$ m in the triplet, where the beams will have their largest size, both absolutely and as a fraction of the available aperture. Hence, the ultimate performance of RHIC rests on achieving the highest possible magnetic field quality in the triplets. The correction of magnetic errors expected in the quadrupole bodies and ends will be attempted by quadrupole body tuning shims, and by lumped correctors.

The large aperture triplet of quadrupoles Q1, Q2 and Q3 on each side of each crossover has associated with them three correctors, for a total of 36 correctors per ring. One, here called C1, is at the crossover end of Q2, a second, C2 is at the crossover end of Q3 and a third, C3 is at the other end of Q3. All have 4 corrector elements in the following combinations, with numbers given for two rings:

Style I: b_0, b_3, b_4, b_5 @ 12 C1 Outer

Style J: a_0, b_3, b_4, b_5 @ 12 C1 Inner

Style K: a_1, a_3, a_2, a_5 @ 24 C2 Inner & Outer

Style L: b_0, b_3, b_2, b_5 @ 12 C3 Inner

Style M: a_0, b_3, b_2, b_5 @ 12 C3 Outer

Table 9-1. Properties of Large Aperture Correctors

Parameter	a_0/b_0	a_1	a_2/b_2	a_3/b_3	b_4	a_5/b_5
Number	48	24	48	72	24	72
Layers	6	2	2	2	2	2
R outer (mm)	97	95	76	82	76	69
R inner (mm)	93	93	73.5	80	73.5	67
Turns/coil/layer	149	79	41	33	23	17
$\int B \bullet ds$ (T·m)*	0.285	44.6×10^{-3}	20.6×10^{-3}	8.64×10^{-3}	5.19×10^{-3}	4.12×10^{-3}
L (mH)	1710	112	30	26	14	8.6

*@ R_{ref} = 40 mm and I = 50 A.

The nominal magnetic length of these correctors is 0.5 m and each element will have a nominal operating current of 50 A. The iron lamination inner diameter is 200 mm; the overall o.d. is 350 mm. These correctors will use the same type of double-layer multiwire coils used in the arc correctors. Table 9-1 shows the winding packages for each corrector element and other salient parameters.

All of the correctors were quench-tested using the same protocol as for the 80 mm correctors. Three coils out of a total of 315 needed to be replaced. Nearly all of the remaining coils reached the test limit of 100 A (70 A for dipoles) without quenching.

The correctors were shimmed based on warm measurements and warm measured a second time to confirm the effect of the shims. The shimming significantly reduced both the field angle and the off-axis distances of the individual layers. The field angles were adjusted to be within ± 1 mrad of nominal. The alignment relative to the center of the yoke was within ± 0.2 mm. A summary of the field quality measurements is given in Table 9-2 .

Table 9-2. Summary of field quality measured at room temperature in all the 130 mm corrector coils.

Coil Type	Integral Transfer Function (T.m/kA at 40 mm)	Std. Dev. of Integral Transfer Function	Harmonics at 40 mm radius
Dipole	5.572	0.15%	< 0.3%
Quadrupole	0.8792	0.09%	< 0.3%
Sextupole	0.4023	0.12%	< 0.7%
Normal Octupole	0.1686	0.17%	< 1.0%
Skew Octupole	0.1678	0.17%	< 0.7%
Decapole	0.1017	0.15%	< 1.2%
Dodecapole	0.0798	0.45%	< 1.0%

x. Insertion Quadrupoles

Three large-aperture (13 cm) quadrupoles are located on either side of all six of the RHIC crossing points. The three quadrupoles are close together as a "triplet" and perform the final strong focusing for the experiments. Because the transverse beam sizes are at their ring-wide maximum in the experimental triplets when β* is small, the ultimate luminosity performance of RHIC depends both on the optimum arrangement of these quadrupoles, and also on achieving the highest possible magnetic field quality.

In the present lattice, a total number of 72 large-aperture quadrupole magnets are needed in six insertions. The maximum operating gradient required is ~48 T/m and the magnetic length is 1.44 m in 24 Q1, 3.40 m in 24 Q2, and 2.10 m in 24 Q3 quadrupoles. The outer dimensions of these quadrupoles are determined by the beam spacing at the entrance of the first two quadrupoles on either side of the crossing point. The minimum radial separation between the inner and outer beams at Q1 is 424 mm.

Basic Design Parameters

Table 10-1 summarizes the basic design parameters of the large-aperture quadrupoles. Following are some basic design features which were developed after optimizing the magnetic and mechanical design of this quadrupole:

A circular iron yoke with an outer diameter of 350.5 mm (363.2 mm including the shell) is used in these quadrupoles. This leaves a minimum separation of ~61 mm between the inner and outer Q1 quadrupoles.

Coil pre-compression is obtained by pressing and keying the yoke halves.

The single layer coil uses the 36-strand cable developed for the outer layer of the SSC 50 mm aperture dipole magnet. The parameters of this cable are given in Tables 2-3 and 2-4.

An RX630 spacer is used between the coil and the yoke, just as it is used in the arc dipole magnets. The azimuthal position of the coil is defined by a notch at the midplane of the magnet.

The iron aperture is a modified circle in order to reduce iron saturation effects. The radius increases from 87 mm at 0^o to 92 mm at 30^0 in the first quadrant, to return to 87 mm at 60^o. These cutouts are symmetric in the other quadrants, as shown in Fig. 10-1 , which shows a cross section of

the coil and yoke. This iron geometry holds the change in $b_{5'}$ and $b_{9'}$ over the nominal operating range to about 0.3 units.

The outer radius of the plastic spacer also changes from 87 to 92 mm. However, Fig. 10-1 shows that a space is left between the plastic spacer and the iron at the eight locations where the circle radius changes. These spaces were used to install tuning shims for field quality correction after the magnets are built.

Two of the four large non-circular holes in the yoke are used for helium flow. The other two are primarily used for the dipole bus. The holes are located to preserve quadrupole symmetry, and thus minimize saturation effects. The net hydraulic impedance is about the same as that of the four circular holes in the arc magnets.

The beam tube is a seamless stainless steel 316LN tube with a bare outer diameter of 121 mm and is wrapped with 25 μm Kapton with 60% overlay.

The iron yoke was designed to maintain quadrupole symmetry so far as possible, while also allowing for the necessary bus work, helium circulation, mechanical features, and saturation control. The yokes are enclosed in a stainless steel shell, along with corrector magnets, to give mechanical rigidity and helium containment. The technique of applying weld stripes to the shell to reduce twist, first used on the arc dipoles, was applied here as well. The rms twist on the Q2's was reduced from 1-2 mrad to less than 0.5 mrad [CO97a]. These cold masses as well as those in the neighboring ring and the adjoining D0 bending magnets were all built into a common vacuum tank in-situ.

Table 10-1. Design Parameters of RHIC 13 cm Bore Quadrupoles

Parameter	Value
Coil aperture	130 mm
Number of turns per pole	27
Number of magnets in machine	72
Magnetic length, Q1, Q2, Q3	1.44, 3.40, 2.10 m
Iron inner diameter at midplane	174 mm
Iron inner diameter at pole	184 mm
Iron outer diameter	350.5 mm
Spacer thickness at midplane	10 mm
Spacer thickness at pole	15 mm
Shell thickness	6.35 mm
Beam tube o.d., bare	(4.763 in.) 121 mm
Beam tube wall thickness	(0.157 in.) 4 mm
Beam tube/coil radial gap	(0.175 in.) 4.4 mm
Operating Temperature	4.6 K
Design current	5.05 kA
Design gradient	48.1 T/m
Computed quench current	8.26 kA
Computed quench gradient	75.3 T/m
Field margin	57 %
Inductance	13 mH
Stored energy in Q2 @ design current	165 kJ
Transfer function	
at low current	9.57 T/m/kA
at design gradient	9.52 T/m/kA

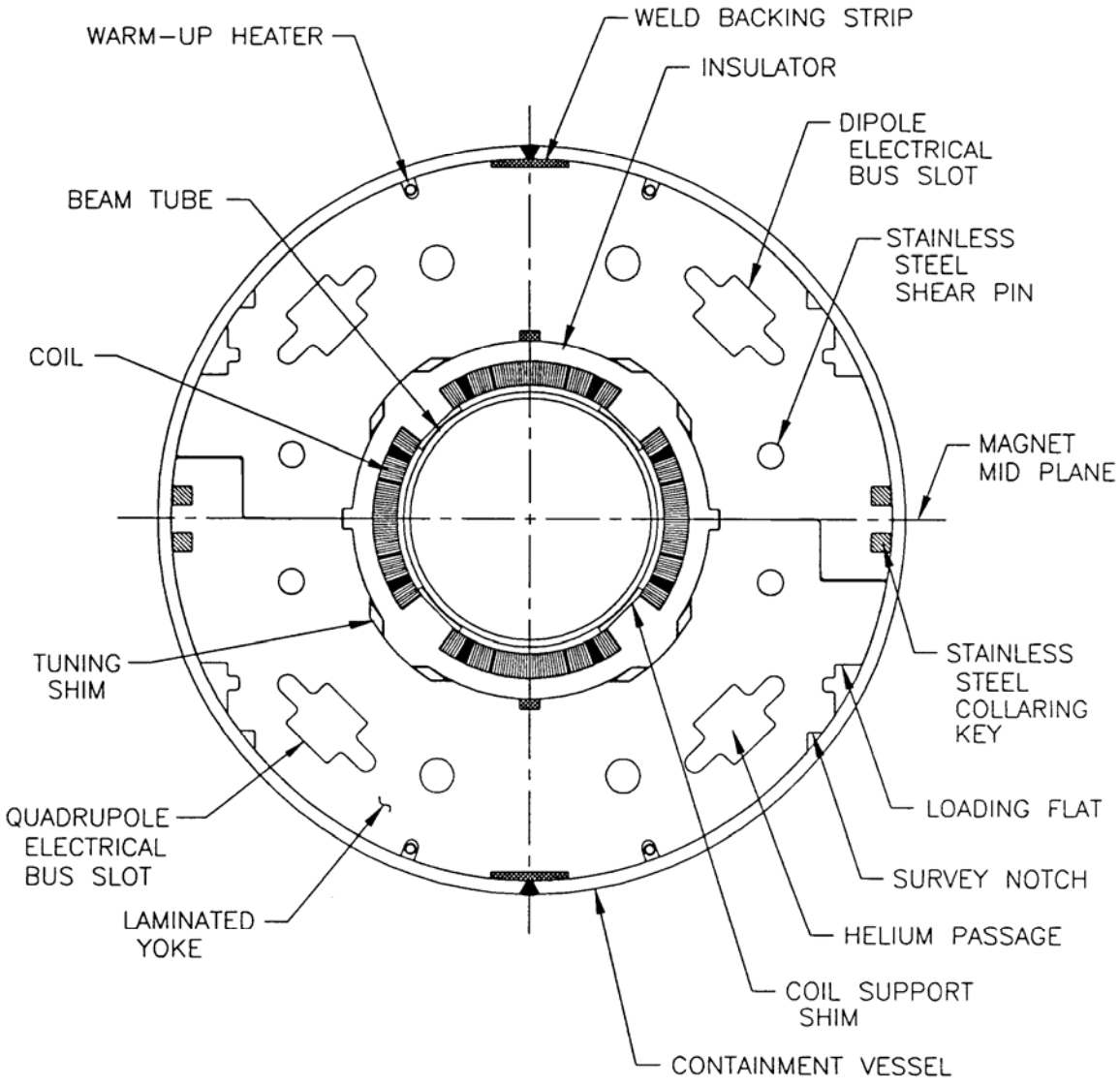

Fig. 10-1. Cross section of 13 cm quadrupole (coil i.d. = 130 mm).

The 13 cm Coil Cross-section

The coil consists of three blocks with 13, 8 and 6 turns, for a total of 27 turns/pole, all with Kapton CI insulation. The larger wedge is a section of an annulus, and the smaller wedge is rectangular. That is, the wedges are chosen to be mechanically symmetric instead of being an exact (but asymmetric) match to the variable radius geometry. The coil cross-section is shown in Fig. 10-2 .

The coil design QRI D86F is based on an insulated cable mid-thickness of 1.346 mm (0.0530 in.) and width of 12.01 mm and is an iteration of a previous design. It is optimized to give quadrupole harmonics (at 40 mm radius) of $b_{5'}$ = -31.4 and $b_{9'}$ = 0.8 with a circular, infinite-μ iron aperture. These non-zero harmonics are partly intended to compensate for the non-circular iron aperture, partly to compensate for the differences between calculations and measurements in QRI001 and QRI002 at the design maximum current and, in the case of b_5, partly to compensate for the effects of the leads.

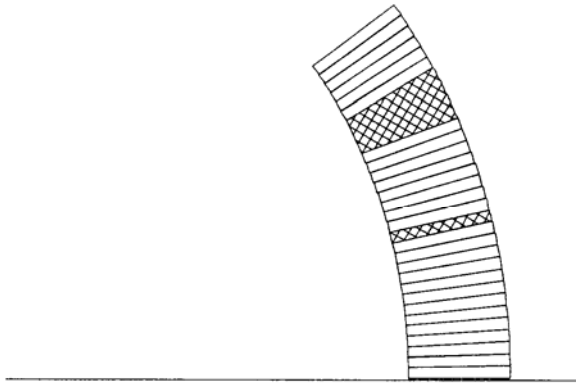

Fig. 10-2 . Iterated coil cross-section and parameters for the RHIC 13 cm aperture insertion quadrupole.

Iron Cross-section

The yoke outer diameter is 350.5 mm. The inner radius of the yoke is 87 mm from midplane to $\theta = 25.8^{o}$, at which angle there is a vertical taper to a radius of 92 mm, with symmetry around a 45^{o} radial line. The angle and the difference between the radii are used as parameters in minimizing $b_{5'}$ saturation. The locating notch at the midplane is 5 mm deep and 10 mm wide. Some other structures in the yoke are shown in Fig. 10-1; although these other structures break a strict quadrupole symmetry, the location of them is such that their influence is minimal. The first sign of symmetry breaking due to this iron geometry is the appearance of b_9 at high current. Nonmagnetic tie rods and shear pins have been located in such a way that $b_{3'}$ is <0.1 at the design current.

The change in the allowed harmonics $b_{5'}$ and $b_{9'}$ due to single magnet iron saturation is about 0.3 unit at design current (5 kA) and about 1 unit at quench current (~8.6 kA). The higher order allowed harmonics remain practically constant up to quench excitation.

At the ends nearest the crossing point, Q1 in the inner arc and Q1 in the outer arc are separated by ~61 mm. This is close enough to break the quadrupole symmetry at the higher excitations, resulting in additional field dependent harmonics.

In RHIC, the ratio of beam rigidities can vary from 1:1 to ~2.5:1. In the anti-symmetric RHIC lattice, the cross talk is maximum when both quadrupoles are excited at high current (1:1 case). The separation increases along the length of the quadrupoles; thus the effect is maximum at the crossing point ends. The dominant cross talk induced harmonic $b_{0'}$ is about 0.1 unit at design currents, and is less than 1 unit at quench currents, according to calculations using POISSON and PE2D. The value of $b_{0'}$ varies significantly over the length of Q1. The computed change in $b_{3'}$ due to non-symmetric iron yoke and cross talk is about 0.1 unit at the design current and about 0.3 unit at quench. All other saturation cross talk harmonics are less than 0.05 unit at design currents, and are less than 1 unit at quench currents.

Post-Construction Harmonic Correction

The desired harmonics in these magnets are much smaller than can be obtained with normal construction techniques. To reduce the measured values of harmonics b_i and a_i, i = 2, 3, 4 and 5, eight tuning shims were placed at the inner surface of the iron of each quadrupole after magnetic measurements have been made at room temperature. The actual tuning shim is a package of a number of low carbon steel (magnetic) and brass (non-magnetic) laminations with a total thickness

of 6.35 mm. The nominal magnetic thickness of a tuning shim is 3.175 mm, but the actual value could be anywhere between the range of 0.0 and 6.35 mm to reduce the measured harmonics. These tuning shims were inserted in the eight spaces symmetrically located between the plastic spacer and the iron yoke. In the first octant, this parallelogram-shaped space is at about 30^o and is between the radii of 87 and 92 mm.

Coil and Lead Modifications Added After Testing

Measurements on the first two magnets built, QRI001 and QRI002, revealed that quadrupole symmetry was not realized during construction. To compensate for this, the coil-to-coil gaps at 0^o and 180^o were increased to 0.25 mm and those at 90^o and 270^o to 0.15 mm.

Measurements also showed substantial harmonics, both normal and skew, in the lead end due to placement of the 8 leads after they exit the coil proper. It was found that this could be ameliorated by rotating all 8 leads (which alternate in current direction) 90^o azimuthally in the magnet end space in such a way that roughly equal lengths of lead, with opposing current direction, occupy each azimuthal position. The integrated harmonics in this space were thereby reduced or eliminated.

The tuning shim packages were adjusted to reduce the measured values of the normal and skew sextupole, octupole, decapole, and dodecapole harmonics, based on the room temperature measurements.

Results for the quench tests of the insertion quadrupoles are shown in Fig. 10-3. The first quenches of all but two of the magnets were above the 5 kA operating current. Later test protocol limited ramping to 7 kA. Quench origins were studied with both voltage taps and a quench antenna [OG96], but no single location was identified as limiting the performance. Additional quench testing was performed to verify that the magnets did not retrain after a thermal cycle. All of the Q1's and Q2's were cold tested, but only 13 of the Q3's. None of the insertion quads has quenched in RHIC.

Plots of the transfer function and first allowed harmonic versus current are given for a Q1 (Figs. 10-4 and 10-5), a Q2 (Figs. 10-6 and 10-7), and a Q3 (Figs. 10-8 and 10-9). The magnets shown are those closest to the mean for that length.

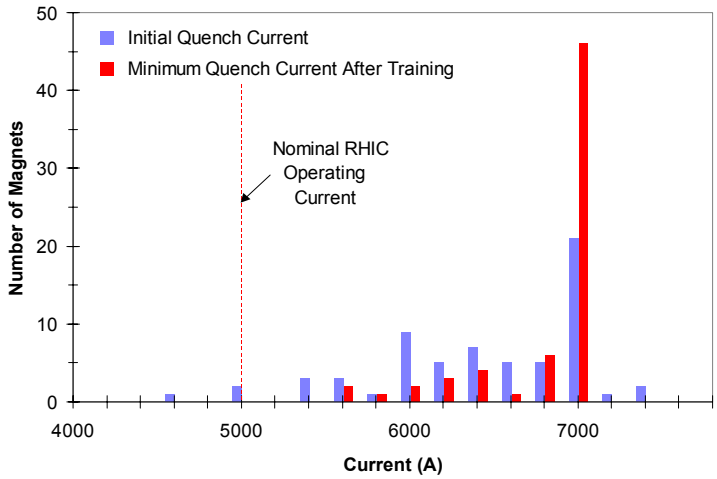

Fig. 10-3. Quench performance of 61 large aperture (130 mm) quadrupoles, tested at 4.5 K.

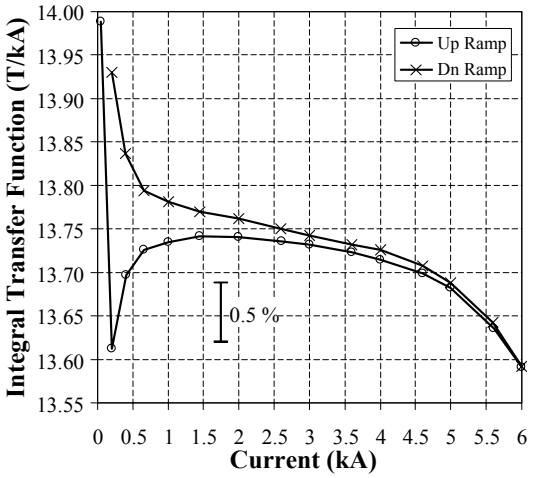

Fig. 10-4. Integral transfer function in Q1 magnet QRI114 (close to mean at 5 kA).

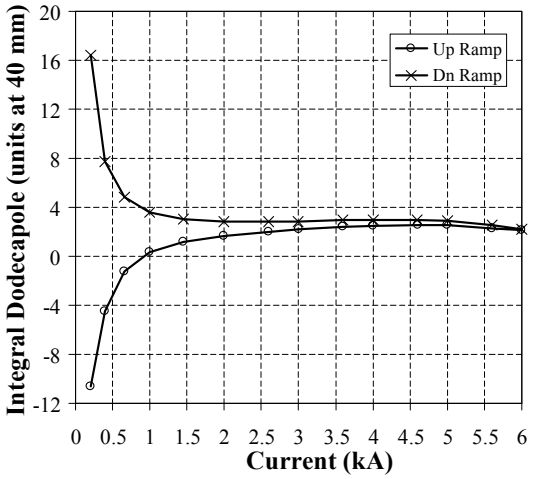

Fig. 10-5. Integral first allowed harmonic (b_5) in Q1 magnet QRI114.

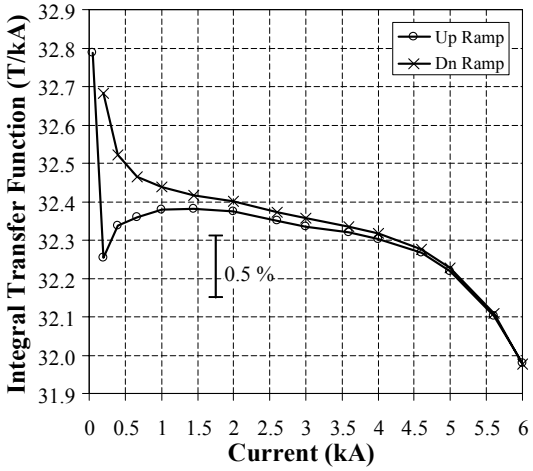

Fig. 10-6. Integral transfer function in Q2 magnet QRK119 (close to mean at 5 kA).

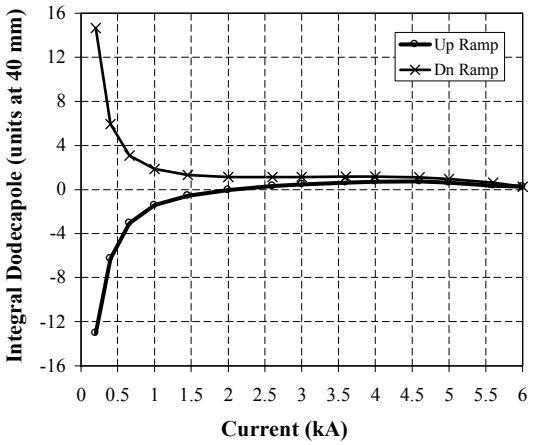

Fig. 10-7. Integral first allowed harmonic (b_5) in Q2 magnet QRK119.

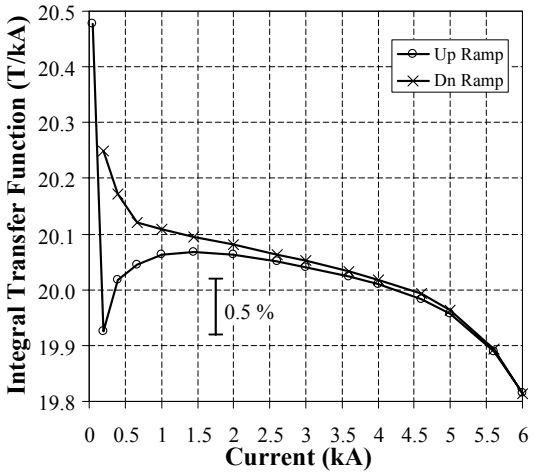

Fig. 10-8. Integral transfer function in Q3 magnet QRJ116 (close to mean at 5 kA).

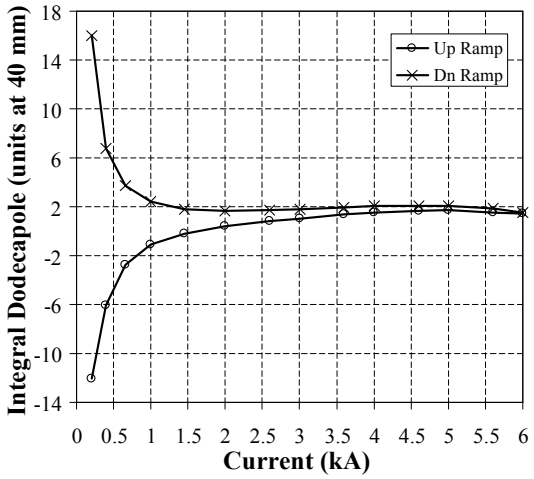

Fig. 10-9. Integral first allowed harmonic (b_5) in Q3 magnet QRJ116.

Tuning shims were used to optimize the field quality at 5 kA, where the quadrupoles play the greatest role in beam performance. The use of tuning shims significantly improved the field quality of the quadrupoles, particularly for the low order terms (Fig. 10-10) [GU99]. There were several practical limitations to improving the field quality with the tuning shims. One is the uncertainty in the correlation between warm and 5 kA measurements. Saturation reduces the correlation with measurements made at lower currents. Figures 10-11 and 10-12 show this effect for the normal sextupole. Also, warm-cold correlations must be established for each length of quadrupole, significantly lengthening the cold test time needed for the first magnets of each type. Another limitation is the change in harmonics with quenching or thermal cycle. Magnetic measurements were made before and after quench and thermal cycles on eight of the Q1's that were thermally cycled [GU97]. The rms of the change in the low-order harmonics due to quenching and thermal cycling was several tenths of a unit, somewhat smaller than the uncertainty in the warm-cold correlation.

The difference in the field quality requirements for the two "golden" IR's ($\beta^* = 1$m) and the other four "non-golden" regions ($\beta^* = 10$m) made it possible to use all of the quadrupoles built in RHIC [WE99]. Nearly all of the quadrupoles met the field requirements for "golden" IR's. The integral field quality data at 5 kA for all the magnets tested cold are given in Table 10-2. In early magnets of the Q1 and Q3 series, the first allowed harmonic, b_5, was larger than in later magnets.

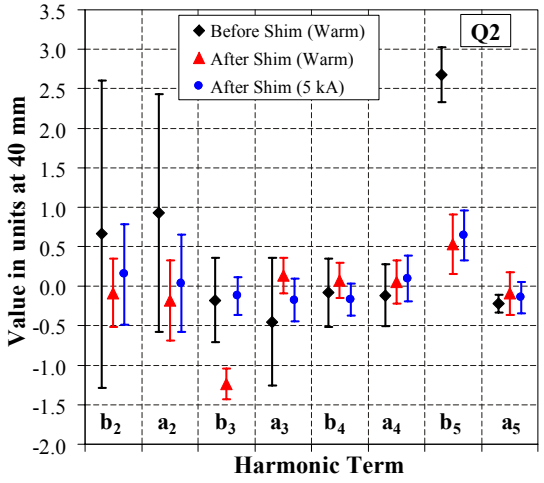

Fig. 10-10. Harmonics before and after shimming in the Q2 quads (QRK).

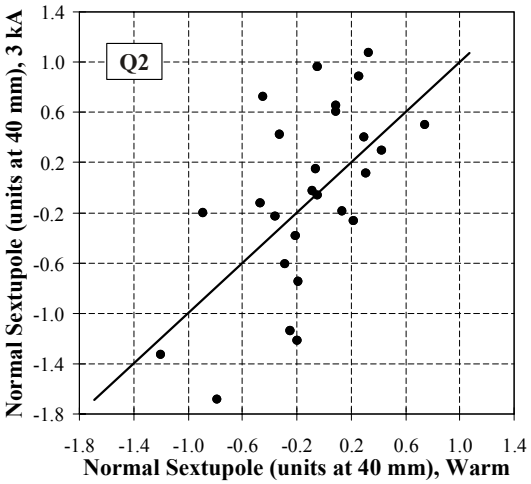

Fig. 10-11. Warm-cold correlation of b2 in the Q2 (QRK) magnets at 3 kA.

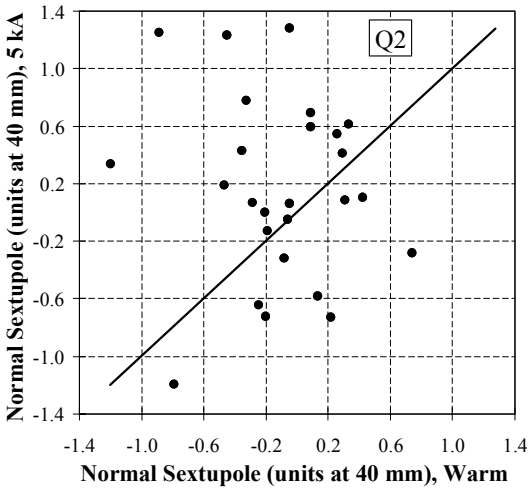

Fig. 10-12. Warm-cold correlation of b2 in the Q2 (QRK) magnets at 5 kA (shim saturation).

Table 10-2. Summary of integral field quality data in 130 mm aperture insertion quadrupoles.

Harmonic at 40 mm	Mean at 5 kA			Standard Deviation at 5 kA		
	Q1 (1.44 m) (26 magnets)	Q2 (3.4 m) (27 magnets)	Q3 (2.1 m) (13 magnets)	Q1 (1.44 m) (26 magnets)	Q2 (3.4 m) (27 magnets)	Q3 (2.1 m) (13 magnets)
ITF(T/kA)	13.658	32.170	19.954	0.32%	0.13%	0.06%
b_2	0.14	-0.08	0.01	0.44	0.43	0.73
b_3	-0.14	-1.24	-0.34	0.44	0.19	0.51
b_4	0.02	0.08	-0.23	0.25	0.22	0.23
b_5	2.15	0.53	1.67	0.59	0.38	0.13
b_6	0.03	0.02	0.07	0.22	0.19	0.17
b_7	-0.14	-0.14	0.00	0.18	0.09	0.13
b_8	0.02	0.00	0.05	0.05	0.05	0.06
b_9	-0.10	-0.37	-0.31	0.17	0.07	0.03
b_{10}	0.00	0.00	0.00	0.02	0.02	0.01
a_2	-0.23	-0.18	0.40	0.56	0.51	0.59
a_3	-0.02	0.13	0.12	0.25	0.22	0.33
a_4	-0.08	0.05	0.06	0.29	0.28	0.15
a_5	-0.74	-0.09	-0.27	0.12	0.27	0.07
a_6	0.20	0.13	0.09	0.29	0.22	0.19
a_7	-0.04	-0.01	-0.01	0.08	0.10	0.07
a_8	-0.02	0.00	0.01	0.05	0.06	0.03
a_9	0.18	0.05	0.08	0.02	0.02	0.02
a_{10}	0.01	0.00	0.01	0.02	0.02	0.02

xi. Large Aperture CQ Assemblies

For these assemblies, the cold mass helium containment half shells were welded around the individual quadrupoles and correctors. This was in contrast to the standard aperture CQS assemblies described earlier, where the half shells were welded around the corrector, quadrupole, and sextupole cold masses as a single unit. There, the shortness of the quadrupoles allowed the use of internal tie rods to support the quadrupole end plates, which restrain the axial Lorentz force of the coils. The greater length of these quadrupoles required the stiffness of the shell to act as support for the magnet end plates. Once fitted with its shell, each Q2 and Q3 quadrupole was welded end-to-end to its respective corrector or correctors to form a single CQ cold mass (Q2's had one corrector, Q3's had two.) Weld stripes on the shell were used to improve the alignment of the correctors with respect to the quadrupoles [CO97a]. For the CQ2 units, the mean corrector offset was 0.15 mm with 0.2 mm rms. For the CQ3 units, produced later, the mean was 0.04 mm, with 0.16 mm rms. Nearly all the correctors had offsets less than 0.5 mm. CQ assemblies were not cold tested.

xii. 100 mm Aperture Insertion Dipole

Each of the 6 insertion regions have a 100 mm coil diameter dipole in each ring on both sides of the intersection region, for a total of 24 dipoles. These dipoles, termed "D0", initiate the beam crossover. Although they contain only a single beam, the relatively large aperture is required to accommodate the large beam size due to the low-beta configuration, as well as variations in beam crossing angles, and collisions between unequal species. The design field, 3.52 T, is about the same as the arc dipole, and the identical superconducting cable is used in a similar, single-layer coil design. Even though the two D0 magnets on one side of the crossover are contained in a common cryostat, the corners of the containment vessels of the two yokes almost touch; in fact, this constrains the yoke outer diameter. Like the arc dipole, the yoke serves as a collar for the coils, and is held together by keys at the horizontal midplane after the halves are pressed together.

Basic Design Parameters

Table 12-1 summarizes the design parameters. The cable used is the same as that in the arc dipoles, see Tables 2-1 and 2-2 with all Kapton CI insulation. In order to achieve good field uniformity at low field, a single layer five-block coil design is needed. It is designated D0GA653D with 16, 10, 6, 5 and 3 turns per block, respectively, from the midplane to the pole for a total of 40 turns in each coil half. The coil design features symmetric wedges to ease construction. With the constraint on the yoke outer diameter mentioned above, the gap between coil and iron, which is occupied by an RX630 molding, is limited to 10 mm in thickness to minimize the flux return path reluctance. With fixed gap, minimum cross-talk between the two side-by-side magnets is obtained by optimizing the coil diameter; it was found that unwanted harmonics at maximum design field are minimized with a coil aperture of 100 mm. To maximize the effectiveness of this relatively small aperture, the D0 magnets are curved, with a sagitta of 7.6 mm. To simplify interconnections, there were two types of D0, with opposite curvatures.

Figure 12-1 shows a POISSON model of one quadrant of the coil and yoke. The helium flow channels are the same as in the arc magnets, 30.1 mm in diameter, and the superconductor bus aperture is also the same, a 31.75 mm square. The keys for holding the upper and lower halves together and the pins for lamination pairs are stainless steel. The helium bypass holes are positioned and suppressor holes added to minimize saturation-induced harmonics. The containment vessel (also not shown) is formed similarly to that of the arc dipole from a stainless steel shell of 6.35 mm thickness.

Table 12-1. Basic Design Parameters for the 10 cm Aperture RHIC Insertion Dipole

Coil i.d.	100	mm
Number of turns per pole	40	
Number of magnets, total	24	
Magnetic length	3.6	m
Iron inner diameter	139.4	mm
Sagitta	7.6	mm
Spacer thickness	10	mm
Iron outer diameter	310	mm
Shell thickness	6.35	mm
Operating temperature	4.6	K
Design current	5.0	kA
Design field	3.52	T
Computed quench current	6.5	kA
Computed quench field	4.42	T
Inductance	16.8	mH
Stored energy @ design current	210	kJ
Field margin	26%	
Transfer function		
@ low current	0.746	T/kA
@ design current	0.701	T/kA
Allowed Design harmonics @ 31 mm		
design field	< 1	
saturation induced $b_{2'}, b_{2'i}, i > 1$	< 3, < 1	
Non-allowed harmonics @ 31 mm		
cross-talk induced $b_{1'}, b_{2'i+1}, i > 0$	< 0.5, < 0.3	

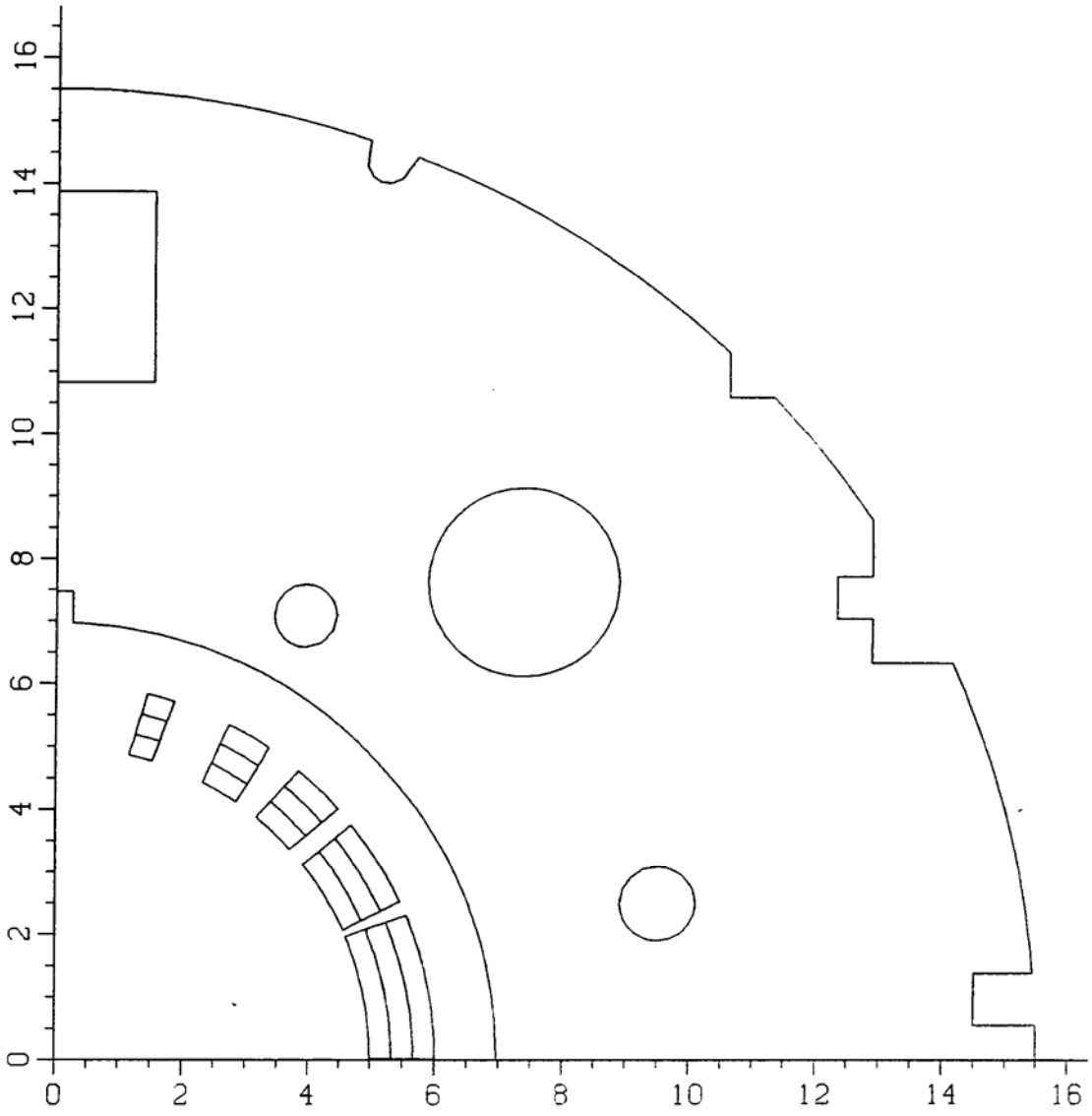

Fig. 12-1 . POISSON model of one quadrant of coil and yoke (dimensions in cm).

Results of the quench tests of the D0 dipoles are shown in Fig. 12-2. Twelve of the 24 magnets had initial quenches below the 5 kA operating current, but all exceeded 5 kA on subsequent quenches. Later magnets were quenched only until they exceeded 6.5 kA (2-6 quenches), a 30% margin. Extra testing was done to verify that the magnets would not quench after a thermal cycle.

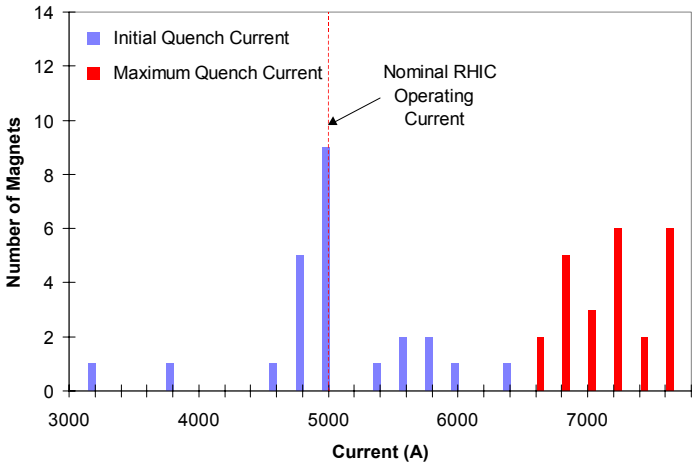

Fig. 12-2 Quench performance of 24 large aperture (100 mm) dipoles, tested at 4.5 K

Field quality improvements were made in two steps, involving five magnets, before the final configuration of coil and yoke was achieved [SC97a]. As it was for the insertion quadrupoles, the focus was on the D0 field quality at 5 kA. The critical data for this work, plots showing the correlation of warm and 5 kA measurements of the low order harmonics, are shown in Figs. 12-3 through 12-7. Figure 12-5 shows the reduction in normal sextupole. As a consequence of the changes made to reduce the sextupole, the normal decapole increased (Fig. 12-7). The remaining harmonics were unaffected. Because of the good warm-cold correlation of the harmonics, it was not necessary to measure the integral harmonics on all the D0's at 5 kA. Warm and cold integral data from the four magnets made in the final configuration were used to predict the integral 5 kA harmonics in the remaining magnets. (Cold measurements of the harmonics of a one meter length in the middle of the magnet were made on an additional 17 D0's as a check of magnetization and saturation behavior.) Table 12-2 gives the warm integral harmonics for all 24 magnets installed in RHIC.

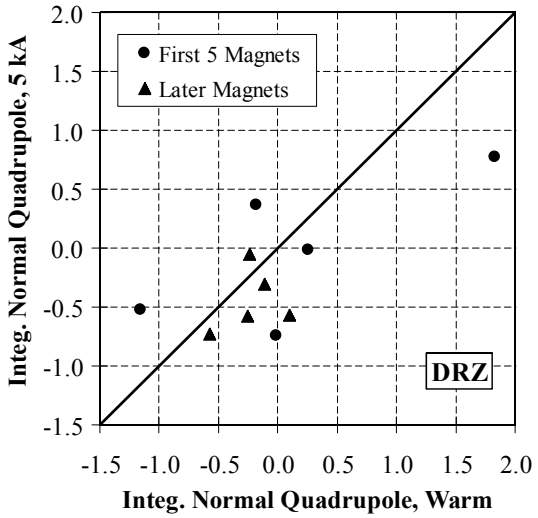

Fig. 12-3. Warm-cold correlation of the normal quadrupole harmonic (b_1) in D0 dipoles.

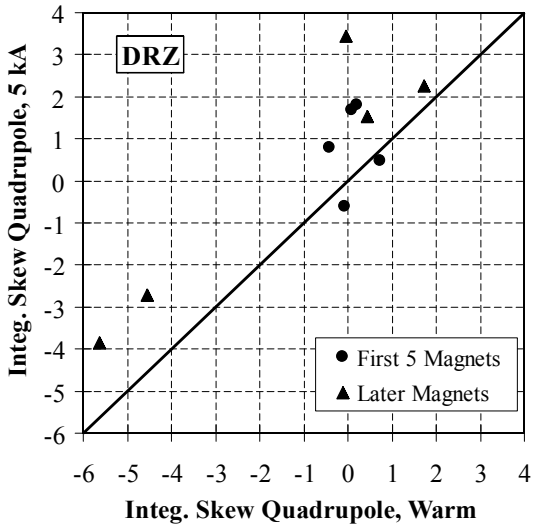

Fig. 12-4. Warm-cold correlation of the skew quadrupole harmonic (a_1) in D0 dipoles.

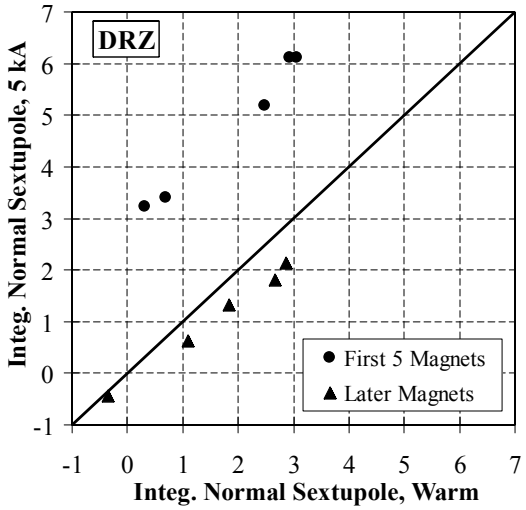

Fig. 12-5. Warm-cold correlation of the normal sextupole harmonic (b_2) in D0 dipoles.

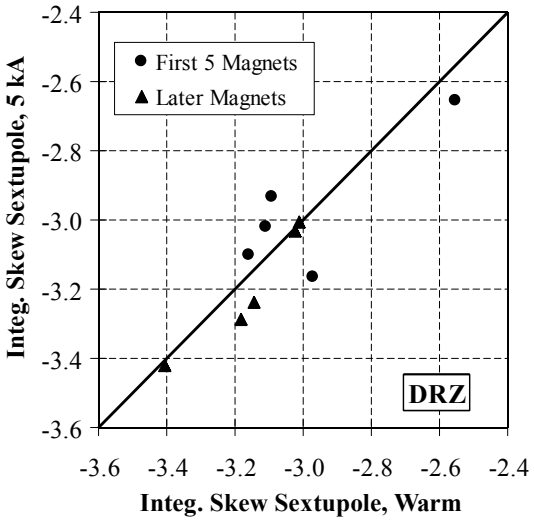

Fig. 12-6. Warm-cold correlation of the skew sextupole harmonic (a_2) in D0 dipoles.

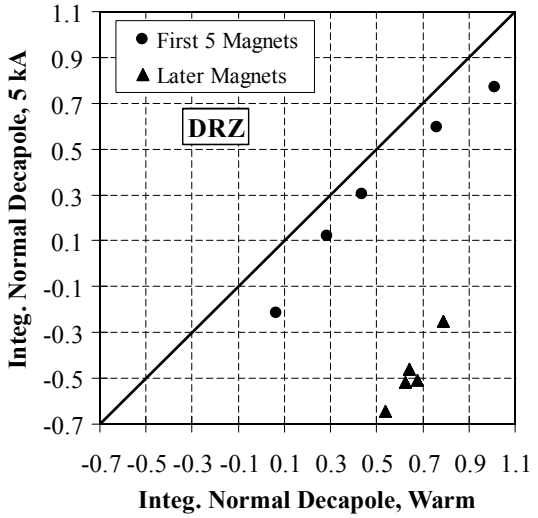

Fig. 12-7. Warm-cold correlation of the normal decapole harmonic (b_4) in D0 dipoles.

Table 12-2. Summary of integral field quality (warm) in D0 dipoles.

Harmonic at 31 mm	Mean (24 magnets)	Std. Dev. (24 magnets)	Harmonic at 31 mm	Mean (24 magnets)	Std. Dev. (24 magnets)
b_1	0.00	0.57	a_1	-0.64	2.03
b_2	2.33	1.27	a_2	-3.24	0.29
b_3	-0.03	0.12	a_3	0.00	0.46
b_4	0.65	0.24	a_4	0.48	0.04
b_5	0.01	0.03	a_5	0.03	0.13
b_6	0.22	0.07	a_6	-0.25	0.01
b_7	0.00	0.01	a_7	0.01	0.03
b_8	-0.01	0.02	a_8	0.04	0.01
b_9	0.00	0.00	a_9	0.00	0.01
b_{10}	-0.12	0.01	a_{10}	-0.02	0.00

xiii. 180 mm Insertion Dipole

Immediately on each side of the six intersection regions is a dipole, "DX", through which both beams pass; there are 12 of these magnets. The strength of DX determines the collision angle. The spacing between the two beams at the end of the magnet away from the intersection determines the aperture required. A coil diameter of 180 mm ensures adequate field uniformity in the case of asymmetric operation, provided that the dipole can be moved sideways to be centered on the beam trajectories. The axial space available necessitates a somewhat higher field, 4.3 T, than is needed for the arc dipoles. To achieve this field with an adequate margin in a single layer coil, a wider cable is used. The cable chosen is similar to the 36-strand cable used in the 130 mm aperture insertion quadrupole, differing only in the keystone angle, 0.6^o vs. 1.0^o in the cable for the quadrupole, see Tables 2-3 and 2-4. The insulation is the same, all Kapton CI, but the design value of the insulated cable mid-thickness is slightly less, 1.341 mm (0.0528 in.).

Basic Design Parameters

Table 13-1 lists the design parameters. A six-block coil design is needed to achieve good field uniformity at low field; all wedges are mechanically symmetric. Unlike all of the other RHIC magnets, the DX uses a stainless steel collar around the coils, similar to that used in the SSC dipoles. This is because the press available can accommodate a moderately thick collar, but not the large diameter of the steel yoke if it were used as a collar. To minimize deflections and thus aid in assembly, a 40.1 mm thick collar is used. Iron saturation is controlled by a series of holes in the iron, near and at the yoke inner radius. Figure 13-1 shows one quadrant of the DX dipole design. Figure 13-2 shows the full cross section. The magnet is considered to be part of the blue ring for cryogenic purposes. The bus cutout is the same size as in the arc magnets, but the helium flow channel is slightly larger (3.175 cm) to assist in the control of iron saturation; there is an additional, smaller hole solely for saturation control.

The rather large stored energy and modest ratio of copper to superconductor in the cable may result in a damaging hot spot temperature during a worst-case quench with passive (double-diode) protection, and active protection consisting of quench detection and firing of heaters was incorporated. A diode was also installed across each of the two coils.

Table 13-1. Design Parameters for the 18 cm Aperture RHIC Insertion Dipole

Parameter	Value
Coil aperture	180 mm
Number of turns per pole	70
Number of magnets in machine	12
Magnetic length	3.7 m
Iron inner diameter	(11.3 in) 287.0 mm
Collar thickness	40.1 mm
Iron outer diameter	(24.5 in.) 622 mm
Shell thickness	9.52 mm
Operating temperature	4.6 K
Design current	6.7 kA
Design field	4.3 T
Computed quench current	8.5 kA
Computed quench field	5.2 T
Inductance	49 mH
Stored energy @ design current	1.1 MJ
Field margin	22%
Transfer function	
@ low current	0.664 T/kA
@ design field	0.643 T/kA
Allowed Design harmonics @ 60 mm	
$b_{n'}$ @ low field (geometric)	< 1
maximum saturation (in operating range) $b_{2'}$	3
$b_{4'}$	0.6

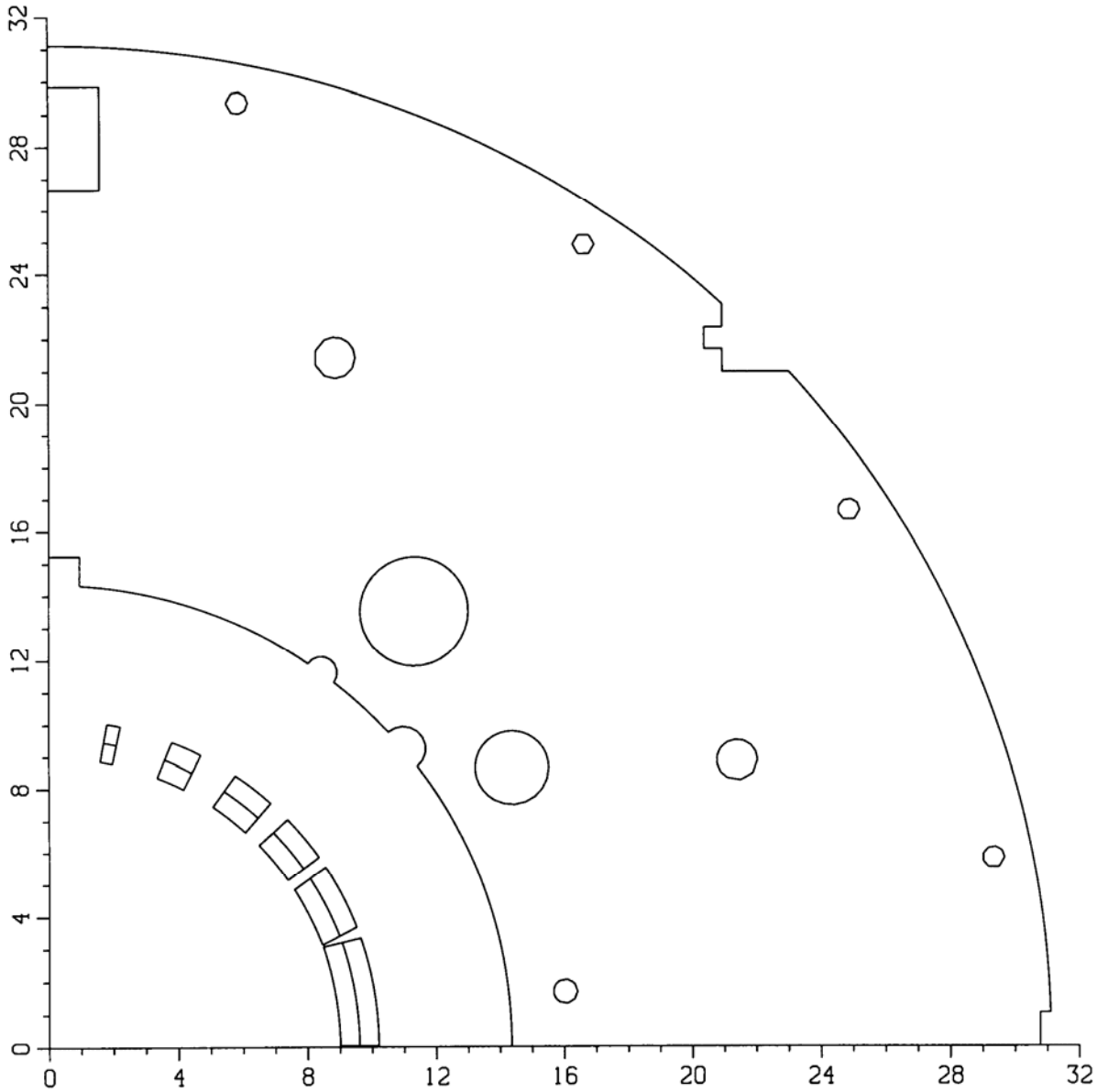

Fig. 13-1. One quadrant of the DX dipole design DXM8A (dimensions in cm).

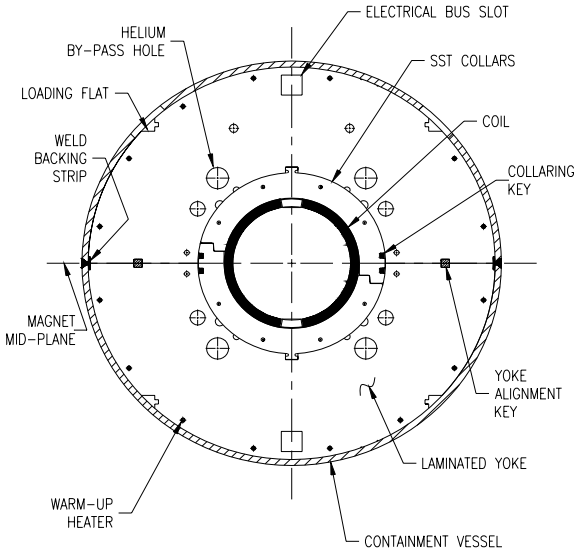

Fig. 13-2. Cross section of the 180 mm DX dipole magnet.

The quench performance of the twelve DX's installed in RHIC is summarized in Fig. 13-3. The dipoles required between one and three quenches to reach operating current. All were trained to at least 10% above the operating current of 6.6 kA. After installation in RHIC, six of the magnets required one quench each to reach operating current after the first cool-down, in agreement with the thermal cycle data obtained during production.

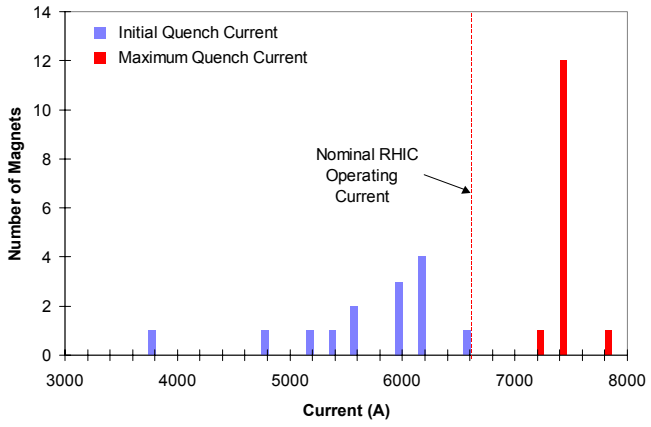

Fig. 13-3. Quench performance of 14 large aperture (180 mm) dipoles, tested at 4.5 K.

Warm integral measurements were made on all 13 magnets. The mean value of the transfer function was 2.5053 T•m/kA with rms variation of 0.03%. Measurements of the integral transfer function and the first two allowed harmonics versus current are shown for a representative magnet in Figs. 13-4 through 13-6. Cold measurements of the harmonics were made on all the magnets, but integral measurements were made on only six. Warm – cold correlations were used to estimate integral values for the remaining six. Warm – cold correlations for several low order terms are shown in Figs. 13-7 and 13-8. The field quality data for warm and cold measurements are given in Table 13-2.

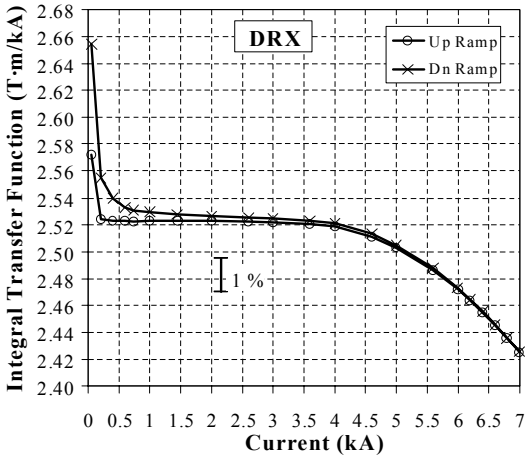

Fig. 13-4. Integral transfer function in DRX110.

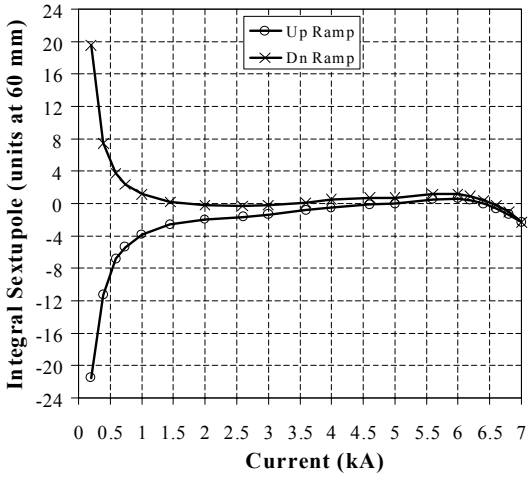

Fig. 13-5. Integral normal sextupole harmonic in DRX110.

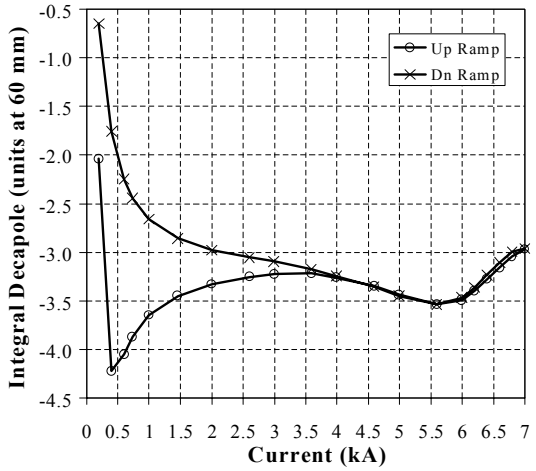

Fig. 13-6. Integral normal decapole harmonic in DRX110.

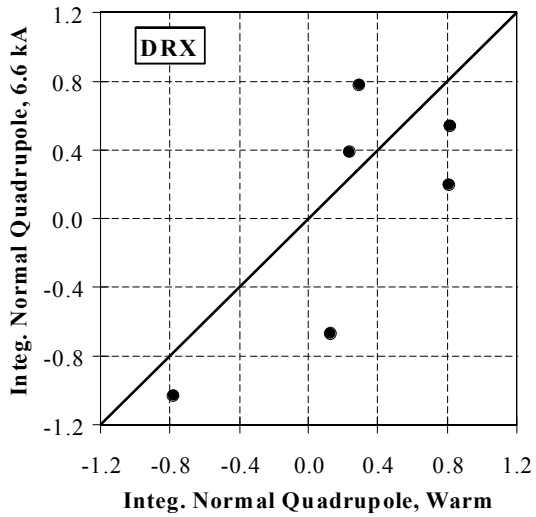

Fig. 13-7. Warm-cold correlation of b_1 in DRX magnets.

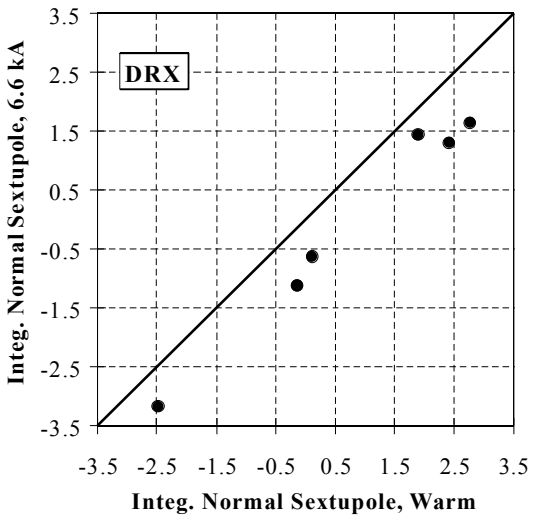

Fig. 13-8. Warm-cold correlation of b_2 in DRX magnets.

Table 13-2. Summary of integral field quality in DX dipoles.

Harmonic at 60 mm	Mean		Standard Deviation	
	30 A (13 magnets)	6600 A (6 magnets)	30 A (13 magnets)	6600 A (6 magnets)
b_1	0.04	0.03	0.63	0.72
b_2	0.53	-0.09	2.09	1.90
b_3	0.00	-0.03	0.19	0.22
b_4	-2.68	-2.95	0.57	0.41
b_5	0.03	-0.05	0.10	0.15
b_6	-1.91	-1.76	0.17	0.12
b_7	0.01	0.01	0.04	0.06
b_8	-1.09	-1.15	0.07	0.07
b_9	0.00	0.01	0.02	0.02
b_{10}	-1.13	-1.15	0.02	0.02
a_1	-1.00	-2.33	2.37	0.96
a_2	-2.54	-2.70	0.53	0.32
a_3	0.38	-0.06	0.99	1.10
a_4	0.30	0.34	0.25	0.16
a_5	0.34	0.19	0.37	0.38
a_6	-0.21	-0.15	0.15	0.08
a_7	0.19	0.15	0.11	0.11
a_8	-0.04	-0.05	0.04	0.04
a_9	0.09	0.08	0.04	0.05
a_{10}	0.03	0.06	0.02	0.02

xiv. Helical Dipoles

Helical magnets control the spin of the polarized protons in RHIC. The basic construction unit is a superconducting magnet producing a 4 T dipole field that rotates through 360 degrees in a length of 2.4 m [WI97, WI99a]. These magnets are assembled in groups of four to build four Snakes that control spin in the lattice and eight Rotators that orient spin axially at two collision points. Thus, the complete program requires 48 magnets.

A cross section drawing of the helical magnet is shown in Fig. 14-1. Parameters for the magnets are given in Table 14-1. Because multiple current leads exit each cryostat, a low current design (320A) was used to minimize the cryogenic load due to the leads. By the standards of superconducting magnets, the field quality requirements are relatively modest (harmonics < 10^{-3} of the main field). The error allowed on the rotation angle is 2°.

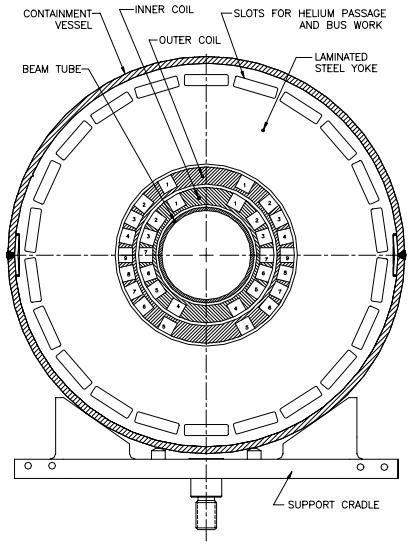

Fig. 14-1. Cross section of the helical dipole magnet. The yoke OD is 356 mm. The innermost conductor is at an ID of 100 mm.

Table 14-1 Selected parameters of the RHIC helical dipole magnets.

Parameter	Units	Value
Aperture	mm	100
Magnetic length	m	2.4
Field	T	4
Current	A	320
Number of turns		1680
Inductance	H	4.8
Stored energy @ 4 T	kJ	240
Diameter of yoke	mm	355.6
Num. of strands in cable		7
Strand diameter	mm	0.33
Cu to non-Cu ratio		2.5:1

The coil structure consists of two aluminum tubes, each with slots as shown in Fig. 14-2. These are filled with Kapton-insulated superconducting cable. The tubes are surrounded by a yoke made of single piece, low-carbon steel laminations. Holes near the outer perimeter of the yoke allow for tie rods, warm-up heaters, passage of helium coolant, and bus work for magnet interconnections. The slots rotate along the length of the magnet but the holes in the yoke do not, so the yoke laminations were designed with rotational symmetry in mind. Azimuthal Lorentz forces are contained in the individual slots. The outward Lorentz forces are ultimately contained by the single piece yoke. In the ends, the difficult Lorentz force problem is again solved by containing the forces in the individual slots.

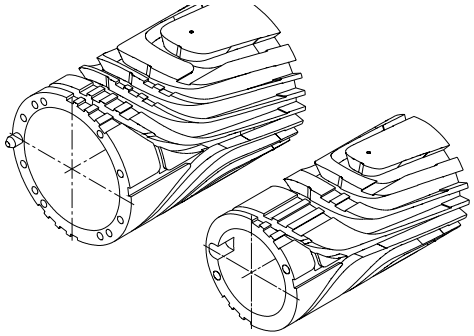

Fig. 14-2. Drawing of the coil tube ends. End Lorentz forces are contained in the slots.

The superconducting cable is placed by hand and without tension into the slots in an ordered array. The width in the slots is such that 12 turns of the round cable, which is about 1.1 mm in diameter, have an average of 25 μm space between turns. A layer of B-stage fiberglass/epoxy with adhesive film on each side is placed between each layer. After winding, press plates of 3.1 mm thick G10 are applied to each slot. A Kevlar wrap is then applied to the tube under tension. In the subsequent curing operation, the stretch in the Kevlar allows the press plates to move radially inward without losing all tension, thereby compressing the windings and removing voids in the slots as the epoxy softens and fills the remaining spaces. Helium is still able to penetrate this package and fill the ~ 10% free space inside the Kapton wrap and around the wires of the cable. At the ends of the magnet, space is left in the slots to accommodate the axial growth of the coil during curing. Voids remaining in the ends after curing are filled with epoxy by hand. After curing, the Kevlar is removed so that the leads can be secured. The coil is then wrapped with fiberglass cloth, Kevlar under tension, and Tedlar. (The Tedlar prevents epoxy in the next layer from seeping into the Kevlar). Multiple layers of fiberglass cloth and epoxy are applied to build the radial thickness needed for the final step, machining the cylinder to a precise radius (~ 50 μm). The epoxy cures at room temperature.

The two coils are assembled, aligned, pinned together, and bolted to a plate that serves as the primary alignment reference of the magnet. The laminations are weighed before assembly to the coils. The length of the yoke is set by tie bars. The tie bars and coils are held on a plate at only the lead end of the coils. Thus, the coils can follow the contraction of the aluminum tube during cooldown. Fig. 14-3 shows a section cut from a prototype helical magnet [OK00].

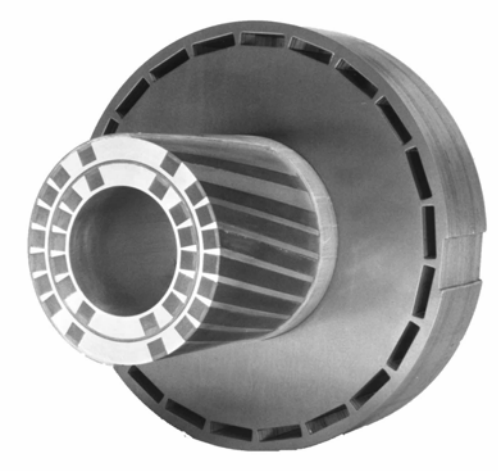

Fig. 14-3. Photograph of a section cut from a prototype helical magnet.

Each of the individual windings is connected in a series connection on a circuit board at the end of the magnet. A 50 mΩ resistor is connected across each of the windings to avoid overheating during a quench. The large inductance of the windings (0.3 H on average) and the 50 mΩ parallel resistance lead to an indeterminate field in the magnet when it is ramped. This is acceptable because the magnet is designed to be operated only in a DC mode or with very slow (< 1 A/sec) ramp rates.

The magnets were tested individually in a vertical dewar filled with liquid helium. Quench test results from the magnets that were installed into the first Snake are shown in Fig. 14-4. Initially, magnets were trained to currents close to conductor limit, ~ 410 A. The training was monotonic but sometimes slow at the highest currents. The test protocol later called for training the magnets to 360 A, about 10% above the maximum operating current. Magnets have typically reached 360 A in a few quenches. See [WI03] for test results from all 48 magnets.

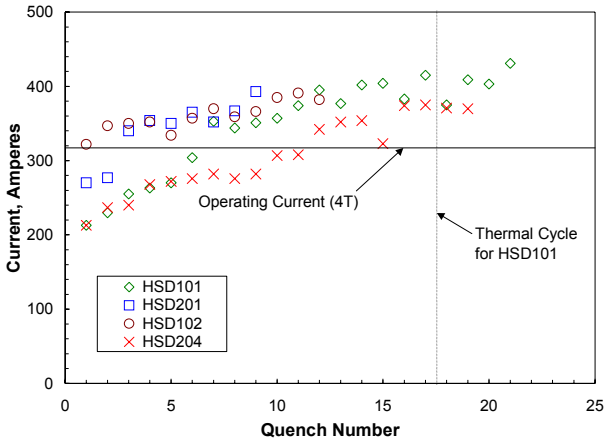

Fig. 14-4. Quench performance of the four magnets of the first Snake. After some initial training, each reached a current comfortably above the maximum operating point of 4 T. A thermal cycle showed no retraining.

Ideally, the integral field of each helical magnet will be zero. The acceptance criterion calls for it to be small: $\left[\left(\int B_y(z)\,dz\right)^2+\left(\int B_x(z)\,dz\right)^2\right]^{1/2} < 5\times10^{-2}\ \mathrm{T\cdot m}$. In terms of the rotation angle of the spin vector, this tolerance is ~ 1.9 degrees. The integral field is measured using a 3.57 m long, 48 mm diameter rotating coil. All magnets tested thus far have easily met this requirement.

Helical magnets have axial fields in the magnet straight section. They can be expressed in cylindrical coordinates using Bessel functions as basis functions [FI97,WI99b]. In these magnets the resulting harmonic coefficients are close to those for straight magnets; the harmonics measured with the short (51 mm) standard harmonic coil used require a correction of only a few percent. This coil has diameter 68 mm. Field quality measurements at the center of a typical magnet as a function of current are shown in Figs. 14-5 through 14-7. The decrease in the transfer function and the increase in the sextupole with current are caused by saturation of the steel yoke, which is undersized in order to limit the physical size of the magnet. Field quality measurements made by stepping the coil through the length of the same magnet at three fixed currents are shown in Figs. 14-8 through 14-11.

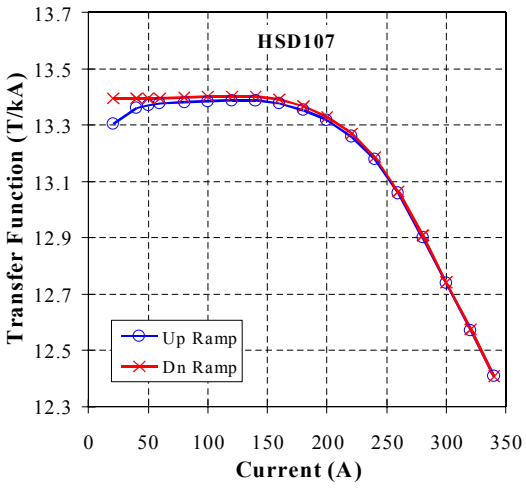

Fig. 14-5. Transfer function at the center of HSD107

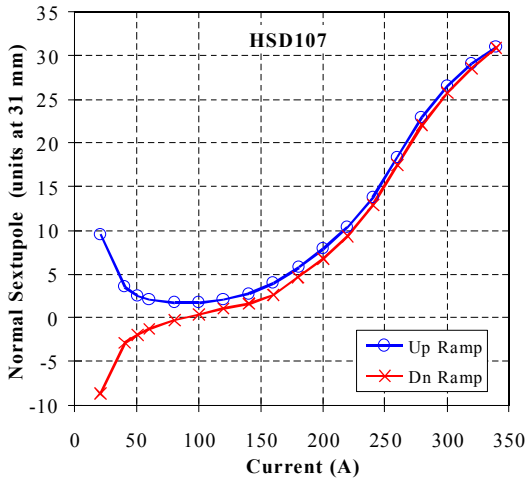

Fig. 14-6. Normal sextupole harmonic at the center of HSD107.

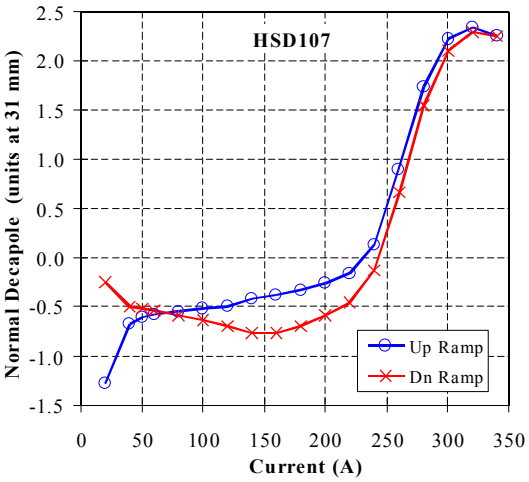

Fig. 14-7. Normal decapole harmonic at the center of HSD107.

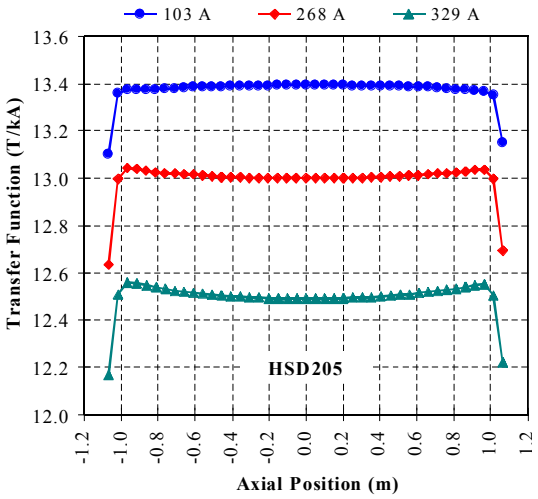

Fig. 14-8. Axial scan of the transfer function in HSD107.

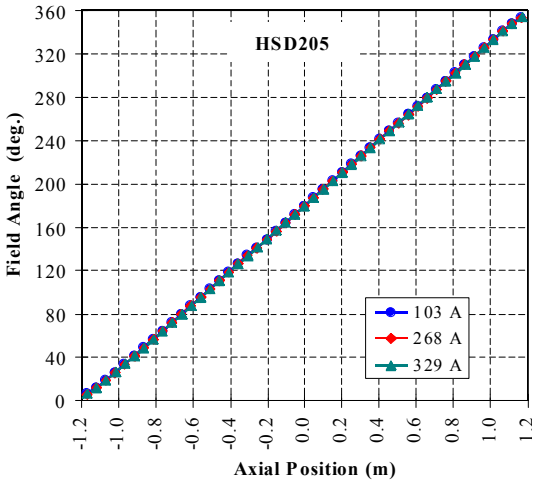

Fig. 14-9. Field angle as a function of the axial position in HSD205.

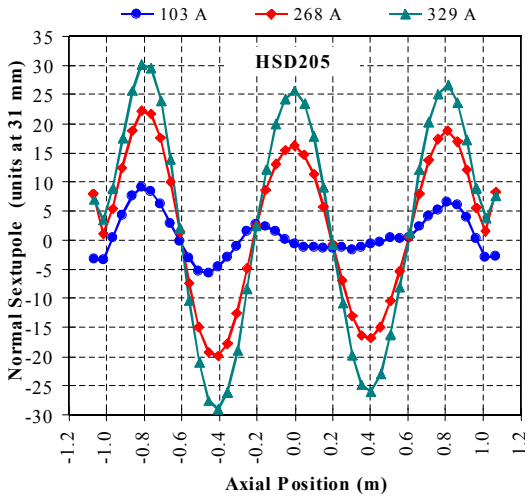

Fig. 14-10. Normal sextupole harmonic as a function of the axial position in HSD205.

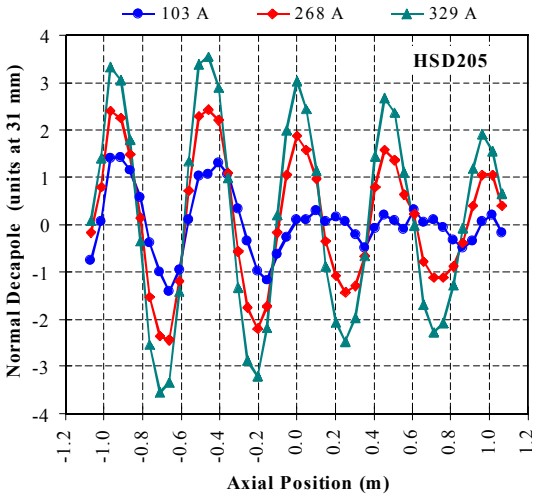

Fig. 14-11. Normal decapole harmonic as a function of the axial position in HSD205.

xv. References

[AN93a] M. Anerella, A. Ghosh, E. Kelly, J. Schmalzle, E. Willen, Improved Cable Insulation for Superconducting Magnets, Proceedings of the 1993 Particle Accelerator Conference, Washington, DC, May 17-20, 1993.

[AN95a] M. Anerella, D. Fisher, E. Sheedy, T. McGuire, Industrial Production of RHIC Magnets, BNL-61361 and Proceedings of the 14th International Conference on Magnet Technology, Tampere, Finland, June 11-16, 1995.

[CO97a] J. Cozzolino, M. Anerella, A. Jain, W. Louie, J. Muratore, P. Wanderer, Removal of Axial Twist in RHIC Insertion Quadrupole Magnets, Proceedings of the 1997 Particle Accelerator Conference, Vancouver, Canada, May 1997.

[DA87a] P. Dahl, J. Cottingham, M. Garber, A. Ghosh, C. Goodzeit, A. Greene, J. Herrera, S. Kahn, E. Kelly, G. Morgan, A. Prodell, W. Sampson, W. Schneider, R. Shutt, P. Thompson, P. Wanderer, E. Willen, Performance of Initial Full-Length RHIC Dipoles, BNL-40545 and Proceedings of the Tenth International Conference on Magnet Technology, Boston, MA, September 21-25, 1987.

[FI97] W. Fischer, M. Okamura, Parameterization and Measurements of Helical Magnetic Fields, Proceedings of the 1997 Particle Accelerator Conference, Vancouver, Canada, May 1997.

[FI99a] D. Fisher, M. Anerella, P. Wanderer, Successful Partnership Between Brookhaven National Laboratory and Northrop Grumman Corp. for Construction of RHIC Superconducting Magnets, Proceedings of the 16th International Conference on Magnet Technology, Ponte Vedra Beach, FL, September 26-October 2, 1999.

[FI00] W. Fischer, A. Jain, S. Tepikian, Beam-based Measurements of Persistent Current Decay in RHIC, Phys. Rev. Special Topics, Vol 4, 041002 (2001).

[FI01a] W. Fischer, A. Jain, S. Tepikian, Beam-based Measurements of Persistent Current Decay in RHIC, Brookhaven Magnet Division Note 600, January 5, 2001.

[GA93a] M. Garber, A. Ghosh, A. Greene, D. McChesney, A. Morgillo, R. Shah, S. DelRe, G. Epstein, S. Hong, J. Lichtenwalner, P. O'Larey, D. Smathers, M. Boivin, R. Meserve, Superconducting Wire and Cable for RHIC, BNL-49321 and Proceedings of the 13th International Conference on Magnet Technology, Victoria, Canada, September 20-24, 1993.

[GO88a] C. Goodzeit, M. Anerella, G. Ganetis, Measurement of Internal Forces in Superconducting Accelerator Magnets with Strain Gauge Transducers, Proceedings of the 1988 Applied Superconductivity Conference, San Francisco, CA, August 21-25, 1988.

[GO93a] M. Goldman, R. Sikora, T. Shea, Preliminary Studies on a Magneto-Optical Procedure for Aligning RHIC Magnets, Proceedings of the 1993 Particle Accelerator Conference, Washington, DC, May 17-20, 1993.

[GR94a] A. Greene, M. Garber, A. Ghosh, D. McChesney, A. Morgillo, R. Shah, S. DelRe, G. Epstein, S. Hong, J. Lichtenwalner, P. O'Larey, D. Smathers, M. Boivin, R. Meserve, Manufacture and Testing of the Superconducting Wire and Cable for the RHIC Dipoles and Quadrupoles, BNL-60350 and Proceedings of the 1994 Applied Superconductivity Conference, Boston, MA, October 16-21, 1994.

[GR95a] A. Greene, M. Anerella, J. Cozzolino, J. Escallier, D. Fisher, G. Ganetis, A. Ghosh, R. Gupta, A. Jain, S. Kahn, E. Kelly, R. Lebel, G. Morgan, A. Morgillo, S. Mulhall, J. Muratore, S. Plate, A. Prodell, M. Rehak, W. Sampson, R. Thomas, P. Thompson, P. Wanderer, E. Willen, The Magnet System of the Relativistic Heavy Ion Collider (RHIC), BNL-61790 and Proceedings of the 14th International Conference on Magnet Technology, Tampere, Finland, June 11-16, 1995.

[GU93a] R. Gupta, M. Anerella, G. Ganetis, M. Garber, A. Ghosh, A. Greene, A. Jain, S. Kahn, E. Kelly, E. Killian, G. Morgan, A. Morgillo, J. Muratore, A. Prodell, M. Rehak, W. Sampson, R. Shutt, P. Thompson, P. Wanderer, E. Willen, Large Aperture Quadrupoles for RHIC Interaction Regions, Proceedings of the 1993 Particle Accelerator Conference, Washington, DC, May 17-20, 1993.

[GU94] R. Gupta, A. Jain, S. Kahn, G. Morgan, P. Thompson, P. Wanderer, E.Willen, Field Quality Improvements in Superconducting Magnets for RHIC, EPAC 94, pp.2928-2930, London, UK.

[GU95a] R. Gupta, A. Jain, S. Kahn, G. Morgan, P. Thompson, P. Wanderer, E. Willen, Field Quality Control Through the Production Phase of RHIC Arc Dipoles, BNL-61226 and Proceedings of the 1995 Particle Accelerator Conference and International Conference on High Energy Accelerators, Dallas, TX, May 1-5, 1995.

[GU95b] R. Gupta, M. Anerella, J. Cozzolino, B. Erickson, A. Greene, A. Jain, S. Kahn, E. Kelly, G. Morgan, P. Thompson, P. Wanderer, E. Willen, Tuning Shims for High Field Quality in Superconducting Magnets, BNL-61106 and Proceedings of the 14th International Conference on Magnet Technology, Tampere, Finland, June 11-16, 1995.

[GU97] R. Gupta, A. Jain, J. Muratore, P. Wanderer, E. Willen, Change In Field Harmonics After Quench and Thermal Cycles in Superconducting Magnets, Proceedings of the 1997 Particle Accelerator Conference, p.3347, Vancouver, BC

[GU99] R. Gupta, Lawrence Berkeley National Laboratory; M. Anerella, J. Cozzolino, A. Ghosh, A. Jain, S. Kahn, E. Kelly, G. Morgan, J. Muratore, A. Prodell, W. Sampson, P. Thompson, P. Wanderer, E. Willen, RHIC IR Quadrupoles and Field Quality State of the Art in Superconducting Accelerator Magnets, Proceedings of the 1999 Particle Accelerator Conference, New York, 1999, p.185.

[JA95a] A. Jain, R. Gupta, P. Thompson, P. Wanderer, Skew Quadrupole in RHIC Dipole Magnets at High Fields, BNL-61362 and Proceedings of the 14th International Conference on Magnet Technology, Tampere, Finland, June 11-16, 1995.

[JA97a] A. Jain, A "Survey Antenna" for Determining Magnetic Center, Presented at the Tenth International Magnet Measurement Workshop (IMMW-10), FNAL, Batavia, IL, October 13-16, 1997.

[JA99a] A. Jain, J. Muratore, M. Anerella, G. Ganetis, A. Marone, G. Morgan, A. Prodell, J. Schmalzle, R. Thomas, P. Wanderer, Quench Performance and Field Quality of DX Dipoles for RHIC, Proceedings of the 1999 Particle Accelerator Conference, New York, NY, March 29-April 2, 1999.

[JA99b] A. Jain, M. Anerella, J. Escallier, G. Ganetis, A. Ghosh, R. Gupta, E. Kelly, A. Marone, G. Morgan, J. Muratore, A. Prodell, W. Sampson, R. Thomas, P. Thompson, P. Wanderer, E. Willen, Superconducting 13 cm Corrector Magnets for the Relativistic Heavy Ion Collider (RHIC), Proceedings of the 16th International Conference On Magnet Technology, Ponte Vedra Beach, FL, September 12-October 2, 1999.

[JA00a] A. Jain, G. Ganetis, J. Muratore, R. Thomas, P. Wanderer, Time Decay, Snap-Back, and Ramp Rate Effects in RHIC 8 cm Dipoles and Quadrupoles, Magnet Division Note 593, May 10, 2000.

[KA93a] S. Kahn, R. Gupta, A. Jain, G. Morgan, P. Thompson, Calculations of Magnetic Field for the End Design of the RHIC Arc Dipole, Proceedings of the 1993 Particle Accelerator Conference, Washington, DC, May 17-20, 1993.

[MO92a] G. Morgan, Final Report of the Task Force on the RHIC Iron Specification, Brookhaven Magnet Division Note 420, February 26, 1992.

[MO93a] G. Morgan, A. Morgillo, K. Power, P. Thompson, New Coil End Design for the RHIC Arc Dipole, BNL-49324 and Proceedings of the 13th International Conference On Magnet Technology, Victoria, Canada, September 1993.

[MO94a] G. Morgan, A B-H Table for the Kawasaki Iron Used in the RHIC Arc Dipoles, Brookhaven Magnet Division Note 535, May 13, 1994.

[MO95a] A. Morgillo, J. Escallier, G. Ganetis, A. Greene, A. Ghosh, A. Jain, E. Kelly, A. Marone, G. Morgan, J. Muratore, W. Sampson, P. Thompson, P. Wanderer, E. Willen, Superconducting 8 cm Corrector Magnets for the Relativistic Heavy Ion Collider (RHIC), BNL-61264 and Proceedings of the 1995 Particle Accelerator Conference and International Conference on High Energy Accelerators, Dallas, TX, May 1-5, 1995.

[MO95b] G. Morgan, Design of the Large Aperture Superconducting Magnet DX, BNL-61425 and Proceedings of the Conference on the Computation of the Electromagnetic Fields Compumag, Berlin, Germany, July 10-13, 1995.

[MU93a] J. Muratore, M. Anerella, G. Ganetis, M. Garber, A. Ghosh, A. Greene, R. Gupta, A. Jain, S. Kahn, E. Kelly, G. Morgan, A. Prodell, M. Rehak, E.P. Rohrer, W. Sampson, R. Shutt, R. Thomas, P. Thompson, P. Wanderer, E. Willen, Quench Propagation Study for Full-Length RHIC Dipole Magnets, BNL-49323 and Proceedings of the 13th International Conference On Magnet Technology, Victoria, Canada, September 20-24, 1993.

[MU95a] S. Mulhall, H. Foelsche, G. Ganetis, A. Greene, E. Kelly, S. Plate, E. Willen, Combined Element Magnet Production for the Relativistic Heavy Ion Collider (RHIC) at BNL, BNL-61234 and Proceedings of the 1995 Particle Accelerator Conference and International Conference on High Energy Accelerators, Dallas, TX, May 1-5, 1995.

[MU97] J. Muratore, A. Jain, G. Ganetis, A. Ghosh, A. Marone, A. Morgillo, W. Sampson, P. Thompson, P. Wanderer, Results from the Completed Production Run of Superconducting Corrector Magnets for RHIC, Proceedings of the 1997 Particle Accelerator Conference, pp.3353-3355, Vancouver, BC

[OG96] T. Ogitsu, A. Terashima, K. Tsuchiya, KEK; G. Ganetis, J. Muratore, P. Wanderer, BNL, Quench Observation Using Quench Antennas on RHIC IR Quadrupole Magnets, IEEE Trans. Magn., July 1996, Vol. 32, No. 4.

[OK00] M. Okamura, T. Tominaka, T. Kawaguchi, T. Katayama, A. Jain, J. Muratore, G. Morgan, E. Willen, Half-Length Model of a Siberian Snake Magnet for RHIC, Nuclear Instruments and Methods in Physics Research A 452 (2000) 53-60.

[RE92a] M. Rehak, R. Shutt, Pressure Drops and Temperature Increases in RHIC Magnets, Brookhaven Magnet Division Note 423, March 4, 1992.

[SC97a] J. Schmalzle, M. Anerella, G. Ganetis, A. Ghosh, R. Gupta, A. Jain, S. Kahn, G. Morgan, J. Muratore, W. Sampson, P. Wanderer, E. Willen, RHIC D0 Insertion Dipole Design Iterations During Production, Proceedings of the 1997 Particle Accelerator Conference, Vancouver, Canada, May 12-16, 1997.

[SC99a] J. Schmalzle, M. Anerella, G. Ganetis, A. Jain, G. Morgan, J. Muratore, P. Wanderer, RHIC DX Dipole Magnet Construction, Proceedings of the 16th International Conference on Magnet Technology, Ponte Vedra Beach, FL, Sept. 26-Oct. 2, 1999.

[SH90a] R. Shutt, M. Rehak, Instabilities of Bellows: Dependence on Internal Pressure, End Supports, and Interactions in Accelerator Magnet Systems, BNL-44548 and Proceedings of the 1990 American Society of Mechanical Engineers (ASME) Winter Annual Meeting (WAM), Dallas, TX, November 25-30, 1990.

[SH91a] R. Shutt, M. Rehak, Stability of Bellows Used as Expansion Joints Between Superconducting Magnets in Accelerators, BNL-45337 and Proceedings of the Third Annual International Industrial Symposium on the SuperCollider (IISSC), Atlanta, GA, March 13-15, 1991.

[SH93a] R. Shutt, K. Hornik, M. Rehak, Corrector-Quadrupole-Sextupole (CQS) Power Leads for the Relativistic Heavy Ion Collider (RHIC) at Brookhaven National Laboratory (BNL), Proceedings of the Fifth Annual International Industrial Symposium on the SuperCollider (IISSC), San Francisco, CA, May 6-8, 1993.

[SO91a] J. Sondericker, L. Wolf, Alternative Concepts for Structurally Supporting the Cold Mass of a Superconducting Accelerator Magnet, Proceedings of the Third Annual International Industrial Symposium on the SuperCollider (IISSC), Atlanta, GA, March 13-15, 1991.

[TH86a] P. Thompson, J. Cottingham, P. Dahl, R. Fernow, M. Garber, A. Ghosh, C. Goodzeit, A. Greene, H. Hahn, J. Herrera, S. Kahn, E. Kelly, G. Morgan, S. Plate, A. Prodell, W. Sampson, W. Schneider, R. Shutt, P. Wanderer, E. Willen, Status of Magnet System for RHIC, BNL-38459 and Proceedings of the Second Conference on the Intersections between Particle and Nuclear Physics, Lake Louise, Canada, May 1986.

[TH89a] P. Thompson, G. Cottingham, M. Garber, A. Ghosh, C. Goodzeit, A. Greene, J. Herrera, S. Kahn, E. Kelly, G. Morgan, S. Plate, A. Prodell, W. Sampson, W. Schneider, R. Shutt, P. Wanderer, E. Willen, Status of the Quadrupoles for RHIC, BNL-41899 and Proceedings of the 1989 Particle Accelerator Conference, Chicago, IL, March 20-23, 1989.

[TH91a] P. Thompson, R. Gupta, S. Kahn, H. Hahn, G. Morgan, P. Wanderer, E. Willen, Revised Cross Section for RHIC Dipole Magnets, BNL-45721 and Proceedings of the 1991 Particle Accelerator Conference, San Francisco, CA, May 6-9, 1991.

[TH92a] R. Thomas, G. Morgan, Measurements of Magnetic Permeability and H_c of Magnet Steels using Digital Techniques, BNL-47851 and Presentation at the Eleventh Annual Conference on Properties and Applications of Magnetic Materials, Chicago, IL, May 12-14, 1992.

[TH93a] P. Thompson, M. Anerella, G. Ganetis, M. Garber, A. Ghosh, A. Greene, R. Gupta, A. Jain, S. Kahn, G. Morgan, A. Morgillo, J. Muratore, A. Prodell, M. Rehak, W. Sampson, P. Wanderer, E. Willen, "B" Series RHIC Arc Quadrupoles, Proceedings of the 1993 Particle Accelerator Conference, Washington, DC, May 17-20, 1993.

[TH95a] P. Thompson, M. Anerella, G. Ganetis, A. Ghosh, A. Greene, R. Gupta, A. Jain, E. Kelly, M. Lindner, G. Morgan, J. Muratore, W. Sampson, P. Wanderer, E. Willen, Superconducting Sextupoles and Trim Quadrupoles for RHIC, BNL-61224 and Proceedings of the 1995 Particle Accelerator Conference and International Conference on High Energy Accelerators, Dallas, TX, May 1-5, 1995.

[TR95a] D. Trbojevic, P. Cameron, G. Ganetis, M. Goldman, R. Gupta, M. Harrison, M. Hemmer, F. Karl, A. Jain, W. Louie, S. Mulhall, S. Peggs, S. Tepikian, R. Thomas, P. Wanderer, Alignment and Survey of the Elements in RHIC, Proceedings of the 1995 Particle Accelerator Conference and International Conference on High Energy Accelerators, Dallas, TX, May 1-5, 1995.

[WA91a] P. Wanderer, M. Anerella, J. Cottingham, G. Ganetis, M. Garber, A. Ghosh, C. Goodzeit, A. Greene, R. Gupta, J. Herrera, S. Kahn, E. Kelly, A. Meade, G. Morgan, J. Muratore, A. Prodell, M. Rehak, E.P. Rohrer, W. Sampson, R. Shutt, J. Skaritka, P. Thompson, E. Willen, Performance of Trim Coils Made by a Novel Method, BNL-45720 and Proceedings of the 12th International Conference on Magnet Technology, Leningrad, USSR, June 24-28, 1991.

[WA93a] P. Wanderer, M. Anerella, G. Ganetis, M. Garber, A. Ghosh, A. Greene, R. Gupta, A. Jain, S. Kahn, E. Kelly, G. Morgan, J. Muratore, A. Prodell, M. Rehak, E.P. Rohrer, W. Sampson, R. Shutt, R. Thomas, P. Thompson, E. Willen, Test of Eight Superconducting Arc Quadrupoles for RHIC, BNL-49348 and Proceedings of the 13th International Conference on Magnet Technology, Victoria, Canada, September 20-24, 1993.

[WA95b] P. Wanderer, M. Anerella, A. Greene, E. Kelly, E. Willen, Technology Transfer for Industrial Production of Superconducting Magnets for the RHIC Project at BNL, Nuclear Instruments and Methods in Physics Research B99 (1995).

[WA97a] P. Wanderer, Status of RHIC Construction, Proceedings of the 15th International Conference on Magnet Technology, Beijing, China, October 20-24, 1997.

[WA98] P. Wanderer, Magnet Measurements for Series Production, CERN Accelerator School, Measurement and Alignment of Accelerator & Detector Magnets, CERN Report, CERN 98-05 August 4, 1998.

[WE95] J. Wei, R. Gupta, A. Jain, S. Peggs, C.G. Trahern, D. Trbojevic, P. Wanderer, Field Quality Evaluation of the Superconducting Magnets of the Relativistic Heavy Ion Collider, Proceedings of the 1995 Particle Accelerator Conference, Dallas, TX, May 1-5, 1995, p.461.

[WE96] J. Wei, G. Ganetis, R. Gupta, M. Harrison, M. Hemmer, A. Jain, F. Karl, S. Peggs, S. Tepikian, P.A. Thompson, D. Trbojevic, P. Wanderer, Misalignment Evaluation of Superconducting Magnets in the Relativistic Heavy Ion Collider, Proceedings of the 5th European Particle Accelerator Conference, p.2222-2224, Sitges, Barcelona, June 10-14, 1996.

[WE99] J. Wei, R. Gupta, M. Harrison, A. Jain, S. Peggs, P. Thompson, D. Trbojevic, P. Wanderer, Real-World Sorting of RHIC Superconducting Magnets, Proceedings of the 1999 Particle Accelerator Conference, New York, 1999, p.3176.

[WI86a] E. Willen, Magnets for RHIC, BNL-38966 and Proceedings of the ICFA Workshop on Superconducting Magnets and Cryogenics, Brookhaven National Laboratory, May 12-16, 1986.

[WI96a] E. Willen, Superconducting Magnets, BNL-64183 and Proceedings of the INFN Eloisatron Project 34th Workshop, "Hadron Collider at the Highest Energy and Luminosity", Erice, Sicily, November 4-13, 1996.

[WI97] E. Willen, R. Gupta, A. Jain, E. Kelly, G. Morgan, J. Muratore, R. Thomas, A Helical Magnet Design for RHIC, Proceedings of the 1997 Particle Accelerator Conference, Vancouver, Canada, May 1997.

[WI99a] E. Willen, E. Kelly, M. Anerella, J. Escallier, G. Ganetis, A. Ghosh, R. Gupta, A. Jain, A. Marone, G. Morgan, J. Muratore, A. Prodell, P. Wanderer, BNL; M. Okamura, RIKEN, Japan, Construction of Helical Magnets for RHIC, Proceedings of the 1999 Particle Accelerator Conference, New York, 1999, p.3161.

[WI99b] E. Willen, M. Anerella, J. Escallier, G. Ganetis, A. Ghosh, A. Jain, E. Kelly, G. Morgan, J. Muratore, A. Prodell, P. Wanderer, BNL; R. Gupta, LBL; M. Okamura, RIKEN, Japan, Performance of Helical Magnets for RHIC, Proceedings of the 16th International Conference On Magnet Technology, Ponte Vedra Beach, FL, September 12-October 2, 1999.

[WI03] E. Willen, M. Anerella, J. Escallier, G. Ganetis, A. Ghosh, R. Gupta, M. Harrison, A. Jain, W. MacKay, A. Marone, J. Muratore, S. Plate, R. Thomas, P. Wanderer, KC Wu, BNL; M. Okamura, RIKEN Japan, Performance Summary of the Helical Magnets for RHIC, Proceedings of the 2003 Particle Accelerator Conference, Portland Oregon, May 12 – 16, 2003, p.164-166.

MAGNET ELECTRICAL SYSTEM (WBS 1.2)

i. Power Supplies

The electric power supply system required to operate the superconducting magnets for RHIC falls into three categories:

The main power supplies - The supplies used to power the main dipoles and the main quadrupoles are similar in that they have a ramp power section to provide a high voltage to bring the magnets rapidly up to full field, and a holding power section to maintain that current in a precise and efficient way during beam storage.

The main dipole and quadrupole power supplies are similar in design. Both use a pair of 12-pulse, phase controlled rectifier power modules. The dipole supply requires a 400 V ramp section and a 30 V holding section, while the quadrupole system uses a 90 V ramp section and a 15 V holding section. The control and regulating system will be interfaced with the main control computer for monitoring and analysis. The digital regulation system will use as its reference a zero flux Direct Current Current Transformer (DCCT), and will also reduce the sub-harmonic component of the ripple voltage through its control of the rectifier commutation. In order to control the betatron tune within $\Delta v=10^{-3}$, it is required that dipole and quadrupole currents track with about 10^{-5} accuracy.

A smaller shunting supply is used to offset the current in the horizontal quadrupole string for the current in the vertical quadrupoles string.

All main power supplies are located in the service building at 4:00 (4 o'clock).

The insertion power supplies - These include the shunts to the insertion dipoles, D0 and DX, the shunts to the insertion quadrupoles, Q1-3, and Q6-9 and the trim quadrupole supplies at CTQ4, 5, and 6. They will be specified in modular sizes to minimize the quantity of types of supplies to maintain, and to simplify procurement.

The unipolar insertion supplies use 12-pulse, phase controlled power sections. The bipolar insertion supplies use switch mode power sections with a linear output stage. While these accept a current set point digitally, the regulator is a precision analog device. All units use a DCCT, as the main supplies do, as a precision current measuring device.

All insertion power supplies are located in the service buildings.

The corrector power supplies. These include the supplies for the dipole correctors, the insertion correctors, the gamma-T jump, and the sextupoles.

These smaller corrector supplies use switch mode power sections with a linear output stage. They use analog regulation loops around a DCCT feedback. Both the current command and current and voltage readbacks are analog signals. All corrector power supplies are located in the ring alcoves.

Summaries. Table 2-1 summarizes the required power supplies, showing voltage, current, and quantity. Power supplies labeled "mono" are units that do not reverse current polarity. Units labeled "bi" are bipolar supplies, and operate with either polarity of voltage or current. At the bottom of Table 2.1 is a footnote marked by an *. This footnote uses a convention to describe the types of Low Beat Triplet magnet correctors. a2 is really a(2+1)2 = a6 which is a skew sextupole type corrector. b2 is really b(2+1)2 = b6 which is a normal sextupole type corrector. b3 is really b(3+1)2 = b8 which is a normal octupole type corrector. b4 is really b(4+1)2 = b10 which is a normal decapole type corrector. b5 is really b(5+1)2 = b12 which is a normal dodecapole type corrector. The “a” refers to a skew type corrector and the “b” refers to a normal type corrector.

Table 2-1. Power Supply Summary

Item	Polarity	Voltage (V)	Current (A)	Quantity (2 rings)
Main Power Supplies				
Dipole Ramp	mono	400	5500	2
Dipole Flat-top	mono	30	5500	2
Quadrupole Ramp	mono	90	5500	2
Quadrupole Flat-top	mono	15	5500	2
Quad H/V Trim	mono	40	300	2
Insertion Dipoles				
Type A	mono	20	2000	14
Type B	mono	20	600	7
Insertion Quadrupoles				
Type A	bi	15	150	96
Type B	bi	15	300	14
Type C	mono	15	200	48
Type D	mono	15	300	24
Type E	mono	15	450	16
Type F	mono	20	600	16
Corrector Supplies				
Dipole	bi	20	50	468
Gamma-T pulsers	pulsed	300	40	24
Skew Quads	bi	20	50	48
Octupoles	bi	20	50	48
Sextupole	bi	100	100	24
Low Beta Triplet*	bi	20	50	56
Snake and Spin Rotator Power Supplies				
Snake	mono	15	440	8
Spin Rotator	mono	15	440	16

*8 a_2, 8 b_2, 16 b_3, 8 b_4, 16 b_5 correctors.

ii. Magnet Bus

The power supplies for the collider magnets are distributed in the service buildings and in the tunnel alcoves. All magnets, with the exception of the sextupoles and the magnets in the corrector packages, are powered from the service building. Power is carried to the magnets from the service buildings using superconductors. These superconductors are bundled into an assembly called the Cold Crossing Bus (CCB). The power leads within each sextant of a ring are carried to the service building in two CCBs, one containing the main dipole current, and the other the quadrupole current. The two CCBs are identical, except that the quadrupole CCB has one additional conductor. The CCB is also used to carry power across warm sections of the ring, such as the space between the CQ3 and CQ4 magnets.

The cross section of the CCB is shown in Fig. 2-1. Wherever the CCB is used, the currents always sum to zero. This means that the critical current rating will be based on a magnetic field of essentially zero strength. The conductors are also given a MIITs $\left(\int I^2\,dt\right)$ rating as a measure of how much energy the copper in the cable can withstand during a quench. Table 2-2 lists these ratings.

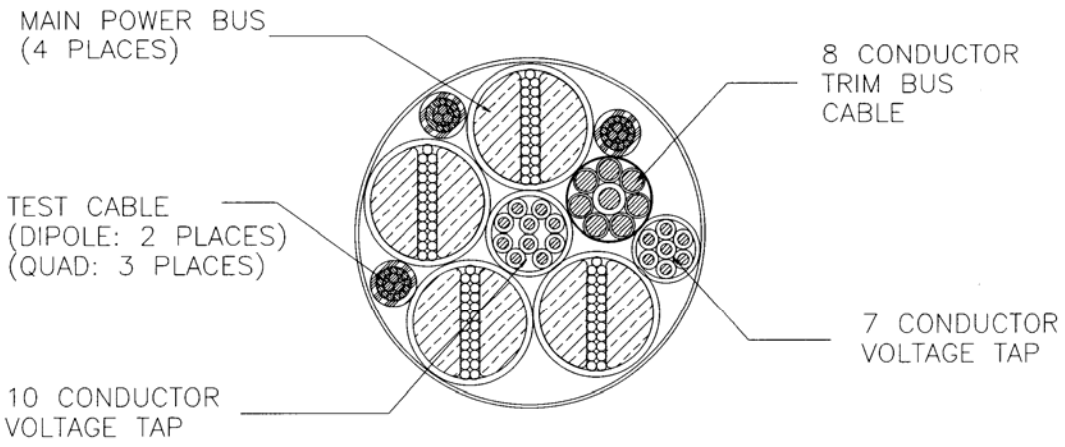

Fig. 2-1. Cold Crossing Bus

Table 2-2. Cold Crossing Bus Ratings

Conductor	Current Ratings, A Critical	Operating	MIITs (10^6 A^2 sec)
Main Power	11000	6600	204
Test Cable	1800	600	1.50
Trim Bus	1800	150	0.11

The diagrams of Figs. 2-2 and 2-3 show the dipole and quadrupole bus arrangements. The dipole circuit is powered from the 4:00 insertion region, with the return busses coming back at 10:00. Dump resistors are at 4:00 and 10:00, and are split for symmetry. The insertion dipoles, D0, and in the blue ring, DX, are connected in the return path. This keeps them near ground potential during a quench, and is done to minimize the stress on power supplies shunting them. In the quadrupole circuit, the H/V Offset also has quench protection, but it is not shown.

The quadrupole circuit is also powered at 4:00 with a return at 10:00. In this configuration, the vertical quads are powered on one bus, while the horizontal quads are on the other. This allows a trim supply to offset the current in the horizontal bus with respect to the vertical bus. The insertion quads placement is also shown here, and the circuits powering Q8 and Q9 will have the capability to offset the trim current, making the base current in the insertion quads independent of the trim setting.

In Fig. 2-2 there is a table of Inductances. The arc dipole is 25mH. The dipole sextant is made up of arc dipoles D10-D20 and D20-D10. Each one of these dipoles is 25mH and the total is 25mH*22 magnets for a total of 550mH. In Fig. 2-2 between 8:00 and 10:00, D5O(I) indicates D5 outer for blue and inner for yellow. Then between 6:00 and 8:00 D5I(O) indicates D5 inner for blue and outer for yellow. The energy extraction resistor values, at 4:00 and 10:00 in Fig. 2-2, for the yellow ring are in parenthesis and the values for the blue ring are not in parenthesis. In Fig.2-3 a quad sextant is defined as $Q_V + Q_H$. Where Q_H = 11 magnets*1.5mH = 16.5mH and Q_V = 12 magnets*1.5mH = 18mH. 16.5mH + 18mH = 34.5mH for a quad sextant. The11 magnets in Q_H are Q11, Q13, Q15, Q17, Q19, Q21, Q19, Q17, Q15, Q13 and Q11. The 12 magnets in Q_V are Q10, Q12, Q14, Q16, Q18, Q20, Q20, Q18, Q16, Q14, Q12, Q10.

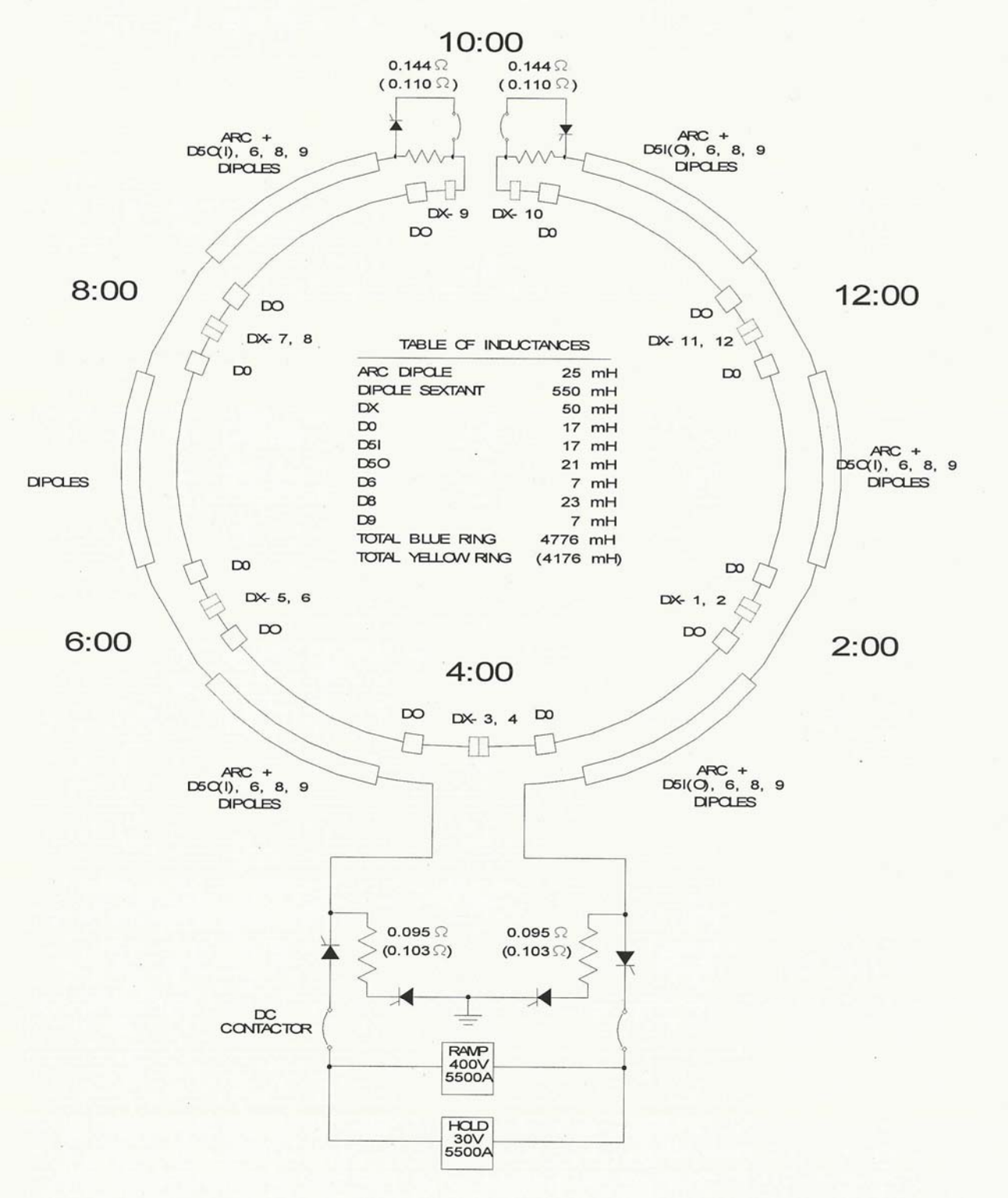

Fig. 2-2. Main dipole bus layout. The DX dipoles are in the blue ring bus only.

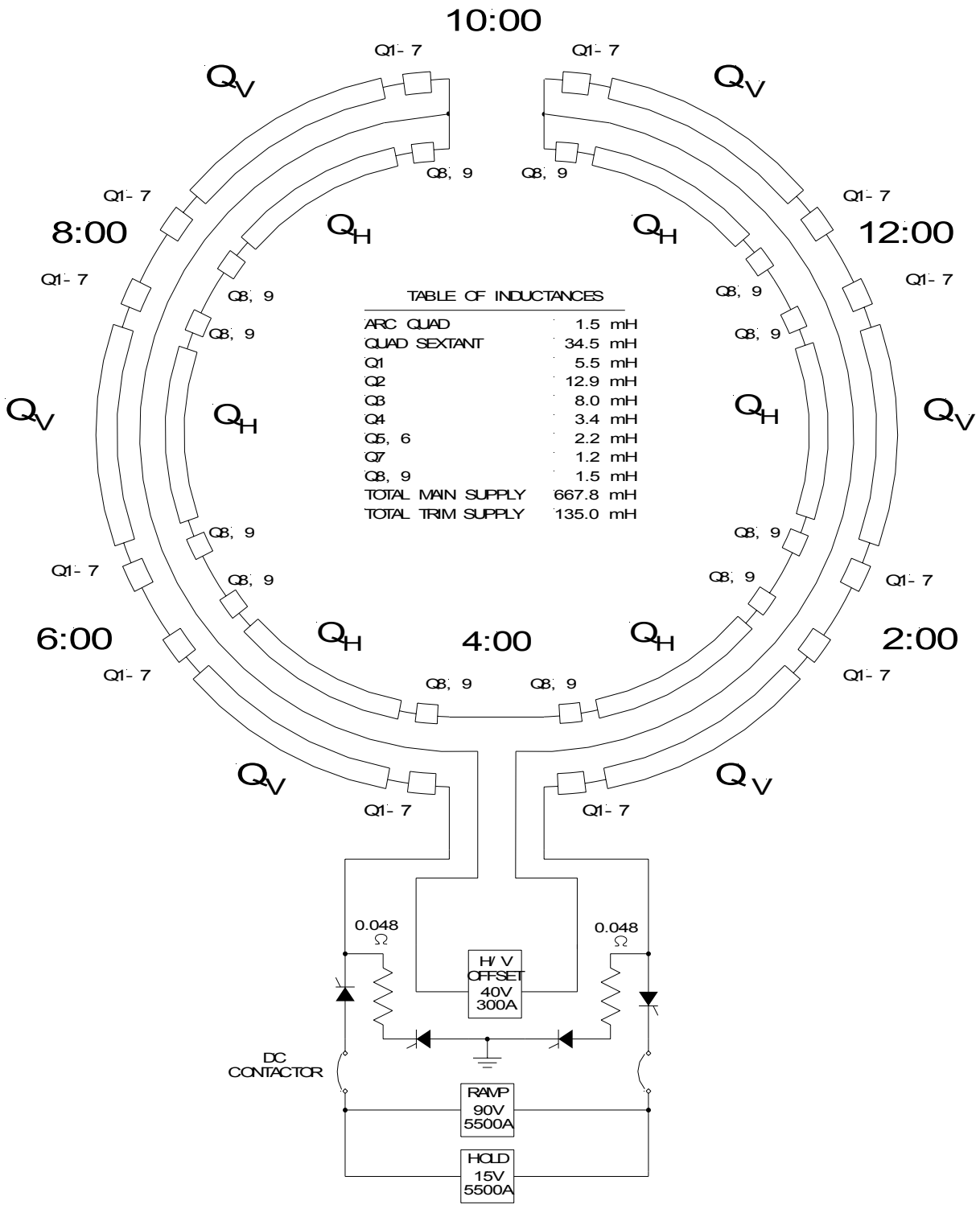

Fig. 2-3. Main quadrupole bus layout.

iii. Cable Tray System

The power supplies for most of the superconducting magnet loads are located in the equipment service buildings. These supplies are connected to gas cooled warm-to-cold power leads that are part of the cryogenic valve boxes, also located in the equipment service buildings. On the warm side of the power leads, copper cables connect to the power sources. On the cold side of the power leads, superconducting Cold Crossing Bus carries the current to the RHIC tunnel, where it is distributed over other superconductors to the magnet loads. The sextupole and corrector supplies are located in the tunnel alcoves, and power from these supplies is carried by conventional copper cables in trays. In addition to power supply leads, the trays also bring beam instrumentation cables and control signals to the alcoves.

In most of the ring, the trays are hung from the center of the tunnel. This is nearly directly above the magnets. The cables drop out of the trays and can either go to the power leads on the CQS assemblies, or to other devices, such as cryogenic, vacuum, and safety equipment. In those areas (typically in the region between each Q3 and Q4) where the vacuum jacketed piping bypasses warm beam tube sections, the cable trays move to the outside of the ring.

Figure 2-4 is a composite of two typical areas in the arch plate portions of the tunnel. The trays have been partitioned to segregate cable types, as required by the National Electrical Code. Each of the partitions in the tray has been labeled, and the cable types that occupy those sections of the trays have been listed in Table 2-3.

Some cables are totally internal to the ring. They might be connections between devices in the ring or between devices in the ring and equipment in the alcoves. Other cables need to go from the equipment service buildings to the ring. These are carried by tray to the ring, where they enter at the same location as the vacuum jacketed piping. At 6, 8, 10, and 12 o'clock this means entering through the top of the ring via conduits. At 2 and 4 o'clock the tray enters through the side of the tunnel. In either case, the cables enter the tray in the ring at a location between the Q1 and D0 magnets.

The cable tray system in each sextant stretches from DX to DX. At 2, 6, 8 and 10 o’clock no cables interior to the ring ever cross the beam crossing point. This avoids interference with equipment in the experimental areas. At 4 and 12 o’clock there are some optical signal cables that do cross the IR region.

Table 2-3. Cable Tray Space Allocation

Conductor		Total Tray Width, cm (in.) DX - Q4			Q5 - Q5	
Correctors	F,H	61	(24)	D,F,H	107	(42)
Beam Instrumentation	E,G	15	(6)	E,G	61	(24)
Vacuum, Cryogenics, Control	A	10	(4)	A	23	(9)
AC Power	B	5	(2)	B	23	(9)
High Voltage	J	15	(6)	J	15	(6)
Security	C	15	(6)	C	15	(6)
Totals		122	(48)		244	(96)

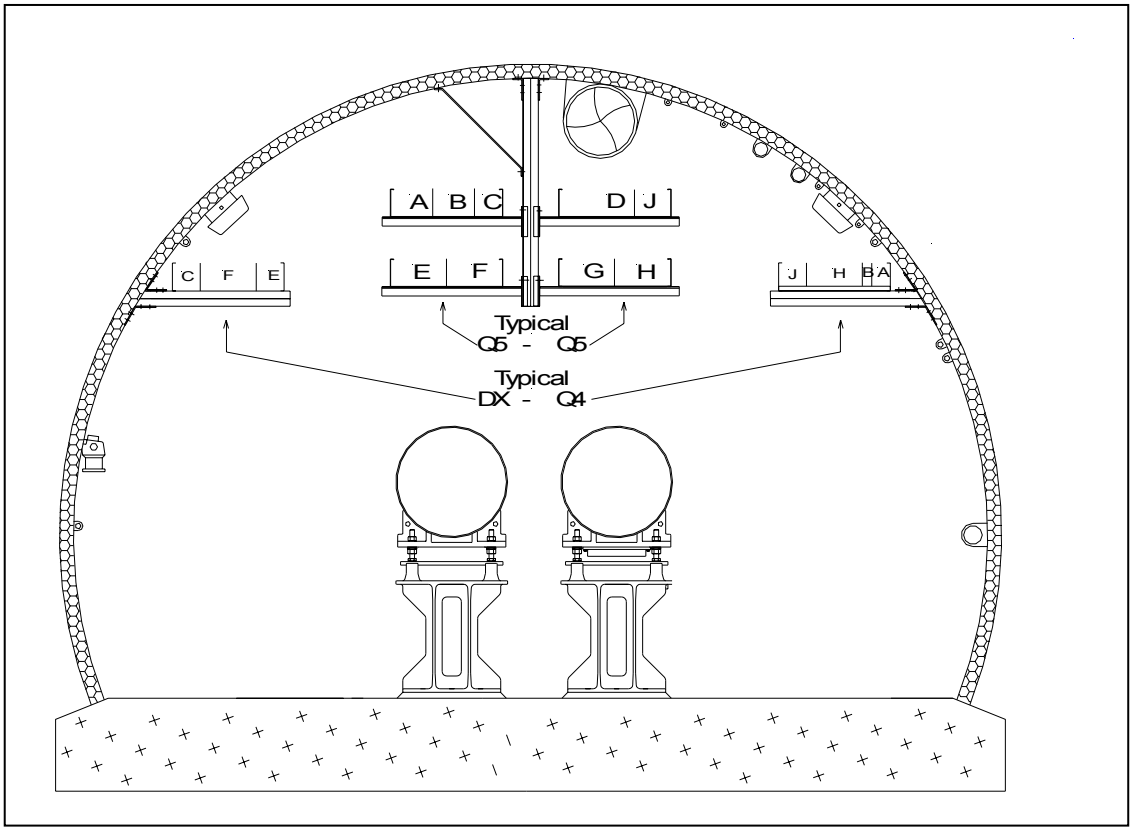

Fig. 2-4. Composite Cable Tray Layout

iv. Quench Protection System

To prevent magnet damage in the event of a quench, the current in the quenching magnet must be reduced to zero before overheating occurs. There are two parts to this system. First, the energy from the non-quenching magnets is bypassed, through the natural switching action of a diode around the quenching magnet. Second, quench detectors "switch in" energy dump resistors that reduce the current, as they absorb the stored energy.

The single-diode bypass system is shown in Fig. 2-5. In this circuit, the current is forced out of the magnet and into the shunting diode by the natural action of the quench developed resistance of the magnet coil. Energy from the non-quenching magnets will not heat the quenching magnet because of the shunting action of the diode. The collider magnets, with the exception of the DX dipole, are able to absorb their own energy without overheating during the time that the current is being reduced by the energy dump resistors.

The DX dipole is different than the other main magnets in two ways. First, because of it's higher inductance (50 mH vs. 25 mH for an arc dipole), the induced voltage during a current ramp will be higher. This requires two series bypass diodes, instead of the single diode shown in Fig. 2-3. Second, since it cannot absorb its own energy, an active quench protection system will be required.

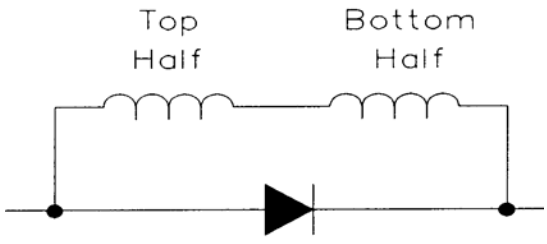

Fig. 2-5. Single diode protection circuit.

Even though the quench-inducing individual magnet is protected, it is necessary to remove the stored energy from the entire series-connected string as rapidly as possible to avoid quench propagation into neighboring magnets and to protect the bus and diodes from overheating. The thermal mass of these elements is large enough to permit a simple solution. Figs. 2-2 and 2-3 show this energy extraction system.

Current is reduced in the non-quenching magnets by a redundant set of switches. The primary switches are solid state silicon controlled rectifiers (SCR). Redundancy is provided by commercially designed dc interrupters commonly used to protect large power systems. When these switches open, the current is diverted into dump resistors which dissipate the stored energy and exponentially reduce the current to zero. The bus and the diodes together with their heat sink have been tested to withstand the rated current for the worst case "dump" period.

v. Insertion Power Supply Systems

The insertion region contains both beam bending magnet and focusing elements. To reduce power supply cost and minimize cold penetrations these elements are connected in series with the main dipole or quadrupole circuits. However, provisions are made to adjust each insertion quadrupole separately as required, either through a shunt, or an auxiliary trim quadrupole.

Insertion Dipole Power Supplies

The regular arc dipoles and insertion dipoles D5, D6, D8 and D9 are in series with the supply side of the main dipole bus. The remaining insertion dipoles, D0, and in the blue ring, DX, are in the circuit return leg. Figures 2-6 through 2-8 shows the detailed circuit arrangement of the dipoles in the insertion regions. The quench protection assemblies and main power supplies are shown there as well. In these figures, three power supplies are shown, PS1, PS2, and PS3. They are connected to the insertion dipoles with a link box, to allow for the best configuration of voltages and polarities for a given species combination. Table 2-4 shows the arrangement of power supplies for typical cases.

Provision for shunting current around D5 and D6 will be provided, but the lengths of these magnets will be adjusted so that no electrical correction is expected.

Table 2-4. Insertion Dipole Configuration

Power Supply	Particle	Current Rating	Polarity
PS1 - Yellow	Au	2000 A	As Shown
PS2 - Blue	Au	2000 A	As Shown
PS3 - Blue		600 A	As Shown
PS1 - Yellow	Cu	2000 A	As Shown
PS2 - Blue	Cu	2000 A	As Shown
PS3 - Blue		600 A	As Shown
PS1 - Yellow	p	2000 A	As Shown
PS2 - Blue	p	2000 A	As Shown
PS3 - Blue		600 A	As Shown
PS1 - Yellow	Si	2000 A	As Shown
PS2 - Blue	Si	2000 A	As Shown
PS3 - Blue		600 A	As Shown
PS1 - Yellow	Au	2000 A	As Shown
PS2 - Blue	d	2000 A	As Shown
PS3 - Blue		600 A	Reversed

The insertion dipole configuration for p-Au is not shown in Table 2-4. This will be determined at the time of the p-Au run.

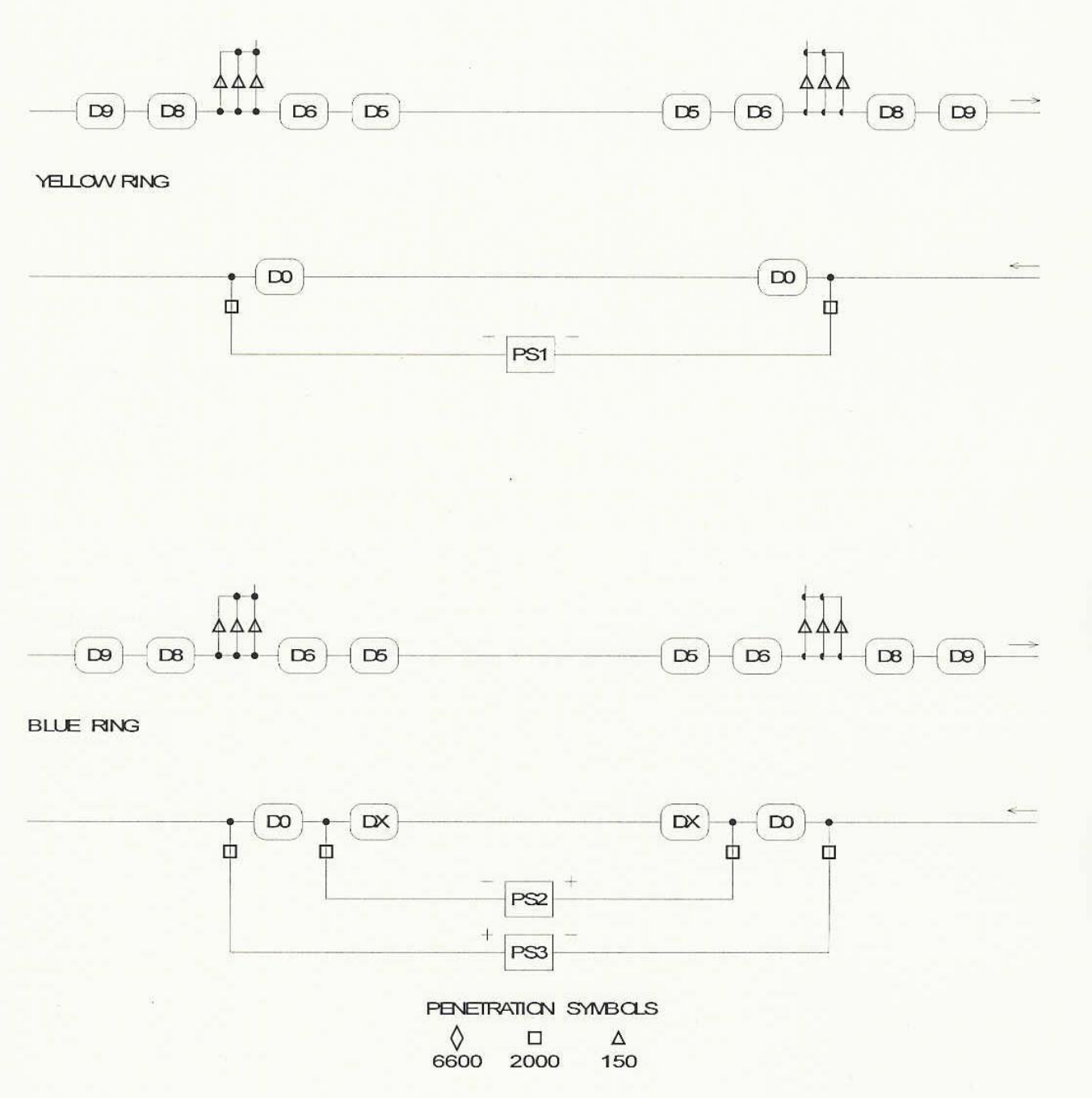

Fig. 2-6. Insertion dipoles at 2, 6, 8 and 12 o'clock.

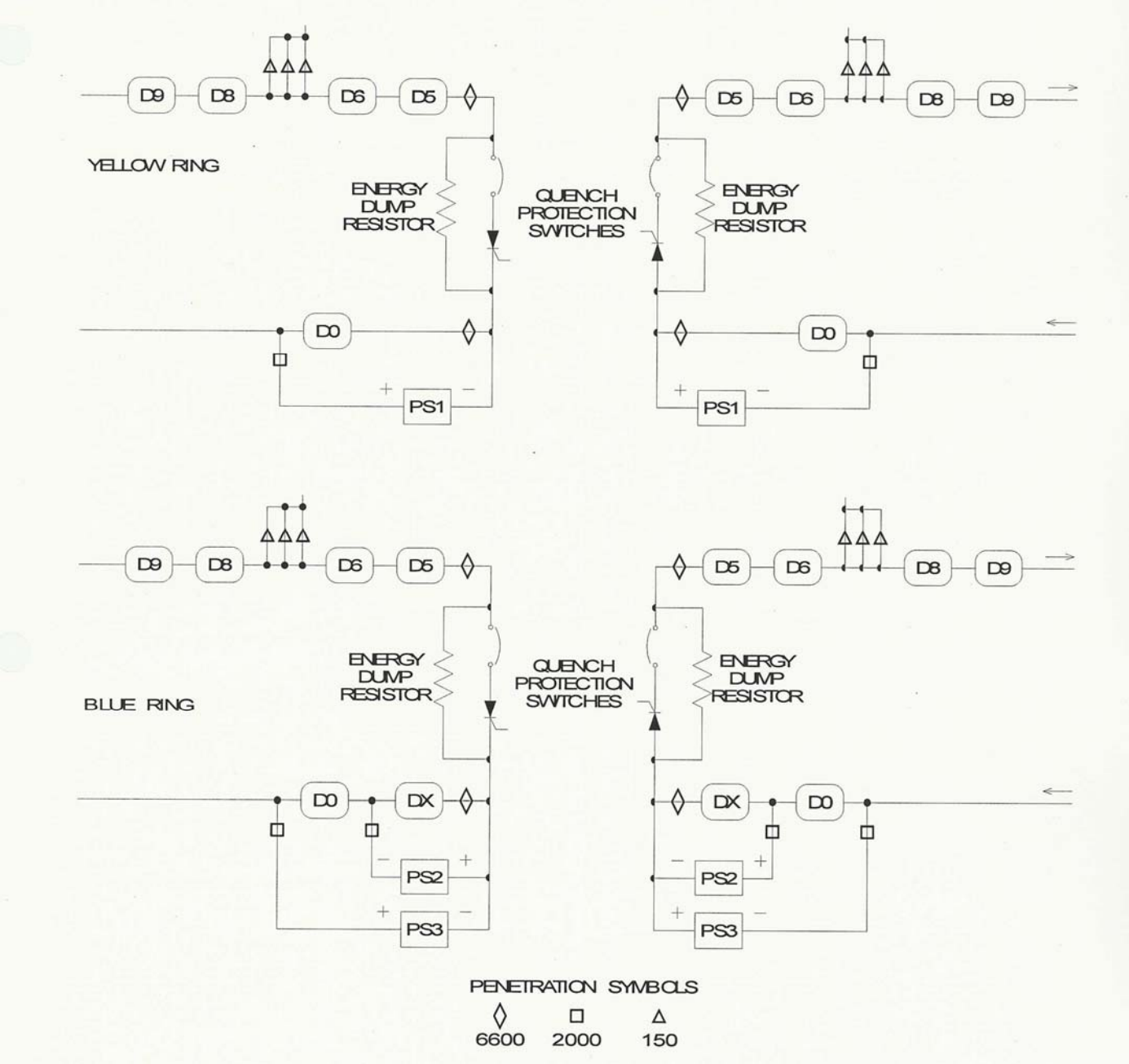

Fig. 2-7. Insertion dipoles at 10 o'clock.

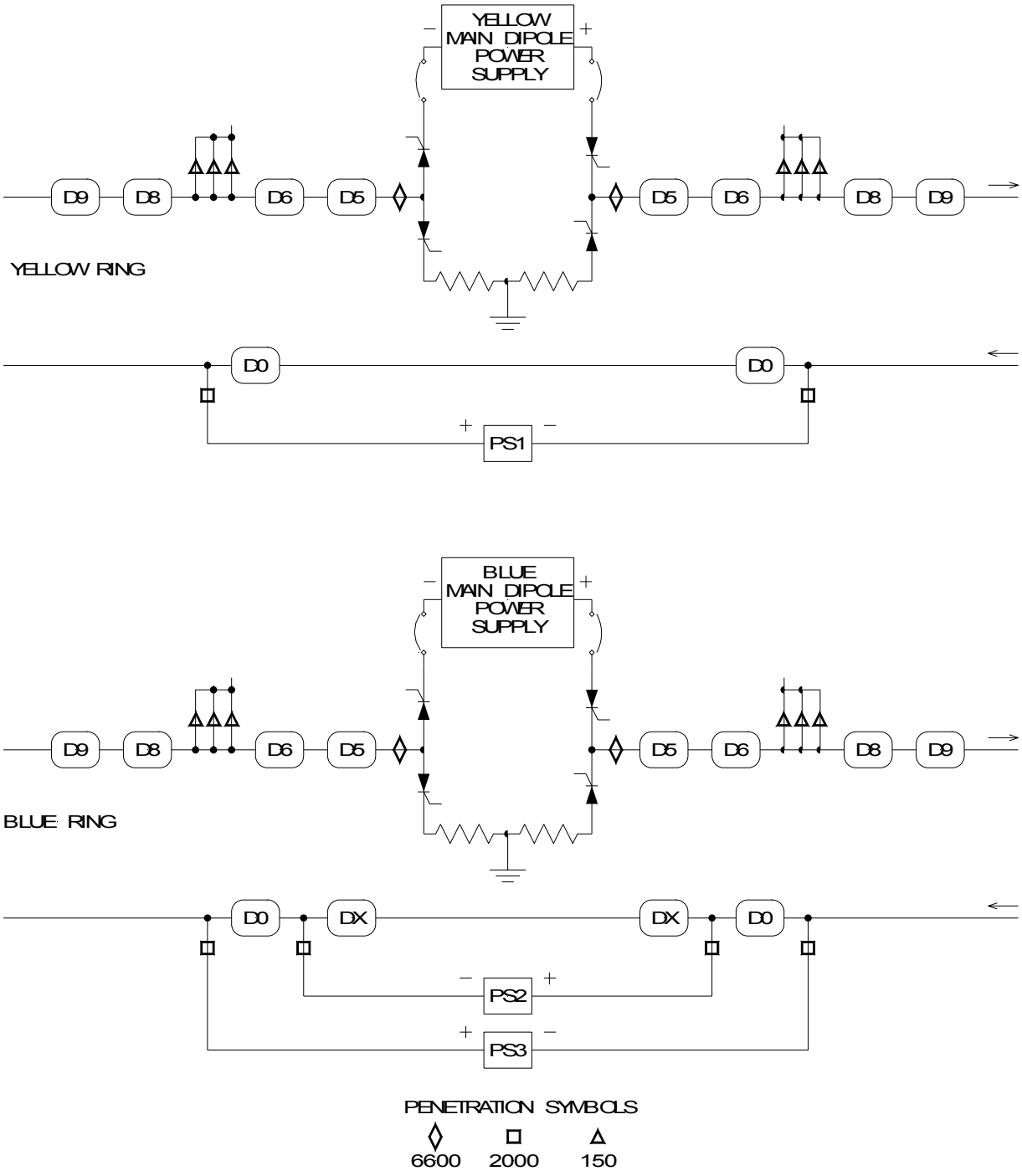

Fig. 2-8. Insertion dipoles at 4 o'clock.

Insertion Quadrupole Power Supplies

The quadrupole insertion schematics are shown in Figs. 2-9 through 2-11. Current flows through the regular Q_V quadrupoles, then through a set of insertion quadrupoles. This pattern repeats until the circuit has gone half way around the ring, then returns through the series connection of the Q_H regular quadrupoles (see Fig. 2-3) and the remaining insertion quadrupoles.

The choice of circuit configuration for the various insertion quadrupoles has been chosen to minimize power supply and current penetration requirements and is sized to allow a continuous change of $ß^*$ between 1 and 10 m. This is implemented in two ways. The current in some of the insertion quadrupoles is varied with shunt supplies. But, in CTQ4, 5 and 6, trim quadrupoles are added where the sextupoles are located in the CQS assemblies. These trim magnets allow tuning the insertions at lower currents. The approximate inductance of each of these trim magnets is 700mH. The shunt supply at CTQ6 is fixed during the $ß^*$ change.

The inner and outer quadrupole currents at Q6, 7 and 9 are close enough that they can share a single power supply that bridges the crossing point. This is not possible at 10:00 or at 4:00 for Q6 and Q7.

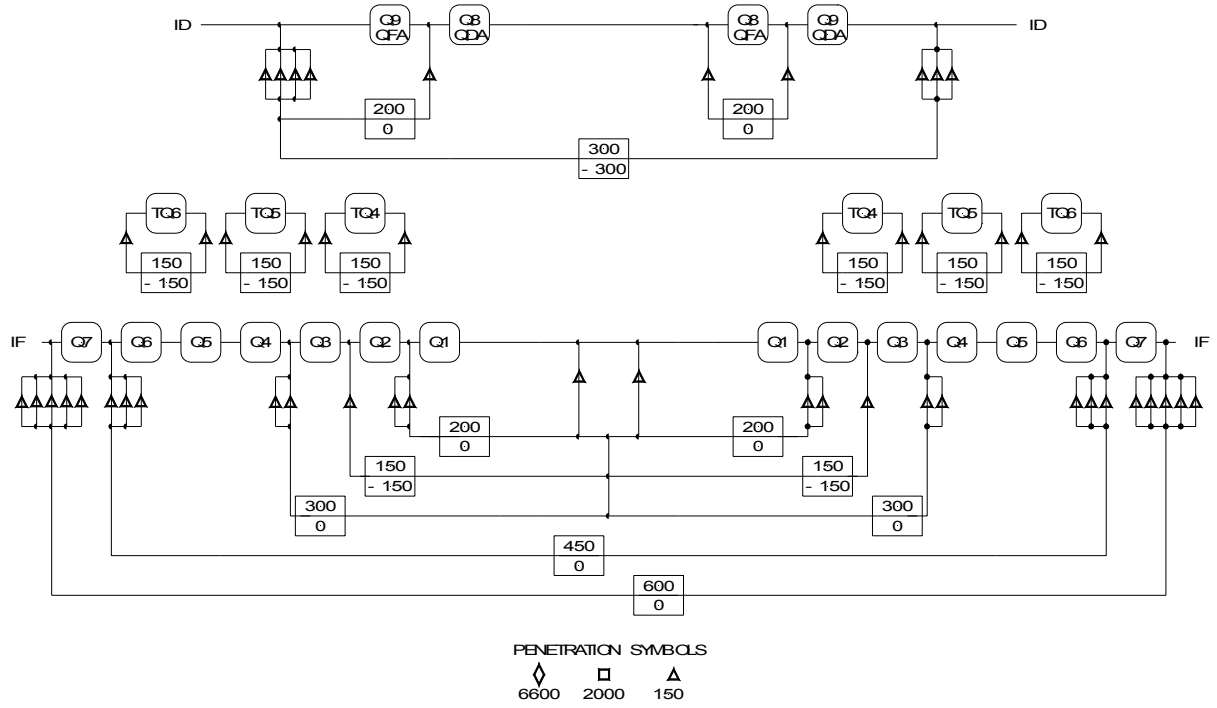

Fig. 2-9. Insertion quads at 2, 6, 8 and 12 o'clock.

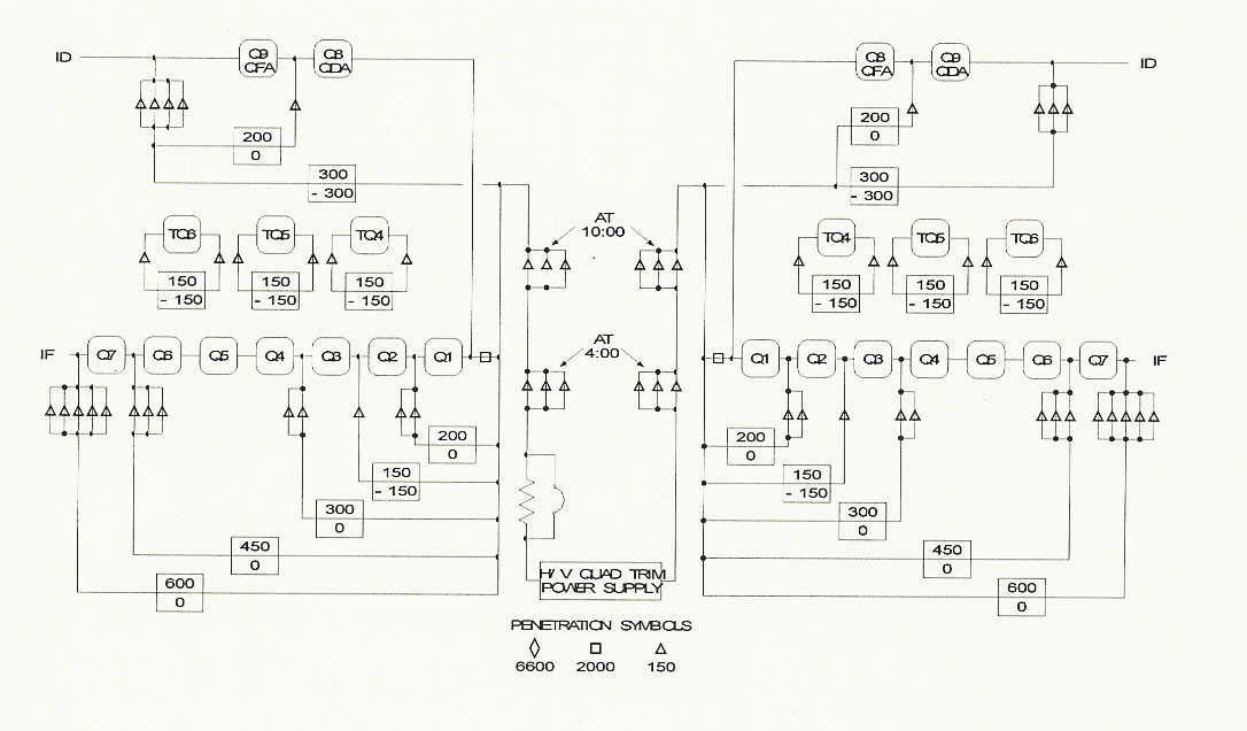

Fig. 2-10. Insertion quads at 10 o'clock.

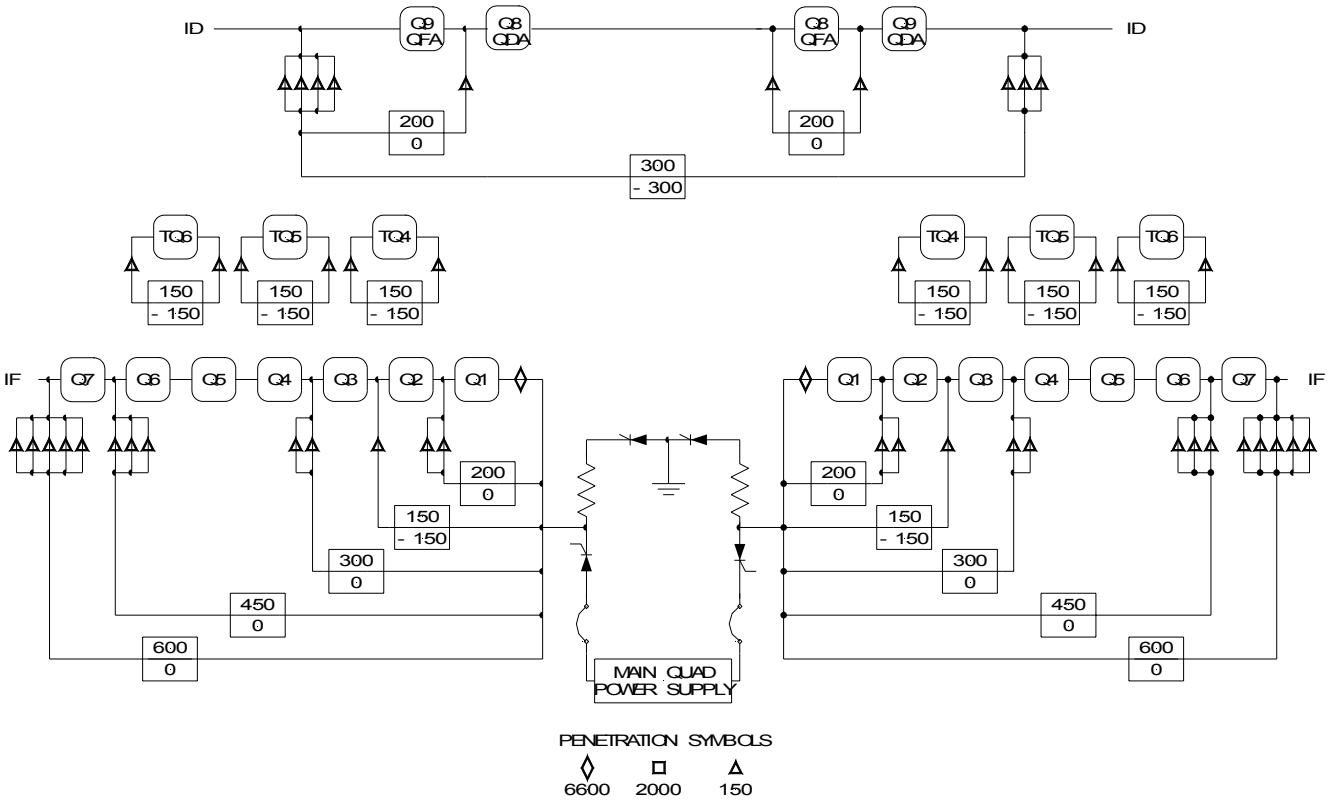

Fig. 2-11. Insertion quads at 4 o'clock.

vi. Correction Magnet Power Supply Systems

There are corrector magnets in each CQ, CQS, or CTQ assembly. The leads for these magnets are brought out individually at each CQ- cryostat. If a corrector magnet should fail, this would make isolating the defective magnet possible.

Figure 2-12 shows the circuit scheme for powering the chromaticity sextupoles, b_2. These elements are connected in two families, focussing and defocussing, in each arc. Each family is powered individually. A sextupole power supply sees a total inductance of approximately 9.6H. There are 12 sextupole magnets connected to each sextupole p.s. There are 4 sextupole power supplies in each B alcove, 2 blue and 2 yellow.

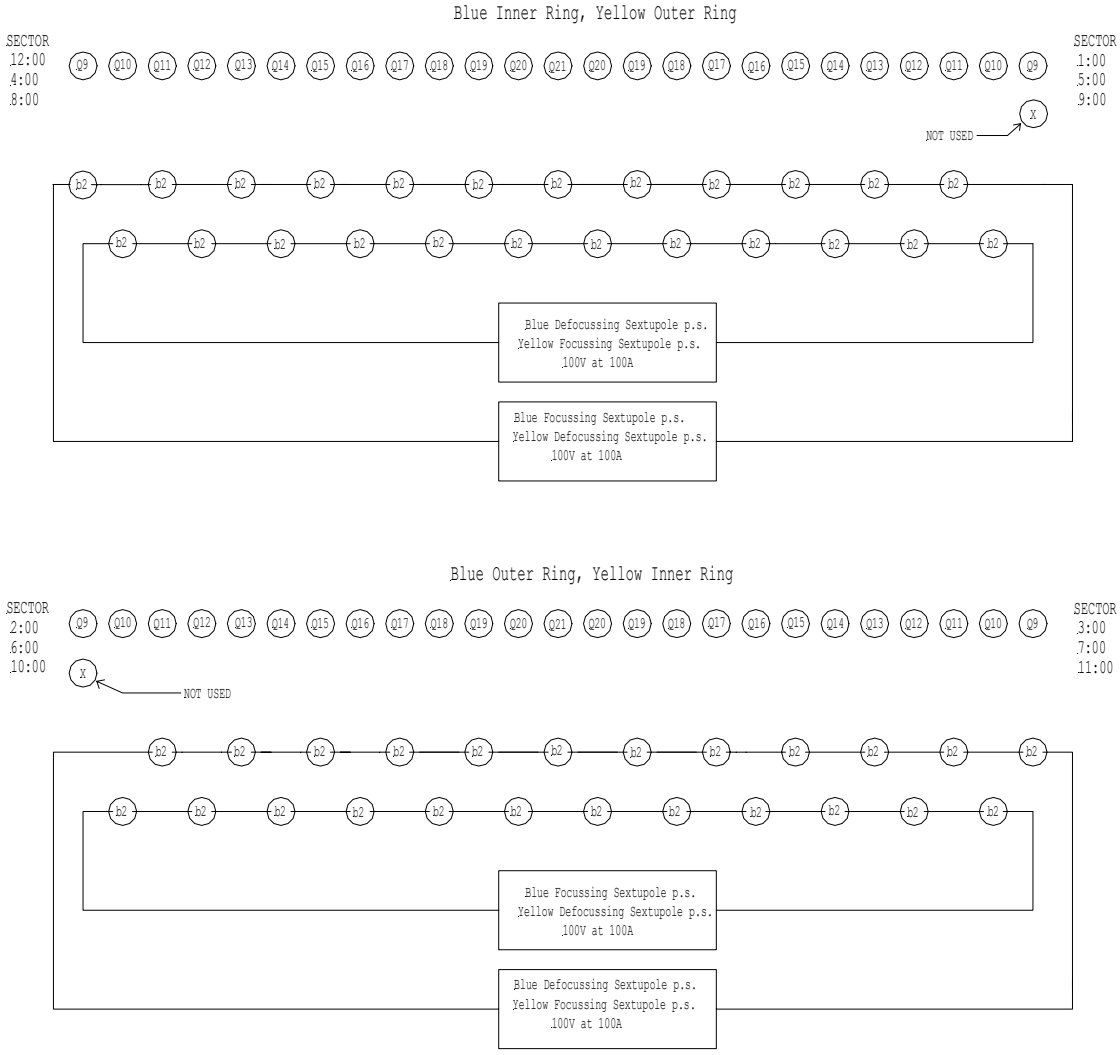

Fig. 2-12. Sextupole circuit.

Figures 2-13 and 2-14 show the configuration of the corrector power supplies for the blue ring. The yellow ring correctors are a mirror image, about the 6:00 insertion region, of the blue correctors. The figures show the correctors in the range, Q10-Q1-Q1-Q18. All the corrector packages in this region are four layers. Outside this range, Q19-Q21-Q10, all corrector packages are single layer (dipole only).

The a_O/b_O closed orbit correction magnets are individually powered in both the arcs and the insertion regions. All are nominally 50 A bipolar supplies.

The dipole and a_1 correctors in the triplet region are individually powered at every insertion region, in the same manner as the other a_0/b_0 elements. In addition, at those regions requiring the lowest β*, the b_2, b_3, b_4, and b_5 elements are also individually powered. This is indicated in Figs. 2-13 and 2-14 by drawing those elements within a dotted circle. In its initial configuration, low β* will be required at the 6:00 and 8:00 regions, but as the leads to all the correctors are available, the other insertion regions can easily be upgraded.

The other corrector supplies are connected as shown. Where circles are shaded, the magnets are not powered, but the leads are available for future use. The "F" and the "+" stand for focus. The "D" and the "-" stand for defocus.

The inductances of the arc corrector magnets are:

Dipole = 840mH, Quadrupole = 29mH, Octupole = 8mH, Decapole = 5mH, The decapoles are not connected to power supplies at this time but the leads are available.

The inductances of the triplet corrector magnets are:

Dipole = 1710mH, Quadrupole = 112mH, Sextupole = 30mH, Octupole = 26mH, Decapole = 14mH, Duodecapole = 9mH

The Gamma-T power supplies are connected as shown in Figs. 2-15 and 2-16. A Gamma-T p.s. is connected to 4 arc quadrupoles which are approximately 29mH each. The total inductance a Gamma-T power supply sees is 116mH.

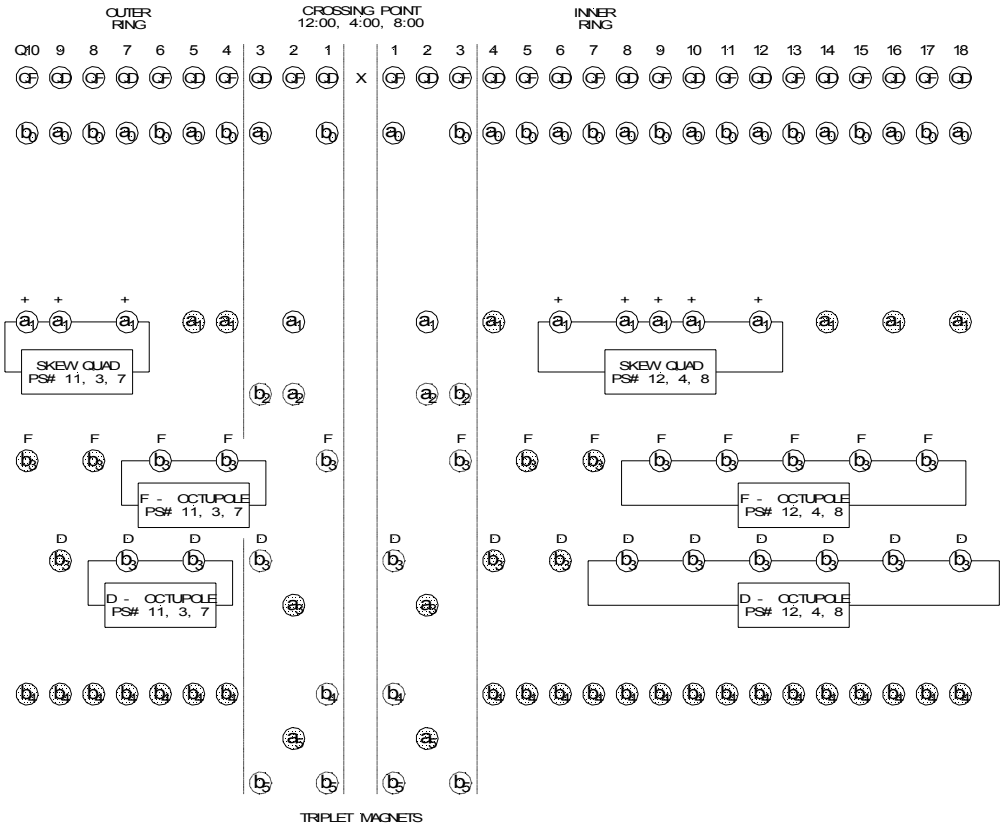

Fig. 2-13. Corrector power supplies at 12, 4 and 8 o'clock.

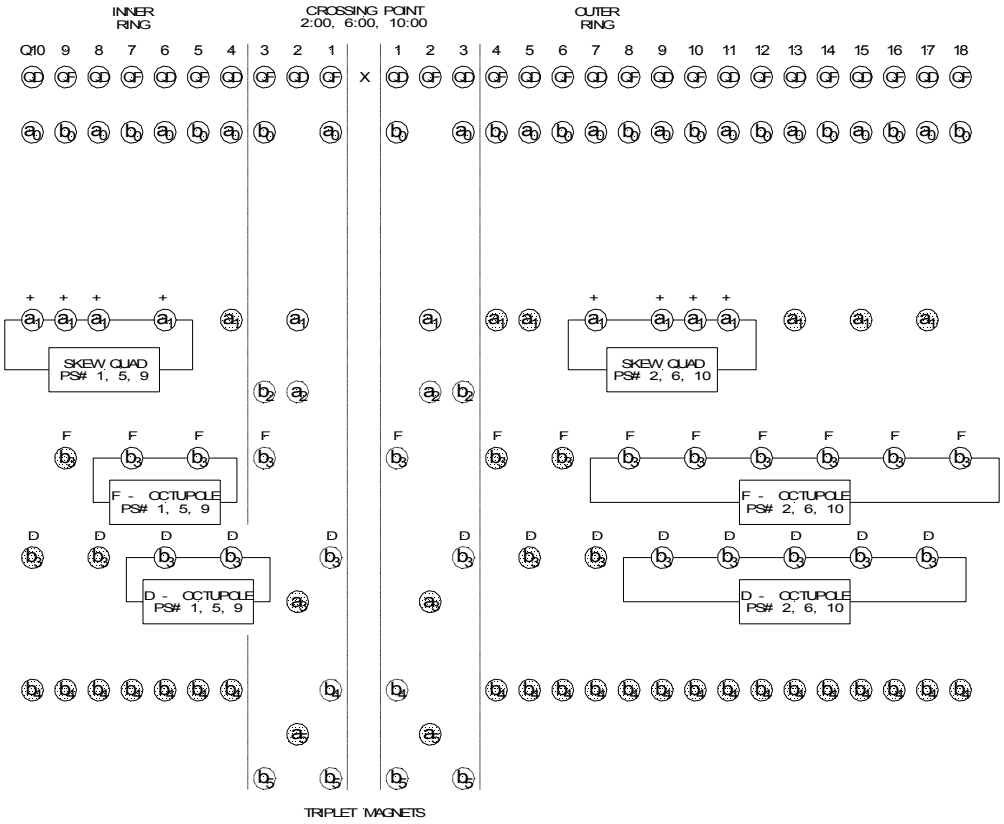

Fig. 2-14. Corrector supplies at 2, 6 and 10 o'clock.

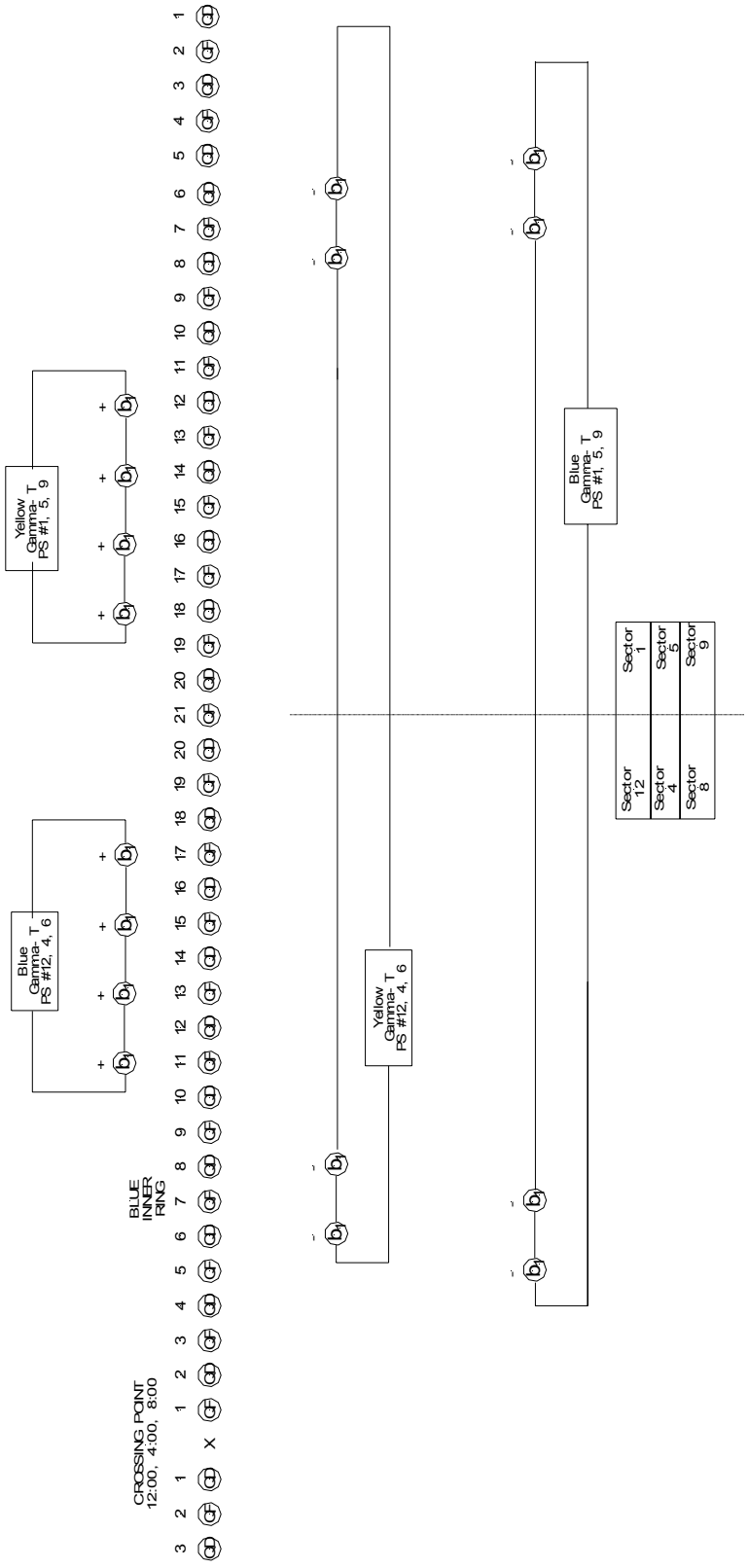

Fig. 2-15. Gamma-T supplies at 12, 4 and 8 o'clock.

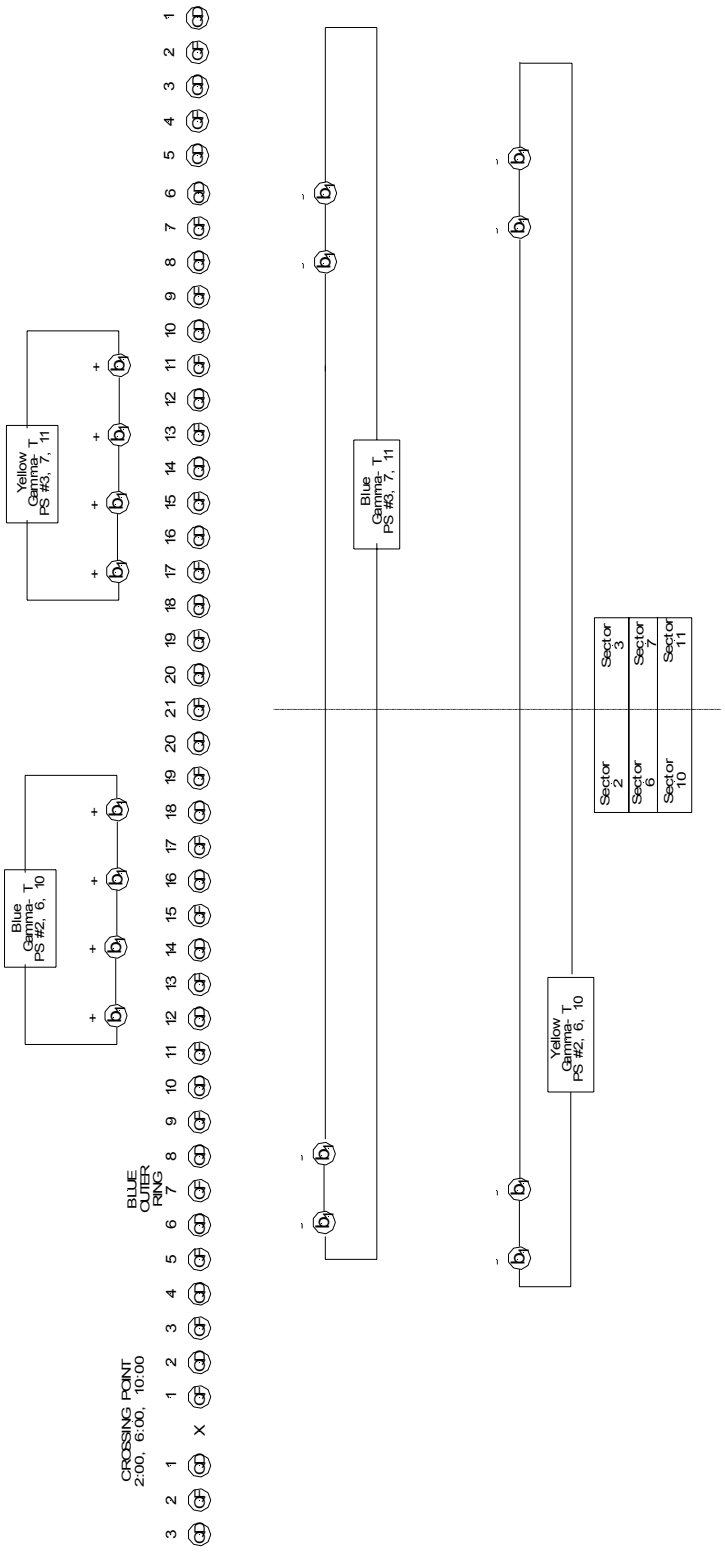

Fig. 2-16. Gamma-T supplies at 2, 6 and 10 o'clock.

vii. Power Supply Connections of Corrector Magnets

Magnetic Measurement Convention

All magnets were measured and the magnetic field information was recorded according to an "intrinsic" convention, which can be summarized as follows:

All measurements are made from the lead end. When looking into the magnet from the lead end of the magnet, the positive x-axis points to the right hand side, while the positive y-axis points upwards. The origin is chosen to be at the center of the magnet. (This is different from the MAD convention, where the x-coordinate always points outward.)

In a nominally single-harmonic magnet, the magnetic field, generated by a positive current into the positive pin, is fully defined by its strength and direction on the right (positive-x) half of the median plan. Here, all normal magnets have a pure positive B_y (pointing upward), and all skew magnets have a pure positive B_x (pointing to the right) field component.

The power supply is connected to the magnet at a terminal, to which the wire pair is brought and numbered so that the positive pin has always the larger number. For example, the 8-cm corrector magnets in the CQS (corrector-quadrupole-sextupole) unit are powered during magnetic measurements as follows:

Dipole, horiz and vert	#12 positive, #11 negative
Quadrupole, normal and skew	#10 positive, # 9 negative
Octupole	#8 positive, # 7 negative
Decapole	#6 positive, # 5 negative
Sextupole magnet	#4 positive, # 3 negative

The 13-cm correctors in the triplet are powered during magnetic measurements as follows:

Dipole, horiz and vert	#12 positive, #11 negative
Sextupole, b2	#8 positive, # 7 negative
Octupole, b3	#10 positive, # 9 negative
Decapole, b4	#8 positive, # 7 negative
Dodecapole, b5	#6 positive, # 5 negative
Skew quadrupole, a1	#8 positive, # 7 negative
Skew sextupole, a2	#4 positive, #3 negative
Skew octupole, a3	#6 positive, #5 negative
Skew dodecapole, a5	#2 positive, #1 negative

Optical Properties of Magnets

In addition on the direction of the exciting current, the "functional" or optical properties of a magnet; i.e, its effect on the beam, will depend on the ring into which it is installed and on its direction with respect to the beam in that ring. For RHIC, the convention defining the "installed" direction of the main dipole and quadrupole magnets in both rings refers to the blue ring, in which the beam travels clockwise (CW).

Extending this convention to corrector magnets has the ring-wide consequence that a clockwise installation in the blue ring implies that the beam enters the non-lead end, whereas in the yellow ring clockwise installation implies beam entering the lead end of any magnet.

All arc dipoles are CW installed.

The installation of the arc quadrupole magnets depends on the sector location as follows:

Sector 2, 3, 6, 7, 10 and 11 is CW

Sector 1, 4, 5, 8, 9 and 12 is CCW

Dipole corrector, sextupole, and trim quadrupole magnets are attached to a main quadrupole and the installation of the combined unit follows the rule for the main quadrupole. Depending on the mechanical arrangement of the magnets within the unit, the attached magnet can be clockwise (CW) or counter-clockwise (CCW). The clockwise unit has the attached magnets installed as

in CW-CQS : Corrector CW, sextupole CCW

in CW-CTQ: Corrector CW, trim magnet CCW

in CW-Q2: Corrector 1 (style I, J) CCW

in CW-Q3: Corrector 2 (style K) CW, corrector 3 (style L,M) CCW

In the triplets, the lead end of Q1 and Q2 is on both sides away from the IP and in Q3 towards the IP.

Prescriptions for the Power Supply Connections

In order to bring the above rules into conformance with the MAD convention used in the RHIC model, the power supply connection of the magnets in the ring will, in some cases, require polarity changes from those used for the magnetic measurements to accommodate the specific ring location and the installed direction of the magnets. The corrector power supply connections have to be done according to the prescriptions of the attached Table 2-5.

Table 2-5. Corrector Power Supply Connections

Positive:	Connected as for magnetic measurements
Reverse:	Connections reversed from magnetic measurements
CW Installation:	Beam enters **non-lead end** in BLUE, **lead end** in YELLOW
CCW Installation:	Beam enters **non-lead end** in YELLOW, **lead end** in BLUE

BLUE	**YELLOW**
b1 (quad), b3 (oct), b5 (dodec)	
CW: Positive	CW: Reverse
CCW: Reverse	CCW: Positive
b2 (sext), b4 (dec)	
CW: Positive	CW: Reverse
CCW: Positive	CCW: Reverse
Skew a1 (quad), a3 (oct), a5 (dodec)	
CW: Reverse	CW: Positive
CCW: Reverse	CCW: Positive
Skew a2 (sext)	
CW: Reverse	CW: Positive
CCW: Positive	CCW: Reverse

viii. Main Magnet Power Supplies

Overview

The RHIC Main Magnet Power Supplies (RMMPS) provide the current for the main dipole and main quad magnet strings. The main dipole and main quad magnet strings are separate electrical circuits; since there is a separate RMMPS for each circuit, and each ring, there are four RMMPS.

Each RMMPS has three major components, the Flat-top Power Module (FTPM), the Ramp Power Module (RPM), and the Output Circuit Compartment (OCC). The power modules supply the current to the magnet strings. The OCC houses the output filter, the quench protection components, the regulator and remote PLC monitoring. Figure 2-17 shows the main power supply block diagram and the interconnection of these sub-systems. Each of these sub-systems is described in a section below.

Sub-System Descriptions

Power Modules

There are two power modules for each RMMPS. Each power supply has one FTPM and one RPM connected in parallel. The two power modules for each RMMPS are 12-pulse, phase controlled power converters. Only one of these power modules is active at a given moment. The regulator selects the active power module based on the instantaneous current slope. When the current slope is low the FTPM is active. During a ramp, when the current slope is above a selected level, the RPM is active. This allows the power modules to be sized for the voltage necessary to maintain the required current slope. This approach provides low voltage ripple when the current is a constant value. The only major difference between the different types of power modules are the rectifier transformers. The RPM transformers are not sized for continuous operation. The voltage and current ratings of the modules are listed in Table 2-6.

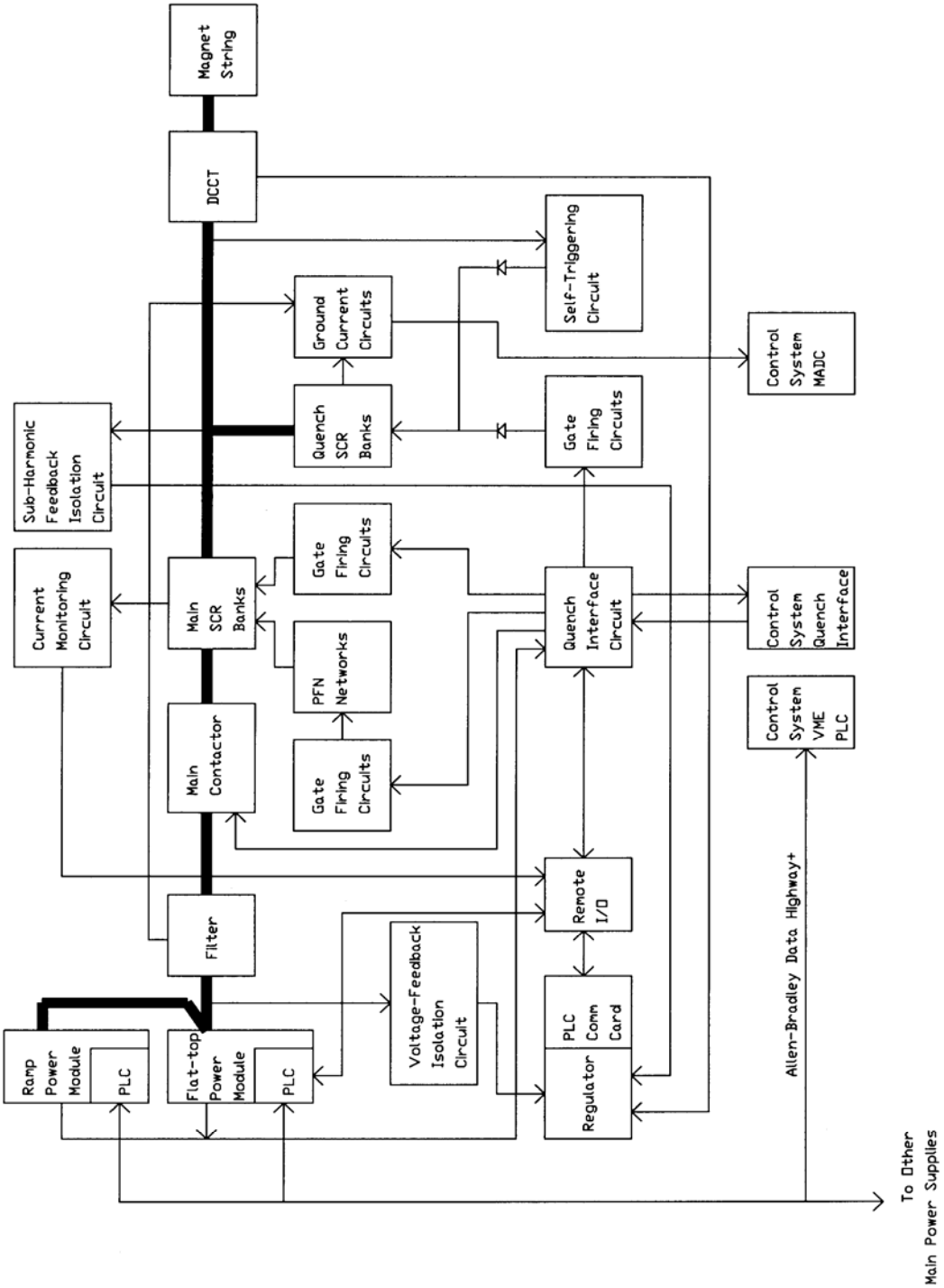

Fig. 2-17 Main Power Circuit Block Diagram

Table 2-6. Ratings of Power Modules

Power Module Type	Voltage Rating	Current Rating	Power Rating
Quad Flat-top	15 V	5500 A	82.5 kW
Quad Ramp	90 V	5500 A pk 3300 A rms	495 kW pk 297 kW
Dipole Flat-top	30 V	5500 A	165 kW
Dipole Ramp	400 V	5500 A pk 3300 A rms	2200 kW pk 1320 kW

Regulator

The regulators for the RMMPSs are digitally based using the TI320C30 Digital Signal Processor (DSP) as the computation engine. Figure 2-18 shows the overall configuration of the regulator. As indicated in the diagram one regulator controls two power modules.

The regulator has a Phase Locked Loop (PLL) that is locked to the power line. This PLL provides all the timing signals for the regulator. The DSP receives voltage, current, and sub-harmonic feedback through A/Ds that sample these parameters at 11520 Hz. The DSP uses this feedback and calculates a command count that is written to the digital firing cards. The digital firing cards use this command count to develop firing signals for the power module's SCRs. The SCR firing signals are sent to the power module's SCR gating circuits over fiber optic cables. There is a separate digital firing card for each power module attached to the regulator. The active power module is selected by enabling the output of its digital firing card.

The current command and the readbacks for the Real Time Data Link (RTDL) are exchanged over a fiber optic link between the waveform generator, in the control system chassis, and the Serial I/O Card in the regulators. This data is exchanged at 720 Hz. The regulator also communicates with a PLC through a PLC communications card. This card provides digital input and output that is used to control the regulator, and return status,

through the control system. There is also a fiber optic lick to the RMMPS control computer. This computer provides program maintenance and diagnostic capabilities.

To insure the stability of the analog feedback circuits the regulator is housed in a temperature controlled enclosure. This enclosure uses thermoelectric modules that provide a temperature stability of +/- 0.2 °C.

The regulator sends analog readbacks to the control system's Multiplexed Analog to Digital Converter (MADC) system. These signals are used for diagnostics and are stored when the quench link goes down. The readbacks for the RMMPS are: reference setpoint, actual current, output voltage, current error, power supply ground current, quench ground current, flat-top power module output current, and the ramp power module output current.

Output Filter

The output filter reduces the current ripple in the magnet string by reducing the voltage ripple at the power module's commutation frequency of 720 Hz. The voltage reduction at 720 Hz is approximately 15 dB.

The output filter is a three pole passive RLC filter with a corner frequency of 90 Hz. This corner frequency insures that the filter's peaking is not at 60 Hz, or its harmonics.

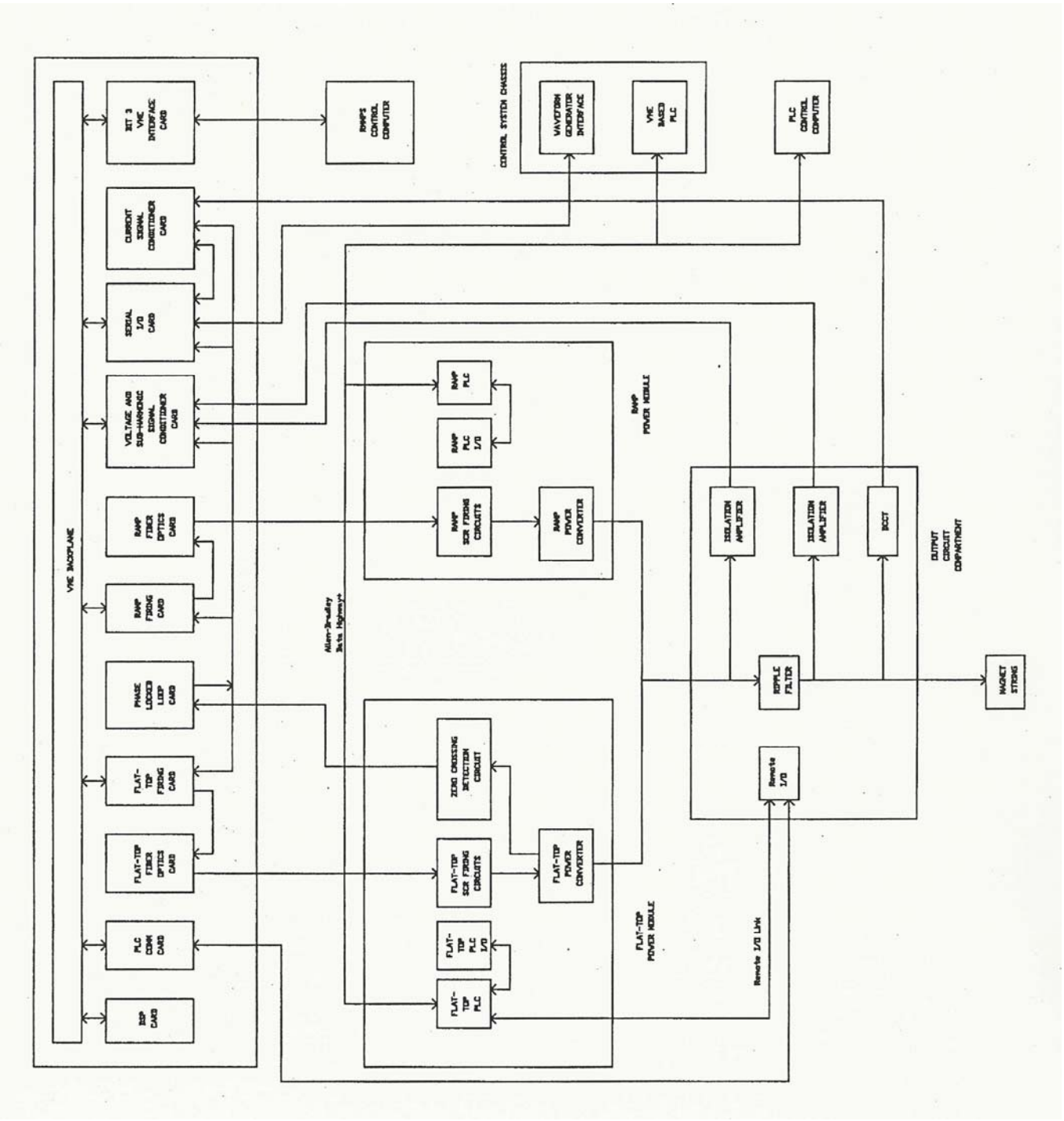

Fig. 2-18 Regulator Block Diagram

Quench Protection and Main Magnet Power Supply System

The quench protection system extracts the stored energy in the main magnet strings. The major system blocks are shown in Fig. 2-19 and are labeled: DC Contactor, Main SCR Firing Circuits, Pulse Forming Networks, and the Quench Control Interface.

The quench link signal, originating in the Control System Quench Interface, is an input to the Quench Control Interface Circuit in the OCC. This signal is a TTL high level during normal operation, it goes low to initiate the energy extraction. When this event occurs the Quench Control Interface Circuit (QCIC) immediately turns off the gate drive to the Main SCR Firing Circuits and triggers the Pulse Forming Network (PFN) attached to the Main SCRs. The PFN shuts off the Main SCRs, this action isolates the RMMPS from the magnet string. The QCIC then fires the Quench SCRs, and the magnet current is now diverted into stainless-steel resistors that extract the energy. The QCIC then opens the Main Contactor, which provides a mechanical backup to isolate the power supplies from the magnet string in the event the Main SCRs fail to open. The QCIC then turns the power modules off. If the QCIC or the Gate Firing Circuits attached to the Quench SCR Banks fail to trigger the Quench SCRs, the resultant voltage rise will trigger the Self-Triggering Circuit. This circuit provides a backup for the QCIC and will fire the Quench SCRs independently.

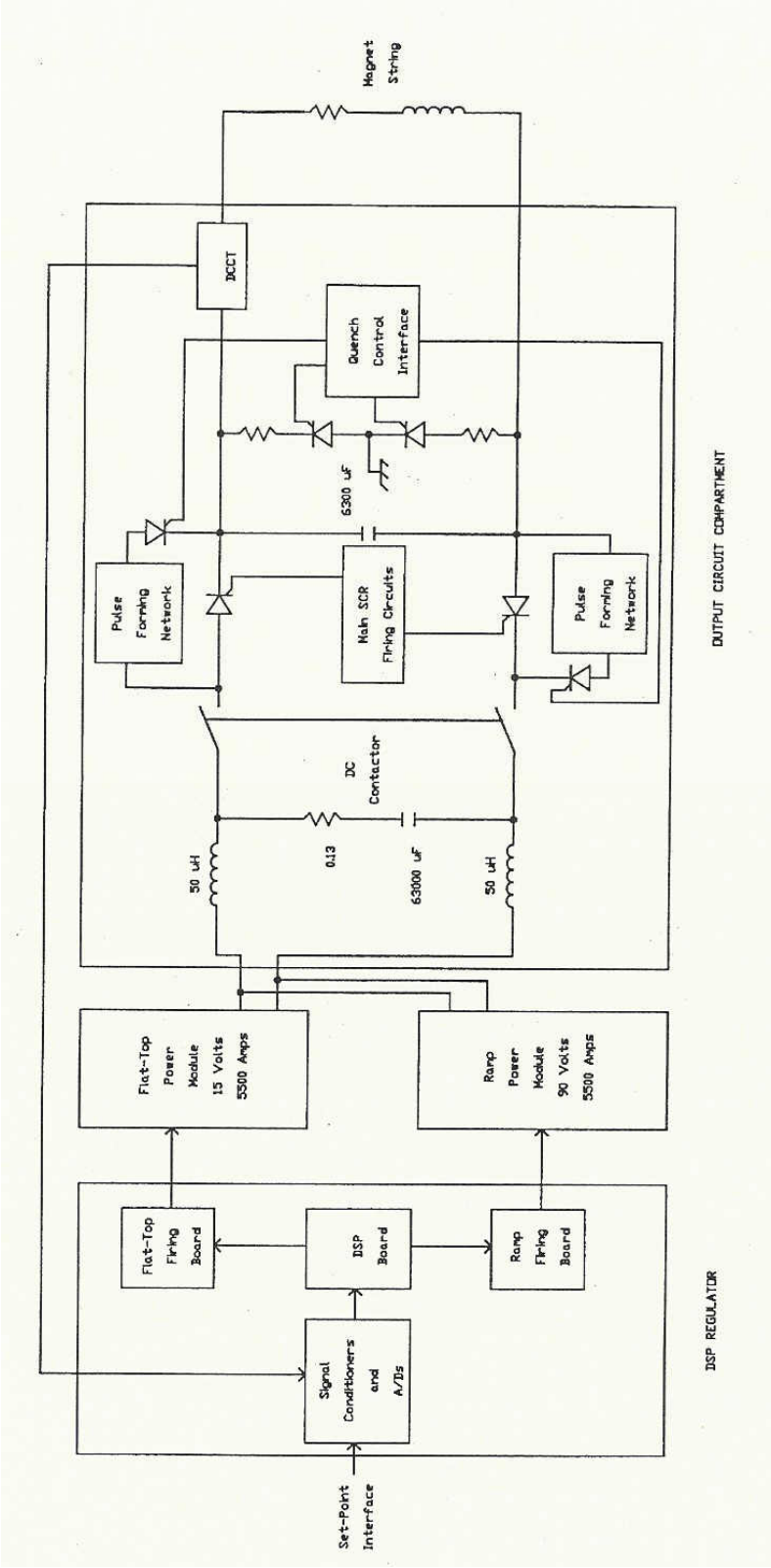

Fig. 2-19 Main Power Supply Block Diagram

PLC System

The PLC system provides status reporting, state control, and local protection of the RMMPS. Each power module contains an Allen-Bradley PLC-5/25. These PLCs are connected to an Allen-Bradley PLC-V5/40, which resides in the Control System Chassis, via the Allen-Bradley Data Highway + serial link. The FTPM PLCs are also connected to remote I/O in the OCCs. These connections tie all the regulators and all the power modules to the control system and provide the status reporting and state control functions.

The PLC-V5/40 collects the status from the power module PLCs and stores this information in dual-port RAM that is accessible to the control system's Front End Computer (FEC), which resides in the same chassis. The FEC can also write commands to this RAM. The PLC-V5/40 contains ladder logic that receives these commands from the control system, and then coordinates turning the power supplies on or off.

The PLC in each power module contains ladder logic that monitors various parameters in that power module. If a failure condition is detected the PLC opens the Master Interlock Relay (MIR) in the power module. Opening the MIR causes the power module to shut down and the power supply fail signal to be sent to the control system. This brings down the quench link signal which activates the quench sequence described above, providing an orderly shut-down of the RMMPS.

The Allen-Bradley Data Highway + also connects to a PLC control computer. This provides PLC ladder logic maintenance capabilities.

ix. Insertion Power Supplies

Overview

The insertion power supplies - these include the shunts to the insertion dipoles, D0 and DX, the shunts to the insertion quadrupoles, Q1-3, and Q6-9 and the trim quadrupole supplies at CTQ4, 5, and 6. They were specified in modular sizes to minimize the quantity of types of supplies to maintain, and to simplify procurement. All of the insertion power supplies are located in the service buildings. The types and quantities of IR power supplies are listed in Table 2-7.

Monopolar Insertion Power Supplies

The monopolar insertion power supplies are current regulated DC power supplies with an inner voltage loop. The AC input to these power supplies is 3 Phase 480VAC for the 2000A and 600A units. The AC input to the rest of the lower current units is 3 phase 208VAC. All of the monopolar power supplies utilize a 12 pulse SCR bridge Power Converter with an output LCRC filter. The current sensing element for current feedback to the current regulator is a DCCT. The required reproducibility is 0.01% of the maximum output current. All of these power supplies have a 100% and 50% voltage tap setting.

Bipolar Insertion Power Supplies

The Bipolar insertion power supplies are also current regulated DC power supplies with an inner voltage loop. However, the bipolar supplies utilize a switchmode DC-DC converter which is controlled by a tracking voltage loop. This tracking voltage loop is in addition to the power supply voltage loop. The DC-DC Converter is a Pre-Regulator for a MOSFET Output Power stage. The voltage across the MOSFET Output power stage is fed back to this tracking voltage loop which keeps the voltage across the MOSFET Power stage low so as to reduce power dissipation across these MOSFETS. The MOSFET Output power stage is an H-bridge configuration. Two of the MOSFETS act linearly while the other two MOSFETS act like a switch controlling which direction the current flows through the magnet load. The number of MOSFETS in the Output Stage of the bipolar 150A power supplies is 24 and the number of MOSFETS in the Output Stage of the bipolar 300A power supplies is 48. The input to these power supplies is 3 phase 208VAC.

Table 2-7. Power Supply Summary

Item	Polarity	Voltage (V)	Current (A)	Quantity (2 rings)
Main Power Supplies				
Quad H/V Trim	mono	40	300	2
Insertion Dipoles				
Type A	mono	20	2000	14
Type B	mono	20	600	7
Insertion Quadrupoles				
Type A	bi	15	150	96
Type B	bi	15	300	14
Type C	mono	15	200	48
Type D	mono	15	300	24
Type E	mono	15	450	16
Type F	mono	20	600	16

Nesting of Monopolar and Bipolar Insertion Power Supply Systems

In any sextant of RHIC there can be as many as 7 power supplies nested inside one power supply. Due to this nesting, all of the insertion power supplies must float off of ground. The DC Output terminals of the 2000A and 600A power supplies have been put through high potential testing of 2500VDC because they are on the Dipole Circuit which has a much higher inductance than the quadrupole circuit. For this reason the 2000A and 600A power supplies will float off of ground to a higher voltage. The lower current units have been put through high potential testing of 1600VDC because they are on the quadrupole circuit which floats off of ground to a voltage which is lower than the dipole circuit.

The nesting of the insertion power supplies and the use of superconducting magnets also created complex time constants which made it very difficult to stabilize the current loops of these power supplies. In some cases the measured admittance of the load was not a pure inductance but also had some capacitive components.

Insertion Power Supply Control System

All of the insertion power supplies use the same 3u chassis control bucket. In this control bucket resides the fiber optic interface card, the current regulator card, the buffer card, the DCCT electronics card, the voltage regulator card, the digital isolation card and the control card. The fiber optic interface card receives the power supply current setpoint over fiber and converts it to an analog current setpoint utilizing a 16bit D/A. This analog setpoint is sent over the 3u control chassis backplane to the BNL designed current regulator card. This current regulator card has a removable PC board for adjusting time constants to stabilize the power supply current loop. The buffer card sends four analog signals back to the Multiplexed Analog to Digital Converter (MADC). These four signals are power supply current setpoint, output current, output voltage and power supply current error. The DCCT electronics card and voltage regulator card were purchased from an outside vendor. The voltage regulator card also contains the isolated shunt feedback voltage which is used in the DC overcurrent circuit which is built into the voltage regulator card. The digital isolation card receives commands from a Node card which is external to the power supply and sends power supply statuses back to this Node card. The Node card communicates over a MODBUS Plus network to a MODICON Programmable Logic Controller (PLC). This PLC communicates with the front end VME computer over an Ethernet connection. A NODE card is an inexpensive multichannel I/O device designed at BNL which receives commands from the PLC and distributes these commands out to as many as 12 power supplies. The power supply statuses are also sent back to the NODE card and then onto the PLC from the NODE card. The control card controls which state the power supply is in and monitors the power supply faults and trips the power supply to a fault state if a fault occurs. This control card employs a micro processor to control the power supply.

The insertion power supplies must also interface with the quench protection system. There are connections made to the Quench Protection Assembly (QPA) and the Quench Detector. The power supply sends the power supply status to the QPA and any QPA faults are sent back to the power supply as well. The power supply output current is sent to the Quench Detector.

x. RHIC Bipolar Corrector Power Supplies

The bipolar 50A corrector power supplies operate on the principles based on the simplified block diagram shown in Fig. 2-20.

The incoming 3 phase 208 VAC, after going through 3-phase rectification and simple LC filtering, is fed into a dc-dc converter. The output of the converter is controlled by a tracking voltage loop, which constantly monitors the difference between the converter output filter voltage and the magnet voltage and make it equal to a voltage set point. What this means is that the converter will track the magnet voltage to keep the voltage drop across the MOSFET output stage constant. 4 MOSFET transistors switching at 100 kHz make up the converter. The four quadrant converter has an H bridge configuration. Output voltage is controlled by pulse width modulation (PWM) technique.

The MOSFET output stage of the power supply consists of 8 transistors and also has an H bridge configuration. Each of the upper MOSFET operates linearly. That is, it regulates the current by acting like a variable resistor. In contrast, each of the lower MOSFET acts like a switch.

There are basically three types of feedback loops employed in the power supplies: an inner voltage feedback loop, an overall current feedback loop, and a tracking voltage loop. With a resistive load, the current feedback has a frequency response of 4 Hz. Putting the power supply into voltage mode disables the current feedback. In this case, the power supply turns into a voltage regulator and has a frequency response of 1 kHz.

The tracking loop minimizes the output stage power dissipation by keeping the voltage drop across the MOSFET transistors to about a volt. Whenever the tracking loop fails to track the output voltage the power dissipation increases, which can lead possibly to a thermal shutdown. Feedback is taken after the dc-dc converter output filter. The frequency response of the tracking loop is about 3 Hz.

Both voltage and current compensation can be accomplished on an external compensation board, which is mounted onto the power supply control board via an opening in the front panel.

Although the power supplies employ dc-dc converters, they have to meet the following noise specifications: For normal mode ripple, Vr < 5mVpp narrow band (20 Hz– 1 kHz) and < 50 mVpp wide band (1 kHz – 1 MHz). For common mode ripple, Vr < 20 mVpp narrow band and < 200 mV wide band.

All of the corrector power supplies provide four analog signals SETPOINT, DCCT, OUTPUT VOLTAGE, and ERROR at the front panel for troubleshooting and testing purposes. The first three signals are also available at the rear panel. In LOCAL mode, the set point for the 50A unit can be adjusted on the front panel by turning a knob.

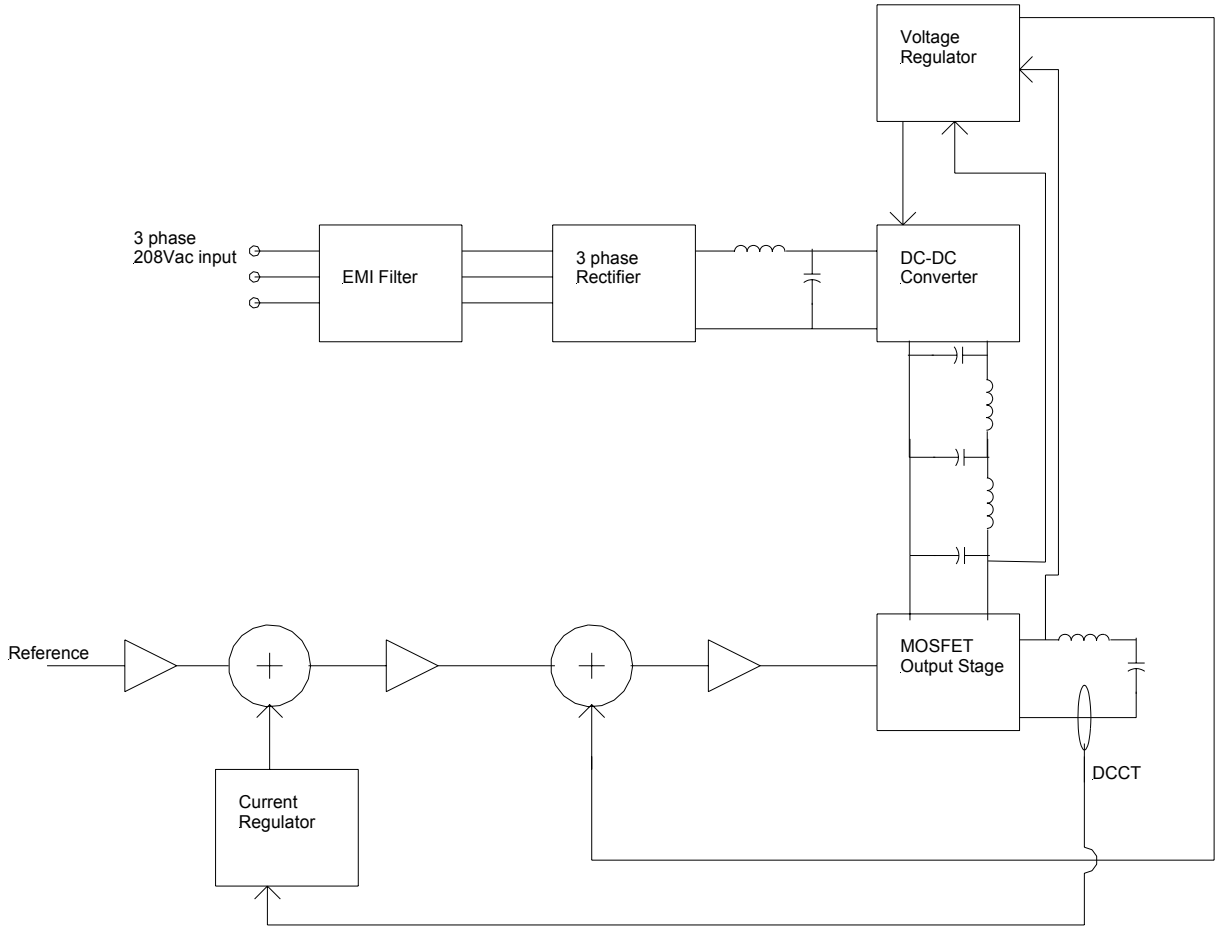

Fig. 2-20 RHIC Bipolar Power Supply Simplified Block Diagram

xi. Sextupole Power Supplies

Power Supplies

There are a total of 24 sextupole power supplies in both rings. All of the sextupole power supplies are located in the alcoves. The sextupole power supplies are current regulated DC power supplies with an inner voltage loop. In addition to this inner voltage loop these sextupole power supplies have a linear MOSFET output stage with a 12 pulse SCR Pre-Regulator. These power supplies use a DCCT as the current sensing element. The required power supply current reproducibility is 0.025% of maximum current rating. The power supply maximum ratings are 100Volts at 100Amps. The AC input is 3 phase 480V at approximately 14 Amps maximum. The maximum voltage ripple is 0.2Vpp in the 100% tap setting. The power supplies have a 70V tap setting as well. The block diagram is shown in Fig. 2-21.

Power Supply Controls

Each power supply receives an analog setpoint from an external fiber optic interface card. This fiber optic interface card receives the setpoint over fiber and converts it to an analog current setpoint utililizing a 16 bit D/A.The OFF, STANDBY and ON Commands to the power supply, as well as the statuses from the power supply, are sent to a NODE CARD which then communicates over a MODBUS PLUS network with a MODICON Programmable Logic Controller (PLC). This MODICON PLC communicates with the VME front end computer over an Ethernet connection. A NODE CARD is an inexpensive multichannel I/O device designed at BNL which receives commands from the PLC and distributes these commands out to as many as 12 power supplies. The power supply statuses are also sent back to the NODE CARD and then onto the PLC from the NODE CARD. There are four analog readbacks which are sent back to the Multiplexed Analog to Digital Converter (MADC). These four signals are Setpoint, Output Current, Output Voltage, and Power Supply Current Error.

Power Supply Magnet Load

Each Sextupole power supply is connected across 12 sextupole magnets. The 12 sextupole magnets are all connected in series. These magnets are connected in two families, focussing and defocussing in each arc. The inductance of each sextupole magnet is about 0.83H. When twelve sextupole magnets are connected in series the total inductance the power supply sees is about 10H. The only resistance the power supply sees is the warm DC cables to each of the sextupole magnets. This resistance is approximately 0.42 ohms.

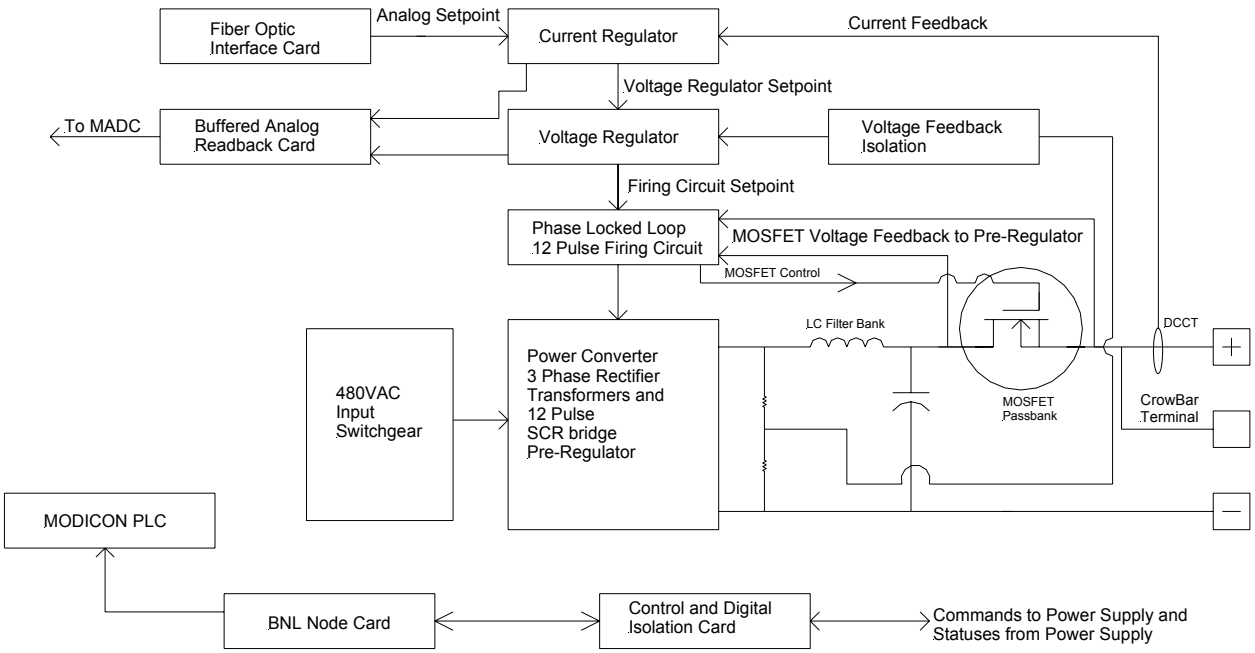

Fig. 2-21 RHIC Bipolar Power Supply Simplified Block Diagram

xii. Siberian Snake Power Supplies

There are a total of 24 snake power supplies in both rings. All of the snake power supplies are located in the alcoves. Each power supply is rated at a maximum of 15Volts at 440Amps DC. The snake power supplies are current regulated switchmode power supplies with a DCCT current sensing element. The switchmode power section is a commercially available voltage regulated power supply, which is inside a BNL designed current regulator.

The snake power supply receives an analog setpoint from an external Fiber optic interface card. This fiber optic interface card receives the setpoint over fiber and converts it to an analog current setpoint utililizing a 12 bit D/A.

The snake power supply must also interface with the quench protection system. There are connections made to the Quench Protection Assembly (QPA) and the Quench Detector. The power supply sends the power supply status to the QPA and any QPA faults are sent back to the power supply as well. The power supply output current is sent to the Quench Detector. Figure 2-22 is a block diagram of the snake power supply.

Two snake power supplies are required to power one snake magnet. Each power supply powers 2 coils that are in series in each magnet. The Inductance of each coil is approximately 5.1H so the total inductance one p.s. sees is approximately 10.2H.

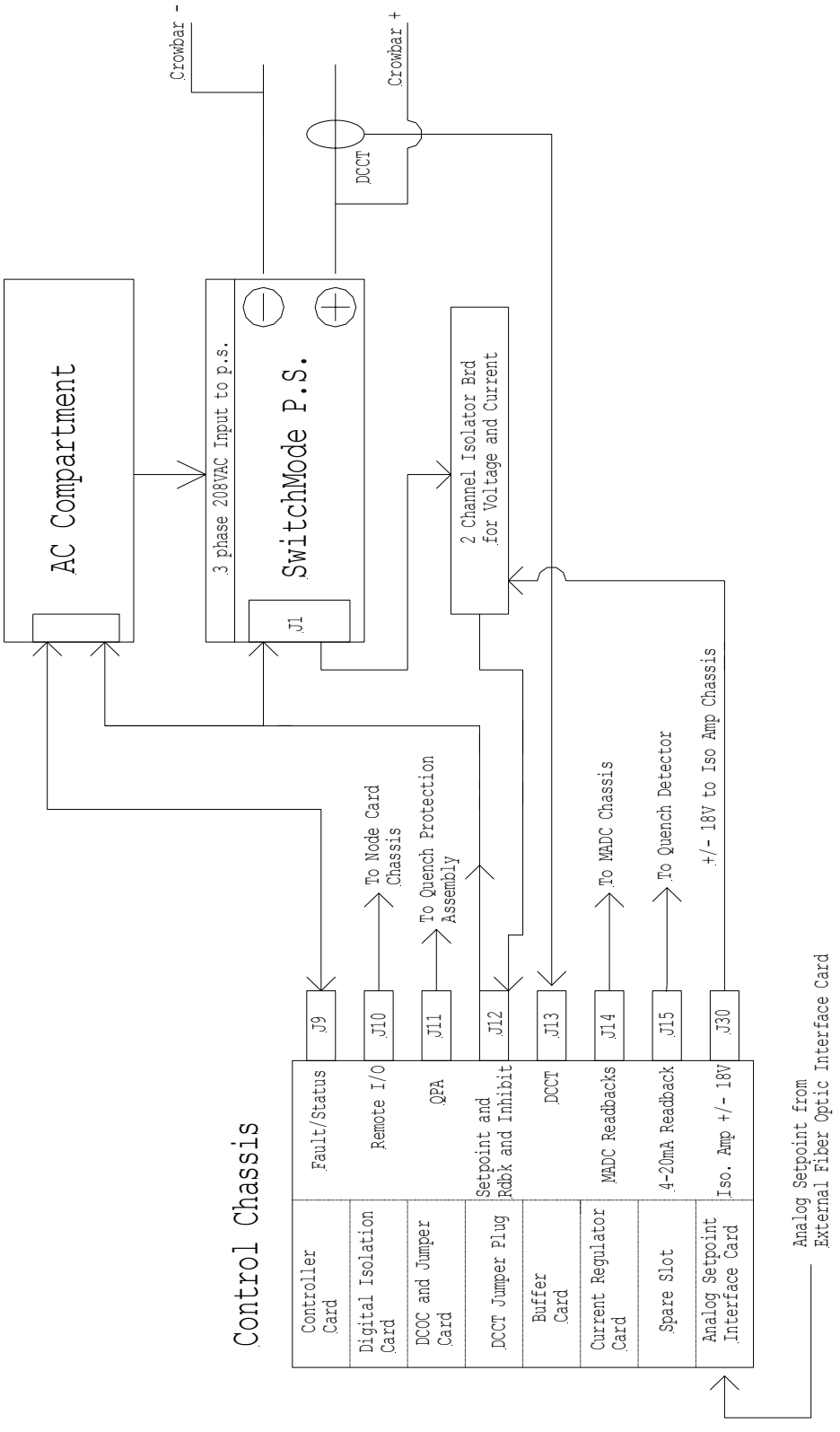

Fig. 2-22 Snake Power Supply Block Diagram

xiii. Quench Protection System

The quench protection system is used to prevent damage to the superconducting cable or wire used in magnets or bus work. This damage will occur when there is sufficient energy deposited at the initial quenching location to cause the location to rise its temperature above safe operating limits. The current in the quenching magnet or bus must be reduced to zero before overheating occurs. They are three parts to this system. First, the cold bypass diodes are used to divert the current from the non-quenching magnets around the quenching magnet. Second, the quench detection system is used to determine when magnet or bus has quenched. The quench detection system will be used to trigger the energy extraction system. Third, the energy extraction system brings the current to zero in the quenching magnets and superconducting buses. This is mainly accomplished by switching in dump resistors in series with the magnet circuits.

Cold Bypass Diode System

Almost all of the collider main magnets are able to absorb their own energy during a quench. With these magnets a passive cold bypass diode system is used to prevent damage to the quenching magnet from current in the rest of the magnet circuit.

The cold bypass diode system is shown in Fig.2-23. In this circuit, the current is forced out of the magnet and into the shunting diode by the natural action of the quench developed resistance of the magnet coil. Current from the non-quenching magnets will not heat the quenching magnet because of the shunting action of the diode. During current ramping the diode must not shunt any significant current.

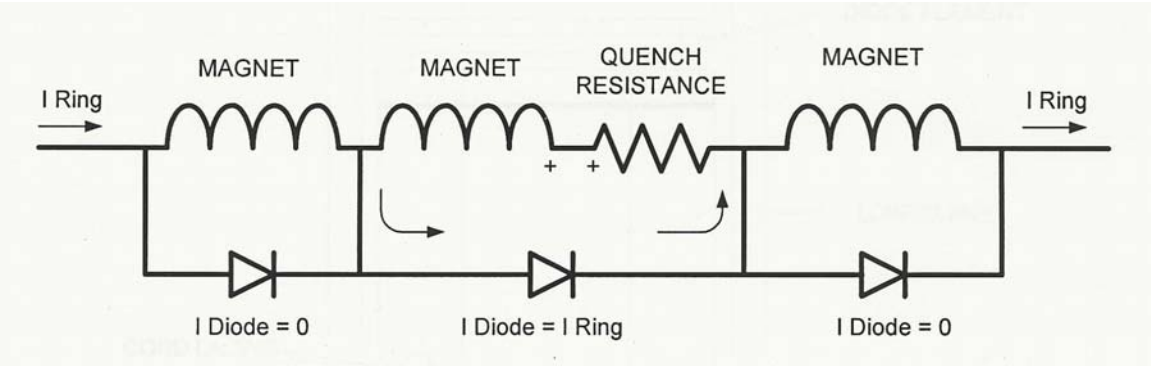

Fig. 2-23 Simplified Circuit of a Quench Protection Diode Bypassing Current During a Magnet Quench

The cold diode assemblies (See Fig.2-24) have two 5 pound copper anvils compressing the diode element. A stainless-steel frame using disc spring washers maintain the large compressive force on the diode element under all operating conditions. This large force is needed for a good electrical and thermal contact between the diode element and copper anvils. Ceramic balls are used to provide electrical isolation between the copper anvils in a stainless-steel frame. The diode elements where specifically passivated for cryogenic temperatures. The large copper anvils are used to limit the maximum temperature of the diode element to below its maximum temperature rating.

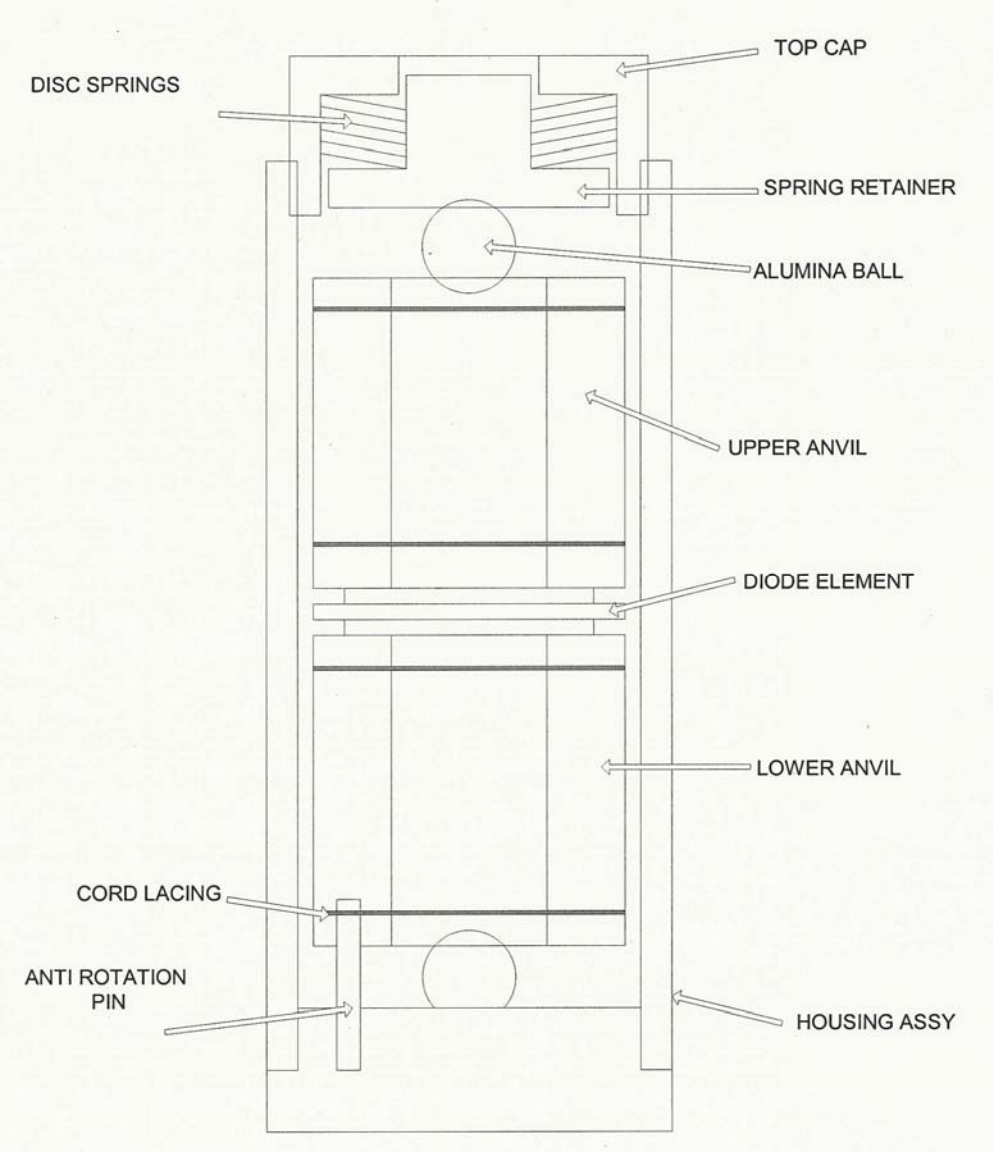

Fig. 2-24 Cold Diode Assemblies

DX Magnet

The DX dipole magnet is different than the other main magnets in two ways. First, because of its higher inductances (50 mH vs. 25 mH for an arc dipole), the induced voltage during a current ramp will be higher. This requires two series bypass diodes, instead of the single diode shown in Fig. 2-23. Second, since the DX magnet cannot absorb its own energy, an active quench protection system will be required. The active quench protection system consists of strip heaters placed along the outer diameter of the DX magnet coil and capacitor discharge power supplies that will pulse the heaters when a DX magnet quench is detected. These power supplies are located in each service building. When the strip heaters are pulsed it will cause a large area of the magnet coil to quench, this in turn will distribute the energy the magnet has to absorb to a much greater volume of the magnet coil thereby preventing any magnet damage due to overheating. To ensure high reliability of the active quench protection system for DX there are two strip heater circuits and two power supplies for every DX magnet.

xiv. Quench Detection System

The RHIC quench detection system monitors various types of superconducting magnets, shunt bus and gas cooled leads continuously to sense magnet quenches and gas cooled lead faults. The method to detect quenches is by voltage sensing, as shown in Fig.2-25 RHIC Quench Detection System Block Diagram. When a quench is determined, the system sends a quench signal for the power supplies to shutdown and energy extraction system to operate, thus protecting all essential parts of the RHIC magnet circuit.

This is a distributed system, it separates into twelve subsystems. Six subsystems located at service buildings and the other six subsystems located at "B" alcoves throughout the ring. Each subsystem is a standalone unit that processes its data locally. All subsystems are networked together via the Ethernet, as shown in Fig. 2-26 RHIC Quench Detection System Layout. The Control System passes Ring Events, RTDL and other parameters to the Quench System Crate controller. Data from subsystems are routed to a concentrator and archived periodically or at the time of a quench. Another PC base system containing the analysis and plotting software is also networked, allowing remote monitoring, analysis and troubleshooting of various components.

Subsystems in alcoves monitor arc-region Dipole, Quadrupole magnet voltage taps. Subsystems at service buildings monitor insertion-region magnets, shunt bus voltage taps, gas cool leads and power supply currents. Each subsystem is divided into three functional sections. The front-end computer section, ADC/timing-control section, and the low level hardware interface section.

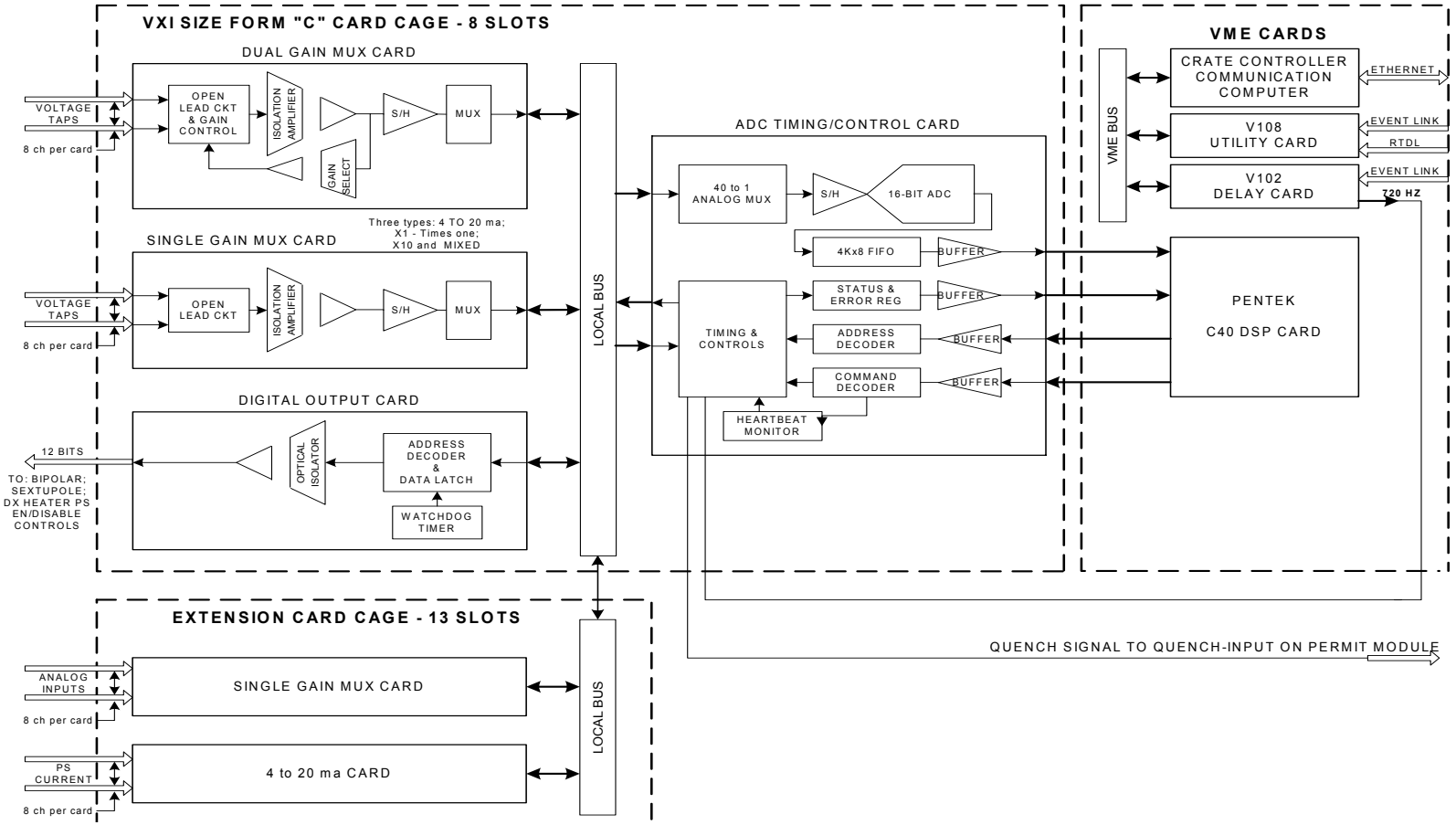

Fig. 2-25 RHIC Quench detection System Block Diagram

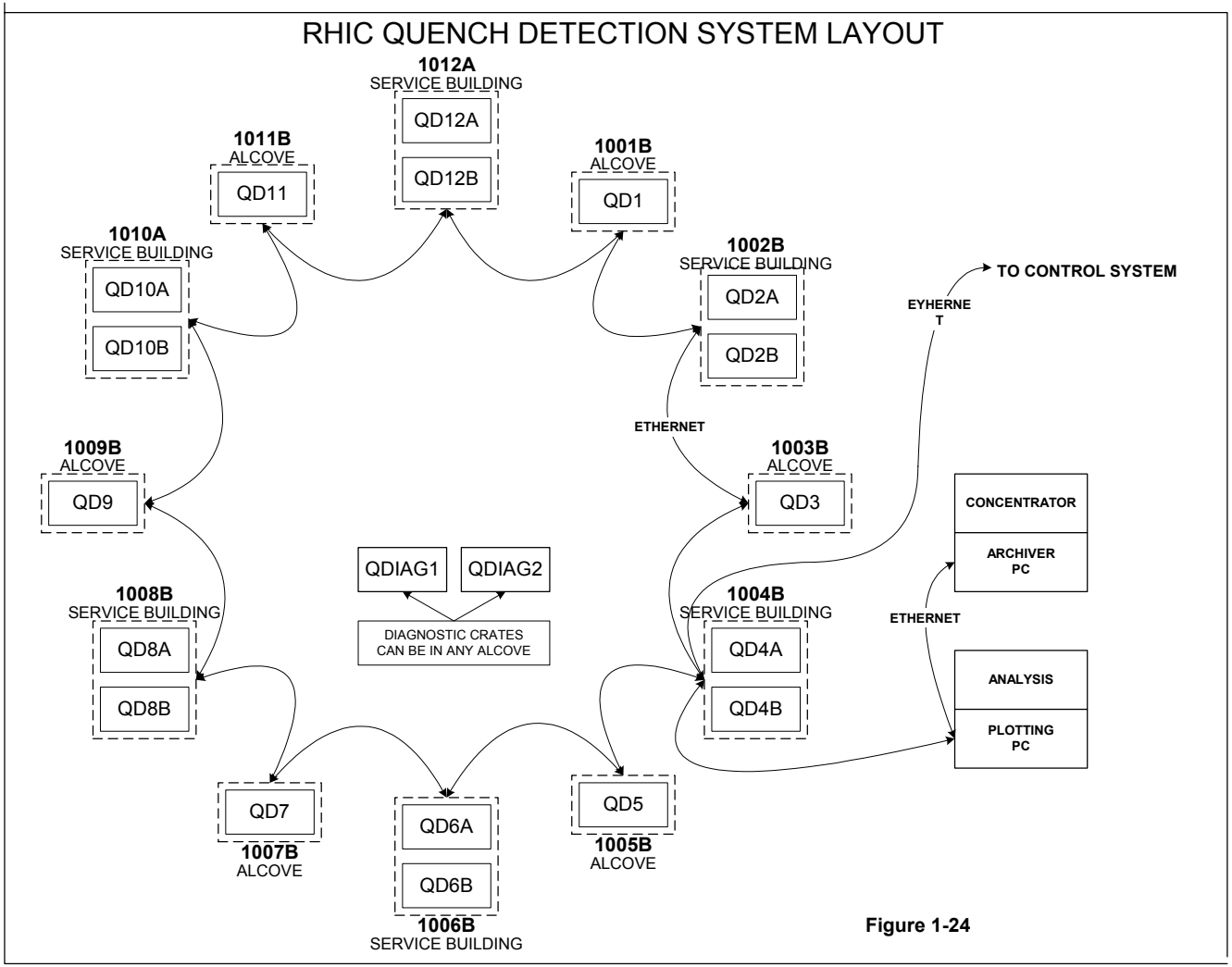

Fig. 2-26 RHIC Quench detection System Layout

The front-end computer section consists of a VME Crate controller, an Utility card, a Delay card and a DSP card. The function of the Crate controller is to communicate with the Control System, download programs and parameters, upload stored data to users and initialize other VME modules. The Utility card extracts Magnet Currents from the Real Time Data Link (RTDL) and passes them the DSP card. The Delay card decodes events from the Event Link and synchronizes the Quench Detection System to the 720Hz master clock at the Control system. The function of the DSP card is to read the magnet currents from the Utility card, current readback from the 4-to-20 ma card, and the magnet voltage taps signals from the analog-to-digital converter card once every 1.389ms. Noise component of 60Hz is removed by averaging twelve acquired samples. Quench condition is determined by performing calculations based on the $Vc(t) = Rc(t) * i(t) + Lc(di/dt)$ formula. Since the gas cooled lead has no resistance nor inductance, its fault is determined by comparing the voltage readback to a fixed threshold value. If the calculated Vc(t) or the gas cool lead readback voltage is outside the band of the expected value that stored in the database, fault is determined. The DSP card then sends a quench signal to the Quench input of the Beam Permit Module via the ADC Card to shutdown power supplies and activate the energy extraction system.

The ADC/timing-control Card generates a simultaneously sample-and-hold signal to all low-level interface cards at the rate of 720 Hz. The holding analog signals are converted by a 16-bit scanning ADC at a fixed rate of about 10μs per channel. Converted data and hardware status are sent to a FIFO that allows the DSP to fetch data at rate up to 80ns. There is a one-second watchdog timer on the ADC card. If this timer is not reset by the DSP software, indicating the software is working properly, then the ADC card will send out the quench signal to shutdown.

There are four different types of analog interface cards to accommodate different input signals. Each card has eight analog input channels and contains open-circuit detection circuitry. The circuit sends a small negative dc current to each voltage tap. If the voltage tap or the wires to the tap are not open, then the readback is around zero volt. When the tap or the wires to the tap break or open, the sensing voltage changes to negative. This fault is sensed and reported by the DSP card to warn users that the tap is not connected correctly. The Dual Gain Mux Card connects to the Dipole and Quadrupole Magnet voltage taps. It has a gain of 0.5 in the normal mode for signals up to ±20 volts, the card automatically switches to a gain of 0.025 during

quench for signals up to ±400 volts. The Single Gain Mux Card has three different versions. The X1 version accepts signals up to ±10 volts, the X10 version accepts signals up to ±1 volt, and the 4-to-20 mA version that connects to Insertion Power Supplies. There is one type of Digital Output Card to enable or disable the Bipolar, Sextupole, and DX Quench Heater power supplies. To protect the DX magnet further with hardware protection, the Digital Output card has a 20ms watchdog timer onboard. If this timer is not reset by the DSP software at the rate of less than 20ms, then the Digital Output Card will trigger the DX Heater Power Supplies and quench the DX magnet.

xv. Energy Extraction System

Even though the individual magnet that quench is protected, it is necessary to remove the stored energy from the entire series-connected string of magnets as rapidly as possible to protect buses and diodes from overheating. The thermal mass of these elements is large enough to permit a simple solution. Figures 2-2 and 2-3 show the energy extraction systems for dipole and quadruples circuits. The main elements used in the energy extraction system for the main circuits are the SCR switches and dump resistors.

The SCR switches consist of six SCR in parallel (see Fig. 2-27). The SCR's are normally conducting when the circuit is operating normally. To insure even current sharing a current sharing resistor is in series with each SCR. The SCR's are specifically selected to have low initial turn on voltage characteristics. The current sharing resistor is size to balance the current at 6000 amps to approximately 10 percent. The switch will open when the energy stored in the pulse forming network is connected across the bank of SCR's by the trigger SCR. This will back bias the six parallel SCRs off. The voltage levels on the capacitors in the pulse forming network are fixed. This voltage level is what's required to open the switch at an operating current of 6700 amps from going through the switch. If the voltage is below this level it to will not have sufficient energy turn the SCR off. The snubber diodes stack is used to limit voltage transients when the pulse forming network is applied across the SCR bank at much lower currents (< 2000 amps). The D.C. interrupter is used as a backup in the SCR's do not open.

A PLC monitors status' and fault conditions of the SCR switch. It also performs control functions of closing and opening the switch by local and remote control.

The dump resistors are large stainless-steel resistors of sufficient mass to limit the temperature rise to acceptable limits after each energy extraction. They are cooled by natural convection. The resistance values are selected to balance the requirements of being able to remove the current fast enough to protect the cryogenic diodes or bus work and to limit the voltage transients from bus to ground and between buses during an energy extraction. The system is now designed to keep the worst-case bus quenches limited to a little over half its allowed maximum temperature rise. For the worst-case condition of a complete magnet group quenching the maximum voltage to ground is 780 volts and bus to bus voltage of 1500 volts.

The basic switch used in building 1004B in the main circuit Output Circuit Compartment (OCC) is of the same design as used in building 1010A. (same PFN, SCRs, snubber diodes

stack, D.C. interrupter, interlocks, etc.) The main difference is the placement of the dump resistors across the circuits. Also there are blocking SCRs that prevent current from flowing in the dump resistors under normal power supply operation (see Fig. 2-2). These blocking SCR's are triggered when there is an energy extraction. The reason the SCR is used here is because the main power supply can operate in the invert mode and generate a large negative voltage. If diodes are used instead of SCR's significant current would flow through the diodes when the power supply went into the invert mode.

Insertion Region Circuits

The insertion region of magnet circuits of RHIC is very complex. There are power supply circuits nested within each main circuit at the six crossing regions. (See Figs. 2-9, 2-10, and 2-11) The nesting of the various circuits makes this region the most difficult to quench protect. The superconducting buses have been sized to match the nominal operating current of the shunt power supplies. At times different size conductors were used in the same circuit. With these different size conductors there are various limits to the amount of energy these conductors can absorb. During a bus quench one has to keep the conductors below the maximum temperature or a fault could occur. The maximum temperature limit varies depending on many factors. The most critical factor is the type of insulation used on the bus wiring. Where Tefzel is used to maximum temperature is 445 degrees Kelvin, or a temperature rise of 440 degrees Kelvin. If this limit is exceeded one could get insulation failure that can cause a short to ground or circuit to circuit short.

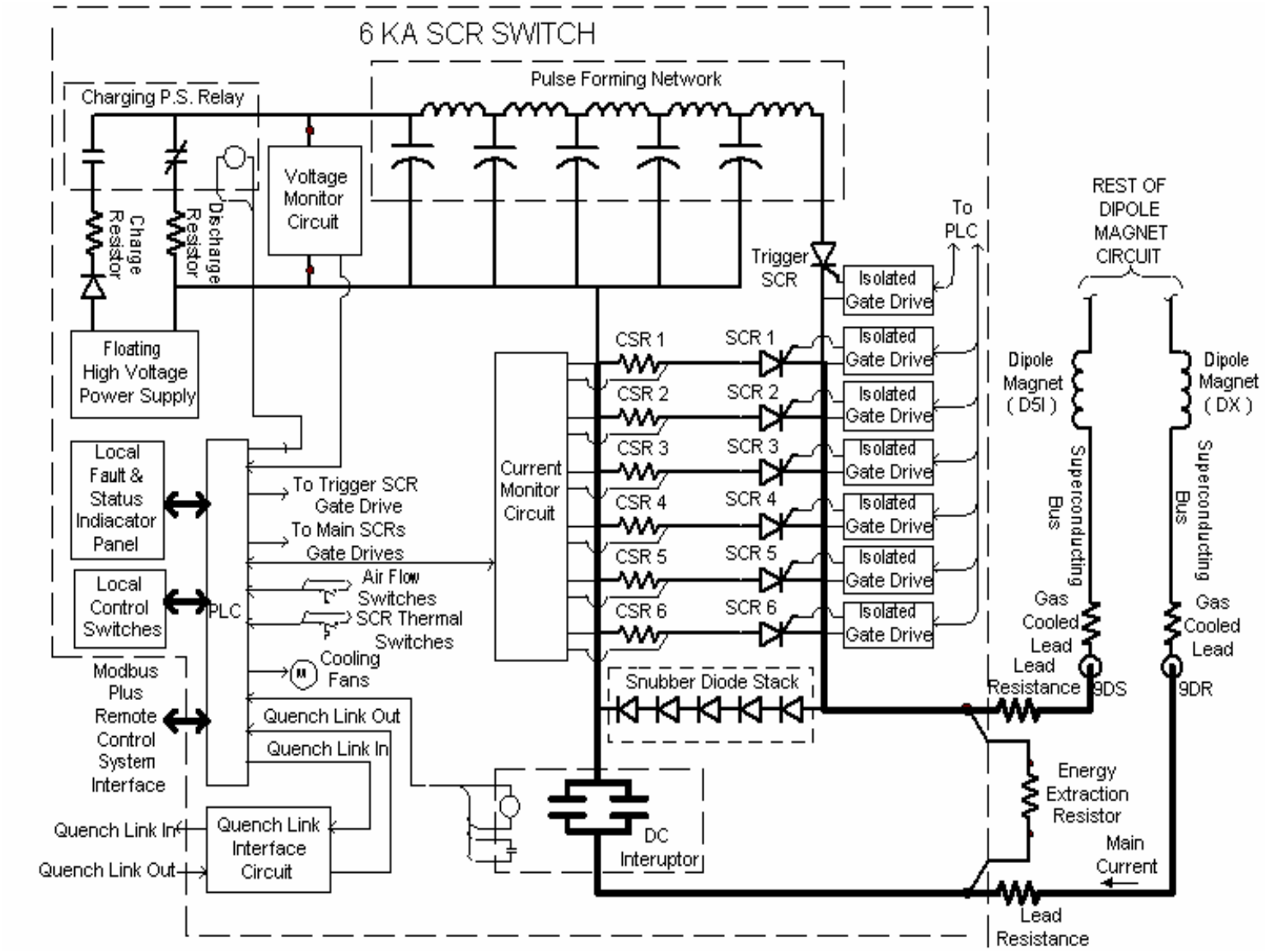

Fig. 2-27 6K SCR Switch

Current in the shunt circuits are at times significantly higher than the current in main circuit. (DX operates at 6400 amps when the arc dipole is that 5050 amps at the top energy of the machine.) During energy extraction significant voltage is undeveloped across the magnet elements. Large currents that could quench the bus will flow in the shunt buses if some action is not taken. If a bus quench work to happen the resistance growth of the quench can be so slow that in most cases it will not decrease the current fast enough to keep the energy deposited by the quench below the safe limit for that bus. Some of the shunt power supplies are configured to subtract current from the main circuit and during an energy extraction the voltage and current flow will reverse.

For all the different insertion magnet circuits there is a unique quench protection assembly (QPA) . These QPAs limit the current of its shunt bus, cause the current in its shunt bus to decrease fast enough to protect the bus, prevent excessive current flow in the power supply, and prevent excessive voltage transients from occurring during main circuit energy extraction. The QPAs are sized to match the current ratings of the various insertion region power supplies.

There are two types of QPAs , an active QPA for high inductance shunt circuits and a passive QPA for low inductance shunt circuits. (See Figs. 2-28, 2-29) The active QPAs use an IGBT (insulated gate bipolar transistor) switch to put a resistance in series with the shunt circuit. This will limit the current in the circuit and cause the current to decrease rapidly. If the IGBT short-circuits during an energy extraction, large currents could flow that will cause the fast acting fuse to blow and thus putting the energy extraction resistor in series with the shunt circuit. The blocking diode is to prevent large reverse currents from flowing through the internal freewheeling diode of the IGBT. The crowbar SCR prevents the current in the shunt circuit from circulating in the power supplies' output stage. It also prevents any large voltage transients that could result in a change in current direction when the main circuit is doing an energy extraction.

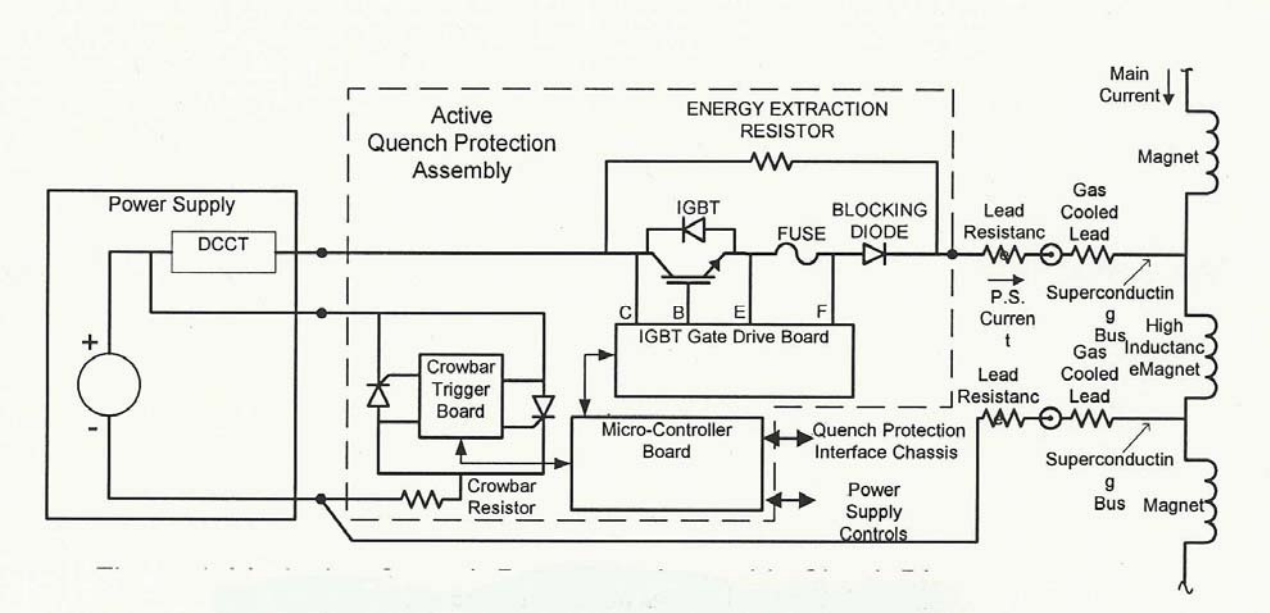

Fig. 2-28 Active quench protection assembly circuit diagram

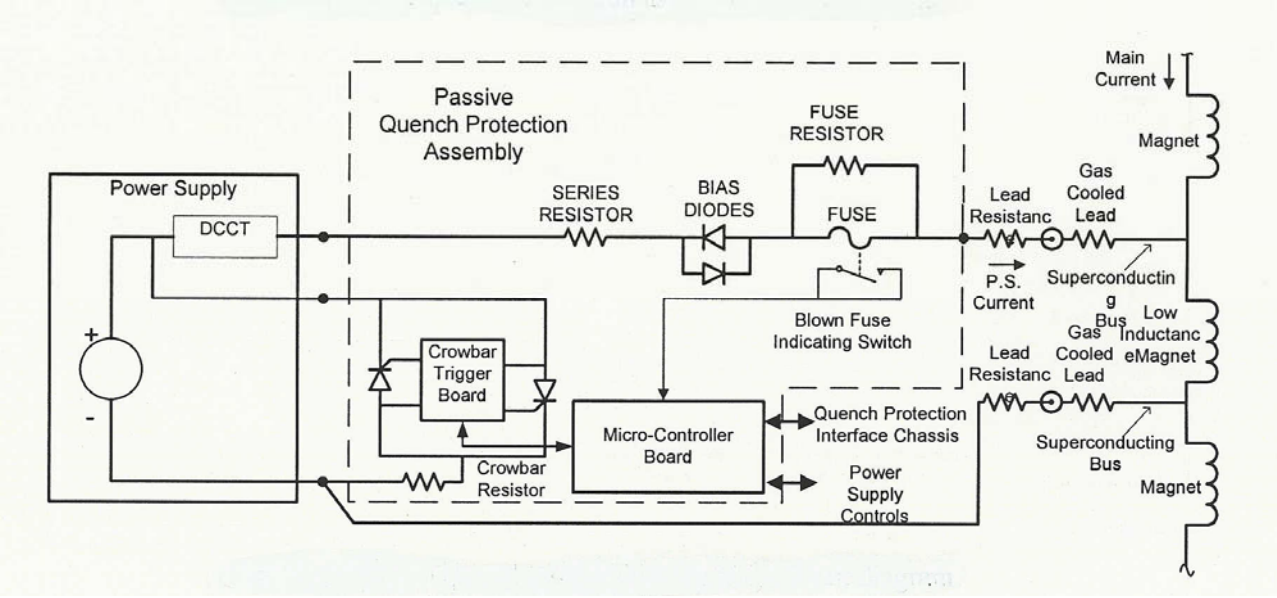

Fig. 2-29 Passive quench protection assembly circuit diagram

The passive QPAs use a simple series resistor and back-to-back biasing diodes to limit the current and enable it to decrease fast enough during the main circuit energy extraction. The fast acting fuse is also used in case there is a condition of high current (shorted crowbar SCR and/or shorted biasing diodes). The crowbar circuit functions the same way as in the active QPA.

Both active and passive QPAs have the same controls. A microcontroller monitors and reports status of interlocks and operational state of the QPAs. It also controls the IGBT and crowbar circuits by input signals from the power supply it is connected to and the quench link signal.

The Quench Protection for Trim Quads, Sextupole, and 50 Amp Corrector Circuits

The trim quad circuits have a high inductance of approximately 0.7 henrys. The single magnet that makes up the trim quad circuit is self protecting but the bus is not. The quench propagation speed of a trim quad bus quench is very slow. If a trim quad bus quench were to occur at maximum current the resistance growth could be too small to decrease the current fast enough to prevent damage to the trim quad bus. Therefore all trim quad magnet circuits use an active QPA to ensure that the current decreases fast enough to protect the trim quad bus.

Sextupole circuits have the largest inductance of all magnet circuits, it is approximately 9.6 henrys. The circuit consists of 12 sextupole magnets connected in series. External SCR crowbars are installed across each magnet. These SCR crowbar circuits have a self trigger circuit that will cause the SCRs to turn on when there is sufficient voltage across the magnet coil. The necessary voltage level and polarity will occur only during a magnet quench to trigger the crowbars. The SCR crowbars are mounted on a large heat sink to prevent the crowbar circuit from overheating while current in the magnet string is brought to zero by an active QPA. This QPA has a slightly different topology then the trim quad or insertion region shunt QPAs to prevent damage of the FET output stage on the sextupole power supplies. The SCR crowbars across each magnet and the active QPA also limits the maximum voltage off ground during a quench and energy extraction for the sextupole circuit. The voltage is kept under 250 volts. This relatively low value is due to a known weakness in the insulation of the internal bus of the sextuple magnets.

All the magnets used in the 50 amp corrector circuits are self protecting for currents up to 60 amps. Therefore the only quench protection needed for the circuits is to shut off the power supply powering them. The 50 amp power supplies have an over-voltage detection and crowbar circuit. The detection circuit will shut off the power supply when the circuit voltage exceeds a fixed limit.

xvi. Quench Link

The quench link is a ring wide interlock system that connects all the power supplies, quench detectors, and quench protection systems together. It is part of the permit module of the control system. It has two independent channels, one for the Yellow ring and one for the Blue ring. The input to the quench link goes low when a quench is detected or power supply or QPA or SCR switch develops a fault. This then causes the link's output to go down around the whole ring. When the link's output goes down it causes all the power supplies to shut off and all the quench protection switches to open up. The quench protection switches place energy extraction resistors in series with the superconducting circuits. This causes the current in the circuits to decay to safe levels. The quench link inputs are time stamped. The quench links are located in every service building and all the center alcoves of the ring.

CRYOGENIC SYSTEM (WBS 1.3)

i. Introduction

The basic function of the RHIC Cryogenic System is to maintain the superconducting magnets and the superconducting bus connecting them in the two rings of the collider at or below their design operating temperature.

The performance specifications, which have a major influence on the design of the cryogenic system, include the following points:

1. All magnets must be maintained below their nominal operating temperature of 4.6 K during steady-state operations.
2. Each sextant of each ring can be isolated for independent warmup and cooldown for repairs if required. During the time required for this procedure the balance of the sextants in the affected ring will not be warmed, but may drift up in temperature.
3. In order to permit system design calculations to investigate "off-design" operations and to size system components, the worst case design heat load is for double the nominal heat load of all magnets in one sextant. Under these conditions, the warmest magnet temperature must still be less than 4.6 K.
4. Reliability of the cryogenic system shall be such that its availability (at nominal design load conditions) is greater than 90%.

The design of the cryogenic system focused on satisfying these requirements while also considering many non-performance constraints, historical and geographical, which must also be factored into the design of the system. The design which has evolved is presented below.

The main feature of the RHIC Cryogenic System (shown schematically in Fig. 3-1) is the helium refrigerator. This refrigerator was fabricated, installed and, after testing, was accepted by BNL in March 1986. The refrigerator was designed to match the load of the CBA Project with a primary capacity of 24.8 kW at about 3.8 K and a secondary, higher temperature capacity of 55 kW at about 55 K. This refrigerator with its matching room temperature compressor system is used to produce the refrigeration required for RHIC.

Cold centrifugal compressors are used to circulate single-phase, supercritical pressure helium in a closed loop through the magnets of each ring and a distributed network of heat exchangers (called recoolers). This is shown schematically in Fig. 3-2. Heat is removed from the circulating helium stream by heat exchange with a boiling liquid helium bath in the recoolers. This type of system is chosen so that the mass of helium in the magnet cooling system can be maintained nearly constant during excursions in temperature due to quenches or other upsets. The pressure in the magnet side of the system is allowed to rise (within predetermined limits) without venting of cold helium. Retaining the helium in the magnets ensures that the refrigeration required to recover from such an event will be minimized and that the refrigerator operation will not be upset by the receipt of excessive amounts of cold helium gas generated by the expansion of the warmed helium in the load. Cold gas from the refrigerator is added to the closed loop of each ring as required to replace the gas removed from the stream to cool the magnet electric power leads.

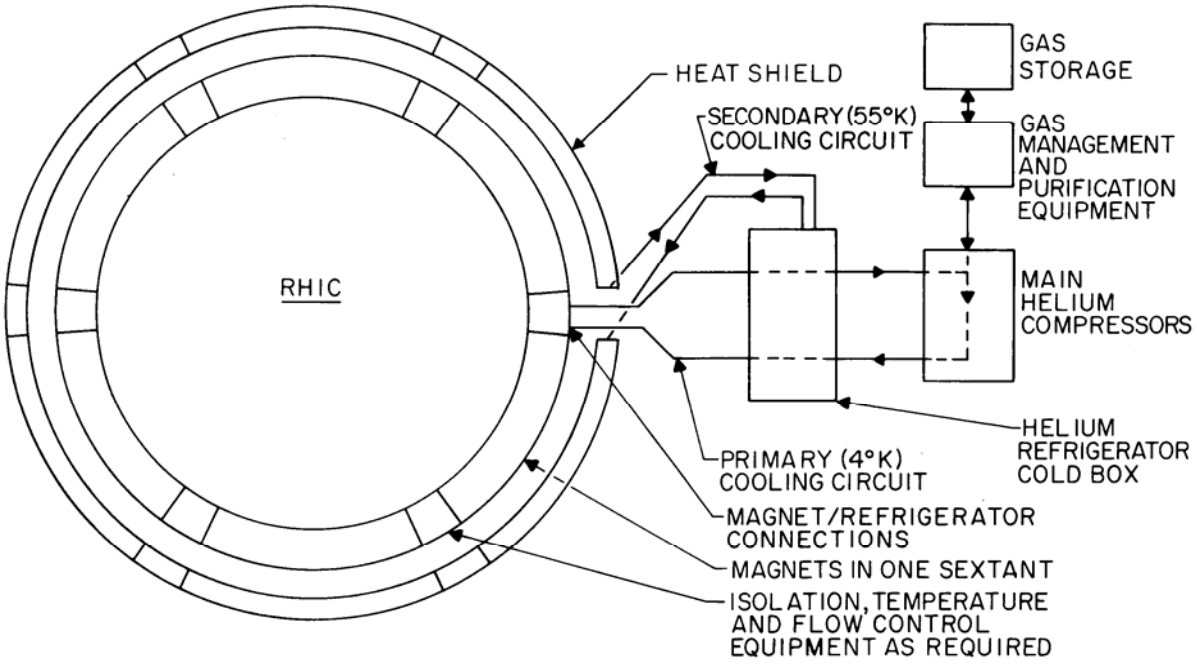

Fig. 3-1. Simplified drawing of RHIC Cryogenic System. Only one of the rings is shown. The second is in parallel with the first.

Connecting the refrigerator and the load is a network of vacuum-jacketed piping. Piping is also required to carry the helium wherever there are long gaps in the magnets in the ring, e.g., across the experimental areas.

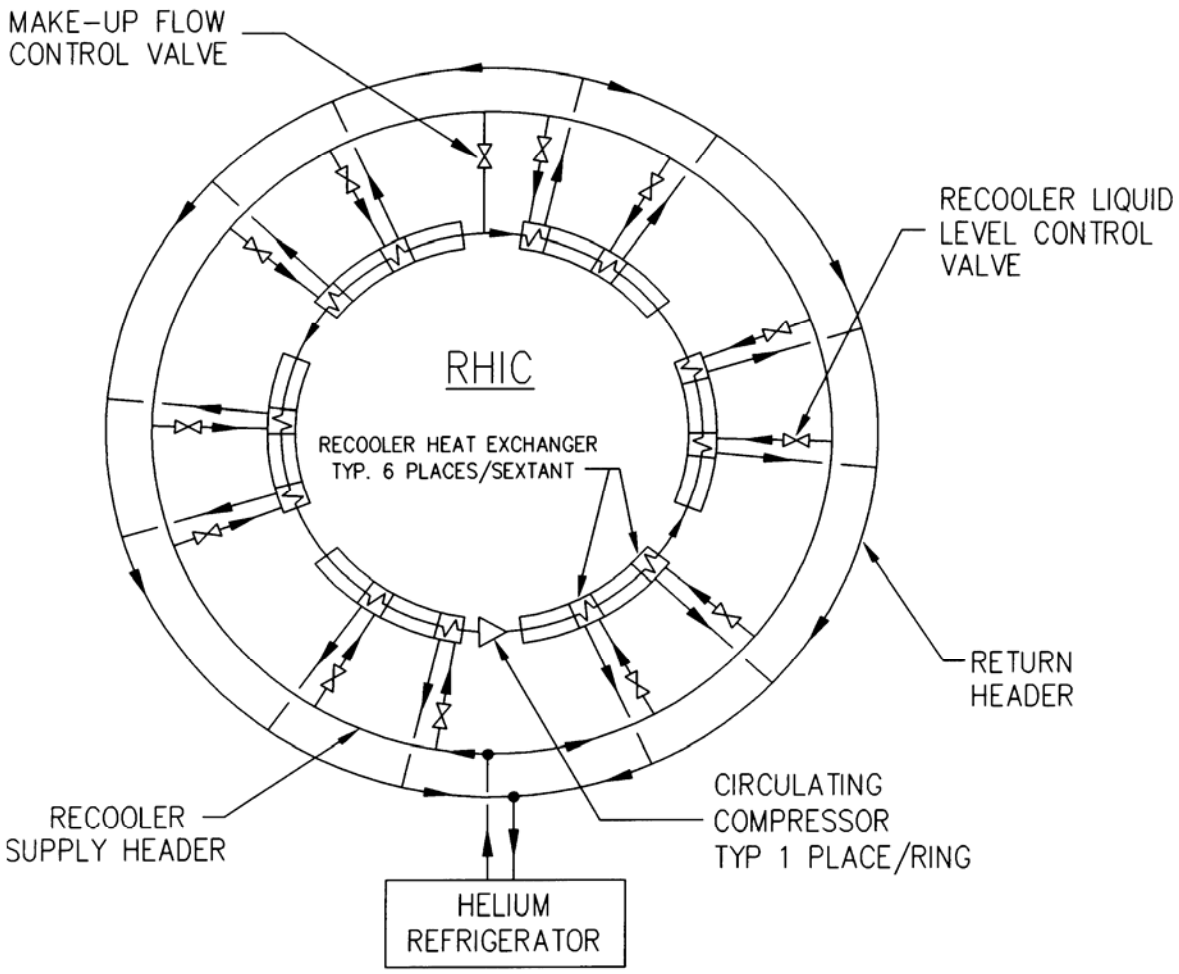

Fig. 3-2. Helium primary flow circuit for steady-state operation.
Only one of the rings is shown.

ii. Heat Load of Magnets and Refrigeration Distribution System

One of the most important factors in the design of the cryogenic system is to properly identify every part of the load imposed upon the system. Wherever possible this load should be as low as is consistent with good design and fabrication practice in order to minimize the operating costs of the accelerator. The aggregate design load, of course, should be kept low enough that a sufficient margin can be maintained between the actual load and the capacity of the existing refrigerator to permit short cooldown times and high reliability.

A heat load budget for the entire RHIC system was maintained throughout the conceptual design period of the project and was periodically updated. The current budget is given in Table 3-1. No refrigeration has been allowed for any item which does not appear in this table. Table 3-2 shows the details of the heat load budget for a 9.7 m Arc Dipole Magnet. Table 3-3 gives the details for an Arc CQS (Corrector-Quad-Sextupole) Magnet. It has been assumed that all dipoles have equal heat loads and that all quadrupoles have the same heat load as an Arc CQS.

Table 3-4 supports the values given in Table 3-1 for the Magnet Power Lead lines of that table. The power bus for the magnets is carried cold (superconducting) in the helium piping which crosses the Intersection Regions (IR). These leads are distributed as shown in Table 3-5. Except at 4 o'clock and 10 o'clock, only two high amperage leads, for the dump resistor, are required per ring per IR. Other leads of lesser amperage also exit at a typical sextant. These leads introduce a conductive load of about 30 W into the magnet helium flow. The penetrations for these leads are incorporated into the design of the valve box. Only one valve box per ring is located at each IR. The remainder of the lead requirements can be handled by low amperage leads (50 A) which are, for convenience, bundled into groups for the gas-cooled penetration. These low amperage leads are located one in each arc CQS assembly and in insertion quadrupoles around the ring.

Table 3-1. Cryogenic System Heat Load Allowance

			Primary Load W @ 4 K			Secondary Load W @ 55 K		
Magnet System:								
Dipoles - 8 cm Aperture	360	ea	@2.51	902		@24.7	8906	
Dipoles - 13 cm (D0)	24	ea	@5.01	120		@49.5	1188	
Dipoles - 20 cm (DX)	12	ea	@7.52	90		@74.2	891	
CQS Assemblies & Insert. Quads	492	ea	@1.78	877		@16.4	8066	
Insertion Magnet Connecting Pipe	1183	m	@0.25	296		@ 1.3	1479	
Corr, Trim, Heater, Volt Tap Leads	492	ea	@3.75	1846		@ 0	0	
Beam Vacuum Pump Connects	48	ea	@1.50	72		@ 5.3	254	
Beam Pipe Warm/Cold Trans	92	ea	@0.50	46		@ 0.2	18	
Magnet System Load Sub-Total					4249			20802
Magnet Power Leads in Lead Pots:								
Main Coils				1282			0	
By-Pass Leads				1189			0	
Magnet Power Leads Sub-Total					2471			0
Cryogenic Distribution System:								
Refrigerator/ Ring Connection Piping	350	m	@0.57	200		@ 2.3	800	
Ring Piping	2400	m	@0.50	1200		@ 2.1	5000	
Valves - 4 K	221	ea		210			1272	
Filters	120	ea		115			974	
Valves - 55 K	47	ea	0	0		@ 3.7	174	
Valve Box with Leads & Recooler	12	ea	@22.0	264		@162.0	1944	
Cryo. Distrib. System Sub-Total					1989			10164
Liquid Helium for Detectors (proposed)					0			0
Sum of Steady-State Individual Component Allowances Above:					8708			30966
Load Contingency and Off-Design Performance Allowance (20%)					1742			6193
Cryogenic System Design Operating Point:					10449			37159
Refrigerator Capacity				24800			55000	
Capacity to Operating Point Ratio:				2.4			1.5	

Table 3-2. Heat Load Allowance per 9.7 m Arc Dipole

Item	Primary W @ 4.6 K	Secondary W @ 55 K
Total Support System	0.30	3.24
Insulation - Radiation & Cond.	1.69	12.70
Interconnect Insulation	0.22	6.80
Other	0.30	2.00
Total for Dipole	2.51	24.74

Table 3-3. Heat Load Allowance for Arc CQS Assembly

Item	Primary W @ 4.6 K	Secondary W @ 55 K
Total Support System	0.20	2.16
Insulation - Rad. & Cond.	0.56	4.23
Interconnect Insulation	0.22	6.80
Beam Position Monitor	0.40	1.20
Other	0.40	2.00
Total for CQS	1.78	16.39

Table 3-4. Magnet Power Leads for RHIC 92 Lattice

LEAD FUNCTION	# of Gas-Cooled Lead Assemblies by current rating				
	12x50A	12x150A	1600A	6300A	TOTAL
Dipole, Main				8	
Quad, Main				8	
DX & D0 Bypasses			44		
Insertion Quad and Dipole Trim and Bypass Circuits		60			
Corrector Coils	492				
TOTAL NUMBER	492	60	44	16	615
LOSS RATE (per kA) USED:					
0.06 g/s + 1.2 W			x	x	
0.085 g/s + 1.7 W		x			
0.08 g/s + 0.3 W	x				
ESTIMATED FLOW (g/s)	20.66	9.2	4.22	3.0	37.6
Equiv. W @ 100 W/(g/s)	2066	920	422	300	3760
ESTIMATED CONDUCTION (W)	89	187	85	60	427
TOTAL LOSS - Equiv. W	2155	1107	507	360	4129
OFF-DESIGN RESERVE (6%)	129	44	23	73	269
MAXIMUM EXPECTED LOAD	2284	1151	530	433	4398

Table 3-5. Distribution of Magnet Power Leads for RHIC 92 Lattice Cold Bus Across Intersection Region

LEAD LOCATION	# of Gas-Cooled Lead Assemblies by current rating					
	12x50A	12×150A	1600A	6300A	TOTAL	Load (W)
2:00 Yellow Valve Box	0	5	4	0	9	
2:00 Blue Valve Box	0	5	6	0	11	
4:00 Yellow Valve Box	0	5	2	4	11	
4:00 Blue Valve Box	0	5	4	4	13	
6:00 Yellow Valve Box	0	5	2	0	7	
6:00 Blue Valve Box	0	5	4	0	9	
8:00 Yellow Valve Box	0	5	2	0	7	
8:00 Blue Valve Box	0	5	4	0	9	
10:00 Yellow Valve Box	0	5	4	4	13	
10:00 Blue Valve Box	0	5	6	4	15	
12:00 Yellow Valve Box	0	5	2	0	7	
12:00 Blue Valve Box	0	5	4	0	9	
TOTAL ABOVE	0	60	44	16	120	1974
Dist. in IR Magnets	204			204	893	
Dist. in Arc Magnets	288			288	1262	
RHIC TOTAL	49260	44	16	612	4129	

Heaters built into the magnets are powered during warm-up. One pair of leads at every CQS is required for these heaters. These leads have been designed into the "bundle" which includes the 12X50 A leads for the correction coils.

Table 3-6 is a listing of each equipment item in a typical sextant (1 and 12 o'clock regions are shown) with its budgeted heat load and the temperature profile which results. This table has been calculated using the baseline load as a model. The baseline flow of 100 g/s is used in this calculation and, as shown, all magnets are below the design maximum temperature of 4.6 K. A similar table has been developed (but is not shown here) for a high heat load model in which each component has twice its baseline heat load. The helium flow rate is increased to 150 g/s and with that change, it is still possible to hold the maximum magnet temperature under 4.6 K.

The parameters used for the calculations in Table 3-6 are as follows:

Recooler Heat Exchanger Effectivity:

Quad	=	0.75
Inlet	=	0.95

(The Recooler Overall Effectivity Used Includes the Effect of By-Pass Flow)

He Bath Temp	=	4.300 K
Magnet Pressure	=	4.5 bar
Magnet Temperature	=	4.5 K
C_P	=	3.956 J/g□K
Flow	=	100 g/s
Dipole Heat Load	=	2.505 W
Quad Heat Load	=	1.782 W
Beam Tube Pump	=	1.500 W

Table 3-6. RHIC Temperature & Heat Load Profile by Element for Typical Sextant of One Ring with Six Recoolers

Element No.	Element Description	Estimated Heat Load (W)	Cumulative for Recool (W)	Gas Temp Out (K)
BI12---	Carryover Prev.	70.6	70.6	4.473
BI12-VJX	Cross-Insert VJP	40.0	110.6	4.575
BI12-VBX	Valve Box	12.5	123.1	4.606
BI12-VBX	Valves	75.0	198.1	4.796
BI12-PL1	Magnet Leads 1	30.0	228.1	4.872
BI12-RCX	Recooler1*Feed	-216.9	11.3	4.328
BI12-VJIN	VJ Line fr Valve Box	10.0	21.3	4.354
BI12-WCX1	Warm/Cold Trans.	0.5	21.8	4.355
BI12-DX	Common Magnet	7.5	29.3	4.374
BI12-WCX2	Warm/Cold Trans.	0.5	29.8	4.375
BI12-WC0	Warm/Cold Trans.	2.5	32.3	4.382
BI12-D0	Dipole	5.0	37.3	4.394
BI12-Q1	Insertion Quad	2.7	39.9	4.401
BI12-PL1	12×50 Corr. #1	2.0	41.9	4.406
BI12-Q2	Insertion Quad	2.7	44.6	4.413
BI12-PL2	12×50 Corr. #2	2.0	46.6	4.418
BI12-Q3	Insert. Quad+WC	2.7	49.3	4.425
BI12-PL3	12×50 Corr. #3	2.0	51.3	4.430
BI12-WC3	Warm/Cold Trans.	0.5	51.8	4.431
BI12-VJ3	Q3 Straight	7.8	59.6	4.451
BI12-WC4	Warm/Cold Trans.	0.5	60.1	4.452
BI12-Q4	Insertion Quad+WC	2.7	62.8	4.459
BI12-PL4	12×50 Corr. #4	2.0	64.8	4.464
BI12-Q5	Insertion Quad+PL	1.8	66.5	4.468
BI12-PL5	12×50 Corr. #5	2.0	68.5	4.473
BI12-D5	Dipole	2.5	71.0	4.480
BI12-RC6	Recooler 2*Quad	-53.3	17.8	4.345
BI12-Q6	Insertion Quad+PL+RC	1.8	19.5	4.349
BI12-PL6	12×50 Corr. #6	2.0	21.5	4.354
BI12-D6	Dipole	2.5	24.0	4.361
BI12-Q7	Insertion Quad	1.8	25.8	4.365
BI12-PL7	12×50 Corr. #7	2.0	27.8	4.370
BI12-Q8	Insertion Quad+PL	1.8	29.6	4.375
BI12-PL8	12×50 Corr. #8	2.0	31.6	4.380

Element No.	Element Description	Estimated Heat Load (W)	Cumulative for Recool (W)	Gas Temp Out (K)
BI12-VJ8	Q8 Straight	1.5	33.1	4.384
BI12-D8	Dipole	2.5	35.6	4.390
BI12-VJ9	Q9 Straight	1.5	37.1	4.394
BI12-Q9	QF+S+C	1.8	38.9	4.398
BI12-PL9	12×50 Corr #9	2.0	40.9	4.403
BI12-D9	Dipole Cell 1	2.5	43.4	4.410
BI12-Q10	QD+S+C+PL	1.8	45.2	4.414
BI12-PL10	12×50 Corr. #10	2.0	47.2	4.419
BI12-D10	Dipole Cell 1	2.5	49.7	4.426
BI12-Q11	QF+S+C+PL	1.8	51.5	4.430
BI12-PL11	12×50 Corr. #11	2.0	53.5	4.435
BI12-D11	Dipole Cell 2	2.5	56.0	4.441
BI12-Q12	QD+S+C	1.8	57.8	4.446
BI12-PL12	12×50 Corr. #12	2.0	59.8	4.451
BI12-D12	Dipole Cell 2	2.5	62.3	4.457
BI12-Q13	QF+S+C	1.8	64.0	4.462
BI12-PL13	12×50 Corr. #13	2.0	66.0	4.467
BI12-D13	Dipole Cell 3	2.5	68.6	4.473
BI12-RC14	Recooler 3*Quad	-51.4	17.1	4.343
BI12-Q14	QD+S+C+RC	1.8	18.9	4.348
BI12-PL14	12×50 Corr. #14	2.0	20.9	4.353
BI12-VP14	Beam Tube Pump	1.5	22.4	4.357
BI12-D14	Dipole Cell 3	2.5	24.9	4.363
BI12-Q15	QF+S+C	1.8	26.7	4.368
BI12-PL15	12×50 Corr. #15	2.0	28.7	4.373
BI12-D15	Dipole Cell 4	2.5	31.2	4.379
BI12-Q16	QD+S+C+PL	1.8	33.0	4.383
BI12-PL16	12×50 Corr. #16	2.0	35.0	4.388
BI12-D16	Dipole Cell 4	2.5	37.5	4.395
BI12-Q17	QF+S+C	1.8	39.3	4.399
BI12-PL17	12×50 Corr. #17	2.0	41.3	4.404
BI12-D17	Dipole Cell 5	2.5	43.8	4.411
BI12-Q18	QD+S+C	1.8	45.6	4.415
BI12-PL18	12×50 Corr. #18	2.0	47.6	4.420

Element No.	Element Description	Estimated Heat Load (W)	Cumulative for Recool (W)	Gas Temp Out (K)
BI12-D18	Dipole Cell 5	2.5	50.1	4.427
BI12-Q19	QF+S+C	1.8	51.9	4.431
BI12-PL19	12×50 Corr. #19	2.0	53.9	4.436
BI12-VP19	Beam Tube Pump	1.5	55.4	4.440
BI12-D19	Dipole Cell 6	2.5	57.9	4.446
BI12-Q20	QD+S+C	1.8	59.6	4.451
BI12-PL20	12×50 Corr. #20	2.0	61.6	4.456
BI12-D20	Dipole Cell 6	2.5	64.1	4.462
BI12-RC21	Recooler 4*Quad	-48.1	16.0	4.341
BI12-Q21	QF+S+C+RC+L	1.8	17.8	4.345
BI12-PL21	12×50 Corr. #21	2.0	19.8	4.350
BI1-D20	Dipole Cell 7	2.5	22.3	4.356
BI1-Q20	QD+S+C	1.8	24.1	4.361
BI1-PL20	12×50 Corr. #22	2.0	26.1	4.366
BI1-VP19	Beam Tube Pump	1.5	27.6	4.370
BI1-D19	Dipole Cell 7	2.5	30.1	4.376
BI1-Q19	QF+S+C	1.8	31.9	4.381
BI1-PL19	12×50 Corr. #23	2.0	33.9	4.386
BI1-D18	Dipole Cell 8	2.5	36.4	4.392
BI1-Q18	QD+S+C	1.8	38.2	4.397
BI1-PL18	12×50 Corr. #24	2.0	40.2	4.402
BI1-D17	Dipole Cell 8	2.5	42.7	4.408
BI1-Q17	QF+S+C	1.8	44.5	4.412
BI1-PL17	12×50 Corr. #25	2.0	46.5	4.417
BI1-D16	Dipole Cell 9	2.5	49.0	4.424
BI1-Q16	QD+S+C+PL	1.8	50.8	4.428
BI1-PL16	12×50 Corr. #26	2.0	52.8	4.433
BI1-D15	Dipole Cell 9	2.5	55.3	4.440
BI1-Q15	QF+S+C	1.8	57.0	4.444
BI1-PL15	12×50 Corr. #27	2.0	59.0	4.449
BI1-D14	Dipole Cell 10	2.5	61.5	4.456
BI1-RC14	Recooler 5*Quad	-46.2	15.4	4.339
BI1-Q14	QD+S+C+RC	1.8	17.2	4.343
BI1-PL14	12×50 Corr. #28	2.0	19.2	4.348

Element No.	Element Description	Estimated Heat Load (W)	Cumulative for Recool (W)	Gas Temp Out (K)
BI1-VP14	Beam Tube Pump	1.5	20.7	4.352
BI1-D13	Dipole Cell 10	2.5	23.2	4.359
BI1-Q13	QF+S+C	1.8	25.0	4.363
BI1-PL13	12×50 Corr. #29	2.0	27.0	4.368
BI1-D12	Dipole Cell 11	2.5	29.5	4.374
BI1-Q12	QD+S+C	1.8	31.2	4.379
BI1-PL12	12×50 Corr. #30	2.0	33.2	4.384
BI1-D11	Dipole Cell 11	2.5	35.7	4.390
BI1-Q11	QF+S+C+PL	1.8	37.5	4.395
BI1-PL11	12×50 Corr. #31	2.0	39.5	4.400
BI1-D10	Dipole Cell 12	2.5	42.0	4.406
BI1-Q10	QD+S+C+PL+PL	1.8	43.8	4.411
BI1-PL10	12×50 Corr. #32	2.0	45.8	4.416
BI1-D9	Dipole Cell 12	2.5	48.3	4.422
BI1-Q9	QF+S+C+WC	1.8	50.1	4.427
BI1-PL9	12×50 Corr. #33	2.0	52.1	4.432
BI1-D8	Dipole	2.5	54.6	4.438
BI1-VJ8	Q8 Straight	3.0	57.6	4.446
BI1-WC8	Warm/Cold Trans.	0.5	58.1	4.447
BI1-Q8	Insert Quad+PL+WC	1.8	59.9	4.451
BI1-PL8	12×50 Corr. #34	2.0	61.9	4.456
BI1-Q7	Insertion Quad	1.8	63.7	4.461
BI1-PL7	12×50 Corr. #35	2.0	65.7	4.466
BI1-D6	Dipole	2.5	68.2	4.472
BI1-RC6	Recooler 6*Quad	-51.1	17.0	4.343
BI1-Q6	Insertion Quad+PL+RC	1.8	18.8	4.348
BI1-PL6	12×50A Lead #36	2.0	20.8	4.353
BI1-D5	Dipole	2.5	23.3	4.359
BI1-Q5	Insertion Quad	1.8	25.1	4.363
BI1-PL5	12×50A Lead #37	2.0	27.1	4.369
BI1-Q4	Insertion Quad + WC	2.7	29.8	4.375
BI1-PL4	12×50A Lead #38	2.0	31.8	4.380
BI1-WC4	Warm/Cold Trans.	0.5	32.3	4.382
BI1-VJ3	Q3 Straight	7.8	40.1	4.401

Element No.	Element Description	Estimated Heat Load (W)	Cumulative for Recool (W)	Gas Temp Out (K)
BI1-WC3	Warm/Cold Trans.	0.5	40.6	4.403
BI1-PL2	12×50A Lead #39	2.0	42.6	4.408
BI1-Q3	Insertion Quad + WC	2.7	45.3	4.414
BI1-PL2	12×50A Lead #40	2.0	47.3	4.419
BI1-Q2	Insertion Quad	2.7	49.9	4.426
BI1-PL1	12×50A Lead #41	2.0	51.9	4.431
BI1-Q1	Insertion Quad	2.7	54.6	4.433
BI1-D0	Dipole	5.0	59.6	4.446
BI1-WC0	Warm/Cold Trans.	2.5	62.1	4.452
BI1-WCX1	Warm/Cold Trans.	0.5	62.6	4.453
BI1-DX	Common Dipole	7.5	70.1	4.472
BI1-WCX2	Warm/Cold Trans.	0.5	70.6	4.473
	Total Sextant Load	467.0		
	Total Recooler Load	-467.0		

The actual RHIC heat load is varies between 11.4 and 12 kW, depending on whether the accelerator is powered to full current. Of this, the conduction and radiation load is approximately 8.4 KW, and the total lead flows vary between 30 and 35 grams/second. All leads are not powered to maximum current at the same time.

The heat load is not evenly distributed throughout a sextant. The first recooler, located at the Q6 magnet, typically sees the highest load, as it sees long transfer lines and triplet magnets. Recoolers in mid arc have lower loads. This pattern is repeated throughout the sextants, as indicated in figure 3-1, which shows the actual measured heat load distribution in the Blue ring.

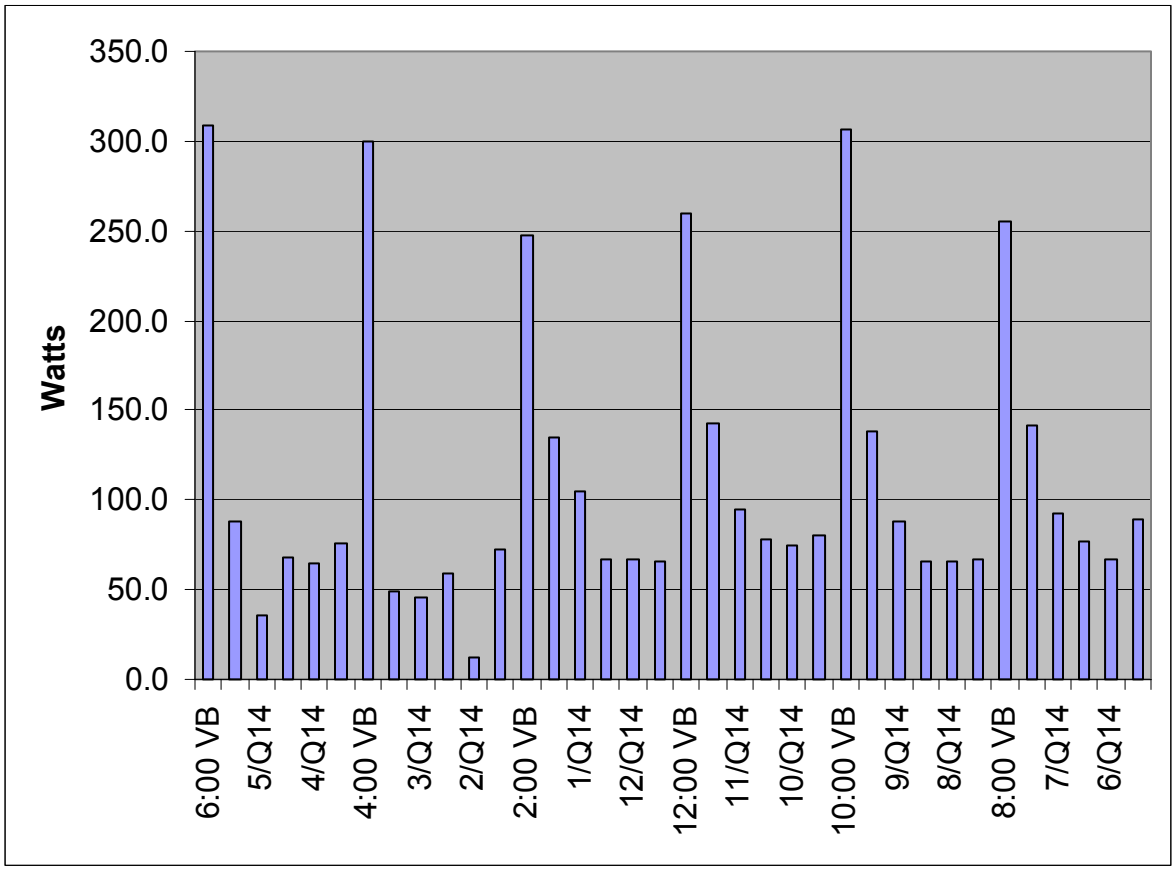

Figure 3-1 .Actual Heat Load Distribution in Blue Ring

iii. Refrigerator Cycle Calculations

The process requirements for the RHIC helium refrigerator to meet the baseline heat load are presented here. The compressor flow required for the refrigerator to meet the baseline load is approximately 50% of the installed compressor capacity. The reference schematic for these calculations is shown in Figures 3-3A and 3-3B. The calculated process state points for this case are given in Tables 3-7A and 3-7B. The electric power currently required for the main compressors to satisfy this operating point is 7.3 MW.

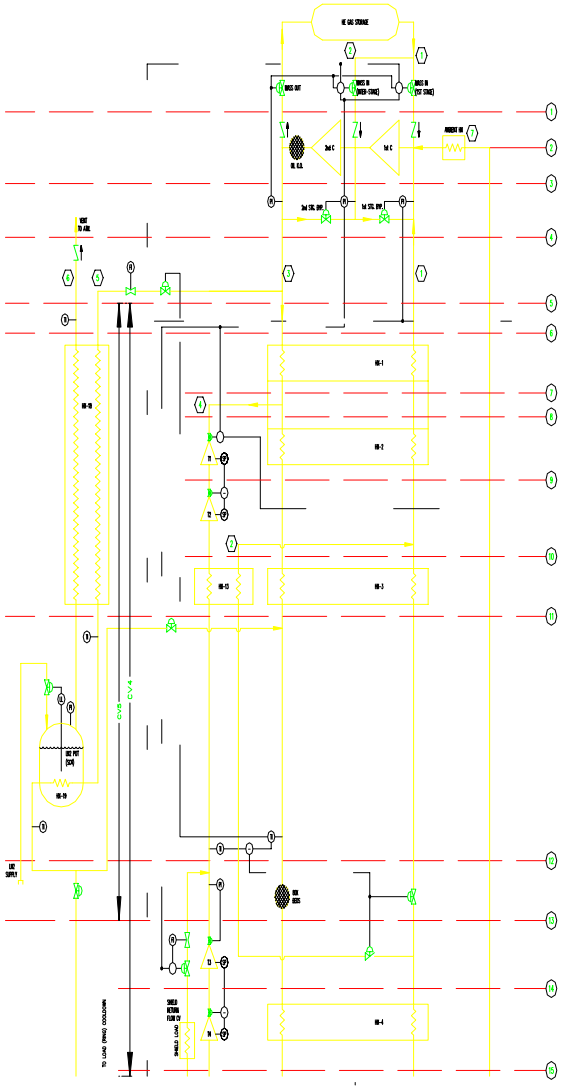

Fig. 3-3A. RHIC refrigerator schematic.

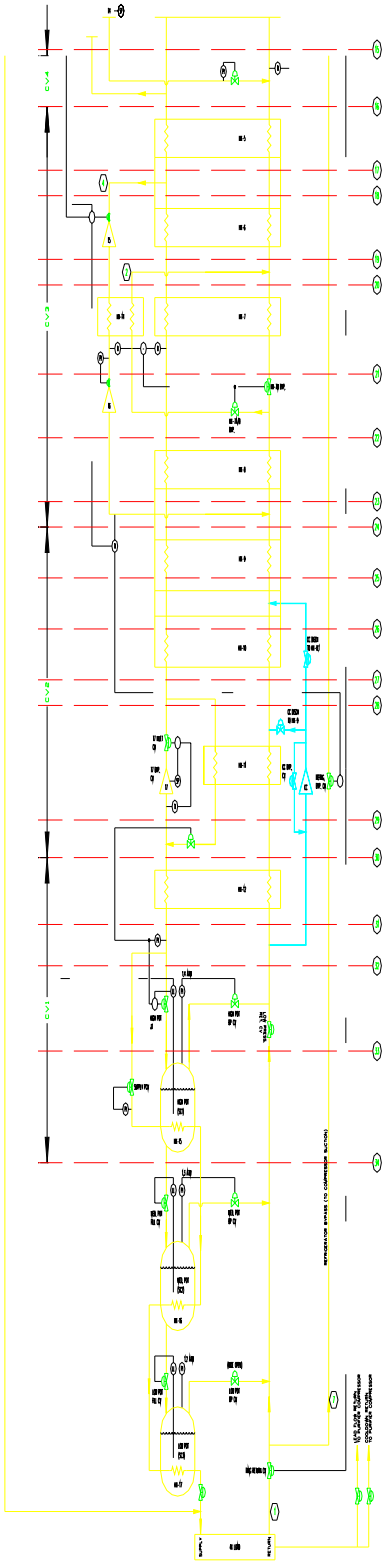

Fig. 3-3B. RHIC refrigerator schematic.

Table 3-7A CYCLE SIMULATION FOR BNL REFRIGERATOR

	HIGH PR.				TURBINE				LOW PR.			
I	T (K)	P (A)	H (J/G)	W (G/S)	T (K)	P (A)	H (J/G)	W (G/S)	T (K)	P (A)	H (J/G)	W (G/S)
1	300.30	15.05	1579.18	.00					292.30	1.05	1532.95	.00
2	300.30	15.05	1579.18	.00					292.30	1.10	1532.97	.00
3	300.30	15.05	1579.18	.00					292.30	1.10	1532.97	.00
4	300.30	15.05	1579.18	1470.15					292.30	1.10	1532.97	1468.15
5	300.30	15.00	1579.17	1470.15					292.30	1.10	1532.97	1468.15
6	300.30	15.00	1579.17	1470.15					292.30	1.10	1532.97	1468.15
7	157.76	14.85	838.56	1470.15					149.03	1.15	788.90	1468.15
8	157.76	14.85	838.56	1190.99	157.76	14.85	838.56	279.16	149.03	1.15	788.90	1468.15
9	129.23	14.75	690.09	1190.99	147.86	11.80	786.12	279.16	125.69	1.18	667.64	1468.15
10	129.23	14.75	690.09	1190.99	137.83	9.30	733.22	279.16	123.82	1.18	657.95	1273.02
11	42.52	14.70	235.52	1190.99	72.12	9.25	390.95	279.16	41.73	1.20	231.35	1273.02
12	42.33	14.70	234.52	1190.99	72.12	9.25	390.95	279.16	41.73	1.20	231.35	1273.02
13	42.34	14.68	234.68	1190.99	72.12	9.25	390.95	297.77	41.73	1.20	231.35	1273.02
14	42.34	14.68	234.68	1190.99	55.52	4.20	303.46	297.77	41.73	1.20	231.35	1468.15
15	40.62	14.64	225.34	1190.99	40.22	1.21	223.49	297.77	40.22	1.21	223.49	1468.15
16	40.62	14.64	225.34	1172.38					40.22	1.21	223.49	1170.38
17	16.70	14.60	90.85	1172.38					14.40	1.22	88.26	1170.38
18	16.70	14.60	90.85	432.77	16.70	14.60	90.85	739.61	14.40	1.22	88.26	1170.38
19	14.53	14.58	77.21	432.77	15.53	7.80	88.34	739.61	13.38	1.22	82.79	1170.38
20	14.53	14.58	77.21	432.77	15.53	7.80	88.34	739.61	12.38	1.22	77.45	785.96
21	11.39	14.56	56.49	432.77	13.19	7.78	74.26	739.61	10.21	1.23	65.72	785.96
22	11.39	14.56	56.49	432.77	13.20	7.80	74.26	739.61	10.21	1.23	65.72	1170.38
23	10.19	14.53	47.53	432.77	9.59	1.23	62.32	739.61	9.59	1.23	62.32	1170.38
24	10.19	14.53	47.53	432.77					9.59	1.23	62.32	430.77
25	4.62	14.51	17.03	432.77					4.60	1.23	31.45	430.77
26	4.62	14.51	17.03	432.77	4.60	1.23	31.45	136.48	4.60	1.23	31.45	294.29
27	4.57	14.48	16.89	432.77	4.45	1.23	29.90	136.48	4.60	1.23	31.45	294.29
28	4.57	14.48	16.89	432.77	4.45	1.23	29.90	136.48	4.60	1.23	31.45	294.29
29	4.57	14.48	16.89	432.77	4.45	1.23	29.90	136.48	4.60	1.23	31.45	294.29
30	4.57	14.48	16.89	432.77	4.45	1.23	29.90	136.48	4.60	1.23	31.45	294.29
31	4.57	14.48	16.89	432.77	4.45	1.23	29.90	136.48	4.60	1.23	31.45	294.29
32	4.57	14.48	16.89	296.29	4.45	1.23	29.90	136.48	4.60	1.23	31.45	294.29
33	5.44	4.50	16.89	296.29	4.45	1.23	29.90	136.48	4.60	1.23	31.45	294.29
34	4.50	4.50	11.91	296.29					4.60	1.23	31.45	294.29

HEAT EXCHANGERS
==== ==========

HX	DTC (K)	DTH (K)	LMTD (K)	UA (W/K)	EFF	NTU	CMIN (W/K)	CMAX (W/K)	QLK (W)	QHX (W)	UAD (W/K)
1	8.729	8.000	8.359	130681.	.9471	17.14	7625.0	7664.0	3600.	1092409.	0.
2	3.545	8.729	5.753	30945.	.8895	4.96	6239.4	7625.0	1200.	178020.	0.
3	.783	5.410	2.394	226837.	.9910	36.22	6262.8	6615.8	1680.	543072.	0.
4	.400	.610	.498	23171.	.8118	3.47	6685.1	7612.2	400.	11532.	0.
5	2.301	.400	1.087	145670.	.9847	23.76	6130.1	6617.3	600.	158273.	0.
6	1.158	2.301	1.664	3845.	.6519	1.30	2952.2	6246.8	500.	6400.	0.
7	1.182	2.156	1.620	5690.	.7266	1.94	2935.7	4255.9	250.	9219.	0.
8	.600	1.182	.858	4636.	.6665	1.40	3318.6	6445.7	100.	3979.	0.
9	.018	.600	.166	79943.	.9968	33.52	2384.6	2662.5	100.	13296.	0.
10	.120	.018	.054	3922.	.8905	2.73	1434.3	4650.4	150.	212.	0.
13	30.383	1.200	9.031	10657.	.9875	10.51	1014.2	1464.6	720.	96243.	0.
14	2.982	.100	.849	12674.	.9812	6.15	2059.9	4596.1	250.	10757.	0.
15	.048	.989	.310	5720.	.9519	3.04	1883.5**********		300.	1775.	0.
TOTAL:				684392.		146.14			9850.		

EXPANDERS
=========

N	PI ATM	PO ATM	PR	TI K	TO K	TR	HI J/G	HO J/G	DH J/G	DI G/CC	DO G/CC	EFFEX	FLOW G/S	WORK W
1	14.85	11.80	1.26	157.73	147.89	1.07	838.39	786.12	52.28	.00453	.00385	.717	279.2	14594.
2	11.80	9.30	1.27	147.83	137.83	1.07	785.97	733.08	52.89	.00385	.00326	.750	279.2	14764.
3	8.85	4.20	2.11	72.12	55.53	1.30	390.90	303.46	87.45	.00589	.00366	.894	297.8	26039.
4	4.20	1.21	3.46	55.51	40.22	1.38	303.40	223.46	79.94	.00366	.00147	.704	297.8	23805.
5	14.60	7.80	1.87	16.70	15.53	1.08	90.84	88.47	2.37	.04433	.02566	.133	739.6	1756.
6	7.68	1.23	6.25	13.18	9.59	1.37	74.26	62.33	11.94	.03107	.00650	.382	739.6	8828.

DEWAR CONDITIONS
================

PSHE ATM	TSHE K	DLIQ G/CC	HLIQ J/G	SLIQ J/G-K	DVAP G/CC	HVAP J/G	SVAP J/G-K	X
1.230	4.452	.120	10.958	3.698	.021	29.900	7.949	.313

HE Warm Make-Up	2.00 G/S	60.0 L/H
HE With-Drawl	.00 G/S	.0 L/H
HE 2-Phase Supply	136.48 G/S	
4K REF Load	5750. W	

COMPRESSOR
==========

NO. OF M/CS.= 10 COMP. TYPE= 321/165. COMP. CAP.(ACFM) = 3051.1
PS= 1.050 ATM PD= 3.550 ATM PR= 3.381 TS = 292.300 K
VOL EFF. = .913 MTR EFF. = .900 ISO EFF. = .608 TOT EFF. = .547

	FLOW (G/S)	ACFM	SCFM	ISO POWER (KW)	ACT POWER (KW)
TOTAL	2521.85	30511.1	32128.3	1867.1	3412.6

iv. Pressure Ratings

Each component of the RHIC Cryogenic System has been designed and tested to meet the pressure conditions which may exist during operation of the system. The major subsystems and their pressure ratings are shown in Table 3-8. The piping design, fabrication, relief valve settings and test pressures are to comply with ASME Pressure Vessel Code, Section VIII and Piping Code B31.3.

Table 3-8. Cryogenic System Pressure Ratings

Sub-System	Pressure (bar, absolute except as noted)				
	Nominal Oper.	Design Working (Max Diff)	Relief Valve Set (Gauge)	Pneu. Test -Piping (Gauge)	Pneu. Test -Vessels (Gauge)
Magnet Loop	5.0	18.7	17.7	20.6	23.4
Recooler Supply Header	6.0	18.7	17.7	20.6	23.4
Return (Cold) Header 1.3	18.7	17.7	20.6	23.4	
Utility Header	1.3	18.7	17.7	20.6	23.4
Heat Shield	15.0	18.7	17.7	20.6	23.4
Ambient Temp. Return	1.4	18.7	18.7	20.6	23.4
Main Compressor Suction	1.05	6.8	5.2	7.5	8.5
Main Compressor 1st Stage Disch.	4.0	6.8	6.8	7.5	8.5
Main Compressor Interstage	4.0	9.1	9.1	10.0	11.4
Main Compressor 2nd Stage Disch.	16.4	18.7	18.7	20.6	23.4

v. Pressure Drop of Magnets and Distribution System

As mentioned in the introduction, the flow through the magnets is driven by a circulating compressor in each ring. Because the work which these compressors perform on the helium is part of the load seen by the refrigerator, it is important that the work input be minimized. The work is a direct function of the pressure drop in the loop which is the output head required from the compressor. In order to maximize the efficiency of the compressors it is necessary to specify the range of operating conditions that will be encountered in RHIC operations so a pressure drop budget was established and adhered in the design of components in the flow loop.

Table 3-9 shows the calculated pressure drops for flow through a model of one RHIC ring. Each component which is known to contribute to the pressure drop has been shown with its budgeted allowance for pressure drop. No safety margins are included in these figures, and they represent expected baseline performance with the minimum flow in any magnet at 100 g/s. It can be seen that the pressure drop for these six sextants is estimated to be about 0.5 bar. A similar table has been developed for the same section of the collider ring but for the high heat model conditions, i.e., minimum flow rate is 150 g/s. Under these conditions the estimated pressure drop is about 1.0 bar. The actual measured pressure drop is approximately .50 bar for each circulator during normal RHIC operating conditions.

Table 3-9. RHIC Circulating Compressor Loop Through 1 Ring - 6 Sextants in Series

MAG IC:2.5"+3" TUBE WITH LEADS AND SPLICE, 2" CVI ISOLATION VALVES,3 1/2"SCH5-I
NOM FLOW = 100 g/s MAGNET LENGTH = 2X TO ADJUST FOR 2X FRICTION FACTOR

	INPUT DATA							CALCULATED DATA			DESCRIPTION
SEC NO.	P_{IN} bar	F_{IN} g/s	T_{IN} K	T_{OUT} K	LEN m	DIA cm	# VEL HEADS	FRIC DROP bar	VEL DROP bar	P_{OUT} bar	
1	5.00	118.0	4.50	4.50	5.0	5.70	10.0	.000	.001	5.00	FEED FROM CIRC COMPR
2	5.00	118.0	4.50	4.50	.0	5.08	4.1	.000	.001	5.00	CVI 2" VALVE
3	5.00	118.0	4.50	4.50	2.0	10.00	2.0	.000	.000	5.00	LEAD POT
4	5.00	9.6	4.50	4.30	9.5	1.60	10.0	.001	.001	5.00	225W RECOOL(.63"X12)
5	5.00	57.5	4.30	4.30	14.0	3.81	12.0	.000	.001	5.00	Q1,Q2,Q3 (2@1.5"SQ)
6	5.00	115.0	4.30	4.30	98.4	4.97	10.0	.000	.000	5.00	Q3-Q4 W LEADS
7	5.00	28.8	4.30	4.40	845.2	3.00	296.0	.025	.017	4.95	636 M RING (68 MAGS)
8	4.95	57.5	4.40	4.40	14.0	3.81	12.0	.000	.001	4.95	Q1,Q2,Q3 (2@1.5"SQ)
9	4.95	73.7	4.50	4.50	75.9	4.26	70.0	.000	.001	4.95	3" W.LEAD(A=35.25)
10	4.95	73.7	4.50	4.50	8.5	3.55	1.4	.000	.000	4.95	3" W.SPLICE(A=31.62)
11	4.95	11.5	4.50	4.30	2.5	1.10	10.0	.002	.005	4.94	50W RECOOL(.43"X10)
12	4.94	11.5	4.50	4.30	2.5	1.10	10.0	.002	.005	4.94	50W RECOOL(.43"X10)
13	4.94	11.5	4.50	4.30	2.5	1.10	10.0	.002	.005	4.93	50W RECOOL(.43"X10)
14	4.93	11.5	4.50	4.30	2.5	1.10	10.0	.002	.005	4.92	50W RECOOL(.43"X10)
15	4.92	11.5	4.50	4.30	2.5	1.10	10.0	.002	.005	4.92	50W RECOOL(.43"X10)
16	4.92	115.0	4.30	4.30	78.0	4.97	30.0	.000	.000	4.91	SEXT CONN
17	4.91	115.0	4.50	4.50	.0	5.08	4.1	.000	.000	4.91	CVI 2" VALVE
18	4.91	115.0	4.50	4.50	2.0	10.00	2.0	.000	.000	4.91	LEAD POT
19	4.91	9.3	4.50	4.30	9.5	1.60	10.0	.001	.001	4.91	225W RECOOL(.63"X12)
20	4.91	55.0	4.30	4.30	14.0	3.81	12.0	.000	.001	4.91	Q1,Q2,Q3 (2@1.5"SQ)
21	4.91	112.0	4.50	4.50	98.4	4.97	10.0	.000	.000	4.91	Q3-Q4 W LEADS
22	4.91	28.0	4.30	4.40	845.0	3.00	296.0	.024	.017	4.87	636 M RING (68 MAGS)
23	4.87	56.0	4.40	4.40	14.0	3.81	12.0	.000	.001	4.87	Q1,Q2,Q3 (2@1.5"SQ)
24	4.87	71.8	4.50	4.50	75.9	4.26	70.0	.000	.001	4.87	3" W.LEAD(A=35.25)
25	4.87	71.8	4.50	4.50	8.5	3.55	1.4	.000	.000	4.87	3" W.SPLICE(A=31.62)

Table 3-9. RHIC Circulating Compressor Loop Through 1 Ring - 6 Sextants in Series (continued)

	INPUT DATA							CALCULATED DATA			DESCRIPTION
SEC NO.	P_{IN} bar	F_{IN} g/s	T_{IN} K	T_{OUT} K	LEN m	DIA cm	# VEL HEADS	FRIC DROP bar	VEL DROP bar	P_{OUT} bar	
26	4.87	11.2	4.50	4.30	2.5	1.10	10.0	.002	.005	4.86	50W RECOOL(.43"X10)
27	4.86	11.2	4.50	4.30	2.5	1.10	10.0	.002	.005	4.86	50W RECOOL(.43"X10)
28	4.86	11.2	4.50	4.30	2.5	1.10	10.0	.002	.005	4.85	50W RECOOL(.43"X10)
29	4.85	11.2	4.50	4.30	2.5	1.10	10.0	.002	.005	4.84	50W RECOOL(.43"X10)
30	4.84	11.2	4.50	4.30	2.5	1.10	10.0	.002	.005	4.84	50W RECOOL(.43"X10)
31	4.84	112.0	4.30	4.30	78.0	4.97	30.0	.000	.000	4.83	SEXT CONN
32	4.83	112.0	4.50	4.50	.0	5.08	4.1	.000	.000	4.83	CVI 2" VALVE
33	4.83	112.0	4.50	4.50	2.0	10.00	2.0	.000	.000	4.83	LEAD POT
34	4.83	9.1	4.50	4.30	9.5	1.60	10.0	.001	.001	4.83	225W RECOOL(.63"X12)
35	4.83	54.5	4.30	4.30	14.0	3.81	12.0	.000	.001	4.83	Q1,Q2,Q3 (2@1.5"SQ)
36	4.83	109.0	4.50	4.50	98.4	4.97	10.0	.000	.000	4.83	Q3-Q4 W LEADS
37	4.83	27.3	4.30	4.40	845.0	3.00	296.0	.022	.016	4.79	636 M RING (68 MAGS)
38	4.79	54.5	4.40	4.40	14.0	3.81	12.0	.000	.001	4.79	Q1,Q2,Q3 (2@1.5"SQ)
39	4.79	66.9	4.50	4.50	75.9	4.26	70.0	.000	.001	4.79	3" W.LEAD(A=35.25)
40	4.79	66.9	4.50	4.50	8.5	3.55	1.4	.000	.000	4.79	3" W.SPLICE(A=31.62)
41	4.79	10.9	4.50	4.30	2.5	1.10	10.0	.002	.005	4.78	50W RECOOL(.43"X10)
42	4.78	10.9	4.50	4.30	2.5	1.10	10.0	.002	.005	4.78	50W RECOOL(.43"X10)
43	4.78	10.9	4.50	4.30	2.5	1.10	10.0	.002	.005	4.77	50W RECOOL(.43"X10)
44	4.77	10.9	4.50	4.30	2.5	1.10	10.0	.002	.005	4.77	50W RECOOL(.43"X10)
45	4.77	10.9	4.50	4.30	2.5	1.10	10.0	.002	.005	4.76	50W RECOOL(.43"X10)
46	4.76	109.0	4.30	4.30	78.0	4.97	30.0	.000	.000	4.76	SEXT CONN
47	4.76	109.0	4.50	4.50	.0	5.08	4.1	.000	.000	4.76	CVI 2" VALVE
48	4.76	109.0	4.50	4.50	2.0	10.00	2.0	.000	.000	4.76	LEAD POT
49	4.76	8.8	4.50	4.30	9.5	1.60	10.0	.001	.001	4.76	225W RECOOL(.63"X12)
50	4.76	53.0	4.30	4.30	14.0	3.81	12.0	.000	.001	4.76	Q1,Q2,Q3 (2@1.5"SQ)
51	4.76	106.0	4.30	4.30	98.4	4.97	10.0	.000	.000	4.76	Q3-Q4 W LEADS
52	4.76	26.5	4.30	4.40	845.0	3.00	296.0	.021	.015	4.72	636 M RING (68 MAGS)
53	4.72	53.0	4.40	4.40	14.0	3.81	12.0	.000	.001	4.72	Q1,Q2,Q3 (2@1.5"SQ)

Table 3-9. RHIC Circulating Compressor Loop Through 1 Ring - 6 Sextants in Series (continued)

	INPUT DATA							CALCULATED DATA			DESCRIPTION
SEC NO.	P_{IN} bar	F_{IN} g/s	T_{IN} K	T_{OUT} K	LEN m	DIA cm	# VEL HEADS	FRIC DROP bar	VEL DROP bar	P_{OUT} bar	
54	4.72	65.2	4.50	4.50	75.9	4.26	70.0	.000	.001	4.72	3" W.LEAD(A=35.25)
55	4.72	65.2	4.50	4.50	8.5	3.55	1.4	.000	.000	4.72	3" W.SPLICE(A=31.62)
56	4.72	10.6	4.50	4.30	2.5	1.10	10.0	.002	.004	4.71	50W RECOOL(.43"X10)
57	4.71	10.6	4.50	4.30	2.5	1.10	10.0	.002	.004	4.71	50W RECOOL(.43"X10)
58	4.71	10.6	4.50	4.30	2.5	1.10	10.0	.002	.004	4.70	50W RECOOL(.43"X10)
59	4.70	10.6	4.50	4.30	2.5	1.10	10.0	.002	.004	4.69	50W RECOOL(.43"X10)
60	4.69	10.6	4.50	4.30	2.5	1.10	10.0	.002	.004	4.69	50W RECOOL(.43"X10)
61	4.69	106.0	4.30	4.30	78.0	4.97	30.0	.000	.000	4.69	SEXT CONN
62	4.69	106.0	4.50	4.50	.0	5.08	4.1	.000	.000	4.69	CVI 2" VALVE
63	4.69	106.0	4.50	4.50	2.0	10.00	2.0	.000	.000	4.69	LEAD POT
64	4.69	8.6	4.50	4.30	9.5	1.60	10.0	.001	.001	4.69	225W RECOOL(.63"X12)
65	4.69	51.5	4.30	4.30	14.0	3.81	12.0	.000	.001	4.68	Q1,Q2,Q3 (2@1.5"SQ)
66	4.68	103.0	4.50	4.50	98.4	4.97	10.0	.000	.000	4.68	Q3-Q4 W LEADS
67	4.68	25.8	4.30	4.40	790.0	3.00	284.0	.019	.014	4.65	636 M RING (68 MAGS)
68	4.65	51.5	4.40	4.40	14.0	3.81	12.0	.000	.001	4.65	Q1,Q2,Q3 (2@1.5"SQ)
69	4.65	62.7	4.50	4.50	75.9	4.26	70.0	.000	.001	4.65	3" W.LEAD(A=35.25)
70	4.65	62.7	4.50	4.50	8.5	3.55	1.4	.000	.000	4.65	3" W.SPLICE(A=31.62)
71	4.65	10.3	4.50	4.30	2.5	1.10	10.0	.001	.004	4.64	50W RECOOL(.43"X10)
72	4.64	10.3	4.50	4.30	2.5	1.10	10.0	.001	.004	4.64	50W RECOOL(.43"X10)
73	4.64	10.3	4.50	4.30	2.5	1.10	10.0	.001	.004	4.63	50W RECOOL(.43"X10)
74	4.63	10.3	4.50	4.30	2.5	1.10	10.0	.001	.004	4.63	50W RECOOL(.43"X10)
75	4.63	10.3	4.50	4.30	2.5	1.10	10.0	.001	.004	4.62	50W RECOOL(.43"X10)
76	4.62	103.0	4.30	4.30	78.0	4.97	30.0	.000	.000	4.62	SEXT CONN
77	4.62	103.0	4.50	4.50	.0	5.08	4.1	.000	.000	4.62	CVI 2" VALVE
78	4.62	103.0	4.50	4.50	2.0	10.00	2.0	.000	.000	4.62	LEAD POT
79	4.62	8.3	4.50	4.30	9.5	1.60	10.0	.001	.001	4.62	225W RECOOL(.63"X12)
80	4.62	50.0	4.30	4.30	14.0	3.81	12.0	.000	.001	4.62	Q1,Q2,Q3 (2@1.5"SQ)
81	4.62	100.0	4.50	4.50	98.4	4.97	10.0	.000	.000	4.62	Q3-Q4 W LEADS

Table 3-9. RHIC Circulating Compressor Loop Through 1 Ring - 6 Sextants in Series (continued)

	INPUT DATA							CALCULATED DATA			DESCRIPTION
SEC NO.	P_{IN} bar	F_{IN} g/s	T_{IN} K	T_{OUT} K	LEN m	DIA cm	# VEL HEADS	FRIC DROP bar	VEL DROP bar	P_{OUT} bar	
82	4.62	100.0	4.50	4.50	26.2	4.97	10.0	.000	.000	4.62	Q7-D8 W LEADS
83	4.62	25.0	4.30	4.40	835.0	3.00	292.0	.019	.013	4.59	636 M RING (67 MAGS)
84	4.59	50.0	4.40	4.40	14.0	3.81	12.0	.000	.001	4.58	Q1,Q2,Q3 (2@1.5"SQ)
85	4.58	60.0	4.50	4.50	55.9	4.26	68.2	.000	.001	4.58	3" W.LEAD(A=35.25)
86	4.58	60.0	4.50	4.50	8.5	3.55	1.4	.000	.000	4.58	3" W.SPLICE(A=31.62)
87	4.58	10.0	4.50	4.30	2.5	1.10	10.0	.001	.004	4.58	50W RECOOL(.43"X10)
88	4.58	10.0	4.50	4.30	2.5	1.10	10.0	.001	.004	4.57	50W RECOOL(.43"X10)
89	4.57	10.0	4.50	4.30	2.5	1.10	10.0	.001	.004	4.57	50W RECOOL(.43"X10)
90	4.57	10.0	4.50	4.30	2.5	1.10	10.0	.001	.004	4.56	50W RECOOL(.43"X10)
91	4.56	10.0	4.50	4.30	2.5	1.10	10.0	.001	.004	4.56	50W RECOOL(.43"X10)
92	4.56	100.0	4.30	4.30	78.0	4.97	30.0	.000	.000	4.56	SEXT CONN
93	4.56	100.0	4.50	4.50	.0	5.08	4.1	.000	.000	4.56	CVI 2" VALVE
94	4.56	100.0	4.50	4.50	5.0	5.70	10.0	.000	.001	4.56	FEED TO CIRC COMPR

TOTAL PRESSURE DROP OVER ALL SECTIONS = .445 ATM

vi. Helium Inventory for RHIC

. The system-wide Helium inventory requirements are summarized in Table 3-10. Total operating inventory is approximately 6.6 million standard cubic feet. Of this, approximately 800,000 scf are in the refrigerator and compressor system, 2.3 million in each ring and about 1.2 million in storage, of which about half is unusable system tare volume.

A bank of 47 warm gas storage tanks has been installed near 1006B, which provides a storage capacity of about 3.3 million scf. Three liquid Helium Dewars have also been installed near 1006B, with a combined capacity of approximately 3.1 million scf. It has proven to be more cost effective to store the liquid helium off site, than to keep the Dewars cold during extended RHIC shutdowns.

Table 3-10. Estimated Helium Inventory

	Physical Volume (liter)	Equiv. Liquid Helium Vol. (liter)	Equiv. Vol. at Std. Cond. 1 atm, 298 K (1000 scf)
I - MAGNET COOLANT LOOP			
Regular Arc Components			
288 Dipole Assemblies	34560	39537	1067
276 CQS Assemblies	20700	23681	639
Sum for Magnet Interconnects	2096	2397	65
Insertion Region Components			
Dipoles			
12 DX Magnets	996	1139	31
24 D0, D5, D6, D8 Assemblies	8424	9637	260
Quadrupoles			
24 Q1-Q9 Assemblies	14688	16803	454
Sum for Magnet Interconnects	4606	5270	142
Vacuum Jacketed Piping			
Sum for Q3-Q4	7685	8792	237
Sum for D0-D0	8128	9299	251
15 Lead Pots	2465	2819	76
56 Cold/Warm Transitions	627	718	19
II - PIPING SYSTEM			
In Ring - 8710 m			
Recooler Supply	32388	37052	1000
Recooler Return	32388	5182	140
Utility Header	32388	5182	140
Shield	20933	3481	94
Refrigerator to Ring - 387 m			
Supply 2180	2494	67	
Return 8049	1288	35	
Shield	7367	1179	32
III - OTHER RING COMPONENTS			
12 - 225 W Recoolers	5220	5220	141
60 - 50 W Recoolers	2094	2396	65
Cold Gas in Storage Tanks	130000	17000	459
Refrigerator Work Inventory		23926	646
Working Margin		18768	507
Gas Storage Tare Volume	3398400	4889	132
TOTAL INVENTORY IN EQUIV. LIQ. LITERS		248148	
TOTAL INVENTORY IN 1000 scf			6600
IN STANDARD m^3			189723
TOTAL INVENTORY IN kg		31019	

vii. System Thermal Mass and Cooldown/Warmup Time Estimates

Based on cool down rates through several thermal cycles of the accelerator, the total thermal mass of the magnets and heat shield is about 200,000 kg. Cool down of the accelerator is done in two phases, first to 80K then to 4.5K. Each wave goes through one ring at a time, with the Blue ring cooled first. A liquid nitrogen based system has been installed near building 1006B to facilitate cooldown to 80K. This system, called the 80K Cooler, takes pressurized Helium from one of two local compressors and cools it to approximately 80K via boiling heat transfer in a liquid nitrogen bath, then routes this cold gas to the accelerator. Typically, this phase takes 12 days per ring, at 120 g/sec of Helium flow through the 80K cooler.

Cool down to operating temperature is done with the main refrigerator and is begun after the 80K waves are complete. The 4.5 K waves are also done in series with it typically takes 5-6 days/ring to reach normal operating conditions.

The energy necessary to warm the magnet to room temperature from operating temperature is provided by electric resistance heaters inserted into the magnet laminations. A small flow of helium is provided during the time that the heaters are powered to spread the heat from the laminations to parts of the system not in contact with the laminations, and to couple magnet temperatures to temperature instrumentation. Warm-up to room temperature takes less than one week.

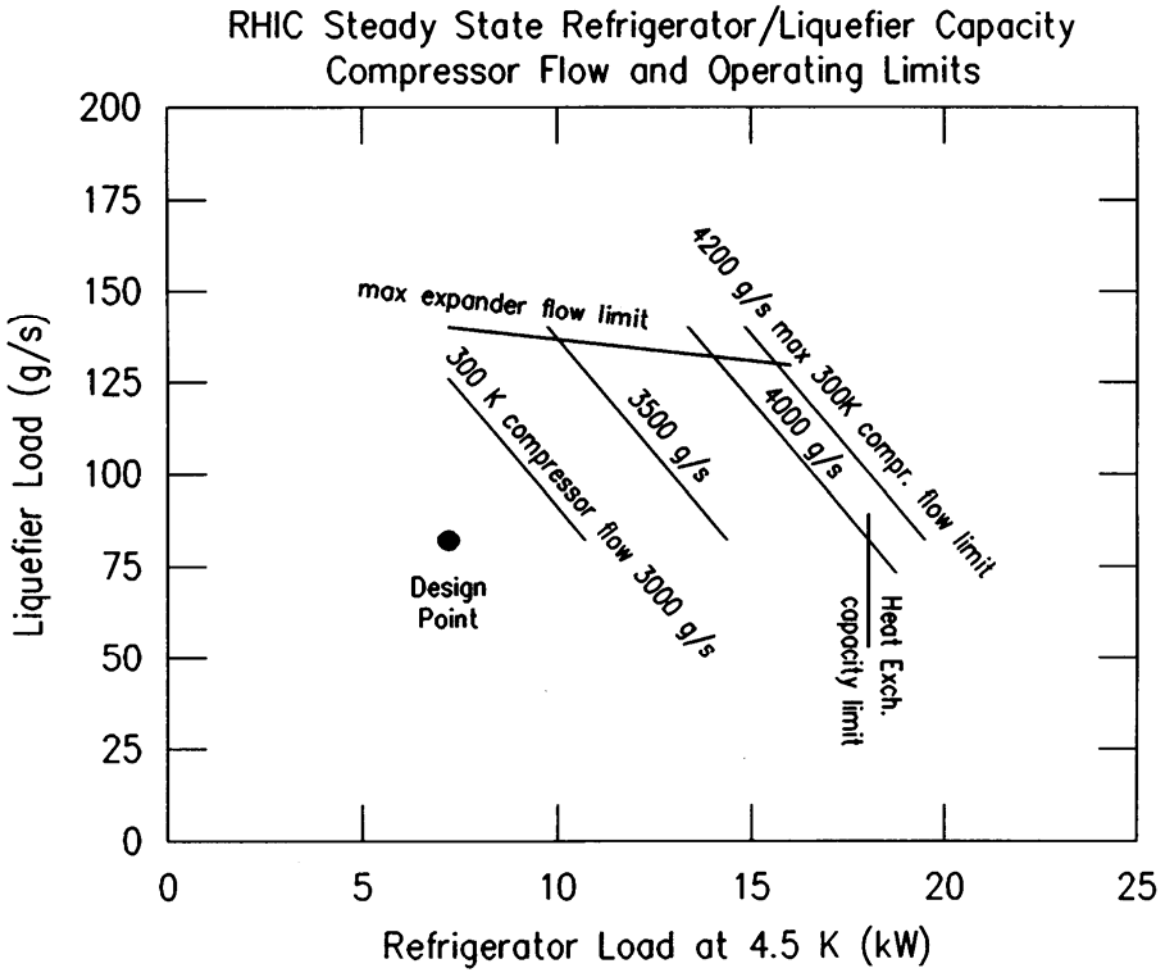

Fig. 3-4. RHIC steady state refrigerator/liquefier capacity compressor flow and operating limits.

viii. System Components

Condensed specifications for cryogenic system related components in RHIC are given below. These specifications indicate the conceptual boundaries of performance, physically and thermally, for each component.

Inlet Recooler

The Inlet Recooler is a heat exchanger assembly located in a valve box. By means of this heat exchanger helium gas, which is about to enter the magnet string at one end (Dipole D0) of a sextant is cooled to a temperature close to the temperature of the boiling liquid helium bath provided on one side of the heat exchanger. The performance required for this heat exchanger is predicated on the analysis of Table 3-6 where this recooler is identified as Element No. BI12-RCX, RECOOLER1*FEED. RHIC Spec. No. 015, *Specification for the Design and Fabrication of a 225 Watt Recooler* is the controlling document for this piece of equipment. The performance requirements from this specification are excerpted below.

1. The recooler shall have sufficient heat exchanger surface to permit the removal of 225 W of heat from the magnet coolant stream and transfer it to a bath of boiling helium. The process diagram is shown in Fig. 3-5. The required process point conditions dictated by the RHIC operating conditions are:

Point	Pressure (bar)	Temperature (K)	Flow Rate (g/sec)
1	4.5	4.825	100
2	See para. 4, below	4.28	100
3	1.024	4.25	--
4	4.22	4.30	As required
5	1.023	Covered elsewhere	As required

2. The sum of the heat flux to the two helium streams shown in Fig. 3-5 from all sources by conduction, convection and/or radiation shall not exceed 5 W.
3. The heat flux to the heat shield circuit shall not exceed 15 W.
4. The total pressure drop in the Magnet Coolant circuit shall not exceed 0.005 bar from inlet to outlet port with fluid conditions as shown in paragraph 1. This is to include allowance for the inlet filter losses and velocity head losses due to direction change as well as frictional losses.

5. Maximum pressure drop from process point 3 to process point 5 including the phase separator shall be less than 0.001 bar.

Quad Recooler

The Quad Recooler is a heat exchanger assembly which has been designed to fit with its piping into an arc quadrupole magnet cryostat (Dwg. No. 12075000). Five of these heat exchangers are located in each sextant as indicated in Table 3-6. The first is located at Q6 where helium enters the regular arc magnets. The next four are located at even thermal intervals. The last is located at Q6 where helium exits from the regular arc magnets. By means of this heat exchanger helium gas, which passes through the magnet string is cooled periodically to a temperature close to the temperature of the boiling liquid helium bath provided on one side of the heat exchanger. The performance required for this heat exchanger is predicated on the analysis of Table 3-6 where this recooler is identified as

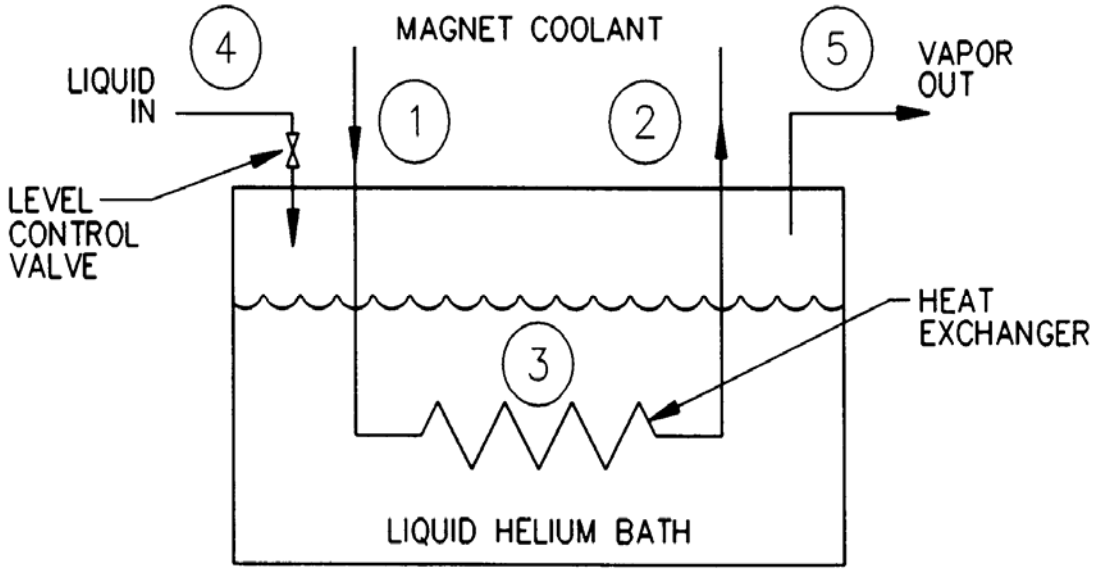

Fig. 3-5. Recooler process schematic.

Element Nos. BI12-RC6, BI12-RC14, BI12-RC21, BI1-RC14 and BI1-RC6. The recooler assembly drawing number is 34015000. The performance requirements are given below.

1. The recooler shall have sufficient heat exchanger surface to permit the removal of 50 W of heat from the magnet coolant stream and transfer it to a bath of boiling helium. The process diagram is shown in Fig. 3-5. The required process point conditions dictated by the RHIC operating conditions are:

Point	Pressure (bar)	Temperature (K)	Flow Rate (g/sec)
1	4.5	4.50	100
2	See para. 4, below	4.28	100
3	1.024	4.25	--
4	4.22	4.30	As required
5	1.023	Covered elsewhere	As required

2. The sum of the heat flux to the two helium streams shown in Fig. 3-5 from all sources by conduction, convection and/or radiation shall not exceed 2 W.
3. The recooler will be located within the 55 K heat shield of the quad cryostat.
4. The total pressure drop (process point 1 to 2) in the Magnet Coolant circuit shall not exceed 0.007 bar from inlet to outlet port with fluid conditions as shown in paragraph 1. This is to include allowance for the inlet filter losses and velocity head losses due to direction change as well as frictional losses.
5. Maximum pressure drop from process point 3 to process point 5 including the phase separator shall be less than 0.001 bar.

Circulating Compressors

A circulating compressor in each ring will be used to sustain the closed loop flow as shown in Fig. 3-2. These compressors are located at the 6 o'clock valve boxes and have the operating characteristics as shown below.

Required Operating Conditions:

	Condition 1	Condition 2
Fluid:	Helium	Helium
Flow Rate:	100 g/s	150 g/s
Inlet Pressure:	4.75 bar	4.50 bar
Outlet Pressure:	5.00 bar	5.00 bar
Inlet Temperature:	4.5 K	4.5 K
Adiabatic Efficiency:	50%	50%

Magnet Power Lead Pot

It is necessary to carry the electric power for the magnets through conductors which pass from ambient conditions (300 K) to the magnets. The lead pot at one end of each sextant must have penetrations for a minimum number of power leads as shown in Table 3-5. The lead pot is designed to share the vacuum tank of the valve box.

Cross-Insertion Vacuum Jacketed Transfer Lines

Piping is required to carry the cryogenic system helium wherever there are long gaps in the magnets in the ring, e.g., across the experimental areas and between magnets Q3 and Q4, and, at 6 o'clock only, between magnets Q7 and Q8 and magnets Q9 and D9. In all areas it is required that the superconducting buswork be carried along with the magnet coolant flow.

All the piping for a ring is carried in a common vacuum jacket with a heat shield. Pipes inside this jacket carry the helium for the following:

Magnet coolant, with leads
Supply Header
Return Header
Utility Header
Heat Shield (55 K)

This connecting piping also contains all the isolation and diverting valves required to meet the RHIC operating scenarios. Groups of these valves have been gathered into a single valve box located between each pair of sextants. These valves are shown on Drawing No. 3A995006, Overall system Block Diagram, 3-6. The isolation valves are sized at 2 inch and the diverting (block and bleed) valves are 1.5 inch. At each place on the drawing where a "B" designates a block and bleed location, there are actually three valves. These valves are arranged so that two valves are in series to

block the flow and a third (smaller) valve is between them which can be used to bleed off pressure in case either of the other two valves leak. This will prevent undetected leaks.

Refrigerator to Ring Vacuum Jacketed Transfer Lines

Five pipes will connect the refrigerator to the ring. Vacuum jacketed piping transports 4.5 K helium from the refrigerator to the tunnel where it feeds into the Supply Headers for the two rings. Helium at 40 K, 15 bar is sent from the refrigerator to the Heat Shield Header.

The cold (4.5 K) helium gas which returns from the recoolers through the Return Headers will be collected and transported to the refrigerator low pressure return. In addition the Heat Shield Headers (70 K, 9 bar) combine and return to the refrigerator where it passes through an expander before joining the low-pressure return stream. Finally a cooldown return line is used during accelerator cooldown as well as during unusual operating scenarios, such as single sextant warmup.

These lines are located in a single 24 inch vacuum jacket. This line connects the refrigerator building to the two valve boxes at 6 o'clock. At the tunnel end of the line, connections will be made to the ring headers which also enter the 6 o'clock valve boxes.

Helium Vent System

A 6-inch vent stack and appropriate piping for each of the rings is provided to vent helium to the atmosphere near the end of each sextant. The stack is located at the service buildings which house the valve boxes. Relief and vent valves for the equipment in the ring are manifolded to this stack. These valves are located at the valve box. The exception to this rule includes the Magnet Circuit relief valve in each ring of every sector. These valves are located between Q6 and Q14. Their location was chosen to minimize pressure drop in the flow path to the relief valves induced by the 50 W recoolers during extreme venting conditions. These relief valves are piped to vent to the outside world.

The relief valve sizes and locations have been chosen so that the system complies with Section VIII of the ASME Pressure Vessel Code. For details, see Tech Note AD/RHIC/RD-64, "Pressure Relief for RHIC Cryogenic System," by K. C. Wu, December 1993. The size of the piping and the valves are based on studies of the magnet system venting rates during a loss of vacuum fault condition. This results in more stringent venting requirements than magnet quench scenarios. This system is designed for large temperature excursions because of the extremely cold gas which will be vented.

Ambient Ring Piping

A Warm Helium Header is provided to return lead flow helium gas to compressor suction. The main flow in this header will be the gas, which exits from the gas-cooled magnet power leads. Small relief valves will also be connected to this header. This header is continuous around the tunnel and is located overhead. During some lead fault conditions, etc., this line may be exposed to cold gas. Pipe supports and thermal expansion compensation are designed with this in mind.

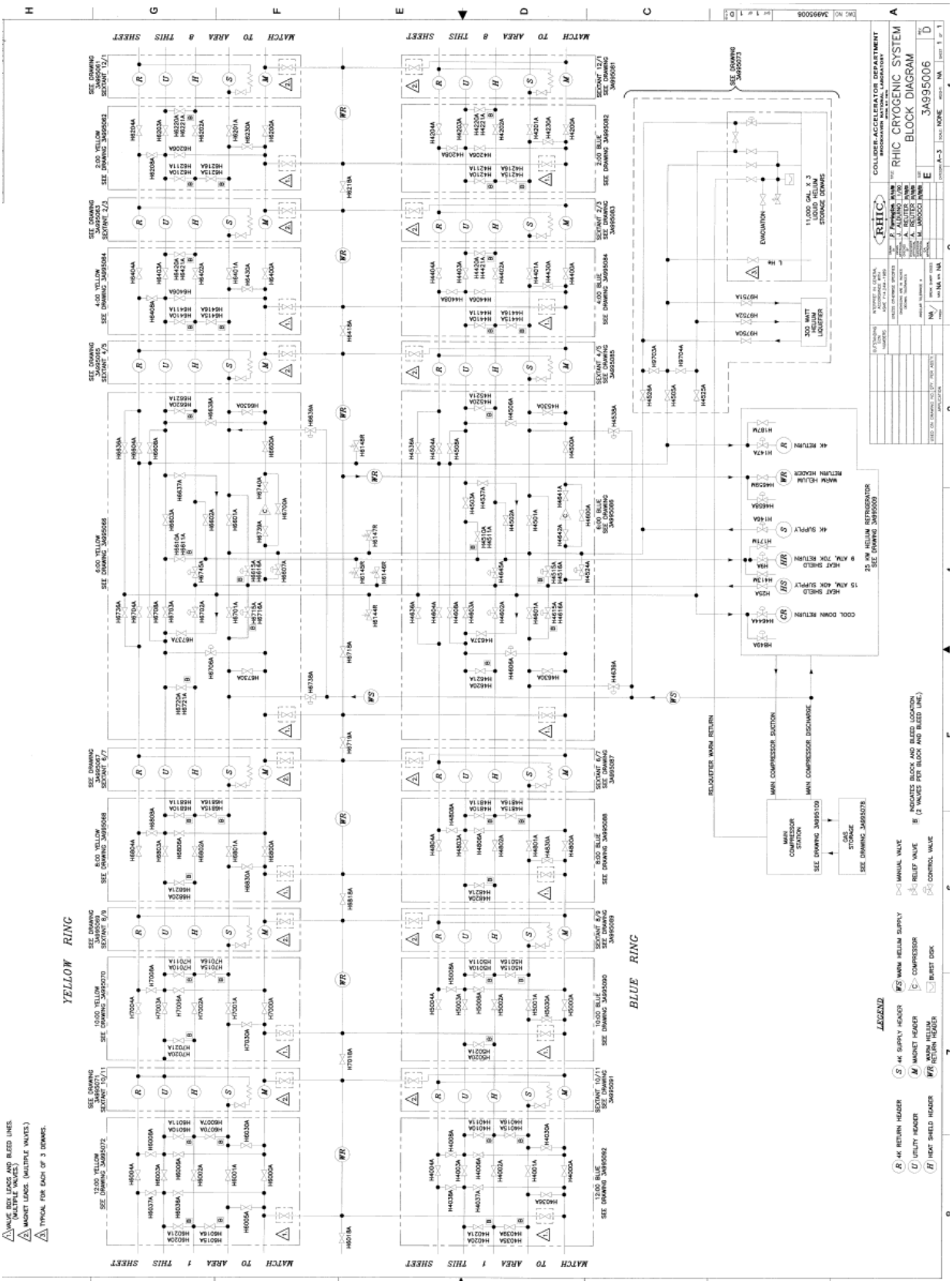

Fig.3-6. Overall System Block Diagram

80K Cooler and Reliquefier Refrigerator

A liquid nitrogen based refrigeration system has been installed near the 6 o'clock beam crossing region. Its primary purpose is to maintain the magnets and heat shield of the accelerator between 80 and 100K during shutdown periods, thus eliminating any stresses associated with thermal cycling. In this mode, Helium is cooled by heat exchange with boiling liquid Nitrogen then forced through the magnet and heat shield lines using three circulating pumps installed in the 80K Cooler cryostat.

The Cooler also has the ability to cool the accelerator from room temperature to 80K. Here, Helium from one of several compressors located throughout the RHIC cryogenic facility is refrigerated to liquid Nitrogen temperatures via pool boiling heat exchangers located in the Cooler, then routed through the ring magnets and heat shield via connections at the 6 o'clock valve box. The cooler has been integrated into the RHIC cryogenic system so as to allow the cooldown and maintenance of the accelerator to be completely independent of the main refrigerator and compressor operations. This allows for maintenance work and scrubbing of the RHIC main refrigerator and compressors while the 80K Cooler is in operations.

A 220 Watt Refrigerator has been installed in the 6 o'clock service building. It is designed to maintain liquid level in the three helium storage Dewars while the main refrigerator is not operating. As with the 80K Cooler this system runs entirely independent of the main refrigerator and compressors. Figure 3-6 describes the integration of the 80K Cooler and Reliquefier into the RHIC cryogenic system.

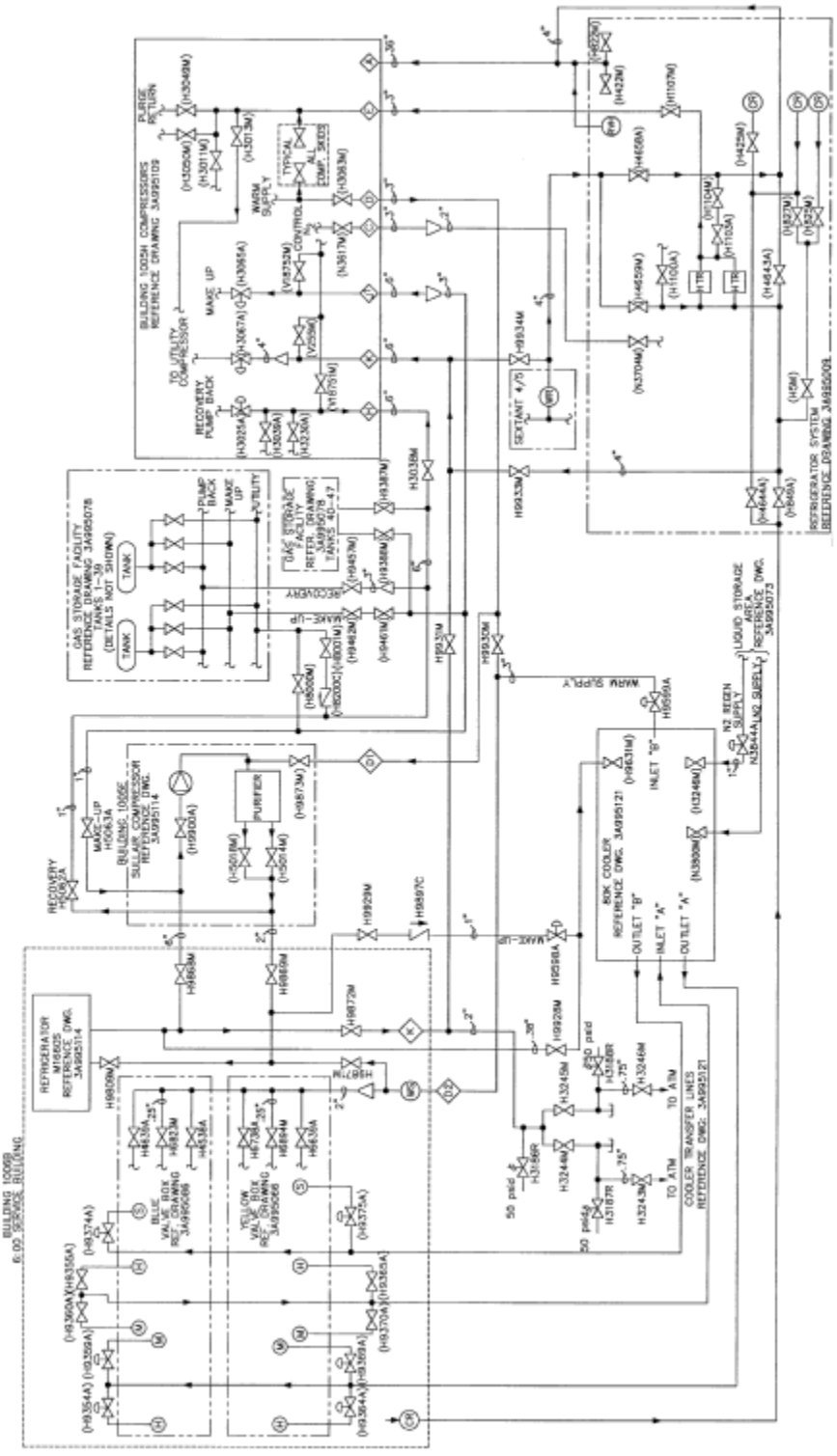

Fig 3-6: Reliquefier and 80K Cooler integration into RHIC cryogenic system

ix. Cryogenic Control System

A stand-alone process control system is required for the Cryogenic System. When desired this will permit operation of the Cryogenic System independent of the main RHIC control system. This may occur quite frequently during periods of cooldown and warmup.

The refrigerator and compressor control sub-system was designed, installed and in operation since 1984. It originally consisted of 3 PDP11® computers and Crisp® software running the refrigerator and compressors via an input/output (I/O) system. The I/O system interfaces a total of about 1700 points consisting of analog and digital input/output points, temperatures and PID loops. Through these points, the I/O system controls the cryogenic vacuum system, purifiers, compressors, refrigerator and gas management.

The current Cryogenic Control System design which also includes the Ring Control Sub-System, replaces the three PDP11® computers with two VAX® 4000/400 computers connected in a hot back-up configuration (Fig. 3-7). The system runs an updated version of the Crisp® Process Control Software in conjunction with a new PLC based I/O system. Included in the current design are multiple operator workstations in various locations running Crisp® Process Control Software. Any workstation can be used to generate or modify databases and programs or perform other functions such as historical trending and analysis and creating reports from the Crisp® system database.

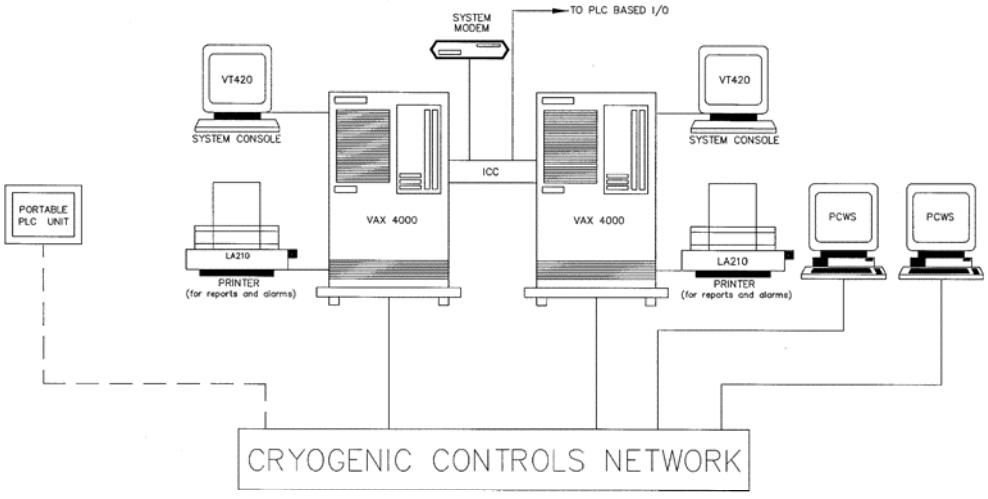

Fig. 3-7. Cryogenic Control System Layout

One of the most powerful tools of Crisp® software is the graphic system which provides the opportunity to create and modify standard and custom process graphic displays on-line without any programming required. Thus, hundreds of pages of graphic display of all cryogenic variables can be generated and linked to the database on the fly, without a glitch or interruption of operation of the process control system.

The dual VAX® computers are connected in a hot-backup configuration. While only one computer is in control, the other one is always updated of the activity of the first one. If the active computer fails, the inter computer communications (ICC) network (Fig. 3-7) which connects the two VAX® together automatically switches control to the backup computer. Since the backup system was continuously updated, the transition is totally smooth with no loss of information and no human intervention.

The Ring Control Sub-System consists of programmable logic controllers (PLC), located at each of the six experimental areas. They are connected to the cryogenic control room via the RHIC Cryogenic Controls network shown in Fig. 3-8. The 10/100 Ethernet switch in the 1005 Communications Hub room distributes the network to the six experimental areas and the B Alcoves. This switch is connected to a similar switch in the Cryogenic Control room that feeds three other switches. The four switches in the control room provide network connections for the dual VAX® 's, local workstations, the Refrigerator room and the Compressor room. Network monitoring and diagnostics are done on a dedicated PC. At each experimental area, the PLC processor manages all cryogenic signals via input/output (I/O) modules located in crates distributed along the RHIC tunnel, connected to the PLC via a local data highway running at a speed of 250 kbaud. There are about 8300 points around the ring to be monitored and controlled for a system total (including refrigerator and compressors) of almost 10000 points.

The ring remote I/O crate consists of a 19 inch rack mountable chassis with its own power supply, I/O scanner and as many I/O modules as needed. Some of the points to be controlled are: Mass flow controllers (MFC) used to control the flow of helium gas, which cools the superconducting magnet power leads. The MFC are located at the room temperature end of the power leads. Magnet current information is received by the VAX® via data transfer with the Main Control Room. The control program running on the VAX® determines the proper control point and this information is passed to the MFC through the PLC analog output module. Flow readback from the MFC is sent back to the VAX® via analog input module.

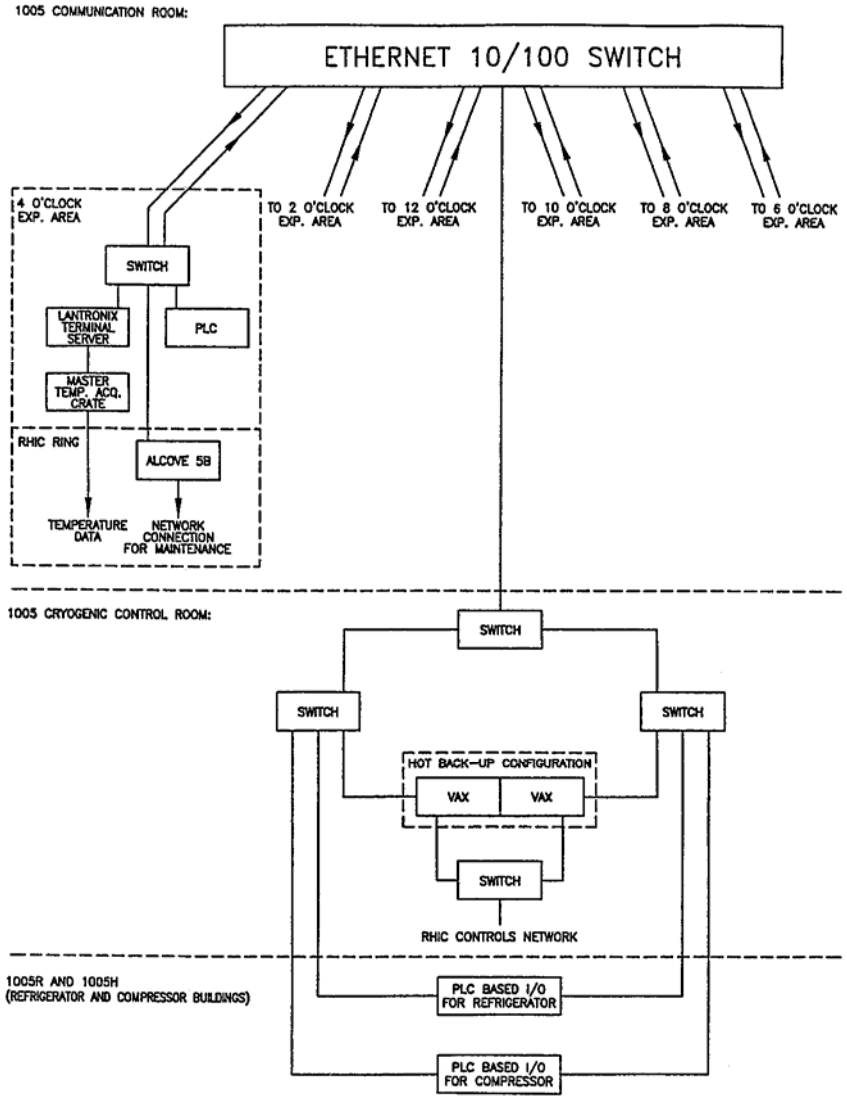

Fig. 3-8. Cryogenic Controls Network

The PLC is also programmed to control the helium liquid level in the recooler at a fixed level. This is achieved by reading the liquid level via analog input module and positioning the opening of the valve via analog output module to keep the liquid level constant.

The rest of the cryogenic signals controlled by the PLC via the I/O crates are pressure sensors and low flow indicators using thermistor resistors in the self-heating mode and cooled by the flow of helium gas.

The ring temperature acquisition crate[1] consists of a 19 inch rack mountable EUROCARD® chassis located in the same cabinet as the remote I/O crate. It is an in house designed multiplexed data acquisition system with an overall accuracy of ± 20 PPM, which translates into a temperature accuracy reading of less than 1mK for temperatures below 10 K. The system reads temperature of pre-calibrated transducers such as germanium, silicon diode, thermistor or platinum temperature sensors. Inside the temperature acquisition system, the raw data associated with these transducers is linearized by use of corresponding polynomial coefficients. The final result (a digitized analog reading) is shipped to the VAX® via a Lantronix terminal server over the RHIC Cryogenic Controls network as shown in Fig. 3-9.

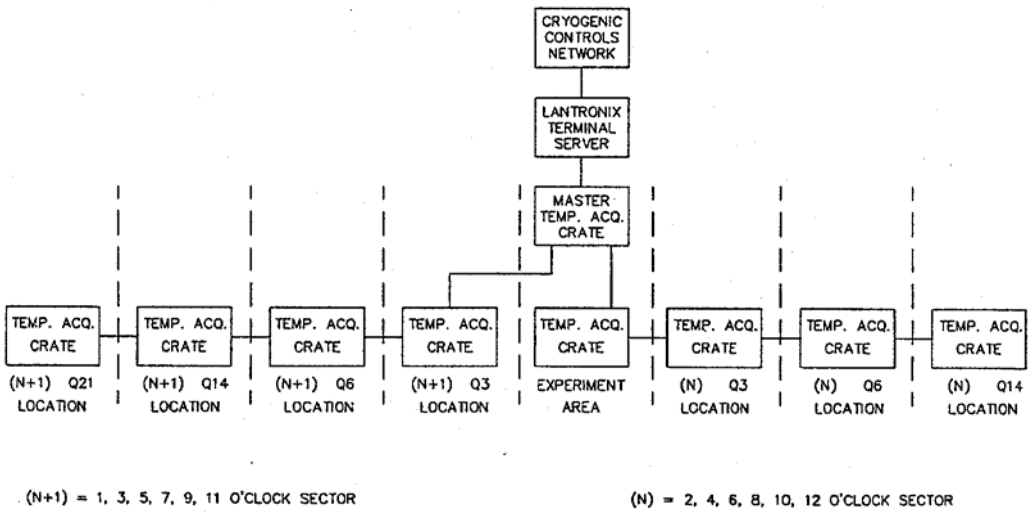

Fig. 3-9. Ring Temperature Acquisition System Layout

[1] Y. Farah, J. H. Sondericker, "A Precision Cryogenic Temperature Data Acquisition System", Advances in Cryogenic Engineering. Vol. 31 (Plenum Press, New York, 1985).

The temperature acquisition system used for the refrigerator and compressors is slightly different from that used in the ring. The temperature devices are wired to a LakeShore Model 218 temperature monitor, where the information can be read locally. Like the ring temperature acquisition system, a Lantronix terminal server is used to take information from the LakeShore device to the VAX® over the RHIC Cryogenic Controls network.

In the design of this system, a clear choice was made in favor of using many remote I/O crates (up to a maximum of 32) distributed along two tunnel sectors, thus minimizing the length of cables between transducers (points) and the electronics. This choice was driven by the low cost of the remote I/O crates in comparison to the cost of fire-retardant cables.

The PLC software is developed at the PC workstation in the Cryogenic Control room. A portable PLC unit complete with a remote I/O and temperature acquisition crates is attached to the PC workstation via the Ethernet hub (Fig. 3-7). This unit located next to the workstation is used to test the PLC software. Once the software is bug free, it is downloaded to the individual PLC in the experimental areas via the RHIC Cryogenic Controls network.

Communication between the CRISP® database in the VAX® computers and the PLC is done via CRISP® intelligent device interface (IDI) over the RHIC Cryogenic Controls network.

The state of the cryogenic system is needed for the operation of some of the components of the collider such as the power supply and the vacuum systems. Therefore, a communication link between the cryogenic and RHIC main computers is necessary. On the cryogenic side, a directory is created under VMS® operating system in which an ASCII input/output file is written. This file will contain all the necessary data to be shared between the two computers over the RHIC controls network. Under VMS® authorize utility, access to variables in the directory by either the main or cryogenic control systems is limited to predetermined status, control and interlock functions.

4. VACUUM SYSTEM

The RHIC vacuum system is divided into four regions: 1) the cold-bore UHV system, housed within the magnet bores and at the interconnects of the superconducting magnets; 2) the standard warm-bore systems residing between Q3-Q4 insertion regions; 3) the cryostat vacuum systems, serving as the insulating vacuum for the superconducting magnets, and 4) the experimental warm-bore regions, having their own unique vacuum materials and pressure requirements.

i. Beam Vacuum

The RHIC machine, must store two counter-rotating particle beams for periods of greater than ten hours. RHIC beams may comprise protons, gold ions (i.e., Au^{+79}), or a wide variety of heavy ions, colliding with each other. The intensity and emittance, and thus usefulness, of the particle beams are diminished when the stored particles are lost from their contrived orbits either due to charge exchange processes or through nuclear and Coulomb scattering with residual gas molecules. Equally important, particle beam collisions with residual gas in regions near the experimental detectors cause background noise in these detectors, and are therefore undesirable. For these reasons, a low operating pressure in the RHIC is very important. The RHIC rings, illustrated in Fig. 4-1, comprise two separate 3.8 km circumference rings. About sixteen percent of the life of each beam is spent in *warm*, RT (i.e., room temperature) sections of the rings; the remainder is spent in beam pipes operating at ~4.5 K (i.e., the *cold-bore*). An average pressure of 5×10^{-10} Torr ($2x10^{+7}$ molecules/cm^3) or less is required in the warm sections, with residual gases comprising 90% H_2, 5% CO and 5% CH_4. The pressure specification for beam components not baked in-situ such as kickers, septum and rf cavities is $\leq 2\times10^{-9}$ Torr, in the same gas species proportions as above. The requirement for the average total pressure of the cold-bore is $\leq10^{-11}$ Torr ($2x10^{+7}$ molecules/cm^3 after correcting for thermal transpiration) comprising exclusively H_2 and He. At this vacuum level, the emittance growth of a gold beam, at $\gamma = 10$, due to elastic scattering in the warm sections, will be $\sim 1\times10^{-4}$ mm mrad per hour, and $\sim 2\times10^{-4}$ mm mrad per hour in the cold-bore sections.

---

[1] M. J. Rhoades-Brown, M. Harrison, *Vacuum Requirements for RHIC*, Informal Report AD\RHIC-106,BNL #47070 December 1991.

The beam lifetimes due to central nuclear collisions of the gold beam with gas, is ~ 600 hours in the warm sections and ~ 240 hours in the cold sections.

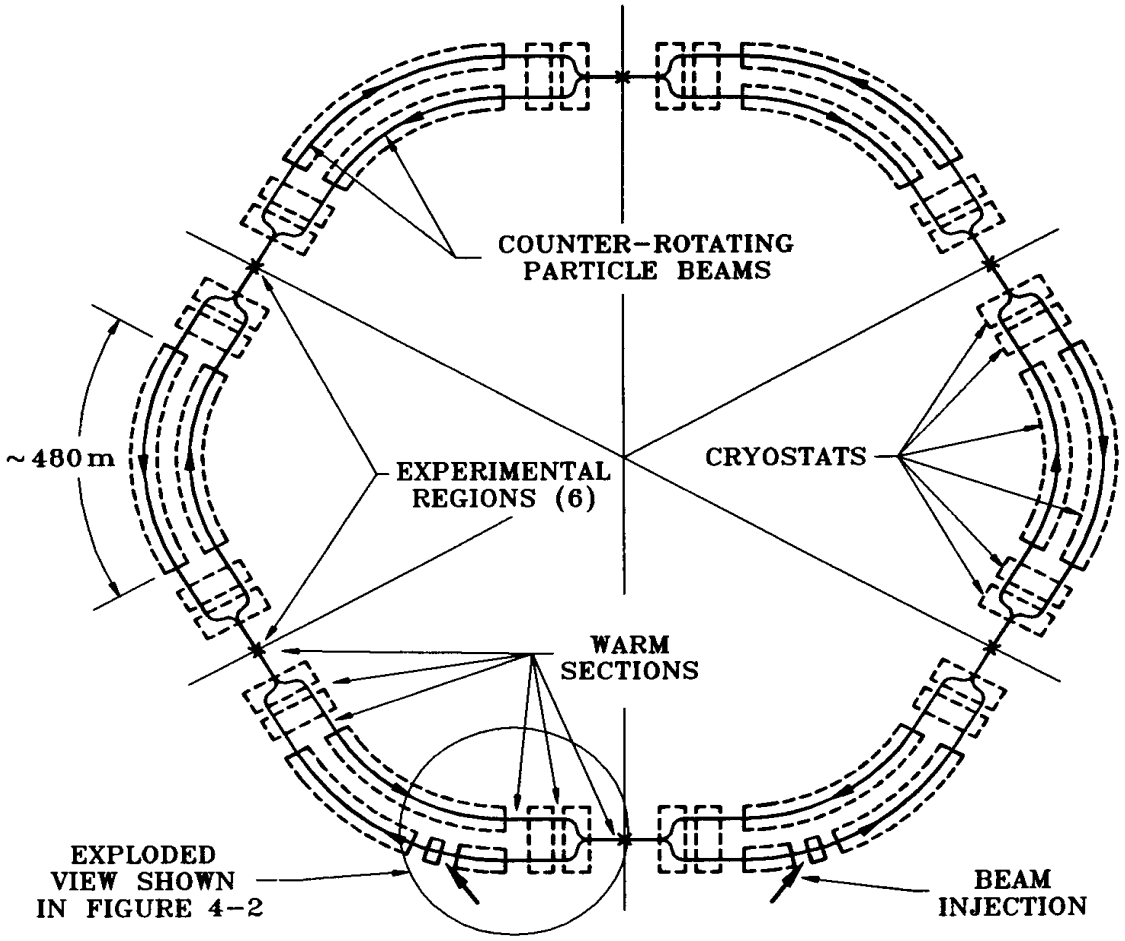

Fig. 4-1. The layout of RHIC vacuum systems.

ii. System Configuration

The total length of cold bore and insulating vacuum for both RHIC rings is ~6.4 km, divided into 12 arc sections and 24 triplet sections. Each 494m arc section consists of a continuous cryostat (without vacuum barriers), housing 64 super-conducting magnets interconnected to form a continuous cold beam tube. The two adjacent triplet magnet strings reside within a common cryostat due to their proximity. The total length of warm bore is approximately 1.2 km, making up roughly 16% of the RHIC circumference. It consists of the 24 Q3-Q4 insertion regions each 34m in length and located between each of the 494m arcs and the triplets, the 12 DX-D0 final focusing regions of 11m each (including the warm bore of the superconducting DX magnets) and the six interaction regions (called IR) of 17m each. There are also two short warm sections between Q7 and Q8 and between Q9 and D9 in each ring for injection lambertson and kicker magnets, respectively. Each warm section is isolatable from the adjacent cold bore sections with the RF-shielded all-metal gate valves mounted on the warm-to-cold transitions. Additional gate valves are also installed at some warm sections to isolate and protect special beam components, such as dump kickers, RF cavities and polarimeters. Figure 4-2 shows a vacuum hardware representation of one-twelfth of the entire ring, including the special beam injection sections at YO5 and BO6.

Warm-Bore Sections

Most warm sections have 12 cm φ beam pipes, made of 304L stainless steel. A list of various beam and diagnostic components residing in warm bore sections is given in Table 4-1. The warm sections are pumped by ion pumps and titanium sublimation pumps (TSP), and monitored with inverted magnetron type cold cathode gauges (CCG) at approximately 16 m interval. Partial pressure analyzers (PPA) are installed in selected warm bore sections, as listed in Table 4-2, to measure the residual gas compositions. Most warm sections are in-situ bake-able up to 250°C including the DX and DX-D0 beam pipes, and at somewhat lower temperature for the experimental region beam pipes. Most warm bore components have been degassed at 350°C in a vacuum furnace prior to installation. Due to the proximity of the IR detectors, the DX beam pipes and sections of the DX-D0 chambers were vacuum fired at 950°C prior to assembly. This reduces the hydrogen content, thus the outgassing and the background to the detectors. The warm sections typically reach vacuum of low 10^{-9} Torr a few weeks after pump down from atmosphere. To achieve the designed vacuum of low 10^{-10} Torr, most warm bore sections have been in-situ baked up to 250°C for 48 hours. In-situ bake is accomplished with custom heating blankets fitted around the pipes and other components, and monitored and controlled with integrated industrial temperature controllers. A local PC is used to down load the bakeout profile to the temperature controllers and to log the temperature data during bake. It usually takes 1-2 weeks, depending on the

complexity of the section, to set up the bake and one week to execute the bake. Pressure of low 10^{-11} Torr has been routinely achieved after a successful in-situ bake.

Pressure rise of a few decades have been observed at all warm bore regions during recent high intensity operations with shorter bunch spacing, resulted from beam induced desorption and electron cloud induced desorption. This pressure rise has caused high beam loss as well as high detector background. To study and combat the pressure rise, electron detectors and solenoids have been designed and installed at selective locations as given in Table 4-2. The electron detectors consist of an anode shielded by two repelling/retarding grid electrodes to allow the measurement of the electron energy spectra. The detector is well shielded by a screen from beam image current. The overall efficiency of the detectors is measured to be 7 ± 2%. The solenoids consist of gage #10 PVC or Kapton insulated wire spirally wound around the bean pipes with ~ 200 turns per meter. Commercial DC power supplies of 40V x 30A are used to power each 4m long solenoid resulted in a 2.7 gauss/amp axial field. This field will confine the electrons near the pipe surface on a spiral orbit of a few mm in radii without hitting the pipe surface, thus reduce the secondary electrons and multi-pacting. Non-Evaporable-Getter (NEG) coated beam pipes have been installed at standard 12 cm φ insertion regions, with a total length of 250m, ~ 50% of the possible length of 500m. The location and length of the NEG coated warm bore pipes are listed in Table 4-2. The low activation temperature Zr-V-Ti alloy NEG coating developed by CERN is applied to the pipe surface using magnetron sputtering, by a vendor licensed by CERN. NEG coated surface has lower secondary electron emission as compared with stainless steel surface, therefore increases the electron cloud threshold. If properly activated, NEG surface has very low electron stimulated desorption and provides very large linear pumping speed, thus further reduces the pressure rise.

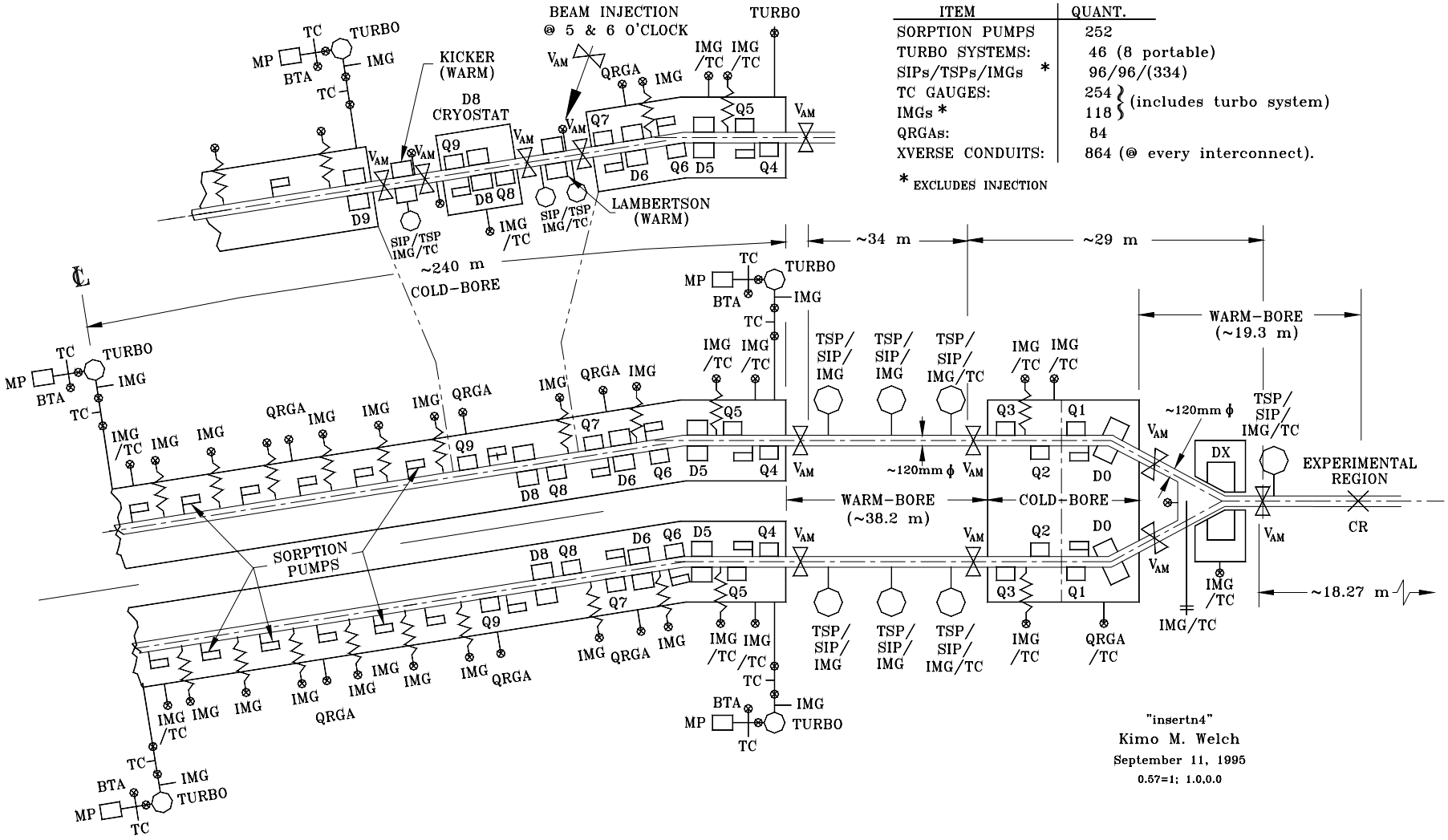

ITEM	QUANT.
SORPTION PUMPS	252
TURBO SYSTEMS:	46 (8 portable)
SIPs/TSPs/IMGs *	96/96/(334)
TC GAUGES:	254 (includes turbo system)
IMGs *	118 (includes turbo system)
QRGAs:	84
XVERSE CONDUITS:	864 (@ every interconnect).

* EXCLUDES INJECTION

Fig. 4-2. Vacuum instrumentation and pumping for one twelfth of RHIC machine.

Table 4-1. Locations of Warm Space Beam Components in RHIC Rings

Sector #	S(m)	L(m)
YO1		
Quad Pickup	40.00	0.25
PLL Kicker	40.63	1.00
Head-Tail Pickup	41.96	1.00
Pickup	42.58	0.25
PLL Kicker	43.21	1.00
Tune Kicker - H	45.15	2.00
Tune Kicker - H	47.15	2.00
Lum. Monitor	52.94	0.33
IPM - V	54.45	1.17
Roman Pot	56.66	0.51
Roman Pot	59.54	0.51
IPM - H	70.74	1.17
BI1		
Movable BPM(2)	40.91	0.38
Kicker	43.42	0.25
ANL Electron Detector	45.64	
TuneK-V+Gap Cleaning K.	52.26	2.00
TuneK-V+Gap Cleaning K.	54.26	2.00
YI2		
Movable BPM(2)	40.94	0.38
Kicker	43.45	0.25
TuneK-V+Gap Cleaning K.	52.16	2.00
TuneK-V+Gap Cleaning K.	54.16	2.00
Button BPM	66.88	0.50
WCM	67.63	1.00
DCCT	68.38	0.50
m Schottky	69.13	1.00

Sector #	S(m)	L(m)
BO2		
ANL Electron Det	39.57	
Quad Pickup	40.00	0.25
PLL Kicker	40.63	1.00
Head-Tail Pickup	41.96	1.00
Pickup	42.58	0.25
PLL Kicker	43.21	1.00
Tune Kicker - H	45.15	2.00
Tune Kicker - H	47.15	2.00
Lum. Monitor	52.94	0.33
IPM - V	54.45	1.17
Roman Pot	56.66	0.51
Roman Pot	59.54	0.51
Button BPM	66.88	0.50
WCM	67.63	1.00
DCCT	68.38	0.50
m Schottky	69.13	1.00
IPM - H	70.83	1.17
IR4		
AC Dipole	4.36	1.35
AC Dipole	2.86	1.35
AC Quad	1.14	1.56
WCM	0.00	0.50
Comm Cavities	5.43	0.74

Sector #	S(m)	L(m)
YO4		
WCM	40.30	0.50
Accel Cavity	46.69	2.93
Accel Cavity	49.93	2.93
Sto Cavities (3)	53.50	0.74
Landau Cavity	60.83	0.74
BPM	69.17	0.42
Cooling Pickup-LF	69.76	0.60
Cooling Kicker- HF	70.64	0.60
BPM	71.24	0.42
BI4		
WCM	38.98	0.50
Accel Cavity	41.42	2.93
Accel Cavity	44.66	2.93
Sto Cavities (3)	56.40	0.74
Landau Cavity	61.74	0.74
YO5		
Warm Dipoles	52, 55	0.6
Lambertson	121.90	
Injection Kickers	146.60	5.70
YI6		
Collimator - V	44.2	0.53
BO6		
Lambertson	121.90	
Injection Kickers	146.60	5.70

Sector #	S(m)	L(m)
YI7		
Collimator-H+V	41.32	0.53
Collimator - H	51.09	0.53
Collimator - V	57.26	0.53
Collimator - H	58.28	0.53
BI8		
Collimator-H+V	41.32	0.53
Collimator - H	51.09	0.53
Collimator - V	57.26	0.53
Collimator - H	58.28	0.53
YO9		
Dump Kicker	42.45	7.24
BPM	51.75	0.38
Dump	69.06	4.87
BO10		
Dump Kicker	42.45	7.24
BPM	51.75	0.38
Collimator - V	63.14	0.53
Dump	69.06	4.87
YI11		
Cooling Pickup	70.96	0.60
IR12		
Gas Jet	0.00	0.62
Shutter-1	6.23	0.07
Shutter-2	6.56	0.07
Shutter-2	6.89	0.07
YO12		
Polarimeter	70.68	1.60
BI12		
Polarimeter	71.19	1.60

S: distance to nearby IP **L:** chamber length

Table 4-2. Locations of RHIC NEG Coated Pipes, Solenoids, Electron Detectors, PPAs,….

NEG Coated Pipes

Sect #	L(m)	S(m) to IP
YO1	3.95	48 - 52
	1.7	57 - 59
	5.2	60 - 65
	4.05	66 - 70
YI2	1.23	39 - 40
	1.61	41 - 43
	5.2	44 - 49
	1.45	49 - 51
	4.93	56 - 61
	5.2	61 - 66
	1.9	70 - 72
BO2	3.95	48 - 52
	1.7	57 - 59
	5.2	61 - 66
YO4	5.2	62 - 67
	1.94	67 - 69
BI5	5.2	39 - 44
	3.1	44 - 47
	5.2	49 - 54
	5.2	54 - 59
YI6	4.14	39 - 43
	2.77	45 - 48
	5.2	49 - 54
	5.2	54 - 59
IP6	2.79	4 - 7
	2.79	4 - 7
BO7	5.2	39 - 44
	3.1	44 - 47
	5.2	49 - 54
	5.2	54 - 59

Sect #	L(m)	S(m) to IP
YO8	5.2	39 - 44
	3.1	44 - 47
	5.2	49 - 54
	5.2	54 - 59
BI8	1.24	39 - 40
	5.2	42 - 47
	1.78	48 - 50
	4.17	52 - 56
BI9	5.2	40 - 45
	5.2	45 - 50
	5.2	50 - 55
	5.2	56 - 61
	5.2	61 - 66
	5.2	66 - 71
BO10	3.41	59 - 62
YI10	5.2	40 - 45
	5.2	45 - 50
	5.2	50 - 55
	5.2	56 - 61
	5.2	61 - 66
	5.2	66 - 71
BO11	5.2	40 - 45
	5.2	45 - 50
	5.2	50 - 55
	5.2	56 - 61
	5.2	61 - 66
	5.2	66 - 71
IP12	5.2	2 - 7
	3.7	2 - 5

Solenoids

SL ADO	S(m) to IP	L(m)
yo1-sl-pw3.1	49.7	2.5
yo1-sl-pw3.2	65.6	2 + 2
bi1-sl-pw3.1	46.8	4
bi1-sl-pw3.2	69.0	4.2
yi2-sl-pw3.1	48.2	3 + 1
bo2-sl-pw3.1	50.3	3
g1-sl-pwx	5.3	2.3
g2-sl-pwx	5.3	2.3
yo4-sl-pw3.3	66.6	4.2
g9-sl-pwx	7.0	~1
g10-sl-pwx	7.0	~1
yo12-sl-pw3.1	50.0	2 + 2
bi12-sl-pw3.1.1	42.4	4
bi12-sl-pw3.1.2	48.1	3.2
bi12-sl-pw3.1.3	52.1	4
bi12-sl-pw3.2.1	58.1	4
bi12-sl-pw3.2.2	63.6	4
bi12-sl-pw3.2.3	67.8	3
g11-sl-pwx.2	3.4	4
g12-sl-pwx	3.5	3

Anti-Grazing Ridges

Sector #	S(m) to IP	ID(cm)
BI5, YO5	39.4	11
	44.5	10
	47.6	10
	53.8	10
	59	10

Electron Detectors

ED ADO	S(m) to IP
yo1-eld-pw3.1.v	48.3
yo1-eld-pw3.2-.v	65.6
bi1-eld-pw3.1.h	45.2
bi1-eld-pw3.1.v	45.4
bi1-ANL ED.h	45.6
bi1-eld-pw3.2.v	71.3
yi2-eld-pw3.1.v	49.3
bo2-ANL ED.v	39.6
bo2-eld-pw3.1.v	48.3
yo12-eld-pw3.1.v	49.9
bi12-eld-pw3.1.v	49.9
g12-eld-pwx.v	1.7
g12-eld-pwx.h	1.8

PPA

Sector #	S(m) to IP
G1, G2, G4	16.5
G5, G6, G7, G8	16.5
G12	7.6
BI1, YI2	55.6
YO4, BI4	60.0
YO9, BO10	58.6
YI10	55.4

H.C. Hseuh
10/15/2004

Cold-Bore Sections

The cold-bore comprises a seamless, austenitic stainless steel tube, extending beyond the end-plates of the magnets, to which it is welded and interconnected with formed rf-shielded bellows. No welded, brazed or bolted vacuum joints serve as barriers between superfluid helium and UHV environments. This is to eliminate the possibility of helium leaks from cold mass, through these joints into the cold bore. The leak rate of 4.5 K, 5 atm helium will be ~ 10^3 times greater than that of a RT 1atm gaseous helium, in terms of molecules per second, through the same leaky passage. The only other means whereby He can leak into the cold-bore UHV system is through metallurgical flaws in the seamless pipe or from the circumstance of gaseous He, in the cryostat insulating vacuum, leaking through a catastrophic failure in the interconnect piping or bellows. For these reasons, cryosorption pumps of activated charcoal are installed at magnet interconnects every 30m to pump helium (and hydrogen). The cold bore is monitored at 30m intervals with cold cathode gauges (CCGs) installed on the cryostat wall. Each CCG is connected to the cold bore through a 1.5m long 1" diameter gauge conduit thermally anchored at RT cryostat wall and at 55K heat shield, and terminated at a port on the rf-shielded bellows adaptor in magnet interconnects. The gauges provide a means of monitoring possible pressure rise in the cold-bore.

Prior to the magnet cool down, the cold bore is pumped down to ~10^{-3} Torr with a turbomolecular pump. After cool down to 4.5K, the CCGs read mid-10^{-10} Torr range when the true pressure, in the absence of helium, in the cold bore is <10^{-11}Torr. The high readings are due to the localized outgassing of the room temperature gauge conduits. The usefulness of the CCGs in monitoring the cold bore pressure was studied during RHIC first sextant test and found to be capable of detecting He pressure changes down to ~10^{-11} Torr.

Pressure rise of a few decades has been observed at a few locations in the cold bore during recent high intensity studies and thought to be caused by electron cloud induced desorption. The real gas density inside the cold bore during this pressure rise could be 10 – 100 times higher than that indicated by the RT CCG, due to the correction to thermal transpiration. Further studies of the relation between surface condensation during cool down and the pressure rise as well as heat load to the cold mass are needed to understand the impact of the cold bore pressure rise.

Cryostat Vacuum Systems

All gases in the cryostat insulating vacuum except helium are effectively pumped by the magnet cold masses. Helium leaking into the cryostats originate from two sources: 1) leaks in welds in the magnet cold mass or He interconnect plumbing; or 2) leaks from the He conduits or interconnecting

bellows running along the full length of the cryostats. To locate serious He leaks to within one magnet interconnect and to institute provisions for local pumping until repairs are implemented, a high conductance transverse vacuum conduit is used at every magnet interconnect to couple the interconnect region to pumping ports located on the magnet cryostats. Most of these ports are capped off with inexpensive manual valves. Initially, one turbopump is mounted at the center of each arc and triplet cryostat to maintain pressure prior to, and during cool down. There are a total of 28 turbopump stations permanently installed in the tunnel for the 28 insulating vacuum volumes. Each insulating volume has one or more cold cathode gauges to measure the pressure levels. Partial pressure analyzers (PPA) are also installed along the cryostats to distinguish air leaks from helium leaks after cool down. Helium pressure gradients, as measured with PPA and portable leak detector through the pumping ports, will facilitate longitudinal location of leaks stemming from interconnect plumbing or magnet cold-masses. Additional turbopumps may be installed to pump on particularly troublesome leaks. Permanent turbopump stations are installed at each of the twelve valve boxes to pump and maintain the insulating vacuum. No permanent pump stations are installed at one hundred plus Vacuum-Jacketed-Refrigerator (VJR) lines. They are pumped periodically with portable pumps before cool down and during operation.

iii. Instrumentation and Control System

The layout of the RHIC vacuum instrumentation and control is depicted in Fig. 4-3. The heart of the system is a network of Allen-Bradley programmable logic controllers (PLCs). There are eight vacuum PLCs, one each at the six ring service buildings and at the two AtR houses. Each PLC consists of a 520/540 CPU, several input and output (I/O) modules, and two sets of coprocessor modules. Each coprocessor set has four serial communication ports, which can be connected through the multi-drop RS-485 serial bus to the vacuum instruments (e.g., vacuum gauge controllers, ion pump controllers, etc.), located either in the service buildings or in the tunnel. Up to 32 instruments of the same protocol can be addressed and connected on the same RS-485 serial bus. Communication driver software is used by the coprocessor's OS-9 real time operating system to communicate with each type of instrument. The transaction time between the driver and each instrument is less than 30 milliseconds, and the total time to update each coprocessor's database is less than 10 sec.

The coprocessors interface with the RHIC control system front-end computers (FEC) located in the service buildings through the Ethernet links. The accelerator device object (ADO) code running in the FEC does most of the data processing before forwarding the information to the high-level application codes for control, display and logging. For faster display and logging, the analog outputs of a few selected vacuum gauges are fed directly into dedicated MADC channels for conversion. During startup or trouble-shooting, portable PCs using vendor-provided software can be connected to an RS-485 bus to operate and diagnose the vacuum instruments.

The RHIC vacuum systems are protected from catastrophic failures by beam vacuum gate valves, which are interlocked by vacuum gauges and sputter ion pumps. Gauges and pumps on both sides of the valves are used in a voting scheme that minimizes valve closure due to false triggering. The gate valves and the set point relay contacts of the gauge controllers are hardwired to the PLC I/O modules. Ladder-logic software in the PLC is used to open and close the gate valves and generates the beam permit link (BPL) signal, either by the FEC or through a man-machine interface (MMI). Valve status and control information is copied from the PLC to the coprocessor by means of data block transfers, and then exchanged with the FEC via the coprocessor Ethernet port. The MMI software runs independently from the PLC software and resides on a PC connected to the PLC Data Highway network that links all eight PLCs.

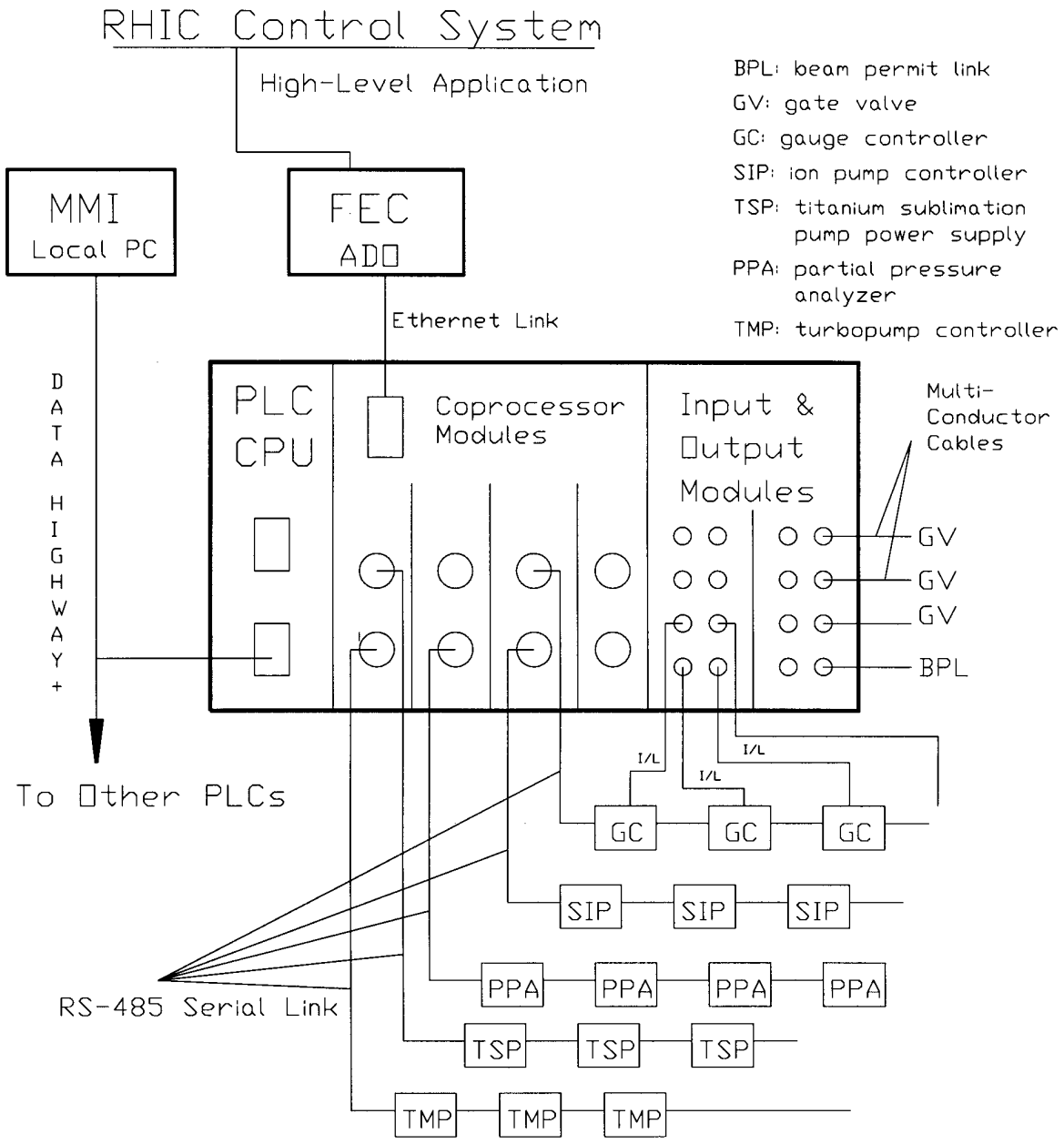

Fig. 4-3. Vacuum instrumentation and control block diagram.

iv. Experimental Vacuum Systems

Each experimental area as defined by the space between the beam pipe end flanges of the two DX magnets is 17.2 m in length. Each area, as shown in Fig. 4-4, is subtended by all-metal, rf-shielded gate valves, beam position monitors, bellows, sputter ion pumps and titanium sublimation pumps. The space available for the experimental beam pipes (EBPs) and detectors is approximately 14.2 m in length.

The beam pipes adjacent to the sputter ion pumps are RHIC standard 304L warm bore tubes with 12.7 cm OD x 3 mm wall and a 5:1 diameter transition down to 7.6 cm OD, followed by 7 cm ID rf-shielded bellows. To maximize the transparency for the experiments, the 1.5 m central sections of the EBPs for three experiments, STAR, PHENIX and BRAHMS, are made of beryllium (Be) with extensions made of either aluminum or stainless steel. The EBPs of PHOBOS consist of three 4m long Be pipes jointed together with Be flanges, bolts and nuts and aluminum gaskets. The outer diameter of Be sections for all four experiments is 7.6 cm and the nominal wall thickness 1 mm. The 7.4 cm ID of the EBP provides the required 10σ beam aperture (up to ± 5 m from IP) for all the RHIC operating conditions.

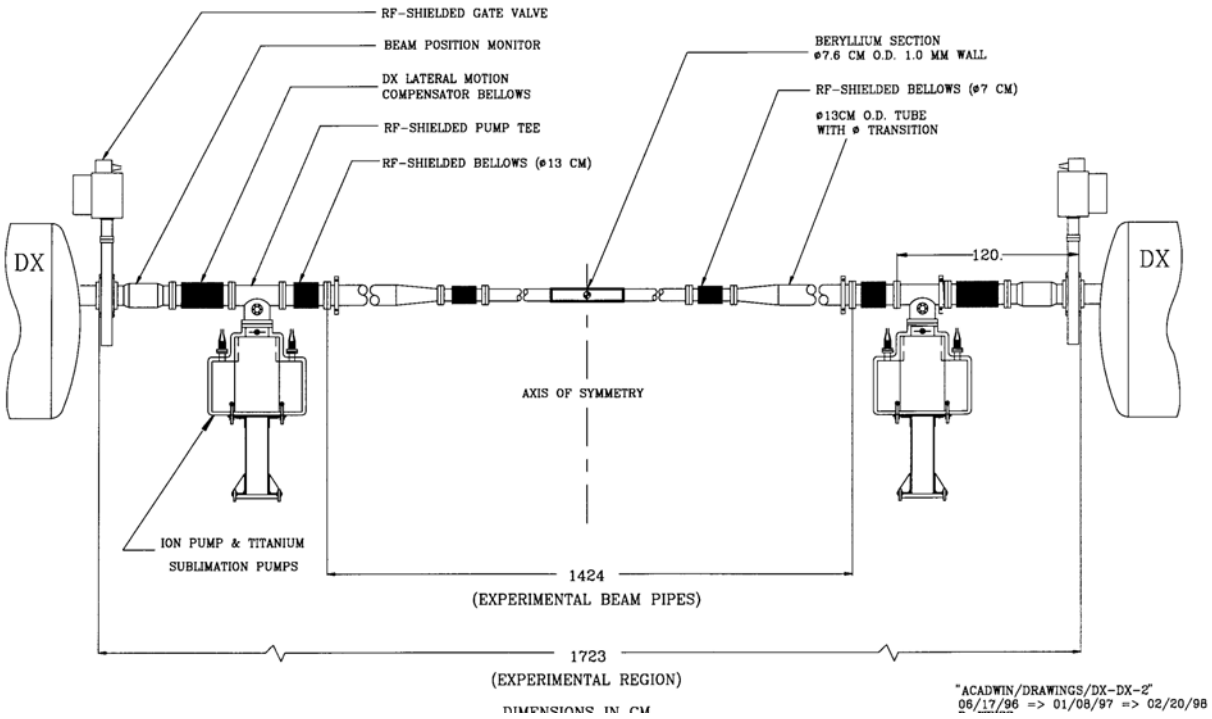

Fig. 4-4. Layout of the vacuum components at experimental regions.

Table 4-3. Experimental Beam Pipes

Experiment	EBP Length	Be Section	Extensions	Flange
STAR	8 m	1.5 m	A1uminum	A1/SS Conflat
PHENIX	5.2 m	1.5 m	Stainless Steel	SS Conflat
PHOBOS	12 m	3 × 4 m	None	Be Conflat
BRAHMS	7.1 m	1.5 m	A1uminum	A1/SS Conflat

The Be section is fabricated from Be sheet rolled into a tube with a longitudinal braze joint. The Be sections are brazed to stainless steel or aluminum extensions and then welded to the 12 cm OD Conflat flanges to form the complete EBPs. Table 4-3 lists the length of the EBPs, the length of the Be sections and the type of extensions and flanges for each experiment.

To achieve the design vacuum of low 10^{-10} Torr, the entire interaction region (from gate valve to gate valve) has been in-situ baked up to 250^{o}C (up to 150^{o}C for EBPs with aluminum extensions). In-situ bake is accomplished with custom heating blankets fitted around the EBPs and other vacuum components. In STAR where installation and removal of heating blankets is not possible after vacuum assembly, the EBP is only wrapped with three layers of 0.025mm thick Kapton foil as thermal insulation prior to installation into the detector. Heated dry nitrogen flow, from liquid nitrogen boil-off, is then used to bake the central section of the STAR EBP to approximately 100^{o} C for 24 hours, to remove surface water and other contaminants. The in-situ bake of EBP region is monitored and controlled with integrated industrial temperature controllers. Bake outs are usually completed in 2-3 weeks, including the time for set up and removal of heating jackets and bakeout equipment, ramp and soak periods and TSP and ion pump conditioning.

The average pressure inside the EBPs after in-situ bake can be approximated by:

$$P_{\text{avg}} = \pi \ \text{Dq} \left(\frac{\text{L}}{\text{S}} + \frac{\text{L}^2}{3\text{C}} \right)$$

with D the diameter of the EBP, q the unit outgassing rate, $2S$ the pumping speed (i.e., $S = 500$ l/s), $2L$ the distance between the pumps ($L = 775$ cm) and C the linear conductance ($\sim 2\text{x}10^4\ l$ .cm/sec for

H_2 and ~ $5x10^3$ *l*.cm/sec for CO of 7.4cm ID pipe). Therefore, the average pressure will be ~ 10 times higher than that indicated by the gauges located at the pumps. The outgassing rate of the EBPs is much below $1x10^{-12}$ Torr·*l* /sec·cm^2 after the in-situ bake, and average pressure of 10^{-11} Torr has been routinely achieved without beam.

Pressure rise of a few decades have been observed at all EBP regions during recent high intensity operations with shorter bunch spacing, resulted from beam induced desorption and electron cloud induced desorption. This pressure rise has caused high beam loss as well as high detector background. NEG coating of the EBPs is proposed to combat the pressure rise. NEG coated surface has lower secondary electron emission as compared with stainless, aluminum, and especially beryllium which has a peak SEY of 2.8, therefore increase the electron cloud threshold. If properly activated, NEG surface will also have very low electron stimulated desorption and provide very large linear pumping speed thus further reduce the pressure rise. The low activation temperature (~ 200^oC) Zr-V-Ti alloy NEG coating developed by CERN may be applied using magnetron sputtering. The small ID and the long length of the EBPs, as listed in Table 4-3, make the NEG coating rather challenging. The vendor for the NEG coating of the 12cm Φ insertion beam pipes can't handle beryllium and the potential residual radiation. Either in-house developed coating or CERN LHC coating facility may be used to coat these pipes. Development of a horizontal cathode coating facility for the EBPs is underway. A careful risk assessment is required if the EBPs are transported to CERN for coating. Proper activation of the NEG in EBP at the interaction regions also needs further development since both STAR and Brahms pipes have aluminum extensions and could not be heated safely in the installed position at higher than 100^o C and 150^o C, respectively. Methods of re-activation after saturation also need to be developed, since all the heating blankets in Phenix, Phobos and Brahms are removed after in-situ bake.

BEAM TRANSFER AND INJECTION SYSTEM (WBS 1.5)

i. Principal Characteristics and Parameters

The AGS will serve as the injector for RHIC. Filling RHIC initially with 56 bunches/ ring will take about two minutes per RHIC cycle of five hours or more. The reference orbit of the AGS has a circumference of 807.12 m and its rf harmonic number is 12. The circumference of each RHIC ring is 19/4 that of the AGS and its harmonic number during injection is 360, the spacing between RHIC rf bucket centers being one-sixth of that in the AGS. The AGS will accelerate a variable number of bunches per pulse (4 heavy-ion bunches with the present booster rf system), and park them on an extraction orbit when the extraction energy ($\gamma \approx 26 \times Z/A$, with Z and A the charge mass and numbers) is reached. These bunches will be less than 17 nsec long; proton bunches will be shorter if bunch rotation in the AGS is used. The distance between bucket centers is 224.4 nsec in the AGS and 35.5 nsec in RHIC. The invariant emittance will be $<20\pi$ mm mrad for protons and 10π mm mrad for heavier ions. The AGS bunches circulate until they are transferred to one of the two RHIC rings, where they are received in designated buckets.

Ring selection is accomplished by means of a switching magnet, which can be reversed on the order of 1 sec, thus allowing a choice of RHIC ring filling scenarios. The rings are filled one bucket at a time, but can be filled sequentially or interleaved. Filling the rings sequentially only requires the switcher magnet to be reversed after the first ring is filled, however this procedure results in the first ring having stored bunches that are older than those in the second ring, and which may have suffered emittance growth. Interleaved filling will allow injection of a small number of bunches, e.g. four, in one ring followed by an equal number in the other ring, the switcher magnet being reversed between AGS cycles.

Injection into the RHIC rings will occur in the 6 o'clock insertion. The insertion quadrupoles are set for $\beta^* = 10$ m during the filling operation in all insertions in order to provide sufficient aperture. The AGS extraction kicker works in the horizontal plane, RHIC's injection kicker in the vertical one. Filling the buckets one by one allows filling every sixth bucket, or any other pattern, depending on the rise time of the injection kickers. The luminosity is proportional to the number of filled buckets per ring. Allowing for the upgraded operation, i.e., filling every third RHIC bucket for a nominal 2×112 bunches, requires the kicker filling time, including time jitter in the switches and other inaccuracies, to be less than 95 nsec. This may be contrasted with the risetime required for the

AGS extraction kicker, which must be ≤207 nsec (always assuming bunch lengths ≤17 nsec). Results of transfer line measurements are reported elsewhere.[1]

[1] T. Satogata et al. "Physics of the AGS-to-RHIC Transfer Line Commissioning", proceedings of the European Particle Accelerator Conference 1996, Stockholm, Sweden (1996).

ii. Equipment

AGS extracted beam bunches pass through a transfer line in moving from AGS to RHIC, a layout of which appears as Fig. 5-1. The transfer line is called the ATR (AGS To RHIC) line, and begins downstream of AGS extraction which comprises the G10 Extraction Kicker and the H10 Extraction Septum. Before exiting the AGS vault, the beam undergoes a 4.25^{o} bend through two dipole magnets accompanied by three quadrupoles. The bunches then traverse a spur called the "U" line, which had been in operation for many years for the AGS neutrino program. The old "U" line has been dismantled, and all components have been either re-furbished or replaced for ATR operation.

An 8^{o} dispersion free bend comprised of four gradient dipoles connected in a modified triplet (FDDF) configuration is found in the "U" line. Prior to the 8° bend, a stripping station is located where the last two electrons are removed from the as yet not fully stripped heaviest species. The stripper can be retracted when it is not needed. Transport optics are designed to form a double waist at the foil to minimize the dilution in phase space of the beam caused by scattering in the foil and to compensate for the associated changes in emittance shape. This first section of the ATR will be shared, at least for the next few years of operation, with the g-2 AGS experiment, and optic components were chosen to accommodate the differing transport requirements. A pair of g-2 deflection magnets (VD3 and VD4) are located just upstream of the 8^{o} bend. Activation of the deflection magnet pair will direct beams to the g-2 target for the AGS experimental program; deactivation allows RHIC injection. Changeover from high intensity protons for g-2 to RHIC beams should be on the order of 1/2 hour for the beamline retuning. Six quadrupoles preceeding and four following the 8^{o} bend allow tuning capability to prepare the bunches for acceptance into the subsequent "W" line spur.

This next section of the beam transfer line, the "W" line, deflects the beam both horizontally and vertically, such that its axis at the entrance to the ring selector runs along the intersection of a horizontal plane, approximately 52 mm above RHIC's median plane, and the vertical plane through the machine center and the crossing point at 6 o'clock. This vertical plane is a plane of reflection symmetry: reflecting one ring and its beam transfer branch in it yields the other.

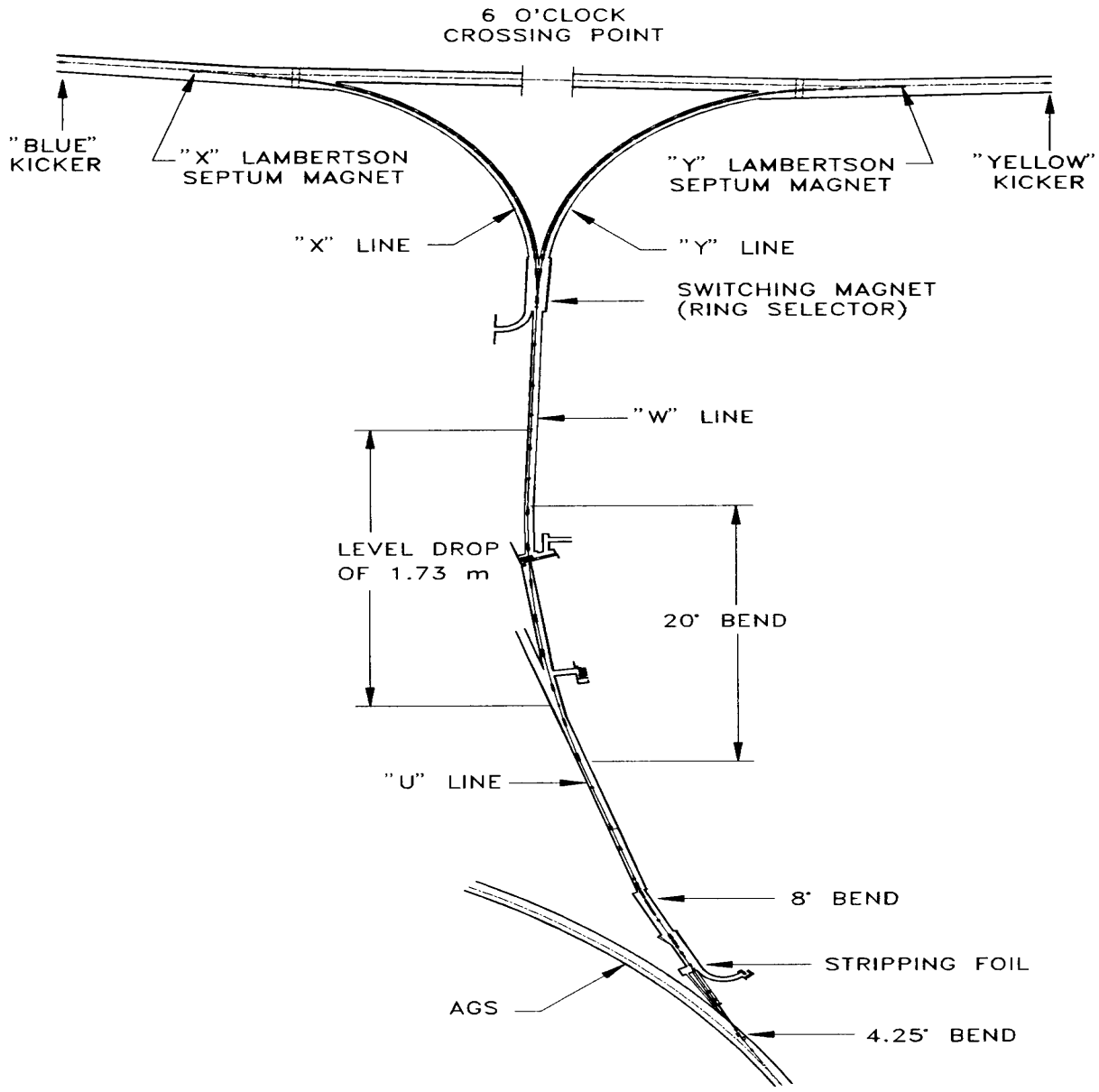

Fig. 5-1. Schematic layout of the AGS to RHIC (ATR) transfer line.

The horizontal deflection in this section is 20^o in an arc with an average radius of 405.82 m, the change in vertical level is approximately 1.73 m. The horizontal deflection and the change in level are entwined: the former is performed by a string of 8 gradient magnets in an AG focusing arrangement, the latter by a pair of vertical pitching dipoles, the first one of which is located between the second and third horizontal deflectors. The gradient magnets are each about 3.66 m long with field strength of about 1.19 T. They are separated from each other by drift spaces of 14.05 m. The second pitching dipole is placed between the second and third quadrupole of a string of six between the last horizontal deflector and the switching magnet (ring selector). These, together with the upstream quadrupoles in the "U" line, provide for flexibility in the choice of focusing parameters at the entrance of the ring selector. Between the second pitching magnet and the switching magnet, the beam line can be nominally free of horizontal and vertical dispersion ($X_p = X_{p'} = 0$ and $Y_p = Y_{p'} = 0$), thus ensuring reflection-symmetric behavior of the beam in the subsequent beam transfer branches into the two rings. The final drop in beam level over about 52 mm in the injection region leaves a small residual vertical dispersion in the circulating beam, thus increasing the vertical emittance by a small amount. This increase can be avoided altogether by resetting the system to compensate for that dispersion.

The next sections consist of the two reflection-symmetric branches, which begin at the entrance to the switching magnet and end in the injection halls. The switching magnet guides the beam via a dispersion match into one of these two "big bend" strings of 25 long plus 1 short gradient magnets, which carry the beam along arcs with average radii of 96.333 m and deflection angles of 48.15 mrad in each long gradient magnet. The gradient magnets in each big bend are arranged in a OFoFOODoDO pattern with horizontal and vertical betatron phase advances of about $\pi/2$ rad per cell.

Each big bend ends in its associated injection hall in the 6 o'clock insertion as shown in Fig. 5-2. There it is followed by a matching section, a string of four horizontally deflecting gradient magnets, one horizontally deflecting dipole, and six quadrupoles, which are excited to match the betatron functions and the dispersion functions of the transfer line to those of the RHIC lattice upstream of the RHIC quadrupole Q8O. The five bending magnets are each about 2.95 m long, and together deflect the beam through about 198 mrad. Three of the six quadrupoles for adjustment of the match between big bend and RHIC are imbedded into this string, the other three form a triplet at the end of the string.

Table 5-1. Injection Magnet Parameters

	Kicker	Septum
Deflection (mrad)	1.86	38
Strength (T·m) @ $B\rho$ = 100 T·m	0.186	3.8
Field (T)	0.044	0.95
Length (m)	4×1.12	4.0
Beam tube aperture, i.d. (mm), circulating beam	41.2	67.4
H×V (mm), incoming beam		63.5×26.1
Risetime (1 - 99%) (nsec)	95	
Flat top (nsec)	20	
Flat top tolerance	±1%	
Fall time (nsec)	800	

Injection occurs downstream of the last transfer line triplet, YQ4, YQ5 and YQ6 in Fig. 5-2. The injected beam lies in a plane vertically about 52 mm above the collider ring midplane. A vertical deflection (~3 mrad) is provided by the pitching dipole magnet (YP1), upstream of the septum, to direct the incident beam downward through the RHIC quadrupoles Q8O and Q9O, so that it will cross the RHIC reference orbit in the center of the injection kicker magnet located downstream of Q9O. The arrangement of the injection magnets is shown in Fig. 5-3 and their principal parameters are listed in Table 5-1.

An iron septum (Lambertson) magnet, bending 38 mrad horizontally, brings the incident beam axis into coincidence, horizontally, with the reference orbit in the outer arc. The iron septum of the Lambertson magnet separates the incident beam from the circulating one. In the region of the circulating beam, the stray field from the septum is held to less than 0.2 G by means of a soft-iron beam pipe, acting as a magnetic shield. The insertion CQS assemblies Q8O and Q7O will be shortened in this region by omitting the blank sextupole correctors, in order to allow sufficient space for the incoming beam to clear the ring components.

Leaving the septum the beam passes off-axis through the aperture of the vertically defocusing ring quadrupole Q8O, and the vertically focusing Q9O, and is finally bent into the

median plane by injection kickers KI1 - KI4. The four injection kicker modules provide a vertical deflection of 1.86 mrad, depositing the beam onto the RHIC orbit.

The Septum Magnet

The Iron Septum (Lambertson) Magnets are designed to horizontally deflect the injected beam onto a path parallel to the circulating beam. Two such magnets are used, each one injecting into one of the counter-circulating beams of the RHIC machine. The two magnets are identical magnetically, but are physically mirror images of each other. The Septum Magnet is the last element in the ATR beam transfer line and is electrically in series with the transfer line dipoles, thus saving the cost of a separate large power supply; a separate trim power supply is connected in parallel across the septum magnet to allow fine adjustment of the injection angle.

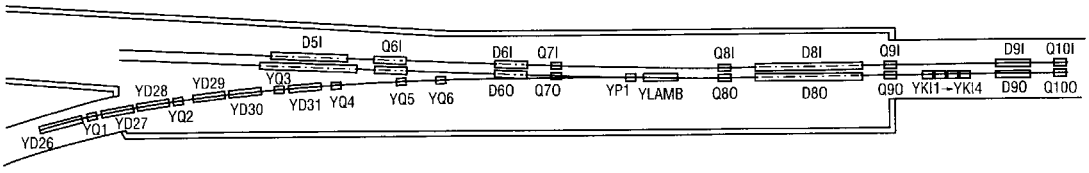

Fig. 5-2. Six o'clock insertion with location of yellow ring injection equipment.

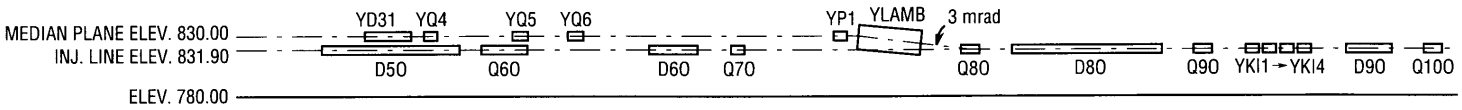

Fig. 5-3. Injection component layout/(elevation).

Table 5-2. Septum Magnet Parameters

Bend angle	38	mrad
Length	4	m
Magnetic field @ injected beam	9.5	kG
Field uniformity @ injected beam	$< 6\times10^{-4}$	
Stray fields @ circulating beam	< 0.2	G
H/V aperture @ injected beam	63.5×26.1	mm^2
Wall thickness @ injected beam tube	0.8	mm
Beam tube i.d. @ circulating beam	67.4	mm
Wall thickness @ circulating beam tube	1.3	mm
Septum thickness	10.8	mm
Vacuum requirement	$< 1\times10^{-10}$	mbar

The magnets are designed to achieve field uniformity of $\Delta B/B < 6\times10^{-4}$ over the width of the incident beam path and stray fields in RHIC's circulating beam pipe of less than 0.2 G at $B_o = 9.5$ kG transverse to the beam direction. In addition, the magnet is ultra-high vacuum compatible in that only the insides of the beam tubes are exposed to the vacuum and the entire assembly is bakeable in situ to 300 ^oC. The principal design parameters are listed in Table 5-2.

The relative location of the magnet with respect to the straight section Q7O - Q8O of the RHIC ring is shown in Fig. 5-4a (top view), 5-4b (side view), and 5-4c (view looking upstream). Figure 5-4a shows the injected beam at the entrance of the magnet, which will bend by ~38 mrad and will then continue at the exit of the magnet on the same vertical plane as the RHIC circulating beam.

The geometry of the magnet changes along the beam axis; one of the cross sections of the magnet is shown in Fig. 5-5 and corresponds to the middle of the magnet. A dimensioned view of the "Y" line injection area, indicating the Lambertson and ancillary devices, is presented in Fig. 5-6.

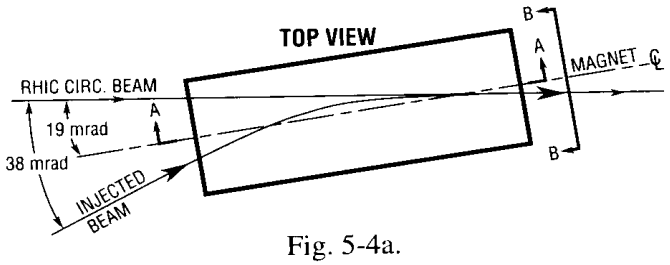

Fig. 5-4a.

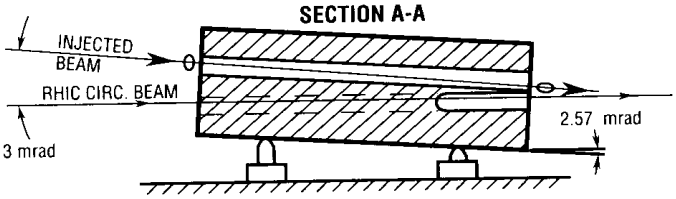

Fig. 5-4b.

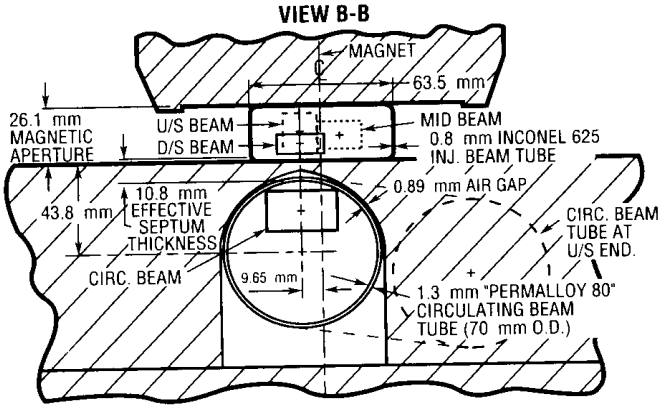

Fig. 5-4c.

Fig. 5-4. Septum Magnet.

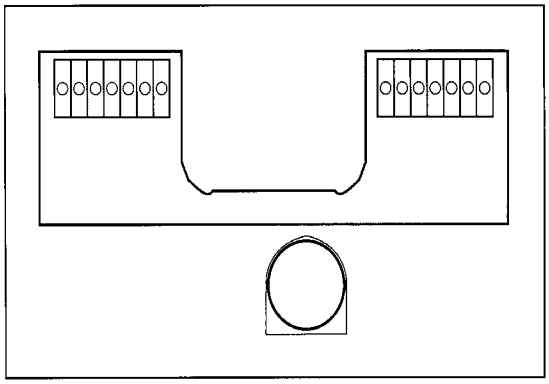

Fig. 5-5. Septum Magnet Cross Section.

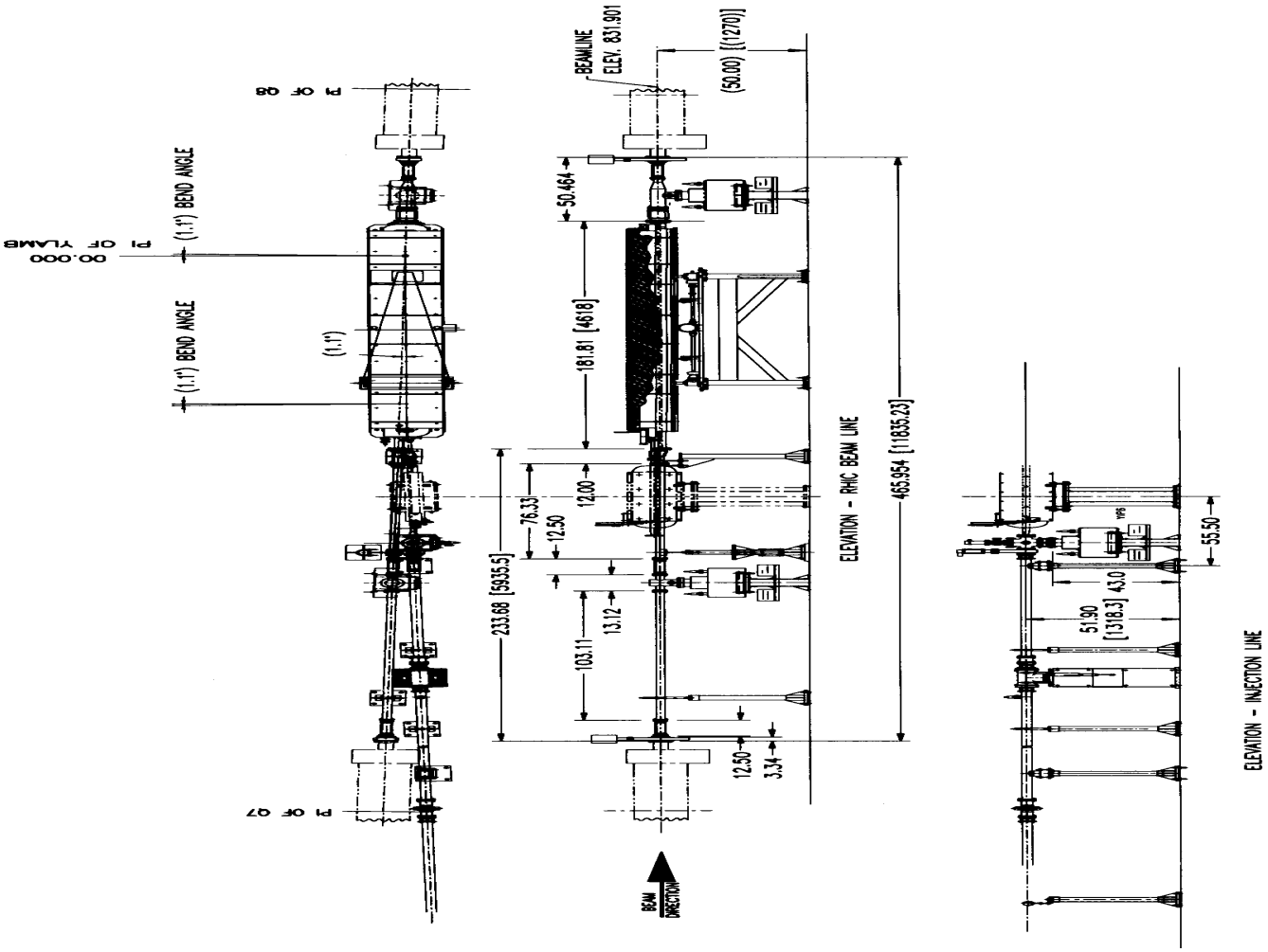

Fig. 5-6. "Y" line Lambertson injection area. (Brackets show dimensions in mm)

Steel Characteristics. Two and three-dimensional computer modeling showed that the design parameters could be met and exceeded by fabricating the magnet body out of an ultra-low carbon (< 0.005%) steel in the unannealed condition. The material (called "INTRAK") is available in large slabs and can be machined without significantly altering the magnetic properties.

Beam tube Materials. The material for the circulating beam tube is critical as it serves a number of functions. First, it must be ultra-high vacuum compatible, which means prefiring at a temperature of at least 950 ^{o}C in a vacuum of at least 1×10^{-5} mbar and should be corrosion-free like stainless steel. In addition, it serves a vital magnetic shielding function. The tube is spaced from the surrounding ultra-low carbon steel by a 1 mm air gap and intercepts leakage fields. For this function, it must have high permeability at low field levels. It must also have sufficient physical strength to resist the vacuum loads with a relatively thin wall. Finally, it helps if the thermal coefficient of expansion is close to that of the magnet body. A material called “Permalloy 80” meets all these conditions. To reach the required annealed condition, it must be heated to 1150 ^{o}C after fabrication. This also serves as the vacuum firing.

The injection tube material selected is Inconel 625. It is completely non-magnetic, has good vacuum and thermal expansion properties, and has high stiffness and yield strength to resist vacuum loading. Both the beam tubes are welded into the common stainless steel downstream chamber (see Fig. 5-7).

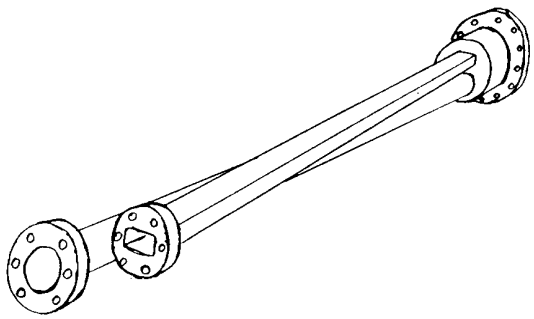

Fig. 5-7. Septum Magnet Vacuum Chamber.

Bakeout. Because of the difficulty of trying to heat the injection tube (which is in intimate contact with the poles) independently of the magnet, it was decided to heat the entire magnet. The coil is thermally insulated from the core and is water cooled during bakeout. A covering heater blanket of 20 kW heats the assembly to 250 ^{o}C in 12 hours.

Injection Kicker System

The purpose of the injection kicker is to provide the ultimate deflection to the incoming beam from the AGS into RHIC. The beam is kicked in the vertical direction to place it on the equilibrium orbit of RHIC. Each bunch in the AGS is transferred separately and stacked boxcar fashion in the appropriate RHIC rf bucket. In order to achieve the required deflection angle, four magnets powered by four pulsers will be used for each ring of RHIC. When the bunches are stacked in RHIC, the last few rf buckets are left unfilled in order to provide a gap in the beam to facilitate the ejection or beam abort process. This also means there is not a severe constraint on the fall-time of the injection kicker. The performance specifications for the kicker are given in Table 5-1. The performance is achieved using four Blumlein pulsers each connected to a magnet forming a matched transmission system. The pulsers will be located outside the RHIC tunnel and will be connected to the magnets by about 75 m of high voltage cable. An overview of the injection kicker system is shown in Fig. 5-8.

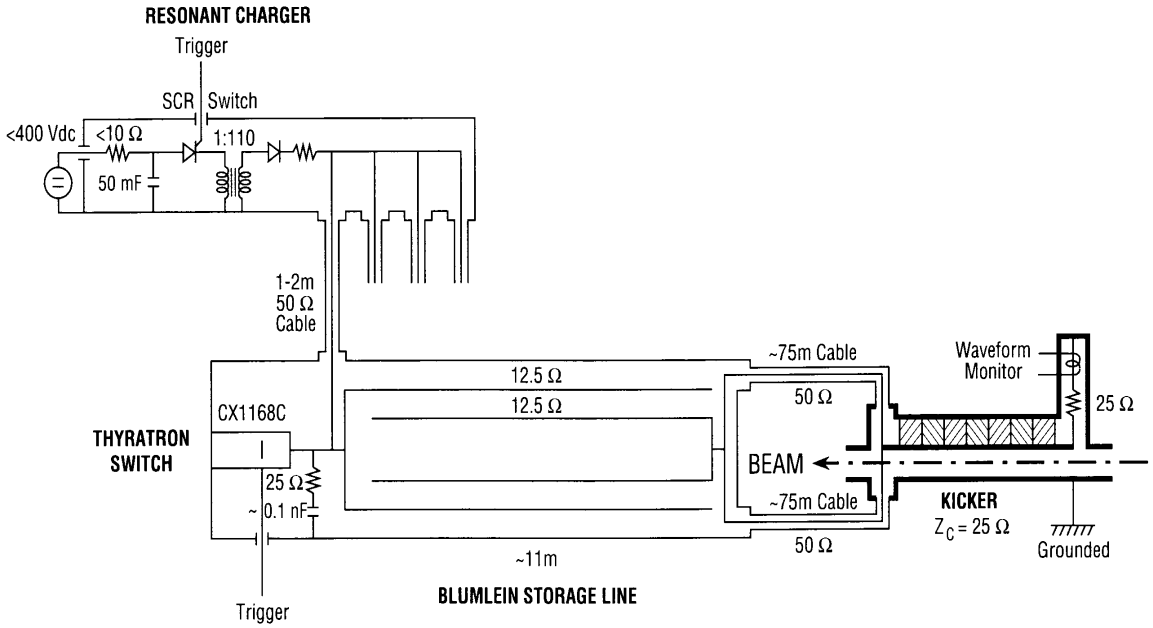

Fig. 5-8. Overview of the injection kicker system.

The Kicker Magnet. The magnet consists of a "C" cross section formed of ferrite bricks that approximates a transmission line as shown in Fig. 5-9. If properly oriented with respect to the beam, both the electric and magnetic fields can contribute additively to the deflecting force, although by far the largest contribution is made by the magnetic field. The characteristics are given in Table 5-3.

The injection kicker is constructed in two functional components, the core and the frame. The core represents and determines the magnet properties and the frame supports the magnet and provides the connection to the terminating resistor and the pulsed power supply. This concept was chosen to allow rapid replacement of damaged cores.

The magnet core is a structure of ferrite blocks and buss bar, solidly held together with epoxy. The ferrite blocks are produced to 50 μm accuracy. Prior to their incorporation into the core, the top ferrite blocks are high voltage tested for 2 ms to 50 kV and the side blocks to 40 kV. The blocks are Al_2O_3 bead blasted to roughen the surface for better epoxy adhesion and cleaned with ethanol and Zero-Tri. The sides of the blocks are primed with Conap-Primer AD1147 and baked to 70°C for 30 min. When ready for assembly, a 0.1 mm thick indium layer is attached with 3M Repositionable Adhesive 75 on the surface, which will contact the buss bar. Proper spacing of blocks is achieved by ~1mm thick, 2 mm ∅, insulating spacers, which are attached with a minimal amount of Loctite 454 Superglue.

The blocks are assembled together with the bus bar in a fixture and impregnated with epoxy. The high voltage capabilities depend completely on full contact between epoxy and ferrite surface and greatest care during the preparatory stages is mandatory. To assure separation of core and core-casting fixture, the latter is prepared by covering it with a thin layer of beeswax at 75°C. The core is formed with the epoxy, Conap RN-1000 and EA-87 hardener in a 100:37 ratio by weight. RN1000 has low viscosity, a long pot life below 22 ^{o}C and only 0.8% shrinkage during cure. The thoroughly mixed epoxy is slowly transferred into the fixture under vacuum, better than 1 Torr, to avoid the formation of bubbles. A gap of 0.7 mm between the bricks can be inspected during and after the pour to ensure no voids exist. After allowing the escape of gases formed during the solidification of epoxy, the fixture is pressurized and remains at 10 psi, typically till the next day.

Surface epoxy and other irregularities are ground off using diamond wheels on a flat milling machine. Prior to the final assembly of the core into the frame, a 0.1 mm thick indium layer is put on the top of the core. Good contact with the frame in order to avoid gaps and local field

enhancements is achieved by assembly under mechanical pressure and voids are filled with Dow-Corning Sylgard Silicone elastomere 184 mixed with hardener in a 10:1 ratio.

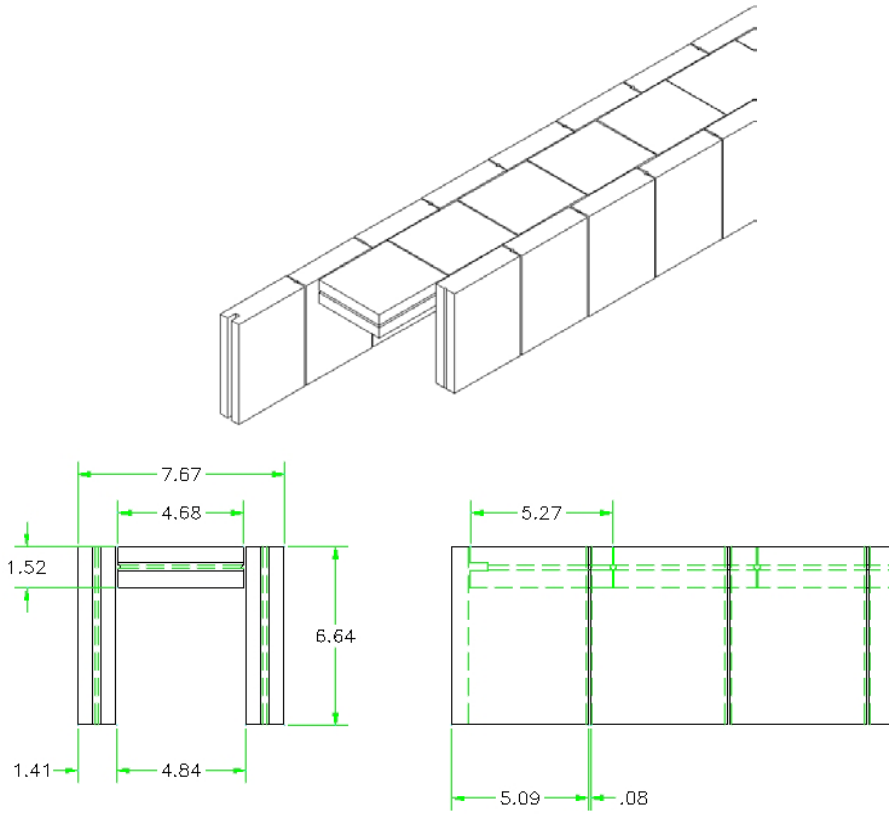

Fig. 5-9. All-ferrite core of RHIC injection kickers (dimensions in cm)

Table 5-3. Injection Kicker Magnet Characteristics (each)

Strength at 2000 A	0.0465	Tm
Number per ring	4	
Propagation time	45	ns
Impedance	~ 50	Ω
High frequency cut off	~ 25	MHz
Magnet aperture, width × height	48.4 mm × 51.2	mm
Magnet length	1.12	m
H field deflection	~94%	
E field deflection	~ 6%	
Ceramic beam tube, circular aperture	41.3	mm
wall thickness	3.2	mm
Min repetition period	33	ms
Life time	10^6	shots
Core material-ferrite,	Ceramic magnetic CMD 5005	
29 sections	50 mm long × 13.9 mm thick	
Bus bar/return frame	Aluminum 6061-T6	
Epoxy potting material	Conap Inc RN1000	

The magnet is designed to permit high temperature bakeout of the ceramic beam tube. For this procedure, the bottom plate shown in Fig. 5-10 is removed and the magnet elevated above the beam tube. The finite elements comprising the magnet result in a frequency cut off in the 25 MHz range: This increases the effective current risetime to about 40 ns. The combination of risetime and propagation time results in an integrated field risetime of about 95 ns.

The pulser. The Blumlein pulser consists of rigid, oil filled transmission lines in a folded, triaxial configuration of the type developed at SLAC. The major dimensions of the storage lines are given in Table 5-4. The triaxial delay line pipes are insulated with Teflon spacers and filled with Calumet Caltran 60-15 oil under slight positive pressure. The dielectric constant is 2.35. The delay lines are assembled from sections each about 2.4 m in length. The combination provides two delay lines of 12.5 Ω impedance, which feed a 25 Ω load, formed by the connecting cables (2×50 Ω in parallel), the magnet and a 25 Ω oil-filled hockey puck resistor assembly. The electrical properties of the Blumlein are shown in Table 5-4. The pulser is switched by a two-gap deuterium thyratron designed for high dI/dt applications (EEV type CX 1168C). An R-C network in parallel with the switch tube provides a small amount of overshoot in the current waveform, this improves the field risetime by a few nanoseconds.

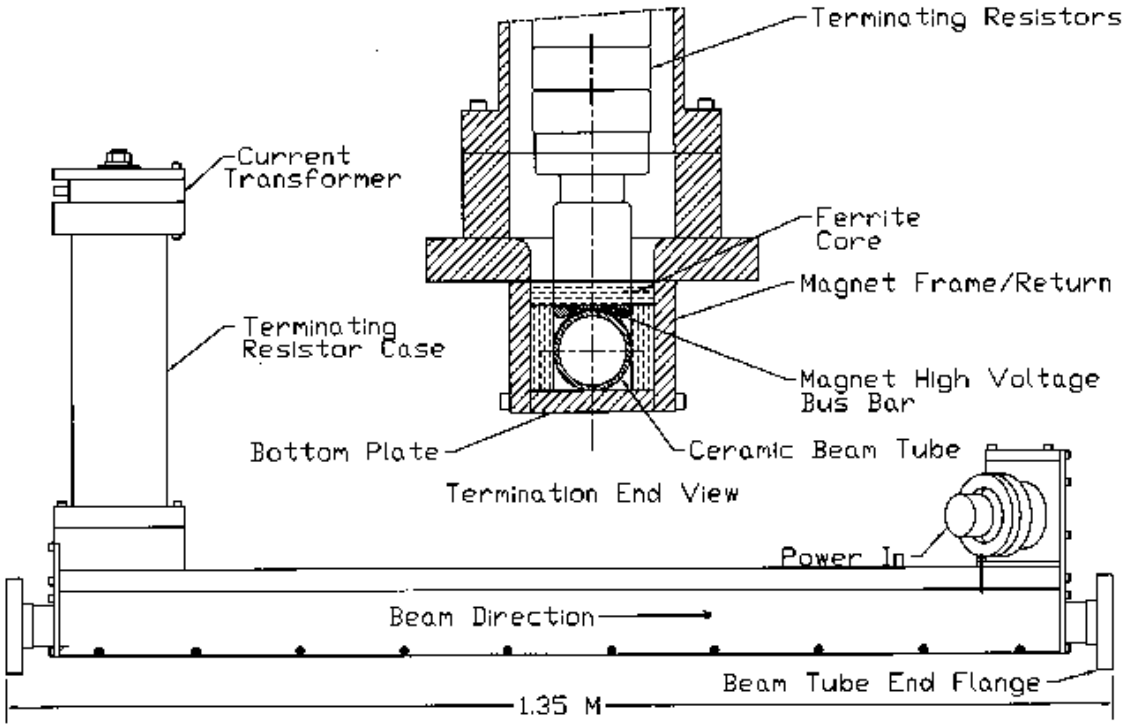

Fig. 5-10. General assembly of transmission line magnet.

Table 5-4. Blumlein Pulser Parameters

	Blumlein Dimensions	
Outer coaxial line	134.5 mm o.d.×98.0 mm i.d. ±0.1	mm
Inner coaxial line	76.2 o.d.×55.5 mm i.d. ± 0.1	mm
Length	10.95	m
Material	Aluminum 6061 - T6	
Insulating oil	Caltran 60-15	
Insulating Standoffs	PTFE Teflon	
	Blumlein Pulser Characteristics	
Load impedance	25	Ω
Two-way propagation time	110	ns
Operating voltage	50	kV
Operating load current	2000	A
Max voltage	60	kV
Current risetime	30	ns
Storage line capacitance	10	nF

iii. Operation

The mode of operation presented here is based on the assumption that the conditions in RHIC represent the standard of reference for all activities. In a setup procedure, RHIC is made ready for filling and then kept stationary in that state until it is filled. In most filling scenarios, with the exception of the switching magnet, all magnets in the ATR are excited and remain stationary. The ATR is designed to transport particles with rigidities up to 100 T·m. Both gold and proton beams are injected at the same rigidity. For transport of gold ions, the rigidity of the line upstream of the stripping foil must be increased by a factor of 79/77 compared to protons, since the charge state is increased when the foil strips the last two electrons. The ATR has a window of spin transparency for polarized protons at $\gamma = 26.75$ ($p = 25.38$ GeV/c) which is sufficiently above transition in RHIC ($\gamma_T = 22.89$).

When used for filling RHIC the AGS may accelerate trains of from 1 to 4 bunches. When the extraction field is reached, the beam is accelerated until the AGS circumference becomes 4/19-δ of the circumference of the injection orbit in RHIC (4/19 is the ratio between the circumferences of the reference orbits, δ is a small number). When the difference has become small enough, a phase-locking loop between the two rf systems takes over and locks the AGS rf frequency to the RHIC rf frequency. The phase is then shifted so that the bunch that is to be extracted from the AGS arrives in RHIC trailing the previous one by a predetermined number of RHIC buckets.

With its phase now as correct as it can be made to be, the bunch keeps circulating until its transfer to RHIC is initiated by excitation of the extraction and injection kickers. This is triggered by coincidence circuitry that produces a signal only when the last bunches of the bunch trains in each ring pass through specific azimuthal positions simultaneously. The waiting period may last up to 19 revolution periods in the AGS and up to 4 in RHIC, thus up to about 51 μsec, which time represents a `superperiod' in the AGS/RHIC cycle. The excitation of the extraction kicker in the AGS drives its last bunch into the transfer line, without disturbing the remaining ones. The extracted bunch finds the injection kicker in RHIC properly excited when it arrives there and becomes the last bunch of the train circulating in RHIC. The phase relationship between the last bunches in the two rings is now destroyed, since the new last bunch in the AGS is passing one AGS bucket spacing earlier than the previous one, while the next empty bucket in RHIC is passing three or, on day-one, six RHIC bucket spacings later than the previous one. That relationship must be restored before the next transfer can take place. The bunches in the AGS are shifted later in time by one AGS bucket spacing plus the appropriate number of RHIC bucket spacings by manipulation of the AGS rf frequency. This

adjustment requires a time interval of the order of 33 msec prior to the next bunch transfer, the recharging times of the kicker power supplies and aperture considerations in the AGS imposing a practical lower limit. A limit on extraction frequency has been set at 30 Hz by hardware considerations. The tolerance on the relative constancy of the guiding fields in the two rings during this process is of the same order as that on the relative synchronous energies, i.e., a few 10^{-5}.

When the AGS has been emptied of its bunches in this manner, it returns for repeated acceleration cycles until all but a few of 56 (later 112) rf buckets in RHIC are filled. The AGS cycle time is about 4 seconds, and 19 cycles of 4 ion bunches each would fill 60 RHIC buckets in one ring. In fact, a gap of about 1 μsec will be left in the circulating beam (omitting 4 of 60 bunches) to facilitate the rise of the RHIC beam dump kicker magnet system.

iv. Tolerances

Transfer of a beam from the AGS to a RHIC ring will in general affect its quality adversely. The deterioration may be the result of the mislocation of a bunch's center of charge relative to its intended synchronous fixed point in 6D phase space, or of a mismatch between the 6D emittance of a bunch and the lattice functions of the ring in which it is to circulate. Tolerances must be established to ensure that such deterioration can be kept within accepted bounds. Some of these tolerances can be relaxed if means are provided for error correction after injection. Dipole errors, i.e., errors in position or direction, and energy or phase, can be corrected to some extent by transverse or longitudinal dampers, which may also be needed to control of beam instabilities.* Normally such dampers are not particularly powerful, since they are intended for damping of coherent motion with very small amplitude. The required power is proportional to the square of the maximum error because the correction must be completed in a time that is small compared to the decoherence time of the error motion, and it turns out that even modest errors require considerable power.*

As far as pulsed magnets are concerned (kickers, septum magnets, orbit bumps), systematic pulse-to-pulse variations are assumed to be tolerable, provided that together they contribute less than 1 mm to the injection orbit error amplitude inside RHIC. The same overall maximum allowance is made for the contributions from all other dc dipole magnets in the transfer line combined. Assuming that about six such error terms from the pulsed systems contribute, that the errors are not correlated, and that vertical and horizontal deflections contribute in equal strength, one may specify that each component can contribute not more than $1/\sqrt{6}$ times the overall allowance. With this requirement, one obtains the systematic error budget for pulsed magnets which is listed in Table 5-2.

Systematic error contributions from other dc dipole magnets in the transfer line, of which there are many, are specified low enough so that together they contribute no more than what is allowed for the pulsed components.

---

* J. Rose et al, *The Conceptual Design of the RHIC rf System*, Report RHIC/RF-22 (1994).
S. Peggs et al, *Collective Instabilities in RHIC*, Report RHIC/AP 36 (1994).

Table 5-5. Parameters and Tolerances of Beam Transfer

	Beta m	Angle mrad	Tolerance % max
AGS Kicker	15	2	0.9
AGS H-10 Septum	15	22	0.09
AGS Orbit Bumps	22	2	0.8
Switch (X-Y)	54	48	0.02
RHIC Kicker	31	1.9	0.7

Random noise while the beam passes through each magnet, i.e. during a time interval of 20 nsec or less, is expected to enlarge the beam emittance incoherently, and it cannot be damped out. If one views this incoherent growth as being the result of mixing of Gaussian error probabilities with a basically Gaussian density distribution of the beam, one may prescribe a random noise tolerance for each component which keeps the overall emittance growth within acceptable bounds. For example, if the final invariant emittance of 10π mm mrad is to be the result of a dilution of no more than 10% (from 9 to 10π mm mrad), one obtains noise tolerances about 50% wider than the systematic tolerances given in Table 5-2. As a practical matter, only the fast kicker systems contribute sufficiently fast random noise to be of any concern, and the septum magnets and other pulsed systems, as well as the dc components, contribute totally negligible noise.

Similarly, quadrupole excitation errors in the transfer line will cause mismatches with respect to the RHIC lattice, which will lead to an effective enlargement of the beam emittance in the collider. Although this mismatch can be minimized by tuning the optics of the line, variations cannot be tracked and corrected from pulse to pulse. Quadrupole power supply tolerances are specified to ensure that the emittance variations from this source alone are unlikely to exceed a few percent.

The principal causes for dilution in longitudinal phase space are errors in the phase between bunch and bucket centers and mismatches between the synchronous energies in the AGS and RHIC.

With a difference between the synchronous energies smaller than $2 \cdot 10^{-4}$ and an error of in the rf phase of less than a few degrees, the longitudinal emittance blowup stays within 15%.

BEAM DUMP SYSTEM (WBS 1.6)

i. System Introduction

This description of the Beam Dump System was updated in October 2002. A few obsolete sections have been revised or corrected consistent with present knowledge and experience. The original sections described the future – the tense of the verbs has not changed in this revision. Add material describes the past and the present.

An internal beam abort system capable of absorbing the full energy heavy ion beam of the RHIC accelerator once per hour has been designed. The system will be comprised of 3 major subsystems, 1) the kicker magnets, 2) the pulsers and pulse forming networks (PFNs) and 3) the dump absorber. The beam abort systems will be located in the outer straight sections downstream of the 10 o'clock IP between Q3 and Q4 (see Fig. 6-1). In this configuration, the lattice parameters favor extraction in the horizontal plane. The kickers, actually composed of five modules, will be located at Q3 downstream of the crossing point. They will deflect the beam horizontally towards the ring center, onto the C-C absorber whose front face will be 23.5 m downstream from the midpoint of the kicker modules, and just upstream of Q4.

The energy stored in the beam will be about 200 kJ at top energy for all species assuming 60 bunches with nominal intensity, i.e. 10^9 in the case of gold beams. This energy is large enough to cause component damage if lost in an uncontrolled manner, but small enough to be disposed of in an internal beam dump system provided that the expected secondary particle spray from the dump absorber can be contained sufficiently well so as not to overheat and, thus, quench the superconducting magnets downstream. The stored beam energy can be disposed of within the constraints of the lattice without damage to the equipment provided that the materials in the dump absorber have been carefully chosen and the beam is dispersed over a sufficiently large area on the face of the dump absorber.

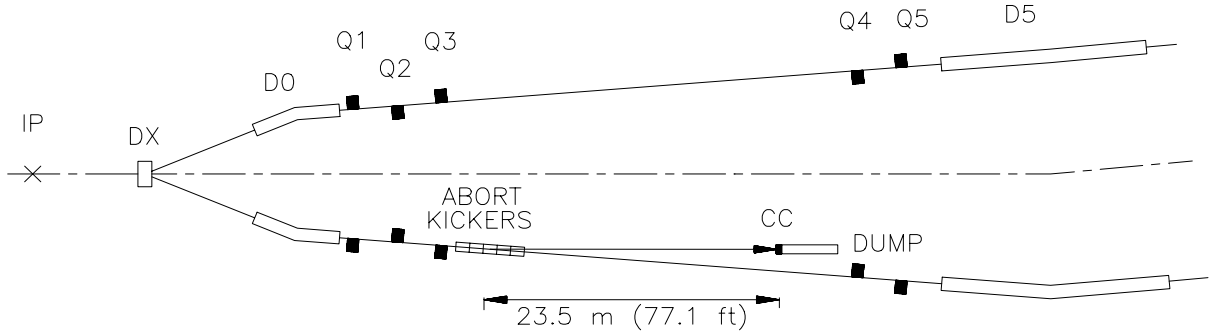

Fig. 6-1. Location of abort kickers and beam dump in the yellow ring at 10 o'clock.

The abort system will be used routinely to safely dump beam when the luminosity has declined to an unacceptable level or whenever deviations from normal operations are detected which may cause the beam to stray beyond a safe region within the vacuum chamber. The system response time will be sufficiently fast to begin safe extraction of the beam in all conceivable cases of accidents or beam instabilities within 4 turns (~52 μsec), and the beam will then be aborted within a single turn (~13 μsec). The 'as built' response time is slightly slower than originally planned. The pulse-forming system delivering the current pulse to the magnets requires approximately a 1–turn delay period to allow the charging supply to be disconnected from the pulse-forming network. The trigger synchronization requires up to another turn. These add to the originally planned delays for sensing fault conditions and transmitting that information to the abort system to begin the abort process. However, a few additional turns of delay do not affect the efficient functioning of the system.

The task will be to eject a small, potentially damaging beam which is traveling inside a larger "dump aperture," i.e. the phase space permitted by physical apertures in the collider. In the event of malfunction, when an incipient excursion toward a physical aperture is detected, the abort system will react quickly enough so that the beam has no chance to escape the dump aperture altogether. At the same time, however, control over the exact beam position or size will be already deteriorating. Therefore, not only the beam, but the entire dump aperture phase space must be transposed onto the dump absorber. This requirement determines the apertures of physical elements within the beam dump channel. The 18 m long beam tube between the five kicker modules and beam dump has the standard warm bore dimensions of 12.7 cm o.d. The layout of the dump components and their locations within the 10 o'clock tunnel structure are shown in Fig. 6-2.

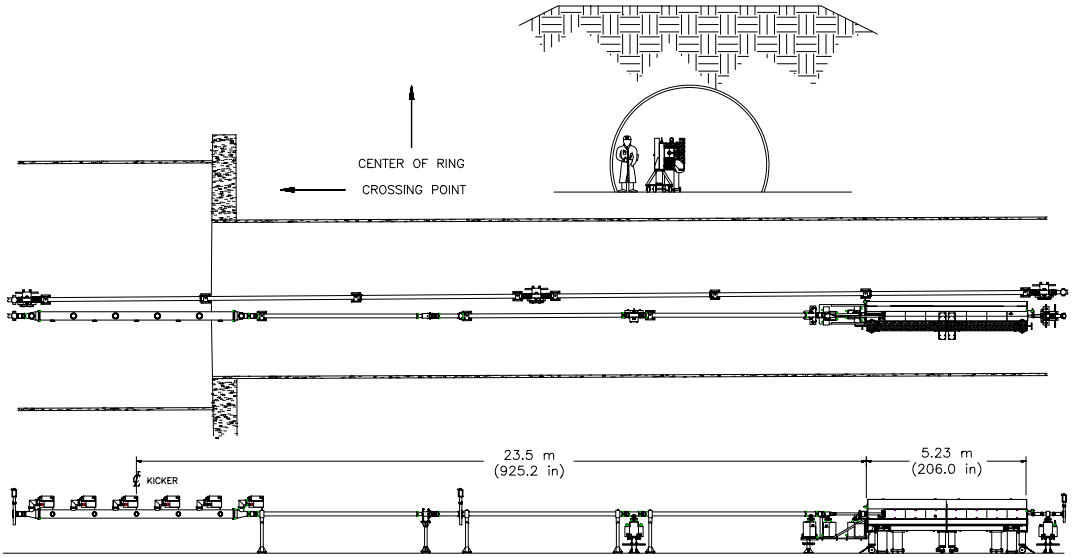

Fig. 6-2. Placement of beam dump components within Collider tunnel. Area shown is yellow ring at 10 o'clock.

In the RHIC rings, physical aperture requirements are determined at injection, with β*= 10 m at all crossing points, to accommodate a 6σ beam halo for gold beams, whose transverse emittance has been enlarged to 15π mm·mrad (from the nominal normalized 10π) by intrabeam scattering. The corresponding (un-normalized) dump aperture is ~7π mm.mrad. In practice, after establishing running conditions at top energy (where physical apertures exceed 10σ, even after intrabeam scattering has enlarged the emittance to 40π mm·mrad), a collimator will be inserted into the beam halo in each ring. A rapid increase in losses on these limiting aperture collimators is expected to be the most likely trigger for the abort system should malfunction occur.

The kicker system must operate over the range of energies from RHIC injection to the maximum energy of RHIC ($B\rho$ = 97.5 to 839.5 T.m). The nominal deflection angle required of the kicker system will be 1.6 mrad at all energies. The total magnetic length of the five kicker magnets is 6.10 m, which then requires a nominal magnetic field strength of 0.22 T in each magnet for the highest RHIC energies to ensure adequate deflection angle. In order to avoid uncontrolled beam loss in case of a single pulser or magnet failure, the kicker module will be built of five individual magnets, each with its own pulser. In the event of a failure to fire of a magnet or pulser, the 80% deflected beam (1.28 mrad) will still clear the limiting aperture of 17.75 mm in the dump and project onto an ellipse having a horizontal extent of ±11.3 mm on the face of the dump absorber. Because of the aspect ratio of the length to diameter dimensions of the structure, it is difficult to visualize the path of the circulating and ejected beams. Figure 6-3 shows this area schematically, with a normal longitudinal scale, but with transverse dimensions increased by a factor of 50. The horizontal beam envelopes of ±11.3 mm width are shown for both the nominal minimum and maximum kicker deflections as they impact the absorber face.

The anticipated failure mode mentioned above where one module fails to fire, which in part motivated the specification for the number of modules to be used, has not occurred in practice. The primary failure mode has been the "prefiring" of one of the five modules with the collider operating with fully loaded rings, at collision energy, and with the Beam Experiment detectors active. All five modules are charged to full voltage. One triggers "spontaneously" – i.e. without the occurrence of a properly timed trigger pulse. In this case the beam kick delivered by the one triggered module is not sufficient to remove the beam from the machine aperture cleanly. It is sufficient to cause the beam to be removed over many turns at limiting apertures around the machine. Most importantly significant beam loss may occur at the Beam Experiments causing damage to the experiment's beam detectors.

It is this mechanism and scenario rather than the quenching of magnets that has been the most significant negative impact of the abort system on RHIC operations.

A subsystem to reduce the impact of prefires is now part of the overall Beam Dump system. The current pulse sent to the magnet for each module is monitored. The signals from the five modules are combined in the ring and produce an additional set of triggers, which are then sent out to all of the modules. If one module prefires, the other four will be triggered within a microsecond. With this configuration active the beam loss at the Beam Experiments has been acceptable. Independent of this new system, other adjustments that fall within the original Beam Dump System description have greatly reduced the occurrence of prefires.

Diagnosing the prefire problem led to an expansion of the planned monitoring equipment for the Beam Dump system. The magnet current pulses from all five modules for both the Yellow and Blue rings are now "logged" – saved into computer memory – with a 10-nanosecond sample rate. A 50-microsecond window of data is collected by oscilloscopes triggered by a pulse occurring on one of the modules in each ring. Voltage waveforms for all of the pulse-forming networks are also logged continuously at the standard 720-Hertz rate.

The circumference of RHIC is 3833.8 m, resulting in a minimum pulse length for the kicker system of 12.8 μs. In order to facilitate the abort system design, a gap of ~1 μsec (corresponding to 4 missing bunches) will be provided. Thus, the kicker pulser and the pulse forming network must be designed with a rise time to achieve the nominal deflection of 1.6 mrad within this gap. After the initial rise, the excitation current will continue to rise by ~45% and oscillate for ~13 μsec, which will provide the necessary horizontal dispersion of the bunches on the face of the absorber.

A beam-based calibration of the strength of the beam dump kick verses PFN voltage was carried out early in the first year of operation. Using Beam Position Monitors in the drift downstream of the kicking magnets it was determined that the required 1.6 mradian kick occurs at the first "dip" in the current pulse (see PFN section below) for 100GeV gold at a PFN voltage of about 27.6 kV.

The timing of the kick relative to the abort gap is also set up by a beam-based procedure each running period after the reference "rev tick" on the beam-sync timing link has been established. The precision required of the kicker pulse timing increases as the abort gap is shortened. The most critical requirement of the timing is to start ramping only after the leading edge of the gap passes the dump kickers to avoid touching beam since the resulting gentle kick will result in beam scraping not in the absorber but rather elsewhere around the ring. The abort gap then has to last long enough to

insure that the first beam coming after the gap receives at least the 1.6 mradian kick. The ramping current get to the amplitude of the subsequent first dip (used for the calibration exercise) in approximately 1.1 microsecond.

The ion beams in RHIC will always be bunched, and as mentioned above, a gap of 1 μsec will be left in the circulating beam so that, in principle, the kicker will be able to rise to nominal field without imparting a partial deflection to some of the beam during the risetime. Even a small amount of partially deflected beam has the potential to quench one of the high β quadrupoles. This "empty gap" concept is partially invalidated by Au ions, which leave their rf buckets and "leak" into the gap.

"Gap cleaning" – the removal of any beam that does manage to leak into the abort gap – has been accomplished by exciting a coherent transverse betatron oscillation for the beam within the abort gap driving this beam out of the machine aperture. Sufficient amplitude is achieved by applying repeated kicks generated by a kicker system independent of the Beam Dump system that are resonant with the beam's betatron frequency. The gap cleaning machinery is active throughout the period when the beams are in collision.

As mentioned above, the beam dump kicker must disperse the beam bunches on the face of the dump absorber to preserve the integrity of the dump material. The worst case will be the ejection of the Au beam immediately after acceleration. In contrast to the situation with proton beams, the energy density will be highest at the dump entrance due to the Z^2 dependence of dE/dx. Dynamic stress analysis showed that the dispersal achievable by the kickers was not sufficient to insure that a dump window would not crack due to thermal shock at the design intensity in worst-case conditions. For this reason, it was decided to forego a window design by making the first element of the dump absorber a stress resistant graphite composite known as carbon-carbon (C-C), placed inside the vacuum chamber. This material is designed for Tokamak walls and missile tips, and is essentially impervious to thermal shock.

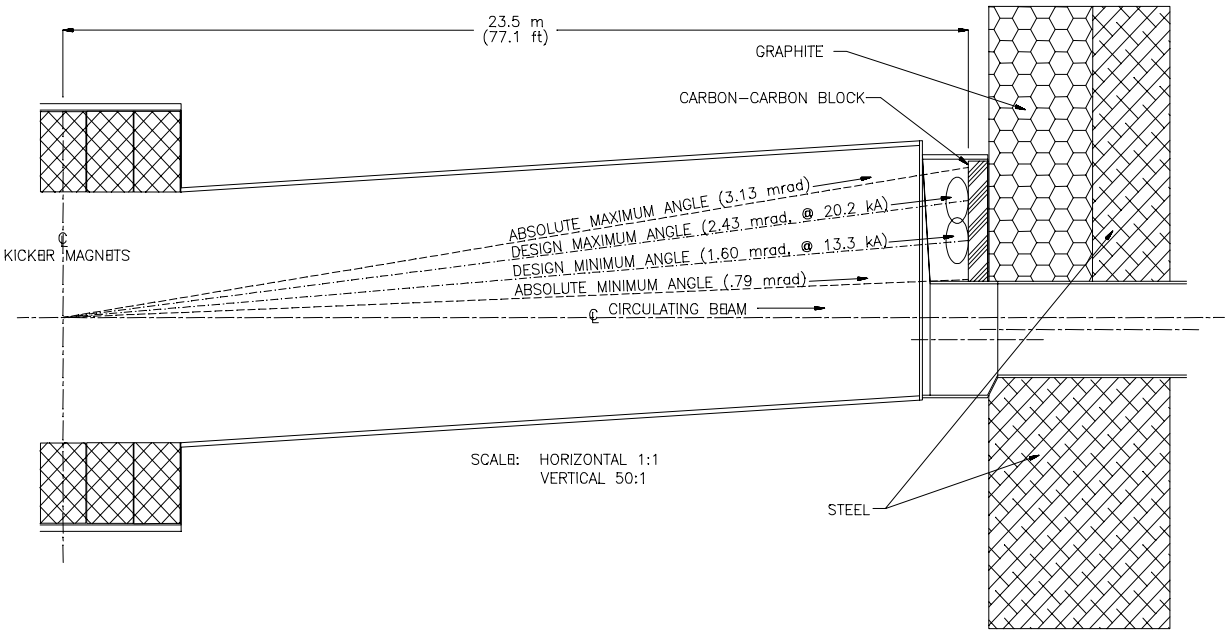

Fig. 6-3. Exaggerated plan view of dump geometry showing beam spots corresponding to acceptance aperture on dump face.

A diagram of the dump proper is shown in Fig. 6-4. As shown, the first element encountered by the extracted beam will be the C-C block, then the vacuum window, ordinary graphite and steel. Since the C-C block out-gasses to some extent, sputter-ion vacuum pumps must be employed to keep the vacuum in the ring sufficiently low. Estimates of the thermal stresses in the various materials of the dump give an adequate margin of safety against cracking and erosion of the C-C material at the design intensity.

Also shown in Fig. 6-4 is the aperture of the dump. At full energy, the circulating beam center line will be displaced horizontally from the physical center of the dump beam tube, so that the ring aperture at the dump is limited to 16.5 mm. This distance corresponds to the 6σ referred to previously. At injection energy, where apertures are tightest, a horizontal orbit bump can displace the beam center line to the physical center of the dump aperture which will then yield over 8.5σ at this location.

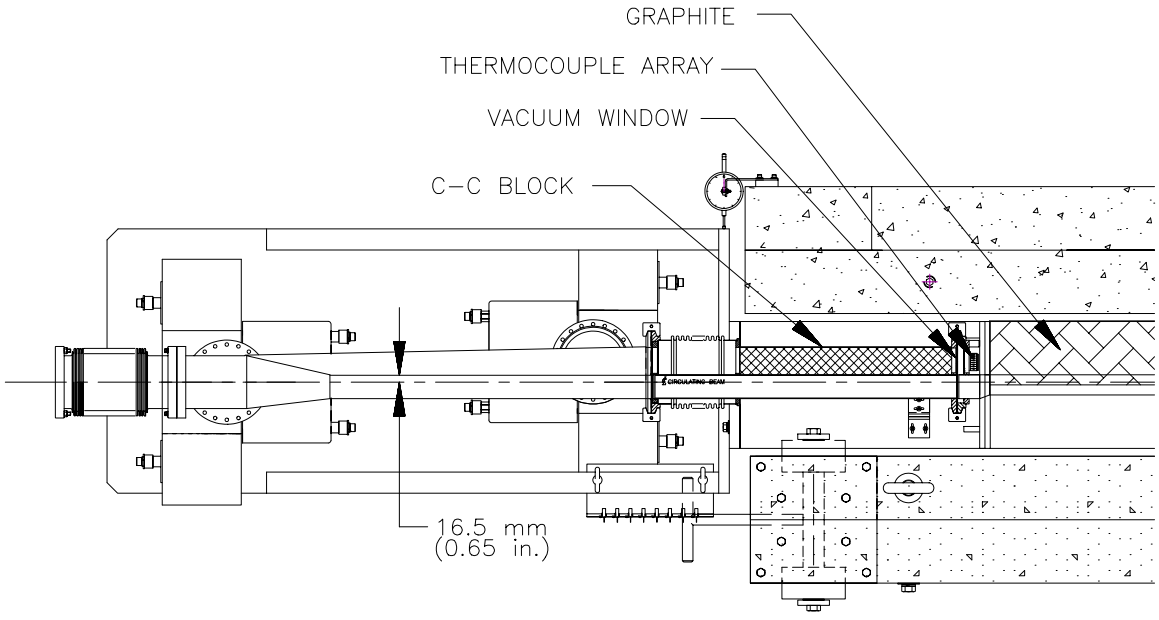

Fig. 6-4. Beam dump absorber details.

Although the dump design described here has a significant margin of safety at the design intensity, it is not clear whether the current design will be adequate for substantially upgraded beam intensities, especially as regards energy deposition in Q4 from secondaries emerging from the dump. Possible upgrades to the internal dump would include vertically deflecting sweeping magnets to increase dispersion of the bunches and a special Q4 magnet with a "liner." Nothing in the current system precludes a future upgrade to a full extraction system to an external dump. Such a system would require a stronger kicker system, the addition of a septum magnet system in place of the current internal dump, and a special Q4 cryostat containing an aperture through which the beam could pass en route to an external dump.

ii. Kicker Magnet Requirements and Design

A series of five H-core magnets constructed of Ceramics Magnetics CMD5005 ferrite will be employed in each of the RHIC abort kicker modules. Details of a single magnet assembly are shown in Fig. 6-5 The aperture of the magnets will be 50.8 mm horizontal ×76.2 mm vertical (2×3 in.) as shown in Fig. 6-6. To produce the nominal minimum magnetic field of 0.22 T, a magnet current of 13.3 kA will be required. Finite element analysis has been performed on the magnet showing a field uniformity of better than 5% over the full aperture of the magnet. The magnets will be located in a common vacuum enclosure (refer to Fig. 6-7) which will operate at ring pressures, the required vacuum levels being maintained by six sputter ion pumps placed atop the vacuum chamber structure. Table 6-1 summarizes the parameters for the RHIC abort kicker magnet.

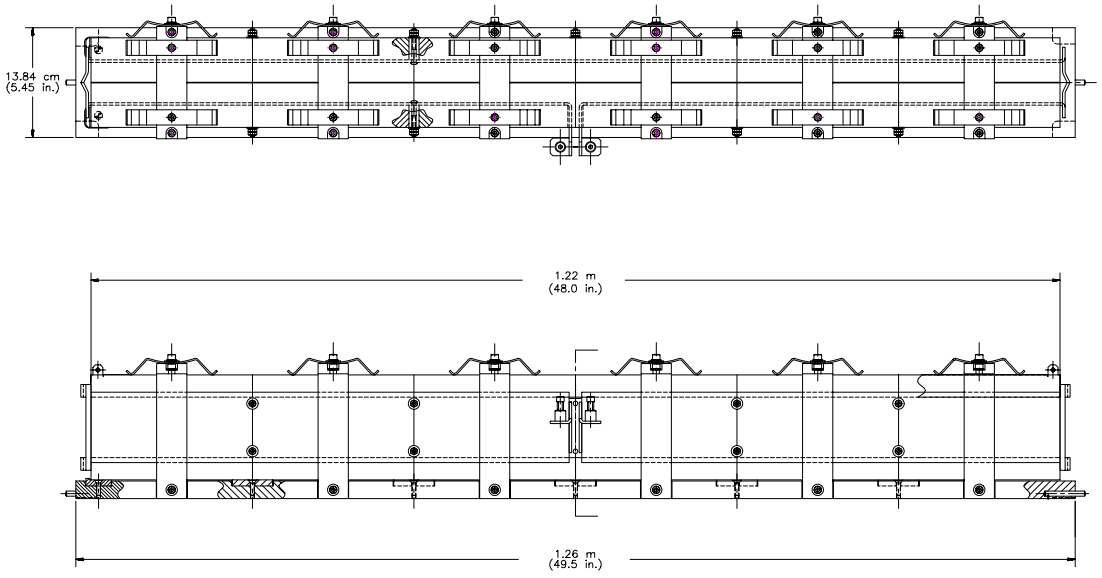

Fig. 6-5. Kicker magnet details

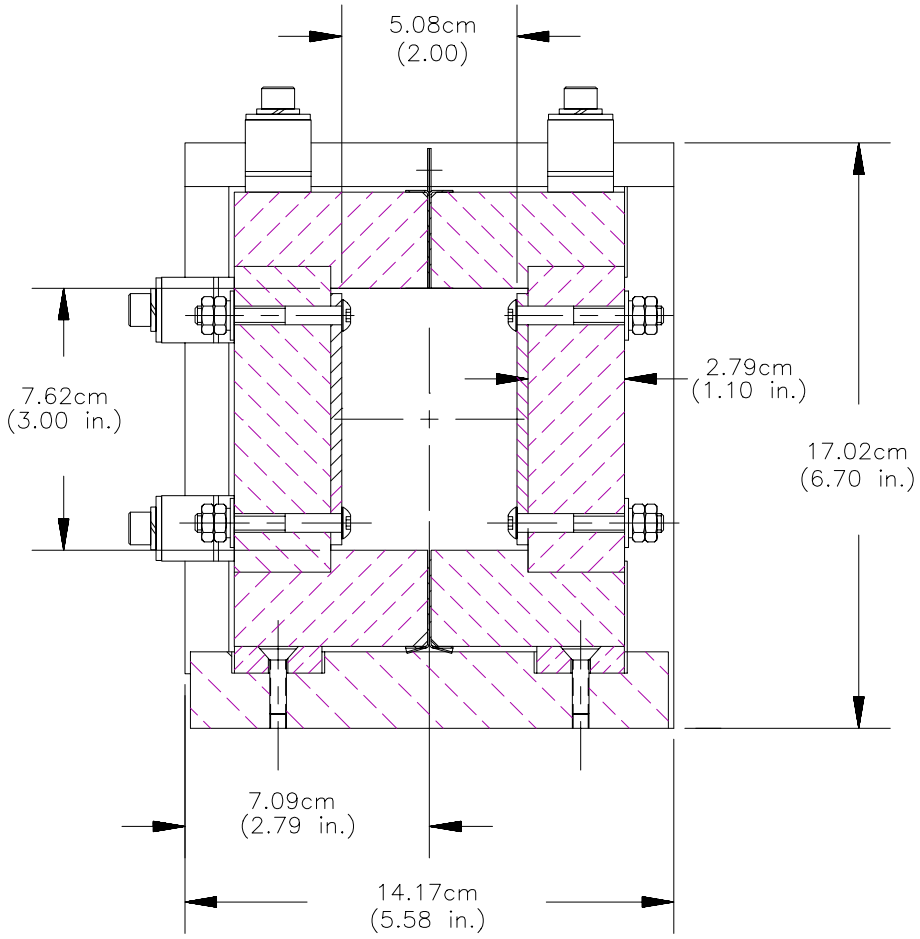

Fig. 6-6. Kicker magnet cross section.

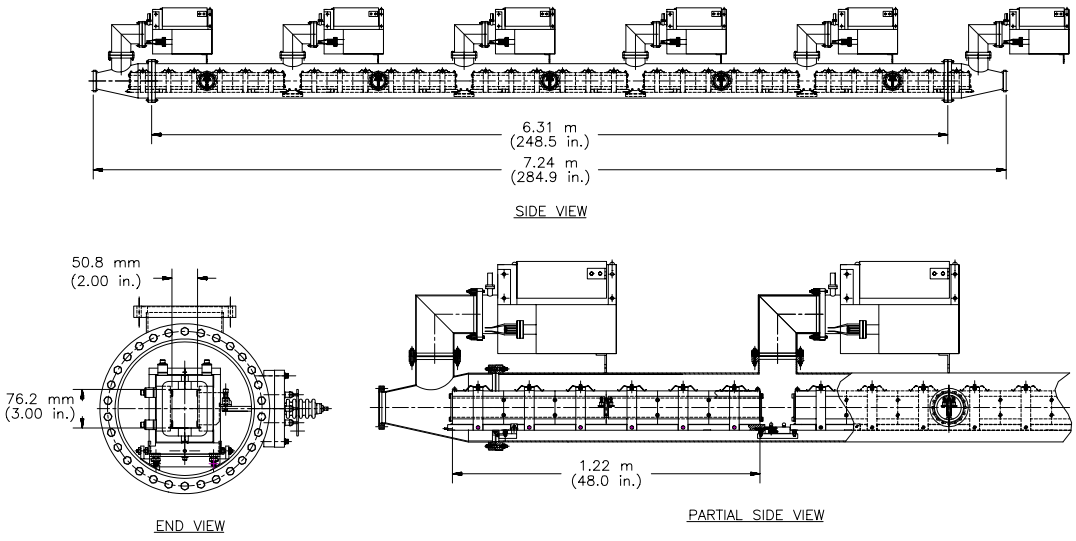

Fig. 6-7. Kicker magnet vacuum enclosure.

Table 6-1. Abort Kicker Magnet Requirements

Requirement	Value
Aperture (H×V)	50.8×76.2 mm (2×3 in.)
Length, each magnet	1.22 m (48 in.)
Number of magnets	5
Nominal minimum magnetic field @ top beam energy	0.22 T
Nominal kicker current	13.3 kA
Field uniformity, (full aperture)	<5%
Inductance, each kicker	1.06 μH
Magnetic field in ferrite @ 20.2 kA	0.3 T
Core material	Ceramic Magnetics CMD5005

iii. Pulser and PFN Requirements and Design

A separate power modulator will provide the drive currents for each of the five abort kicker magnets in each RHIC ring (see block diagram Fig. 6-8). For each modulator an inductance of 100 nH was assumed for the sum of the inductance of the switch tube (80 nH) and the inductance of the cable connecting the modulator to the magnet structure. An additional inductance of 0.87 μH/m or 1.06 μH for the 1.22 m long magnet (including fringe fields) was calculated by finite element analysis run on the ferrite H-core magnet. Therefore, the total load inductance seen by the modulator is approximately 1.16 μH, and in order to achieve the ≤1 μsec rise time a PFN impedance of approximately 1 Ω is required if the modulator is operated into a shorted magnet.

The beam absorber will be capable of sustaining a bunch overlap of less than 10 (the equivalent of 10 bunches hitting the same spot on the target). To accomplish this, the beam must always be moving across the face of the target. Simulations show that a magnetic field pulse which rises by approximately 45% in oscillatory fashion during the 13 μs pulse length will sufficiently spread the beam resulting in a bunch overlap of less than 10. Both the ramp and the oscillations can be accomplished by using a PFN in which the impedance of the network is tapered from one end to the other and the impedance of the output cell is mismatched. Table 6-2 summarizes the power modulator requirements and design.

SPICE simulations have been run and a model has been built for variations of the basic circuit shown in Fig. 6-9 which meet the above requirements. A computed output current is shown in Fig. 6-10 for PFN parameters, including parasitic components, adjusted to reasonably reproduce the waveform actually observed.

The PFN charging supply will have to track the beam energy from injection through acceleration and make up any lost charge due to leakage currents while the beam is stored. The supply will be required to ramp the voltage on the PFN from the injection energy voltage to full voltage in ~1 min. The modulator tubes will always be sitting at the proper voltage (± 5%) required for safe extraction for all points along the injection, acceleration and storage cycles. Failure in any of the critical components, in particular the 50 kV power supply and delay generators, must cancel the "beam allowed" status. In the event of sensing loss of, or out of specification voltage, on any modulator, the beam abort link will be pulled in order to effect safe extraction immediately. The most economical way of ramping up the charging voltage on the five PFN's is by using a single

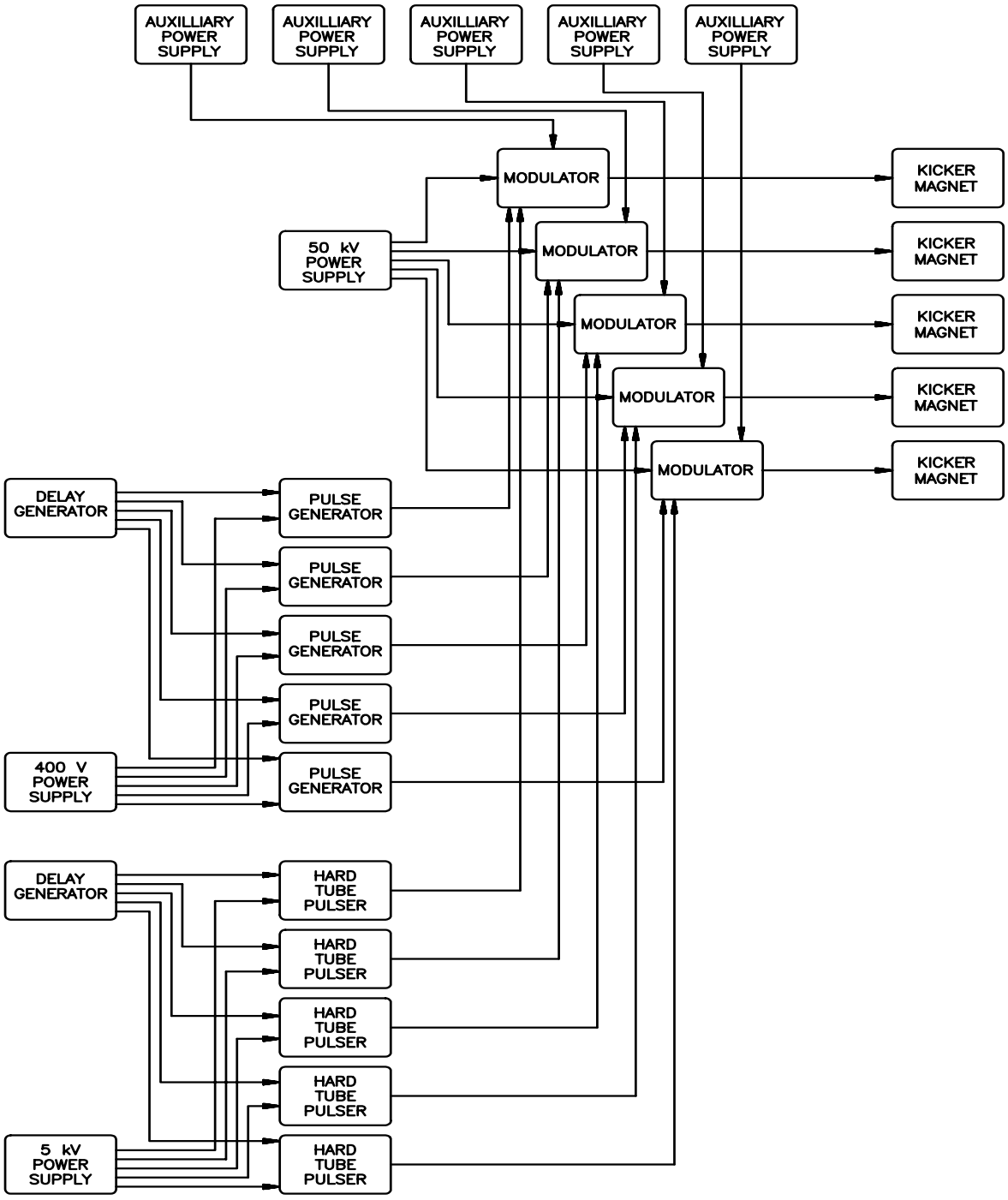

Fig. 6-8a. Preliminary Abort kicker power supply block diagram

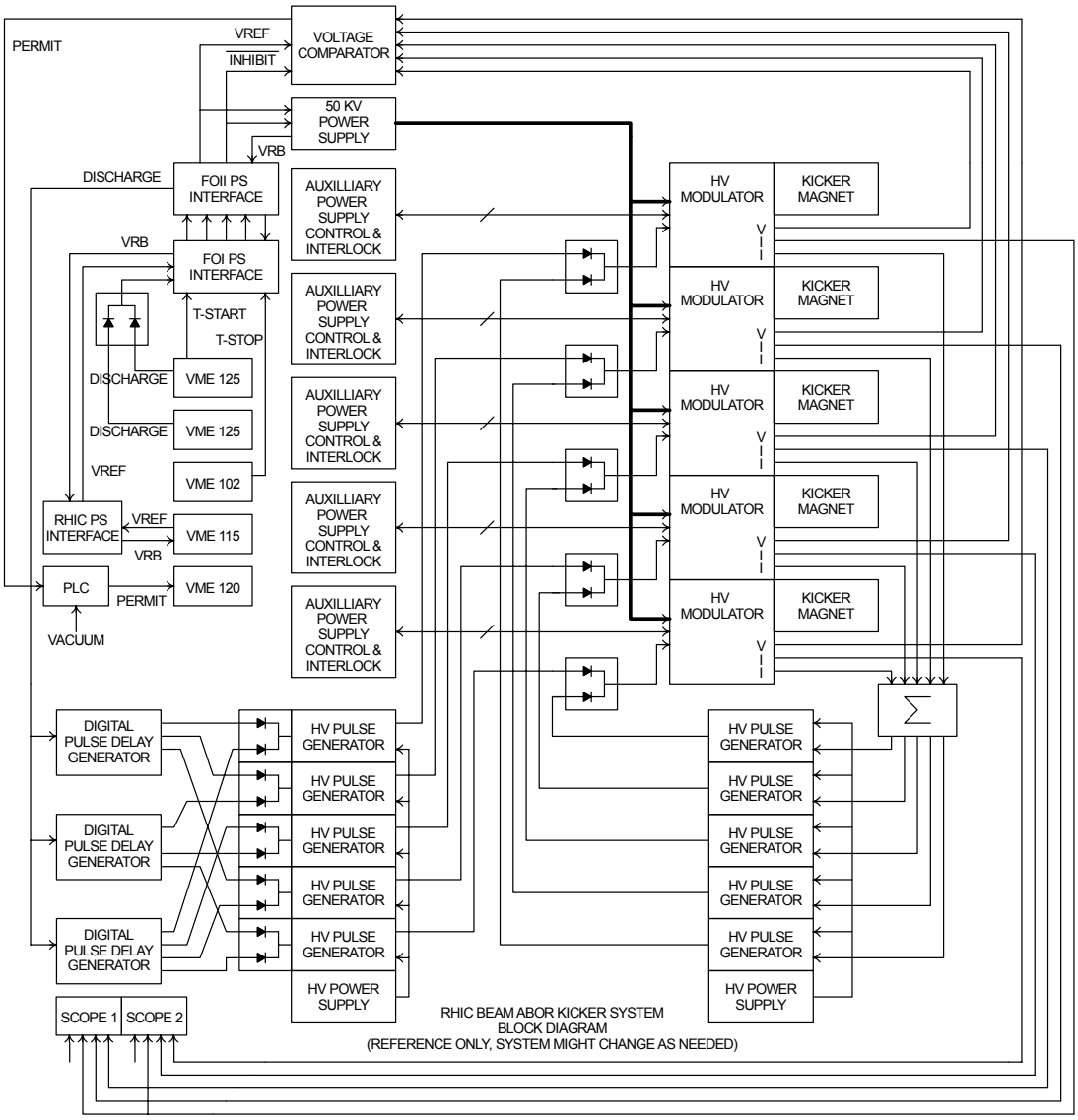

Fig. 6-8b. Simplified block diagram of RHIC beam abort kicker system as built (for reference only, actual system is an ever evolving enterprise).

Table 6-2. Kicker Modulator Requirements

Requirement	Value
Power supply rating	50 kV
Charge voltage @ top energy @ injection	33.3 kV 4 kV
Voltage tolerance	± 5 %
Minimum voltage charge time from injection to top energy	60 s
Kicker current min. @ top energy max. @ top energy	13.3 kA 20.2 kA
Current tolerance	+10%/-20%
Pulse width	>13 μs
Rise time	<900 ns
Fall time	Not Applicable
Jitter	<10 ns
Maximum pulse repetition rate	1 pulse per minute
Load impedance	1.16 μH
Dimensions, each modulator (H×W×D)	183×61×94 cm (72×24×37 in.)

power supply feeding the five PFN's (refer to block diagrams Fig. 6-8 a and b) which tracks the ring dipole magnet current through a Real Time Data Link (RTDL) from the central control system. Tracking and coordination are handled by the standard RHIC Ramp Manager program, with the necessary time-dependent voltage references for the Blue and Yellow ring PFNs generated by standard RHIC waveform generators (WFGs).

In order to minimize the cable lengths between modulators and kicker magnets, each PFN will be contained in a separate enclosure, which will be placed underneath the beamline directly below its corresponding magnet.

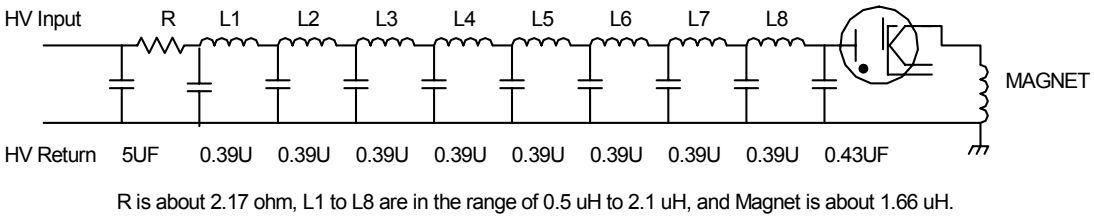

Fig. 6-9. Simplified schematic of RHIC beam abort pulse forming network

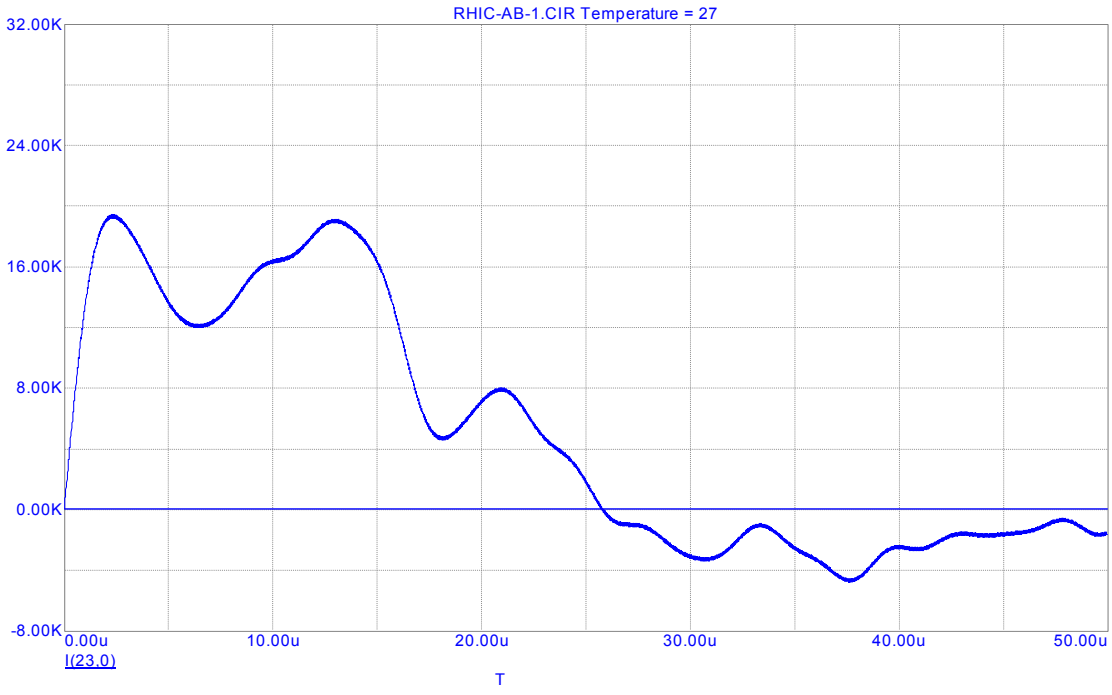

Fig. 6-10. Simulated magnet current waveform with estimated parasitic parameters to match the observed waveform.

iv. Beam Absorber

The dump absorber will be approximately 5.2 m long and composed of three sections. The first and most critical will be composed of a special carbon-carbon material (C-C) having extremely high thermal shock resistance. This section will be about 0.5 m long and will be within the vacuum chamber. The aborted beam will exit the circulating beam tube through an opening into a side parallel vacuum chamber. This side chamber, while open to the main beam pipe, will be differentially pumped along its length and will have the carbon-carbon absorber face exposed at the end (refer to Fig. 6-4). This arrangement will eliminate the necessity of a vacuum window being the first element the ejected beam encounters. After passing through the 0.5 m of the C-C absorber, the beam will lose sufficient energy so that a high strength stainless (17-7PH) vacuum window can withstand the thermal stress of its passage to the next absorber. This second absorber will be a block of ordinary graphite and will be about 2.7 m long. The graphite block will be contained in a sealed enclosure containing nitrogen at one atmosphere to preclude the possibility of ignition due to the thermal load of the beam absorption, and will be capped top and bottom by steel shielding slabs. The final absorber, 2 m of steel, will be located downstream of the graphite section. In addition to the absorber structure, the adjacent circulating beam tube downstream of the C-C section will also be surrounded by steel.

The entire core section will be surrounded by 15 cm (6 in.) of steel shielding on the top, bottom and both sides, with an additional 15 cm (6 in.) of marble on the sides to aid in personnel shielding from the activated steel and graphite components. The removable blocks of shielding (steel and marble) on the aisle side will be mounted on rollers to afford quick access to the core. Figure 6-11 shows some details of the dump/shielding structure. The core itself can be removed from the beam tube for vacuum leak checking or repair of the integral bakeout heater. Because of the small core beam tube (46×42 mm inside), some horizontal position adjustments are thought to be necessary to maximize the available circulating beam tube aperture. Consequently, the entire dump will be positioned on an adjustable table allowing a manual (not remote) adjustment of ±1 cm horizontally. Dial indicators at both ends will monitor the absolute position of the assembly. Lateral movement of the dump assembly will require re-programming of the kicker current as the deflection angle will be altered; therefore remote motion will not be allowed and the positioning devices will be lockable. The off-center configuration of the core can also be ameliorated by the use of a bump magnet mentioned earlier. Inclusion of a bump magnet will also need to be included in the voltage

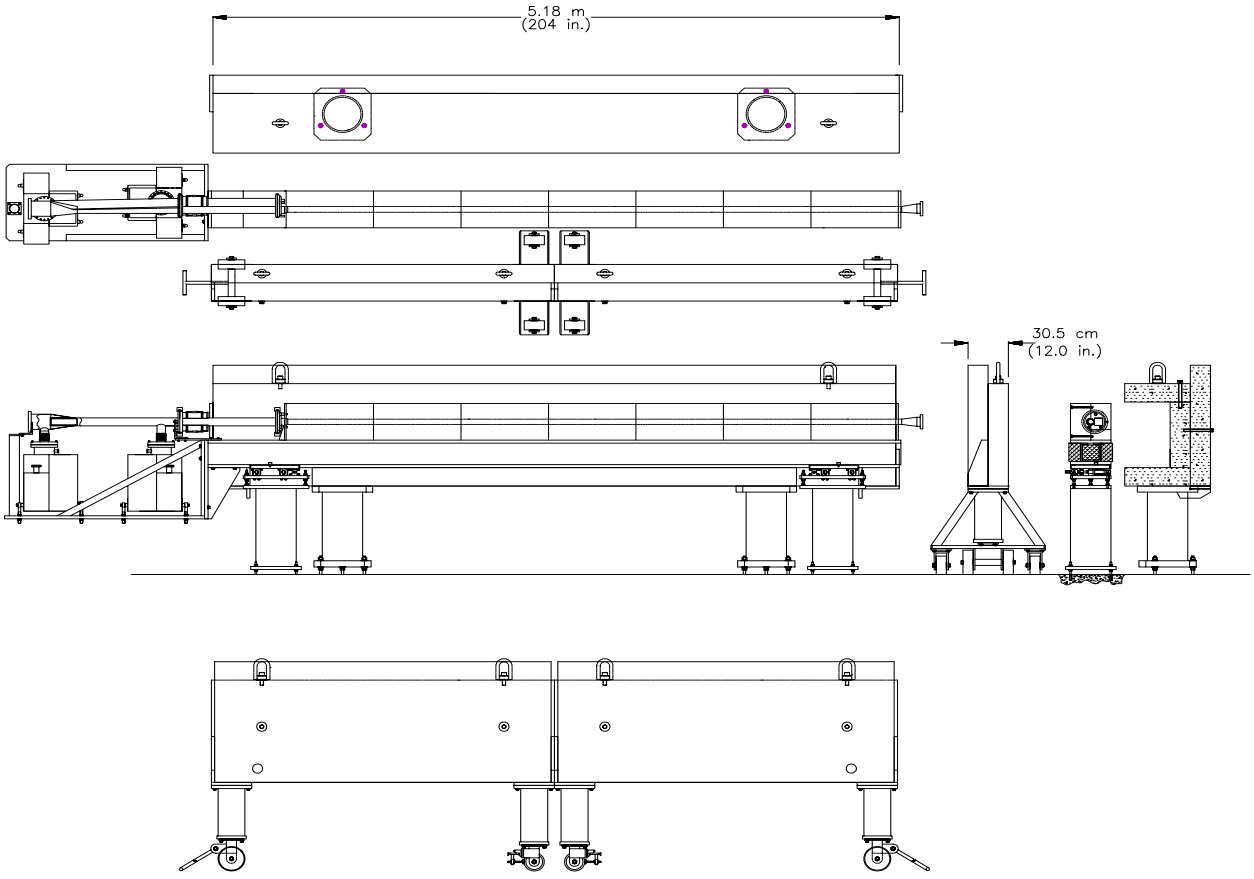

Fig. 6-11. Beam absober and shielding

programming of the abort waveform to ensure that the ejected beam impinges on the proper area of the C-C absorber.

The mechanical location of the absorber was resurveyed after the first year of beam operation with only slight repositioning required. The absorber was left at the original design values. Also, although time dependent horizontal orbit bumps are applied in the absorber region, no modification of the PFN voltage function from one simply following the beam momentum has been found to be necessary.

The C-C absorber section will be contained in a thin wall stainless steel chamber with chain clamp flanges at either end for quick removal. This arrangement will afford ease of C-C block replacement with minimum personnel exposure (ALARA). The thin side walls are designed to bend inward against the C-C material under vacuum to increase thermal contact and subsequent convective cooling to the outside air. Just downstream of the C-C section will be a small 2.5 cm (1 in.) air gap for insertion of an array of thermocouples to monitor the integrity of the carbon-carbon absorber block.

The entire dump vacuum system will be bakeable. This will be accomplished by standard fiberglass insulated heater tapes in areas outside of the core and by a special Kapton-wire heater (wrapped with fiberglass tape) around the oval tube through the core. No forced cooling of the dump core will be necessary for beams up to 4 times the design intensity dumped once per hour.

The external (earth) shielding in the dump area has been analyzed with respect to groundwater activation, sky shine, air activation and muon radiation. Based on the analysis for ~2400 annual dumps/ring of gold beams at top energy and 4× design intensity, an additional 1.5 m (5 ft) of earth will be added atop the nominal berm thickness at the dump locations to meet the sky shine criteria of 1 mrem/yr at the site boundary. An impervious liner will be placed just below the surface of the berm to prevent infiltration of rainwater into the earth shielding, and groundwater monitoring wells will also be installed in these areas.

Groundwater concerns also motivated the extension of the waterproof liner upstream from the absorber area to cover the kicker magnets. These magnets become under some running conditions chronic vertical beam apertures.

v. Beam Instrumentation

The detector for the following diagnostic was installed. The readout system has not been completed and the system has never been commissioned.

Beam position information, both during normal running and during the abort cycle, will be provided by a standard BPM located approximately halfway between the kickers and the dump face. An additional piece of instrumentation is being developed that will determine the extent, if any, of the ablation or cracking of the front face of the C-C absorber. Studies have shown that the beamlets will disperse as they travel through the absorber material, such that a cone-shaped path will be made in the C-C block. As the absorber face is lost, or if microscopic cracks form in it, the diameter of the spot emanating at the downstream end of the block will diminish.

To monitor the spot size an array of very small thermocouples (see Fig. 6-12) will be placed in the 2.5 cm (1 in.) gap that has been left immediately downstream of the C-C block housing. Since the position of the train formed by the 60 bunches will vary modestly along the horizontal axis due to the fine structure of the shape of the leading edge of the abort pulse, and also since the vertical position will be more stable, the array will be more dense in the vertical dimension than in the horizontal. The increased vertical resolution will allow for monitoring of the absorber face for abrupt failure, and through trending analysis will be capable of monitoring slow degradation of the material as well. The present design calls for 126 thermocouples, arranged in a 9 high by 14 wide array. The vertical spacing will be 1.25 mm while the horizontal spacing will be 1.5 mm, covering an area 1 cm high by 2 cm wide. Four off-the-shelf 32-channel signal conditioning boards will be utilized, the outputs of which will be sent to a standard RHIC MADC module. The size and shape of the array is easily altered if future conditions warrant, and doubling the number of monitoring points can be attained at a modest additional cost.

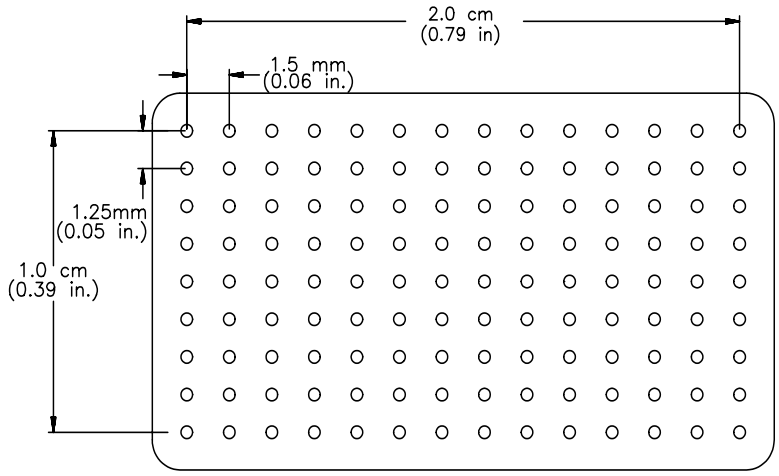

Fig. 6-12. Beam dump thermocouple array (spot size monitor).

CONVENTIONAL FACILITIES (WBS 1.10)

i. Ring Tunnel and Experimental Halls

The availability of the CBA conventional facilities for use in the Relativistic Heavy Ion Collider represented an unprecedented opportunity to build the collider at minimum cost. The existing tunnel configuration provides for six experimental areas where the ring beams will cross. Four areas have been provided with the major structures necessary for an operating experimental area. The RHIC lattice will use these existing areas, which are at the 2, 6, 8 and 10 o'clock locations (see Fig. 10-1). The 4 o'clock facility was an "open area" but was enclosed with portable shielding prior to machine turn-on, and is being used for the high frequency rf system. It is also suitable for small experiments. In order to make the ring operational, the gaps at each of the two undeveloped areas - 10 and 12 o'clock - had to be closed. Multi-plate arch tunnels 4.9 m (16 ft) and 7.9 m (26 ft) in diameter have been erected at 10 o'clock, along with a service building. The 10 o'clock area is the location of the beam dump and is used for a small experiment called PHOBOS. At 12 o'clock, 4.9 m and 7.9 m diameter multi-plate arch tunnels have been erected, along with 2 concrete headwalls, 2 stair structures, a base slab and service building. Multi-plate arch magnet access tunnels have also been constructed at either side of the 12 o'clock facility. The interaction point is presently closed by portable shield blocks. This area will be available for development at a later date, thus maintaining the option of adding an experimental hall for future experimental needs. Additional multi-plate arch magnet access tunnels spurs have been constructed at either side of the 8 o'clock facility. A complete list of RHIC buildings and tunnel identification is given in Table 10-1.

The experimental halls at 2, 6 and 8 o'clock are fully enclosed structures complete with support buildings. The area and height of the facilities vary and each is equipped with overhead cranes, air conditioning, and sprinkler protection and has direct access from grade. Table 10-2 gives the dimensions, crane capacities and beam heights in each of these facilities as well as the 4 o'clock open area. The open area, as noted above, has a concrete deck capable of supporting portable shielding blocks in varying configurations. All conventional services, including a support building, are in place. The experimental hall at 6 o'clock has an assembly building addition constructed similar to the existing assembly building at 8 o'clock.

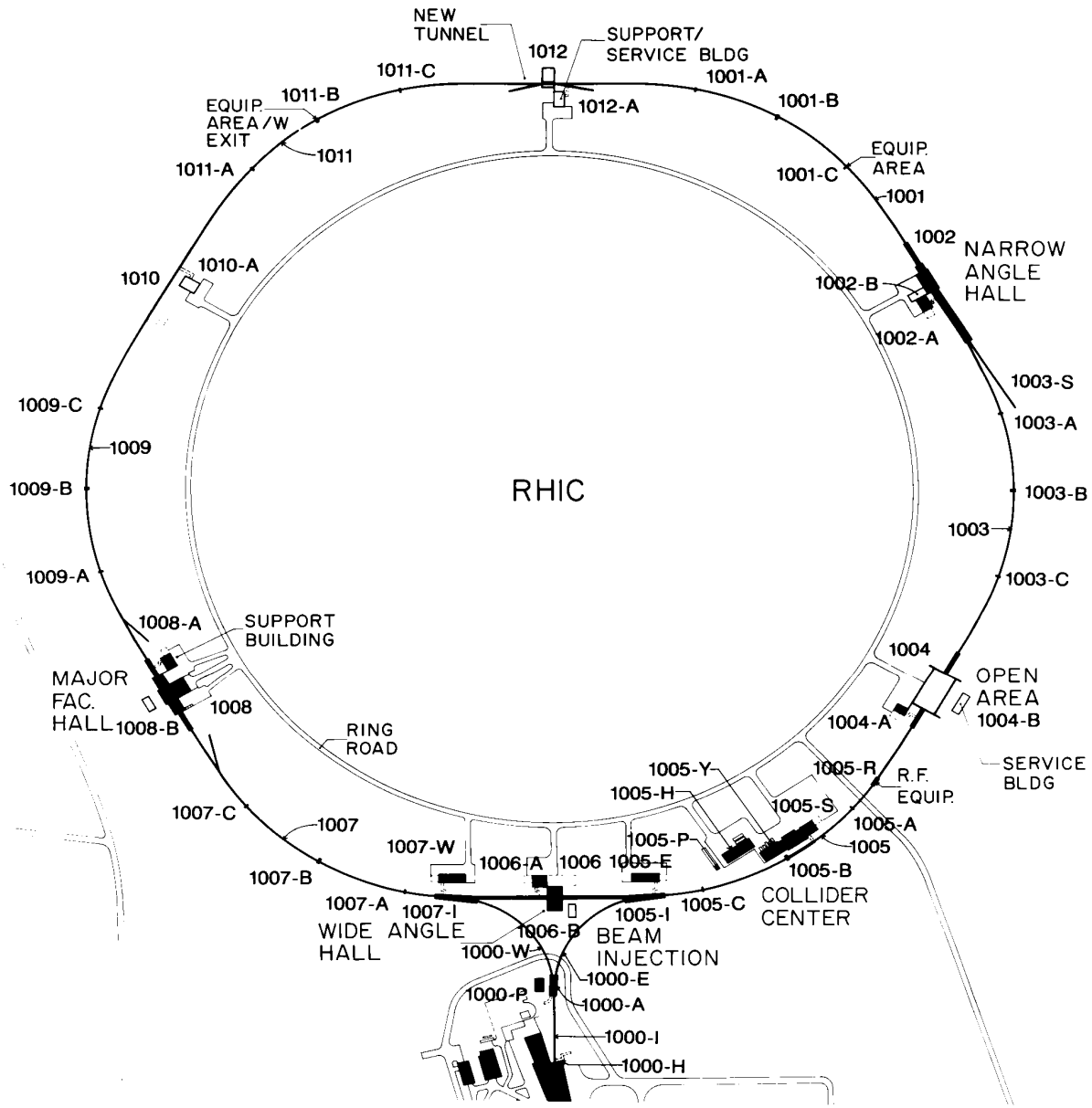

Fig. 10-1. RHIC building and tunnel identification.

Table 10-1. RHIC Building and Tunnel Identification

		1000A	Injection Conjunction Structure
		1000E	East Injection Tunnel
		1000H	Injection Access
		1000I	Injection Tunnel
		1000P	Injection Power Supply Building
		1000W	West Injection Tunnel
1001	1 O'Clock Sextant	1001A	1 O'Clock Sextant Electronics Alcove
		1001B	1 O'Clock Sextant Electronics Alcove
		1001C	1 O'Clock Sextant Electronics Alcove
1002	Narrow Angle Hall	1002A	Narrow Angle Hall Support Building
		1002B	Narrow Angle Hall Service Building
1003	3 O'Clock Sextant	1003A	3 O'Clock Sextant Electronics Alcove
		1003B	3 O'Clock Sextant Electronics Alcove
		1003C	3 O'Clock Sextant Electronics Alcove
		1003S	3 O'Clock Sextant Spectrometer Tunnel
1004	Open Area	1004A	Open Area Support Building
		1004B	Open Area Service Building
1005	5 O'Clock Sextant	1005A	5 O'Clock Sextant Electronics Alcove
		1005B	5 O'Clock Sextant Electronics Alcove
		1005C	5 O'Clock Sextant Electronics Alcove
		1005E	East Injection Power Supply Building
		1005H	Compressor Structure
		1005I	East Injection Transition Structure
		1005P	Cooling Tower Pump House
		1005R	rf Structure
		1005S	Collider Center
		1005Y	Cryogenic Structure
1006	Wide Angle Hall	1006A	Wide Angle Hall Support Building
		1006B	Wide Angle Hall Service Building
1007	7 O'Clock Sextant	1007A	7 O'Clock Sextant Electronics Alcove
		1007B	7 O'Clock Sextant Electronics Alcove
		1007C	7 O'Clock Sextant Electronics Alcove
		1007W	West Injection Power Supply Building
		1007I	West Injection Transition Structure
1008	Major Facility Hall	1008A	Major Facility Hall Support Building
		1008B	Major Facility Hall Service Building
1009	9 O'Clock Sextant	1009A	9 O'Clock Sextant Electronics Alcove
		1009B	9 O'Clock Sextant Electronics Alcove
		1009C	9 O'Clock Sextant Electronics Alcove
1010	Experimental Facility	1010A	Support/Service Building
1011	11 O'Clock Sextant	1011A	11 O'Clock Sextant Electronics Alcove
		1011B	11 O'Clock Sextant Electronics Alcove
		1011C	11 O'Clock Sextant Electronics Alcove
1012	Future Major Facility Hall	1012A	Future Major Facility Hall Support/ Service Building

Table 10-2. Summary of Hall Dimensions (m)

	Length	Width	Beam Height	Hook Height/ Capacity (tons)
2. Narrow Angle				
Central Hall	28	12	1.7	6.1/20
Forward Exp. Bldg.	68	7.9	1.7	5.3*
"Stub"	91	2.4	1.0	2.0*
4. Open Area	57†	29†	2.2	---*
6. Wide Angle				
Central Hall	16	32	4.3	9/20
Assembly Building	31	18	4.3	12.2/40 + 12.2/10
8. Major Facility				
Assembly building	18	16.8	5.2	11/40
Experimental area				5.2/12
Forward Exp. Bldgs. (2)	16	9	3.3	3.3/15
Assembly Building	19	19	5.2	11.3/40+15/5**

*No crane - ceiling height given
†Pad dimensions given
**Rails installed, no crane

The Collider Center, approximately 4650 m^2 (50,000 sq ft), consisting of a Cryogenic Wing, a Compressor Structure and a four level Main Building, is complete. The air-conditioned main building contains technical shops, an RF/Power Supply wing, office and conference room space, and space for the collider cryogenics control center. The RHIC funding included installation of a power substation for the accelerator rf and Power Supplies Wing, site improvements such as paved access roads, hardstands, parking areas, yard lighting and general restoration of facilities and grounds. Additional power supply service buildings have been constructed at various locations around the ring. The 2, 6 and 8 o'clock service buildings are 300 m^2 (3200 sq ft) and the 4 o'clock building will be 450 m^2 (4800 sq ft). Dimensions of support and service buildings are given in Table 10-3.

Construction of the utility services, roadways, drainage and other site improvements for the CBA have been underway since 1979. All have been completed except for some paving and site work. The extension of the 69 kV substation was completed in May 1982.

Table 10-3. Summary of Building Dimensions (m)

Location	Building	Length	Width	Building No.
2	Support	14	18	1002A
	Service	24	12	1002B
4	Support	14	10	1004A
	Service	38	12	1004B
6	Support	14	18	1006A
	Service	24	12	1006B
8	Support	14	18	1008A
	Service	24	12	1008B
10	Support/Service	15	27	1010A
12	Support/Service	15	27	1012A

The underground ductbank for electrical power and communication distribution was completed in 1981. Installation of conventional power feeder cables to the Collider Center was finished in 1982. Installation of the balance of the power cables around the Ring Road ductbank and the unit substations at areas 2, 4, 6 and 8 o'clock location was completed in the Spring of 1983. The Main Ring Sector 11 and Sector 1, approximately one-third of the enclosure, which had remained unfinished during CBA, has been provided with permanent power, lights, fire alarm, HVAC and dehumidification. The Main Ring has been completed, and the two support buildings at areas 10 and 12 o'clock have been constructed as required to supply the utility services to these areas to make the ring operational.

ii. Shielding

The design basis for earth shielding surrounding RHIC is shown in Figs. 10-2 and 10-3. Figure 10-2 shows the radial "lobes" of earth which are required to extend outward to a maximum distance of 90 m from the tunnel center line at the center of each arc and to present a minimum thickness of 4 m in the vertical direction as measured from the beam elevation. These lobes were designed to attenuate radiation from (penetrating) muons to a level of less than 5 mrem/yr at the nearest site boundary.[1] The "typical section" through the shielding shown in Fig. 10-3 shows two thicknesses of earth above the tunnel enclosure. Most of the ring has a 4 m vertical earth cover, but in the region of the Collider Center, where non-radiation workers are present and where occupancy

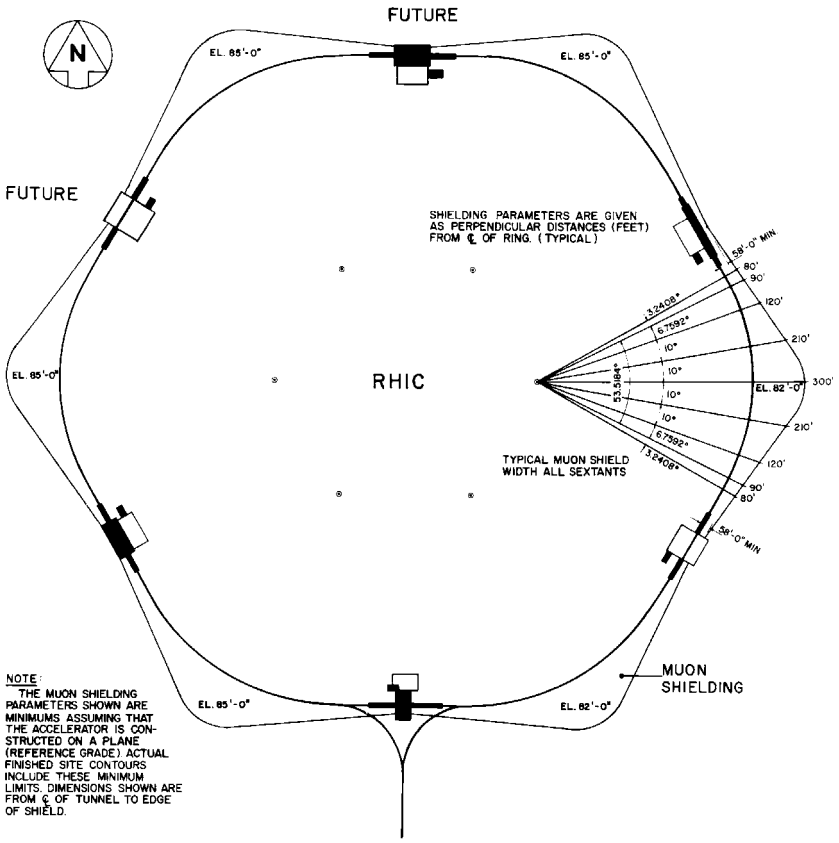

Fig. 10-2. Plan of accelerator ring.

---

[1] P. J. Gollon and W. R. Casey, *ISABELLE Shielding Criteria and Design*, Health Phys. 46, 123-131, (1984).

is high, the vertical cover has been increased to 6 m. The berm cover will also be increased over the locations of the internal dumps, where beam "loss" is expected to be high, in accordance with basic ALARA principles.

Because the existing shielding was designed for the ISABELLE project, it is necessary to compare anticipated loss between ISABELLE and RHIC. ISABELLE was designed to accelerate 3×10^{17} protons per ring per year to 400 GeV, or 2.4×10^{20} GeV/yr. Although RHIC is designed to operate with many species and energies, a conservative estimate of the annual accelerated energy has been placed at the equivalent of 5.5×10^{14} Au ions per ring per year at 100 GeV/nucleon,[2] or 2.2×10^{19} GeV/yr. The radiation burden of RHIC will therefore be approximately one order of magnitude less than that for which the shielding was designed.

A variety of calculations have been performed to verify the adequacy of the RHIC shielding. These calculations rely on the computer code CASIM[3,4] to simulate the intra-nuclear cascade.

Radiation at the site boundary is dominated by neutron skyshine, airborne radioactive emissions, and muons escaping the shielding lobes. Using the (conservative) scenario for "normal" beam loss given in Ref. 2, together with CASIM results and the methodology of Stevenson and Thomas,[5] a skyshine dose of 0.5 mrem/yr is predicted[6], while airborne emissions should contribute only 0.02 mrem/yr.[6] Muon dose at the site boundary has been calculated to be ~0.3 mrem/yr.[7]

---

[2] M. Harrison and A. J. Stevens, *Beam Loss Scenario in RHIC*, AD/RHIC/RD-52 (1993). This reference assumes an "upgraded" RHIC with 4 times the initial design beam intensities.

[3] A. Van Ginneken, *High Energy Interactions in Large Targets*, Fermilab, Batavia, Il, (1975) and *CASIM. Program to Simulate Hadronic Cascades in Bulk Matter*, Fermilab, FN-272 (1975).

[4] A. J. Stevens, *Improvements in CASIM; Comparison with Data*, AGS/AD/Tech Note No. 296, (1988).

[5] G. R. Stevenson and R. H. Thomas, *A simple Procedure for the Estimation of Neutron Skyshine from Proton Accelerators*, Health Phys. 46 115-122, (1984).

[6] *RHIC Preliminary Safety Analysis Report* (1991).

[7] A. J. Stevens, *Radiation from Muons at RHIC*, AD/RHIC-49 (1989).

As mentioned above, the collider center is a special location because of high occupancy and the presence of non-radiation workers. The combination of direct radiation (from beam-gas interactions and aperture-limiting collimators assumed to exist near the entrance to each arc) and skyshine amounts to less than 6 mrem/yr, well below the laboratory guideline limit of 25 mrem/yr for on-site non-radiation workers.

The maximum dose rate near the collider is expected to occur directly over the dump location and is calculated to be ~75 mrem/hr during periods of beam studies at the 4 m berm cover. Although additional berm will be added here, it will still be necessary to designate this location as a "controlled area" and to restrict access appropriately.

In addition to "normal" loss, the possibility of fault conditions must also be considered. An example of a "credible fault" would be failure of the beam dump kicker coincident with a magnet quench. Such a fault would likely result in ~20% of the beam interacting at a single point and would require considerable accelerator downtime to repair the resulting damage. We define a "Design Basis Accident" (DBA) fault as loss of the entire full energy beam on any magnet near the limiting aperture or loss of one-half of the full energy beam on any other magnet. A DBA fault would result

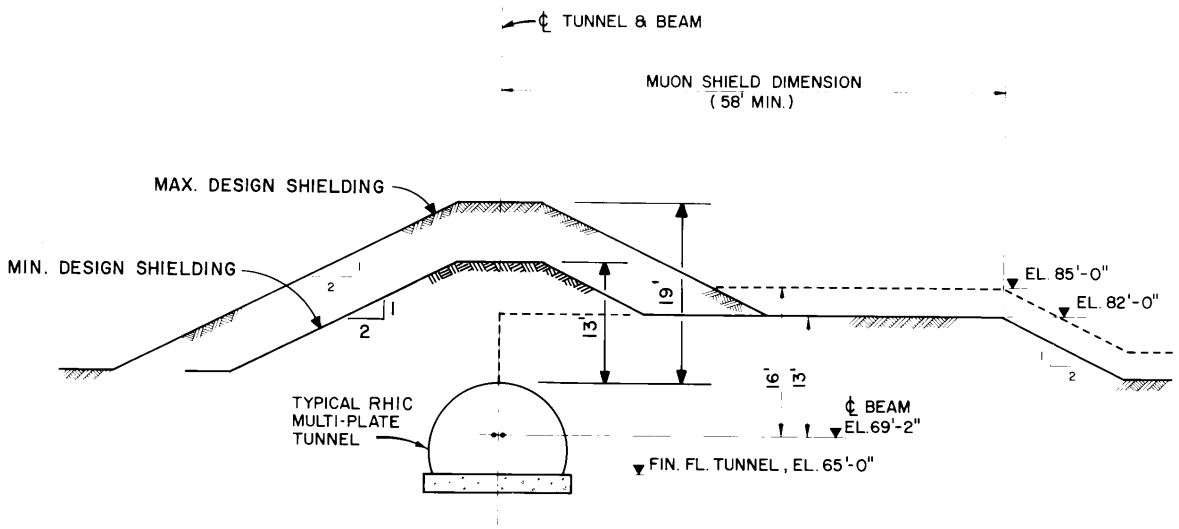

Fig. 10-3. Typical section through RHIC tunnel showing maximum and minimum earth cover.

in a dose at the top of the 4 m shielding berm in the 100 - 200 mrem range. One DBA fault per year (in the worst possible location) would increase the annual dose in the Collider Center by up to 1.7 mrem and at the site boundary by <0.01 mrem (due to skyshine). These levels are much less than the dose from normal operation and are therefore of no concern.

An aerial photogrammetric survey of the terrain cover of the RHIC and AGS regions of Brookhaven National Laboratory has been made.[8] Topographic contour curves were determined at 0.6 m (2-foot) elevation intervals which allows the design berm cover to be verified and/or "low points" to be discovered and corrected.

A detailed analysis of radiation dose levels exterior to the transfer line between the AGS and RHIC has been made.[9] Although dose resulting from normal beam loss is expected to be very small, ≤ 300 mrem/yr on top of the berm in the worst case, the (warm) transfer line magnets do not intrinsically limit fault conditions as is the case in the collider. For this reason, a combination of access restrictions and interlocking radiation monitors must be employed to limit potential fault dose. Access restriction will also be required around limited regions of the transfer line where beam shaving or beam dumping for diagnostic studies are planned.

Configuration control

Periodic inspection of the earth shielding is performed to check for erosion that could reduce the effectiveness of this shielding. The earth shielding configuration is documented by the RHIC A300 series drawings.

Located at the intersection regions and at the five equipment access ports is portable shielding documented by the RHIC 900 series drawings.

---

[8] Aerial survey of April 3, 1992 prepared by Chas. H. Sells, Inc.

[9] A. J. Stevens, *Analysis of Radiation Levels Associated with Operation of the RHIC Transfer Line*, Draft Version 6 (1992).

COLLIDER INSTALLATION (WBS 1.0)

i. Ring Element Nomenclature System

The nomenclature system presented here identifies main magnets and other ring elements and their positions in the ring structure. The present designation takes into account practical considerations, such as machine installation and operation. Since RHIC will become part of an ever increasing string of machines, to be operated from a central control facility, the nomenclature system is compatible with the requirements of the Control Group data base design.[1]

Details of the nomenclature system have been reviewed and accepted by the RHIC Layout Task Force and the scientific and professional staff of the Collider -Accelerator Department.

The convention upon which the new nomenclature system is based consists of the use of two fields separated by a dash. The first set of symbols specifies graphical location in the ring (zip code) and the second to the right of the dash describes the tag name of the machine element, element properties, etc.

RHIC Ring Geographical Structure

The two rings are identified as *yellow* (Y) and *blue* (B). Particles in the Y-ring travel in the counterclockwise direction, and clockwise in the B-Ring. For practical reasons the sextants are also identified as *inner* (I) and *outer* (O).

Each ring is divided into 12 half-sextants, hereafter called sectors. Each sector is fully defined by

- the blue/yellow label
- the inner/outer position
- the clock position 1 to 12

taking the crossing point between the injection points as 6 o'clock on a clock face as illustrated in Fig. 0-1.

For instance, the one o'clock position starts at the center of the arc at one o'clock and ends just before the cross-over point at the two o'clock position. The two o'clock position starts with the cross-over point at two and ends just before the center of the arc at

---

[1] E. H. Auerbach, Booster Tech. Note No. 166 (24 May 1990)

the three o'clock position, etc. The position of an accelerator element is therefore given by the set of geographical identifiers listed in Table 0-1.

A dash (-) separates the geographical identifier from the element description. Thus, a typical address would look like this: BO11-XXXX where the four X's indicate the machine element name or qualifier.

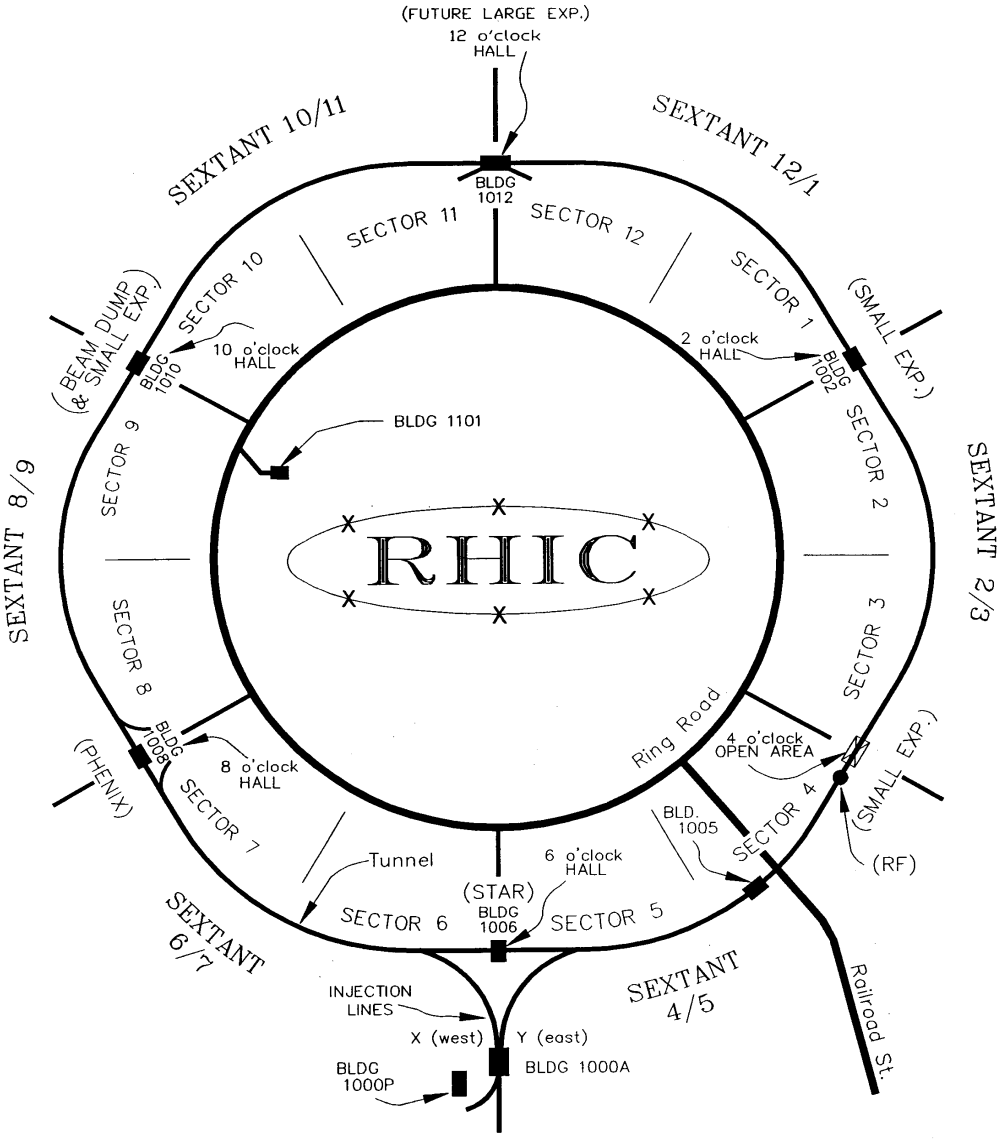

Fig. 0-1. Map, region names and main buildings.

Table 0-1. Geographical Identifiers

Inner Sectors either/	or*	Outer Sectors either/	or*
BI1	I1	YO1	O1
YI2	I2	BO2	O2
YI3	I3	BO3	O3
BI4	I4	YO4	O4
BI5	I5	YO5	O5 (injection)
YI6	I6	BO6	O6 (injection)
YI7	I7	BO7	O7
BI8	I8	YO8	O8
BI9	I9	YO9	O9 (dump)
YI10	I10	BO10	O10 (dump)
YI11	I11	BO11	O11
BI12	I12	YO12	O12

*On drawings and schematics and where there is no loss of clarity, the shortened geographical identifiers may be used.

Numbering of Dipole and Quadrupole Magnets and Quadrupole Assemblies

The quadrupoles of a sector are numbered consecutively, starting from the crossing point and going either in clockwise or counterclockwise direction, as Q1 to Q20 for even sectors and Q1 to Q21 for odd sectors. This is illustrated for sector 1 in Fig. 0-2.

The dipoles of a sector are numbered according to the quadrupole position, e.g. the dipole number follows the quadrupole number. The dipole common to both beams near the crossing point is called DX. Figure 0-2 explains the scheme.

Correctors "C", sextupoles "S", and trim quadrupoles "T" form together with a quadrupole "Q" permanent subassemblies, the so-called cold masses, in a common cryostat. The cryostat assemblies are named corresponding to their cold masses as CQS, CQT, CQB, CQC, CQ, or Q. They carry the same ring location number as their associated quadrupole. In the CQB assembly, the sextupole is substituted by a blank yoke without coil. CQ contains no sextupole and is physically

shortened to provide space for the injection devices. CQC is a cold mass in the interaction region triplet containing the quadrupole Q3 and corrector packages at each end. Q is the triplet quadrupole Q1 without attached corrector.

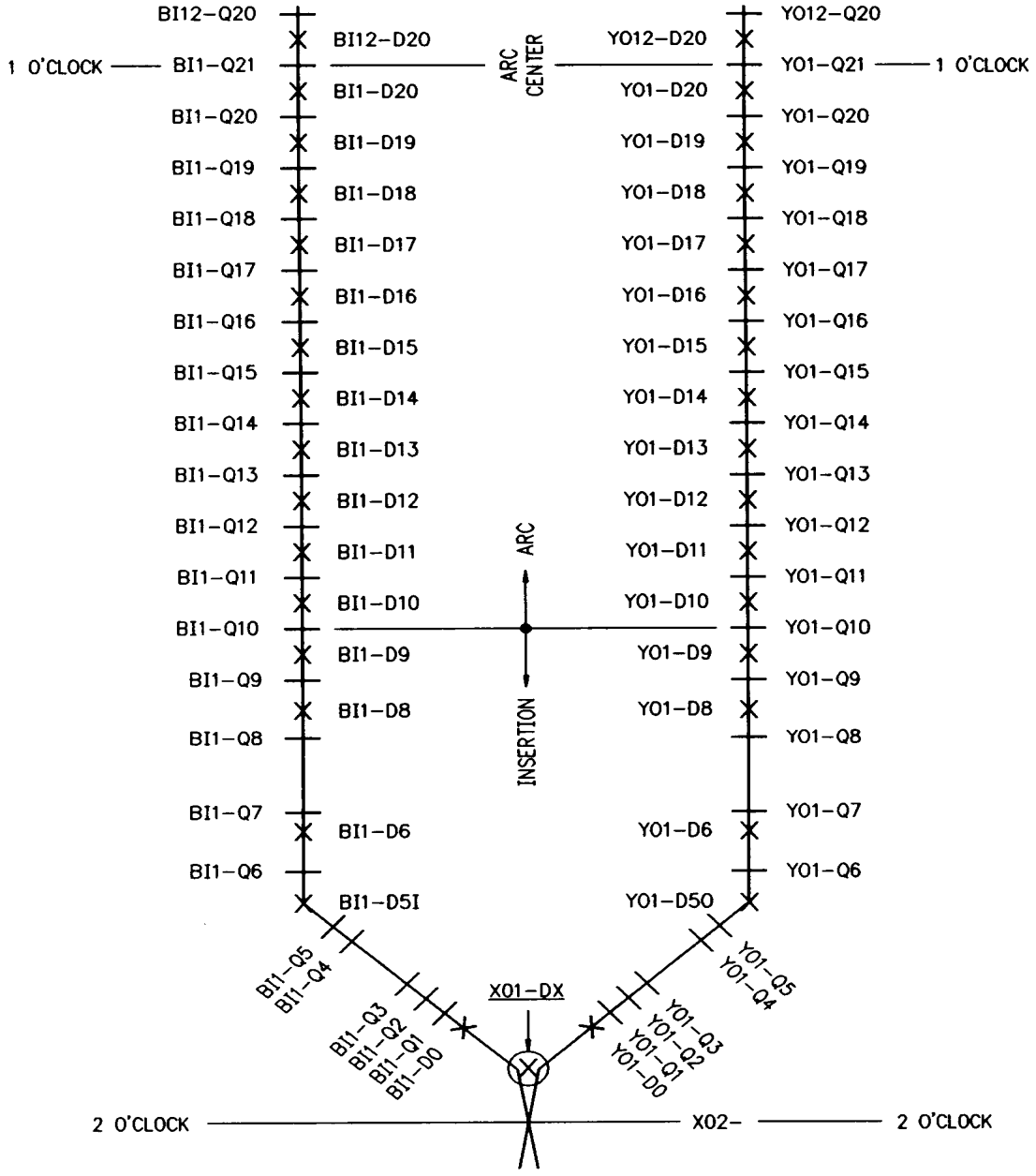

Fig. 0-2. Sector (half sextant) magnets.

A Structured System of Element Description

Machine elements are called by their generic names with qualifiers added. Abbreviations to be chosen should be suggestive to initiated persons, as short as possible, and be unique. For instance, dipoles may be of the following kinds:

Dipole	D
Dipole Vertical	DV
Dipole Horizontal	DH

The letter D in the first position is therefore reserved to identify a dipole class of magnets. The second letter always identifies the kind of dipole or its action on the beam. [Note:An exception to this is the DU or dummy magnet. Dummy magnets are non-magnetic elements, but fill a lattice space traditional held by a dipole class of magnet.] The third qualifier, if needed, provides further qualifications, such as machine element association or more operational information. . Examples are:

Dipole Kicker Injection	DKI
Dipole Kicker Ejection	DKE
Dipole Septum Injection	DSI
Dipole Septum Ejection	DSE
Dummy Magnet	DU
and so on...	

Another frequently occurring class of magnets are quadrupoles. Applying the above scheme one has:

Quadrupole	Q
Quadrupole Focussing	QF
Quadrupole Defocussing	QD
Quadrupole Skewed	QS
and so on...	

The magnets installed for spin physics are the helical dipoles. Again, applying the scheme above:

Helical Snake Dipole	SNK
Helical Rotator Dipole	ROT

The above list is not inclusive, but showed as a guide for the creation of additional symbols and logic abbreviations for all machine-associated data base variables. Since the control system data base is the one area where all tag names are gather together, system managers should be sure that their element descriptions are unique, suggestive of use or purpose, and should check with the C-A Controls Division to be sure that no conflicts or other problems arise when added to the control systems data base.

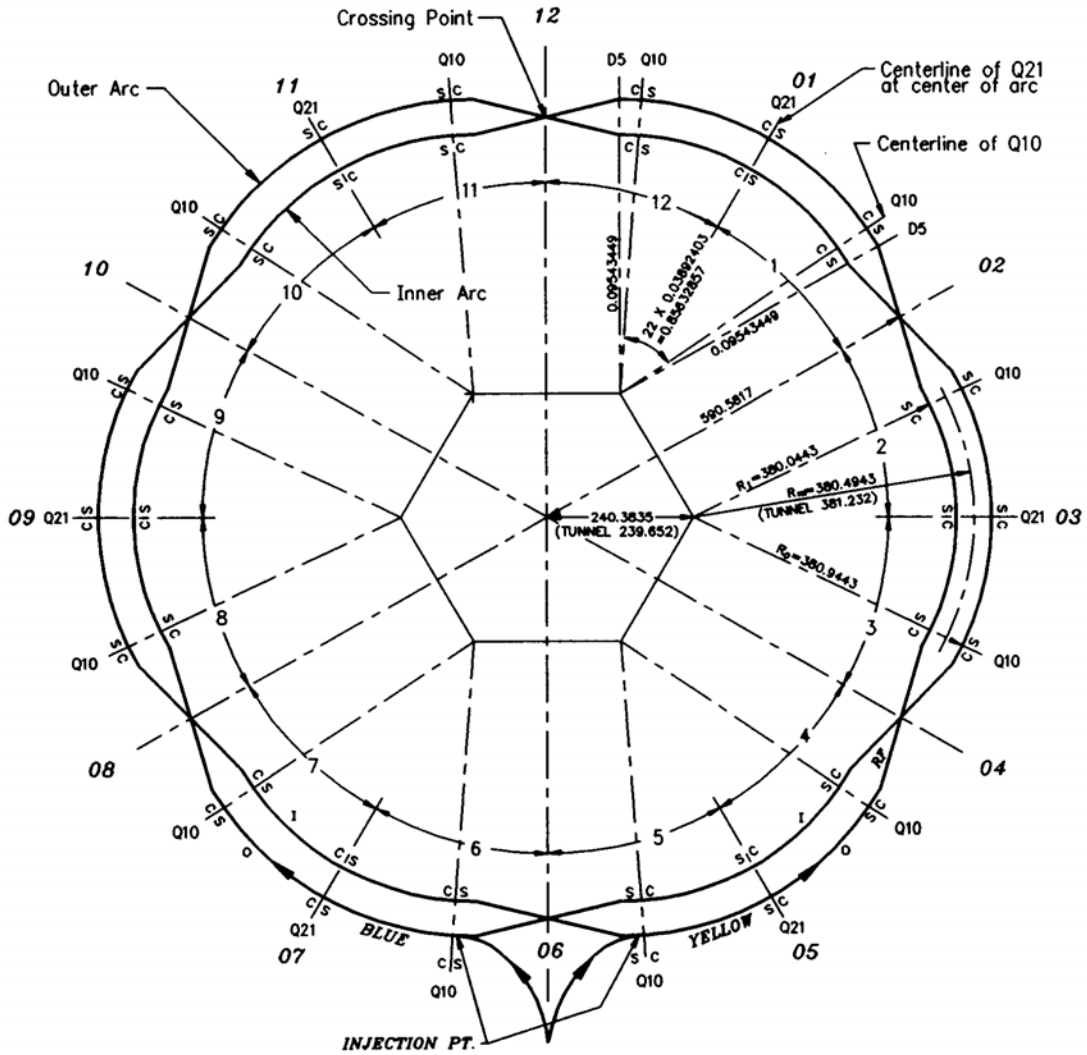

Fig. 0-3. Reference geometry and collider layout. (Ring radii defined by quadrupole center, dimensions in m).

ii. Tunnel Survey and Magnet Alignment

Survey utilizes state-of-the-art technology yielding accurate geodetic information in a fraction of the time required by conventional means. RHIC R&D fostered an integrated plan which includes geodetic survey of primary monuments, establishment of a tunnel net, cryostat design engineering and magnet positioning as a mix of input variables leading to a series of steps to attain positional and smoothness accuracies required for RHIC magnet installation in the accelerator tunnel. The RHIC reference geometry and the collider layout in the tunnel are shown in Fig. 0-3.

Primary Monument Survey. Twelve primary survey monuments located on top of the berm around the RHIC ring were surveyed by the National Geodetic Survey (NGS) in 1981 and must be remeasured to correct for earth settlement that has occurred over the ensuing years. The original quoted error of primary monument survey was about 2×10^{-6} or an uncertainty of one to two millimeters over the RHIC ring radius of 620 m. Measurements were carefully done using conventional triangulation techniques to extend a geodetic grid already in existence at Brookhaven. Accuracies of a few millimeters uncertainty are necessary for a project of this scale but proved very labor intensive, consuming man-years of effort only to be stopped before completion at the termination of the CBA project.

Today, primary survey data of higher accuracy can be obtained in terms of days, not years, by utilizing new technologies. For RHIC's primary monument survey and the tie to the BNL grid, a Kern Mekometer (ME-5000) precision laser distance meter was employed. This instrument has been thoroughly characterized and evaluated for accelerator survey work at the Stanford Linear Accelerator[8] and checked for accuracy at Kern's "Aare Test Facility" and DGFI, the German Geodetic Research Institute. Field accuracies for the ME-5000 show errors to be typically a few tenths of a millimeter over 432 and 864 meter distances, an improvement of an order of magnitude or so over CBA measurements. The ME-5000 measures the phase of a periodically modulated He-Ne laser beam reflected from a precisely fabricated corner cube retroreflector. By modulation of both polarization and frequency of the light beam, unambiguous distance measurements can be made to 0.01 mm resolution and 0.1 ppm accuracies over distances from 10 m to 10 km.

---

[8] T. W. Copeland Davis, Report SLAC-375, Conf.-890 7/90, VC-419, October 1990

The Mekometer was mounted on the primary monument stands and towers around the RHIC ring and a trilateration survey was performed. The Mekometer measured to the neighboring two monuments to the left and right and to the monument at the approximate center of the RHIC Machine.

A second, optional, method to measure the position of the 12 primary monuments could employ satellite based Global Positioning System (GPS) technology. Typically one receiver is placed at a known NGS control point and others at primary control points to be measured. Each receiver accumulates data of satellite time synchronization, orbit information and simultaneous phase measurement of at least four satellite carrier frequencies for a minimum period of 45 minutes. Received information is stored on cassettes and post processed by computer to yield the longitude, latitude, height of unknown stations, distance between each station and azimuthal directions between all points. Six "orders" of GPS geometric relative positioning accuracy standards are defined by the Federal Geodetic Control Committee (1988) document,[9] the highest being classified as order AA. Its accuracy standard for three dimensional surveys using space system techniques is defined in terms of base error and line length dependent error. The maximum allowable error for a single dimensional measurement at 95% confidence level is:

$$S = 3 \text{ mm} + 10^{-8} \times (\textit{Line Length})$$

For RHIC the longest line length is no more than a few kilometers, making line length errors inconsequential. One sigma error can be expected to be less than 2 mm in all three dimensions. An NGS calibrated base line of 14000.0138 m, located in St. Petersburg, Florida, was used by a commercial survey company to check the accuracy of GPS technology. Two antennas were set up at either end of the base line and satellite data was recorded for 1 hour. The data was reduced and the GPS derived length agreed to within 3 mm of the NGS calibration. GPS technology is clearly a time saver, without a sacrifice of accuracy, when compared to conventional means. This method was not used to establish the control for the RHIC Machine.

Standard 30 mm diameter CERN type self-aligning stainless steel bushings are grouted into the floor of the RHIC tunnel beneath twelve 12-inch vertical pipes located in the ceiling. These transfer points act as primary monuments and are located near the ends of each arc sextant of the machine. The measuring instruments are positioned on top of the berm over the primary monuments and collimated. Once positioned, data taking begins and continues to accumulate data measuring relative position of the primaries with respect to the ring center monument and the existing geodetic

grid. When enough data has been accumulated to gain the desired accuracy, the reflectors are moved to new positions and set up for another Mekometer session. Survey jobs of a size larger than RHIC have been completed in one to two months of work, which includes setup, session and data reduction time.

Secondary Tunnel Net. Once the coordinates of the tunnel primary monuments are known, secondary control points are located in *x, y* and *z* around the remainder of the ring. These monuments are physically the same as the primaries and are installed in their rough positions before magnets are placed in the tunnel. Accuracy of placement of the secondaries is unimportant, so long as the monuments are placed about two feet away from the inner and outer tunnel walls, positioned opposite each arc dipole location and slightly offset from its magnet stand center support leg. A similar scheme was used to extend monuments through the insertion regions of the sextants with minor adjustment because of the non-periodicity of its magnetic elements.

The exact three-dimensional positions of the secondaries are carried from the primaries at each end of the sextant through twelve secondary monument pairs and are closed at the midpoint of the sextant. The geodetic figure (Fig. 0-4) of the RHIC arc full cell shows a braced quadrilateral framework of a width to length ratio of approximately 1 to 4. From experience gained at CERN's ISR and SPS projects, length measurements were used employing laser distance meters to keep errors down to the 0.025 mm range. Additional stiffening of the tolerances can be obtained by measuring

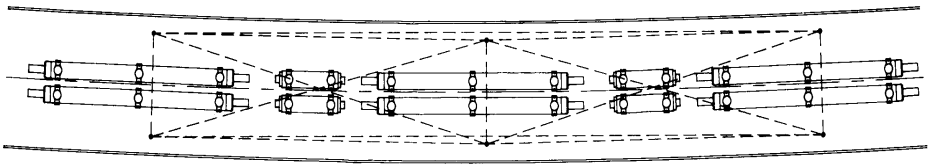

Fig. 0-4. RHIC secondary monument distance measurement.

offsets of two consecutive quadrilaterals to assure the precise position measurement of secondaries of the geodetic framework of each sextant. Vertical positional measurement is done by conventional angularity measurements. Errors in closure at the center of the sextant are less than 0.5 mm plus the relative position error differential of the primary monuments.

Magnet Installation and Positioning. Final positioning of magnet elements to meet machine accuracies (Table 0-2) is simplified by integrating these requirements at every stage of planning starting with cryostat design. Figure 0-5 shows a cross-section of the cryostat, including removable survey targets mounted on its cold mass and base.

Magnet stands were placed in the RHIC tunnel to a few millimeter accuracy and secured in place. Two stands are required to support each blue and yellow ring magnet and were cast to shape to reduce costs as opposed to cutting and welding plate stock.

Absolute position of the cold mass in the cryostat, through the cradle assembly, post support and base, is controlled by machining tolerances; thus the position of the cold mass with respect to cryostat base fiducials should be reproducible to within the stack-up of specified machining errors. Before shipment to BNL, the supplier measured and recorded the offset dimensions of the end fiducials of the cold mass with respect to cryostat base fiducials as specified in the RHIC Dipole Request for Proposal (Section 4.1.4 Position and Orientation Measurements). Upon receipt at BNL, the cryostat was resurveyed to assure that the assembly has not been damaged in shipment by comparing suppliers fiducial data to as-received at BNL and to check that the cold mass was correctly assembled in its cryostat, based upon deviations from normally expected variances of fiducial values. After the magnet assemblies passed cold tests, they were trucked to the RHIC site. There, a specially designed cart carried the cryostats into and along the tunnel and placed the dipoles and quads on their stands. The stands were designed to accommodate a sliding plate and vertical screws so that each cryostat can be independently positioned in *x, y* and *s* space and corrected for rotation errors of the magnetic field.

Table 0-2. Magnet Position Tolerances at 4 K

Beam Position Monitor - Reference Orbit†	$\Delta x = \Delta y = 0.25$ mm rms
Sextupole - Beam Position Monitor This tolerance refers to the magnetic center of the sextupole relative to the center of the BPM, all along the axis of the sextupole.	$\Delta x = \Delta y = 0.13$ mm rms
Quadrupole - Beam Position Monitor This tolerance refers to the magnetic center of the quadrupole relative to the center of the BPM, all along the axis of the quadrupole.	$\Delta x = \Delta y = 0.25$ mm rms
Dipole - Reference Orbit Tolerance refers to the magnetic center as given by fiducial marks of the dipole relative to the reference orbit all along the axis of the dipole. The dipole magnetic center is defined as the magnetic center of its magnetization sextupole.	$\Delta x = \Delta y = 0.50$ mm rms
Dipole Rotation The average horizontal component of the dipole magnetic field is to be less than 1×10^{-3} rms of the vertical component of the field.	$\Delta\Theta = 1$ mrad rms
Quadrupole Rotation	$\Delta\Theta = 1$ mrad rms
Longitudinal Error Refers to the longitudinal position of all magnets with respect to their ideal position along the reference orbit.	$\Delta s = 1.0$ mm rms
Long Term Position Stability The design shall make every effort to keep the long-term position stability, including creep effects, consistent with above position tolerances.	

†Reference orbit positions are based upon tunnel net and primary monument measurements.

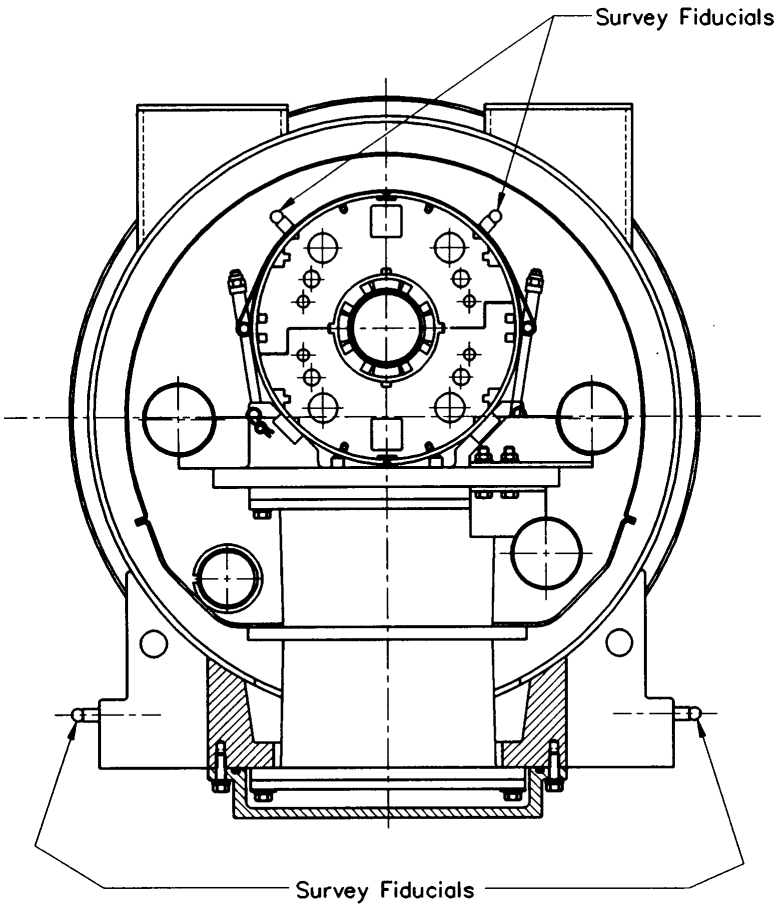

Fig. 0-5. Cryostat showing survey targets.

Final positioning and smoothing of the magnetic elements to the machine's reference orbit was done in one operation utilizing digitally encoded electronic theodolite systems. Electronically encoded T 3000 theodolite heads were plugged into the secondary tunnel net monuments as shown in Fig. 0-6. Positional tolerances for dipoles are less stringent so the secondary monuments were pre-positioned opposite the center support legs of these elements to afford larger sighting angles for the quadrupoles where greater accuracy is demanded. Up to eight theodolite heads can be connected to an on-line personal computer, each having angularity setting capability of less than 0.5 arc seconds which translates to errors of less than 0.025 mm in a 10 m sighting distance. The electronic theodolite system has many features that enhance useability and speed setup time, including an automatic electronic leveling feature with compliance to ±10 minutes and a setting accuracy of ±0.1 seconds. As long as the 30 mm CERN bushings are grouted to a verticality of no more than 10 minutes maximum error, there will be no need for manual adjustment procedures.

Real time saving is afforded by the use of the computer interface. Since the position of the tunnel net secondaries and primaries are known from previous measurements, a computer program will be written to smooth the measured positions of the tunnel net monuments. Placement of the quadrupole and dipole magnetic elements in their proper positions with respect to the machine reference beam orbit therefore becomes a less laborious task. Since the position of the center of the quadrupole and dipole magnetic fields are known with respect to the cold mass fiducials, the cryostats are moved to position the cold mass fiducials to precalculated locations in space so that the magnetic elements are longitudinally centered and radially located as per RHIC lattice design. Cryostat base

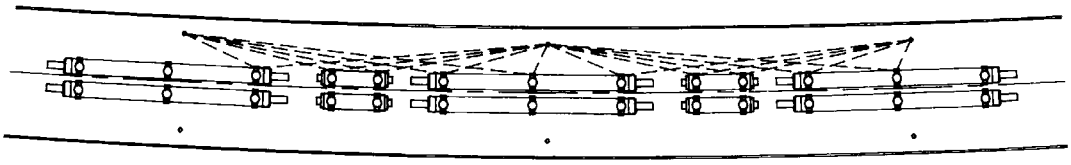

Fig. 0-6. Electronic theodolite positions for magnet installation.

fiducial positions are checked against offset measurements obtained during incoming test and , along with cold mass position data, become a permanent record data base for future reference.

The electronic survey system can be operated in two modes to assist placement of the magnets in their final positions. The inspection mode can be used where the operators set the theodolite cross hairs on the cryostat targets, coordinate values are computed. Deviations from the desired positions stored in memory are displayed on the screen of the CRT. Cryostat position would then be adjusted until the computed deviations are driven to zero. The second method employs laser heads mounted on the optical telescopes of the theodolites. Each of the theodolite heads are positioned to pre-calculated angles and the cryostats are moved to a point where the laser beams intersect at the cryostat targets. In both cases there is no need for manual data taking or hand calculations, for magnet position is based only on smoothing calculations from the original measured positions of the primary and secondary monument locations and offsets to the beam reference orbit position.

Four or more theodolite heads would be optimum for cryostat positioning in the tunnel. Two would be plugged into the tunnel net sockets along the wall and two or more heads positioned in tripods at appropriate positions to minimize angle measurement error. The exact position of each of the auxiliary heads is calculated by system software after a tunnel net theodolite and auxiliary sight a reference bar of known length. Once all measuring element positions are known in three dimensional space coordinates, methods described above can be used to place the cryostats in their smoothed locations, and in one case, without having to change the position of the theodolite heads. The ability to utilize numerous measuring elements is clearly an advantage. All measurements for magnet installation can be done from one or the other side of the tunnel and, in the second mode, at least, setting errors are minimized because the theodolite heads remain in static position, untouched after initial setup.

The concept and use of electronically encoded theodolites, an on-line computer to pre-smooth magnet positions and essentially "point" to their final positions not only increase accuracies but save time as well. As magnets are initially installed in the tunnel by electronically aided methods, results were checked by conventional means and the best method of magnet installation and smoothing was adopted.

iii. Tunnel Equipment Clear Zones

The tunnel cross section in Fig. 0-7 shows the two "clear zones" that were established by the Collider Ring Division in early 1992. The 1.4 m (55 in.) wide by 2.13 m (7 ft) high "clear zone" is to be kept open in the inner aisle, even during construction and installation of RHIC equipment. The outer aisle may have large, temporary equipment (welders, pump stations, etc.) blocking it during installation or repair steps. Equipment causing temporary blockage of inner aisle space should be on wheels and be able to be placed under magnets, or otherwise moved out of the clear zones, to allow the passage of personnel, electric carts, and other equipment. Since any protrusion into the "clear zone" can impede the progress of a repair, maintenance, or magnet replacement, both aisle "clear zones" must remain free of permanent structures now that RHIC is completed. In some cases, certain equipment may reside in the "clear zone" of the aisles during RHIC operation. This equipment must be designed and constructed to allow its removal within an eight (8) hour shift.

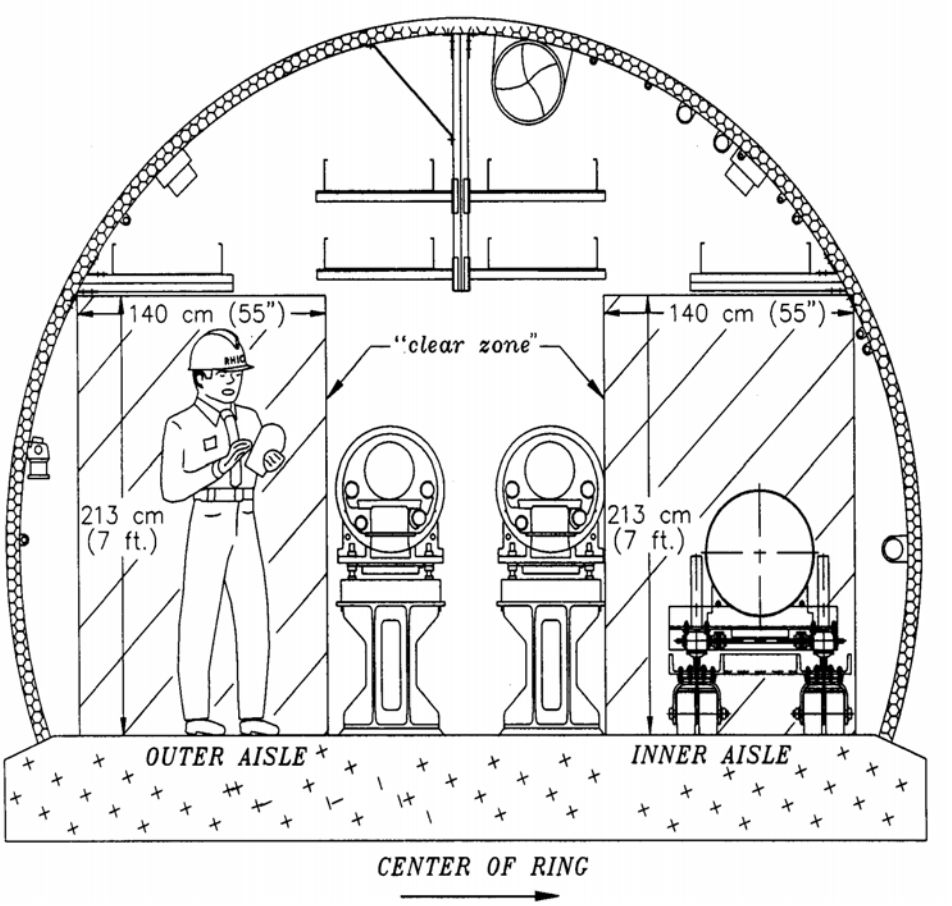

Fig. 0-7. Tunnel cross section clear zones.

iv Warm Space Components

In this section, the space allocations of ring devices and components in the warm sections are defined. The data given here is being used in the development of the RHIC Space Allotment Drawings. These drawings together with the Optics Database represent the source for the Survey Database and, consequently, define the installed location of the warm space components.

The magnet positions in both RHIC rings are fixed and defined by the RHIC Optics Database. The RHIC Optics Database includes, in addition to magnets, all components that affect the beam or perform beam diagnostics, in particular rf cavities, BPMs, wall current monitors, gate valves, etc. These elements are defined in "slots" which are delimited between two connecting flanges at the ends of the element. Correspondingly, a warm space is defined as drift space between the magnet elements, with the warm space being measured as the distance between the vacuum flanges at the ends of the cold cryostats. AUTOCAD coordinates of the magnet centers and component positions are provided directly from the Optics Database in "dxf" format, readable by AUTOCAD. In the RHIC Space Allotment Drawings for the warm spaces, the component locations are defined by the distance from the nearby Interaction Point (IP), as measured on the "equivalent" orbit. The drawings are updated through the C-AD Engineering Change Notification (ECN) system. Images of these drawings, in ".tif" format, are available through the C-A Engineering Archives (drawing prefix 0105-) under the "Useful Information" section of the Accelerator Divisions webpage. In order to keep track of the location of these components with respect to the Optics Database, any new component to be installed in the Warm Space must be approved using the Engineering Change Notice (ECN) system. Following the C-A Operations Procedures Manual 9.3.3, "Procedure for Obtaining Approval to Place Devices into the RHIC Warm Beam Tube Regions", device placements are reviewed, approved and incorporated into the RHIC Space Allotment Drawings.

Layouts of the components in the six interaction regions (IR) are illustrated in the "tif" images noted above. All warm spaces, other than those across the IPs, are jumpered by cryogenic by-passes, within the tunnel, which start and end with cold-to-warm transitions. The warm space length is defined between the vacuum flanges of the transitions. The warm spaces are terminated by bakeable beam vacuum gate valves. These valves are directly attached to the flanges at all cryostat ends of Q4s, Spin Rotators, Q3s, Triplets and DXs (IP side only). Warm bakeable devices and vacuum pipes are connected between the valves, usually by bellows. The space allocation for warm

devices and the interconnecting beam tubes and bellows is detailed in the RHIC Space Allotment Drawings. The warm spaces are classified as *long* and *short* warm drift spaces as follows:

Long Warm Drift Spaces at each of the six interaction regions (IRs).

1. From the IP to DX magnets on each side. This warm space is to $l = 7.120$ m in every IR, and is defined as the distance from the crossing point to the flange on the bellows of the ion pump stand connected to the warm beam position monitor at the DX cryostat. (The distance from the IP to the DX flange is 8.614 m).
2. From the end of the cryostat at the Q3 magnet to the beginning of either a Q4 magnet or a Spin Rotator. The length of the warm space from the triplet cryostat flange (38.439 m from the IP) to the flange of the Q4 quadrupole is $l = 34.122$ m. On both sides of the 6 and 8 o'clock interaction points, cold spin rotators are connected to the quadrupole Q4, reducing the warm space to $l = 21.660$ m in the 6 and 8 o'clock IRs.

Short Warm Drift Spaces between the D0 and DX magnet in every IR.

The DX-D0 warm space of $l = 4.895$ is identical at every IR, and represents the distance between the flanges at the end of the DX cryostat and at the vacuum valve connected to the D0 cryostat. Located on either side of the 6 o'clock IP, in the *yellow* ring of sector 5 and the *blue* ring of sector 6, there are two *additional* short warm spaces in each ring. These warm spaces contain the injection magnetic septum (Lambertson) magnets at Q7-Q8 and the fast injection kicker magnets at Q9 - D9.

SAFETY SYSTEMS (WBS 1.12)

The collider personnel will be protected against Radiation Hazards and Oxygen Deficiency Hazards (ODH) using a single "RHIC Personnel Safety System" in full compliance with regulatory requirements. Ensuring personnel safety at older accelerators meant an Access Control System designed to protect personnel from radiation hazards. Other safety hazards to be found within accelerator enclosures or support buildings were mitigated by their own independent administrative controls or engineered safety solutions, often after the initial accelerator design phase and independent of the Access Control System design. Integrating all personnel safety systems in RHIC is expected to result in a superior level of personnel safety and equipment protection, while providing greater operational efficiency. It is also intended that the Personnel Safety System have a closer interface to the fire protection elements installed as part of our conventional construction than has been the case in other accelerator construction.

i. Personnel Safety Systems (WBS 1.12.1)

Required safety systems for Oxygen Deficiency Hazards (ODH) and Radiation Hazards are integrated into a single system. The Personnel Safety System will employ fourteen small Programmable Logic Controllers (PLC) interconnected as two sets of seven peers, channels "A" (otherwise refer to as A-divison) and "B" (B-division) in Fig. 12-1, rather than a few larger units hierarchically connected to multiple remote I/O chassis. This is done to achieve a redundancy level, for the most complex part of the system, greater than that provided by the dual level achieved by other designs.

Control Devices

Commercially available Programmable Controllers are configured so as to attain the level of redundancy necessary to achieve compliance with DOE 5480.25. A network of PLC units compensates for the complex set of failure mechanisms exhibited by individual processors as compared to designs based upon relays, much as a OP-Amp compensates for component variability with gain and feedback or a bridge is supported by its interconnecting I-beams. In order to reduce the potential for Common Cause failure events, the core PLC system will be comprised of two different brands or models of PLCs such that basic

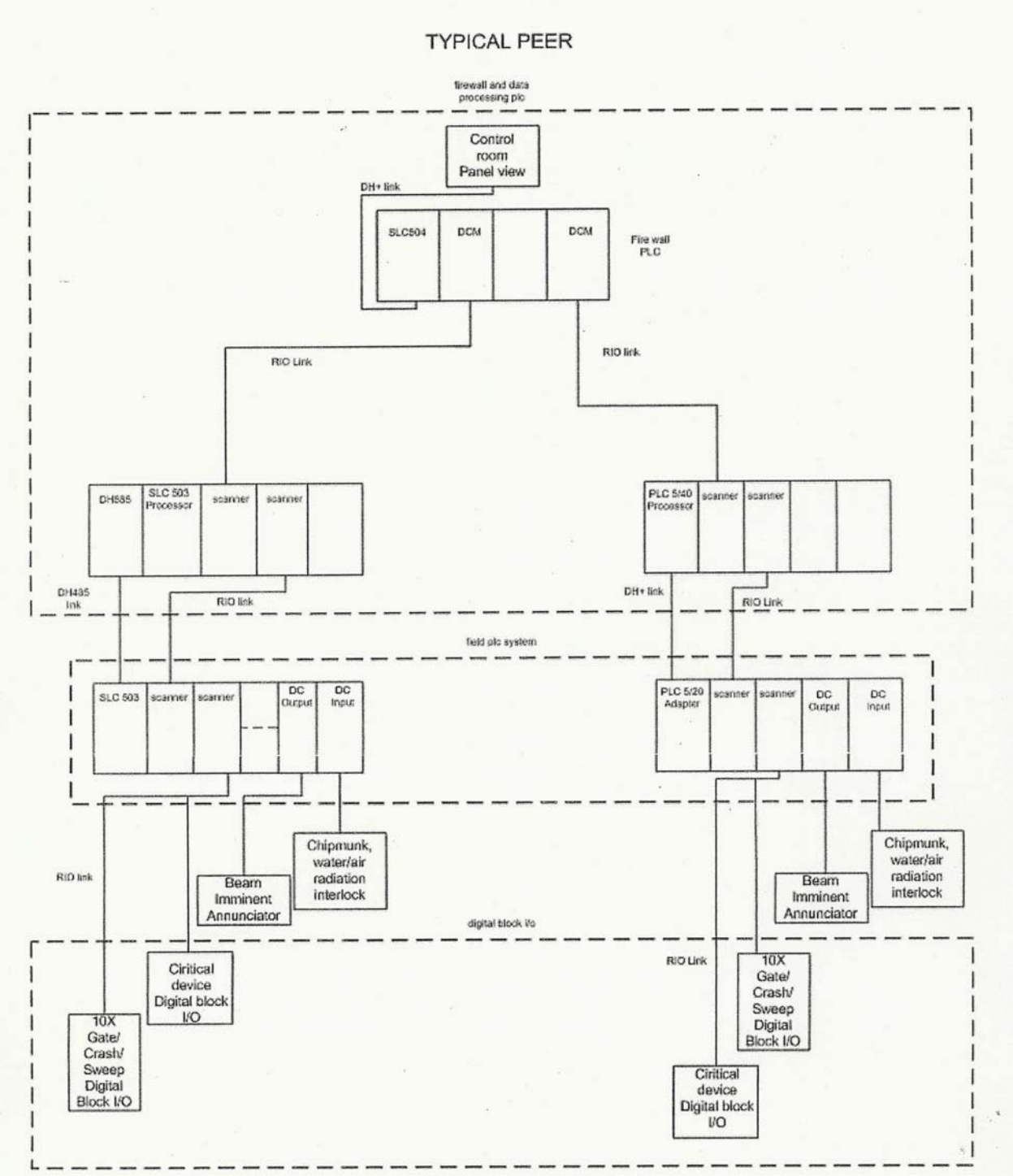

Fig. 12-1. Personnel Safety System Block Diagram.

hardware and software elements will be of different origin; each PLC has its own independent UPS and line power feed. Complications introduced by physical bus limitations result in a rather complex interconnection pattern, however, a minimum of two independent divisions "A" and "B" is always maintained. The "A" and "B" divisions are in turn connected to one of two Command and Control processors which provide supervisory control and monitoring functions. These processors are in their turn redundantly connected to a Personnel Safety System generated Display located in the

C-AD Main Control Room.

Safety Devices

An Emergency Shutdown System labeled CRASH will use "pull cord" type switches. They will be installed throughout the Collider enclosure. With minor exceptions, there will be essentially continuous coverage on both sides of the enclosure tunnel. Because of magnet locations, coverage in supported injection areas will be made on one side only. Each unit will protect 65 m (200 ft) of tunnel. The CRASH switches are not hard wired into a lockout system, but are connected in a redundant manner to a PLC in the "A" division and to another PLC in the "B" division. When a CRASH is called for, the Personnel Safety System will remove power from selected critical power supplies or close selected critical vacuum valves. In addition, the Beam Dump System will be activated. This dual approach is necessary because the Beam Dump system, while engineered and constructed to high standards, is not considered part of the Personnel Safety System.

The Gate system is comprised of thirty-five (35) Gate packages and nineteen (19) Emergency Entrance and/or Exit Doors packages. Redundant interlock switches will be mounted on each of these doors. In addition, the external entry gate has control points (electric strikes) which are monitored for to verify a gate being locked. At this Main Gate will also be a standardized electronics system for information, display and access purposes; this package will include TV monitoring capability in the MCR. All access gates (external and internal) have a card reader based entry logging system and information display. The Main Control Room (MCR) will have a bank of captive access and sweep keys interfaced into the PLC logic such that if any key is missing from the key bank, then the Collider (and Collider injection) cannot be started.

The Radiation Monitoring system will employ the "Chipmunk" design used at the AGS and at FERMILAB. Interlock outputs will be connected to system PLC units. Eighteen (18) units are

planned for initial startup. The most likely distribution is twelve (12) units for experimental area monitoring and six (6) units for RHIC injection.

Distribution

The PLCs will be wired and programmed so that each will independently supervise the interaction area and the sextant areas nearest their physical location. In simple terms, they will provide coverage both clockwise and counterclockwise for the half-sextants nearest the location. Sensor and control elements within the tunnel enclosure will operate at 12 or 24 Vdc (Gate switches, ODH alarms, etc.). Distribution boxes located approximately every 65 m (200 ft) will be interconnected via dual multi-drop supervised cables to the PLC units, as will the wiring for Gate and Emergency Entrance/Exit Doors.

Redundant signals are carried via separate cables except when a conduit is used; safety system cables are carried either in their own tray or via conduit. Properly secured, supervised cables may be optionally employed outside the tray system.

Event Logging

All events from both divisions are monitored using a Windows PC and application written with the Rockwell RSView software package. The Logs are backed up three times per day on a Linux based server PC. The logs can be viewed via the web browser using Java based applications and html. Redundant firewall hardware is used to protect the PCs from access outside the CA department.

Testing

OPM procedures are used to perform functional and acceptance testing of the PSS annual or prior to the beginning of each running cycle.

Personnel Safety System Support

As per the laboratory RADCON manual and the SBMS module on “Software Quality Control” all changes or modification to the software and hardware follows the ECN guidelines as related to approval and reporting format.